

University of Strathclyde
Department of Chemical and Process Engineering

Characterisation of Turbulent Mixing and its
Influence on Antisolvent Crystallisation

Andrew Brown

A thesis presented in fulfilment of the requirements
for the degree of Doctor of Philosophy

2012

Copyright Statement

This thesis is the result of the author's original research. It has been composed by the author and has not been previously submitted for examination which has led to the award of a degree.

The copyright of this thesis belongs to the author under the terms of the United Kingdom Copyright Acts as qualified by University of Strathclyde Regulation 3.50. Due acknowledgement must always be made of the use of any material contained in, or derived from, this thesis.

A handwritten signature in black ink, consisting of a large, stylized 'G' followed by a large, stylized 'P' and a smaller signature below it.

May 2012

Acknowledgements

There are many people to whom I am indebted to for the help, support and guidance that was graciously provided to me in the duration of PhD. First and foremost I would like to thank my supervisor Dr. Ján Šefčík for guiding me through the process and always making himself available for enlightening discussions.

I would also like to thank the technical support staff (Jim, John, Stuart, Ian and Les) at the chemical engineering laboratory for assisting me with many of the practical problems which arise on a day to day basis in the laboratory. Additionally, I would like to thank the many postgraduate researchers who have come through the door during my spell here, each of whom has made the experience more enjoyable and made the long hours seem a little shorter.

I was fortunate enough to have considerable support in the form of an engineering and physical sciences research council (EPSRC) grant with industrial support from Xstalbio limited. This afforded me the opportunity to test some of the ideas and concepts explored during my PhD on real industrial processes and the collaborative relationship has kept industrial relevance foremost in my thoughts. I am particularly thankful to Dr. Barry Moore, Dr. Marie-Claire Parker and Dr. Jan Vos for providing me with this opportunity and assisting me. Several of the experiments were conducted at the Swiss Federal Institute of Technology in Zurich and I am grateful to Dr. Miroslav Soos and Prof. Massimo Morbidelli for arranging this.

Finally, I would like to thank my friends and family for their support and friendship over the years.

Table of Contents

Abstract	ix
Table of Nomenclature	xi
1 Introduction	1
2 Turbulent Mixing - Theory and Introduction	4
2.1 What is mixing?	4
2.2 Turbulence and turbulent mixing.....	5
2.3 Mixing quantification using parallel reactions	14
2.4 Bourne IV reaction scheme.....	16
3 Antisolvent Crystallisation - Theory and Introduction	24
3.1 Crystallisation theory	24
3.2 Mixing sensitivity in antisolvent crystallisation	31
3.3 Formation of protein coated microcrystals (PCMCs)	34
3.4 Objectives of Investigation	35
4 Experimental Techniques and Methods	36
4.1 Mixing characterisation	36
4.2 Mixing influenced precipitation of valine	57
4.3 Testing the vortex mixer in commercial applications	66
5 Micromixing Reaction Models	69
5.1 Interaction by exchange with the mean (IEM model).....	69
5.2 The engulfment model (E-model)	73
5.3 Comparable volume engulfment.....	77
6 Micromixing Reaction Models - Results and Discussion	85
6.1 IEM results	85
6.2 Comparable volume engulfment results	91
6.3 Comparison of the IEM and E-model results	100
6.4 Modelling conclusions.....	104
7 Mixing Characterisation – Results and Discussion	105
7.1 Relative mixing performance of various continuous mixers	105
7.2 Total energy dissipation rate.....	109
7.3 Estimation of an absolute mixing time	123
7.4 Comparison of estimated mixing times with literature	132

Contents

7.5	Viscosity and volume fractions.....	133
7.6	Fraction of total energy utilised for mixing	144
7.7	Comparison of mixing and residence timescales	151
7.8	Mixing characterisation conclusions	157
8	Mixing Influenced Precipitation - Results and Discussion	159
8.1	Mixing influenced precipitation of Valine.....	159
8.2	Testing the vortex mixer in commercial applications	174
8.3	Conclusions - Mixing influenced precipitation	183
9	Concluding Remarks.....	184
	References.....	187
	Appendix 1 - Physical Properties.....	- 1 -
	Appendix 2 - Mixer Geometries	- 3 -
	Appendix 3 - Mixing Characterisation Data	- 7 -
	Appendix 4 - Comparison of Timescales	- 15 -
	Appendix 5 - Fractional Conversion Regression Plots.....	- 24 -
	Appendix 6 - Research Outcomes	- 29 -

List of Figures

Figure 2.1. Segregation of mixing.....	4
Figure 2.2. Eulerian view of local velocity	5
Figure 2.3. Immiscible volume exposed to turbulent flow.....	6
Figure 2.4. Diffusing volume exposed to turbulent flow.....	6
Figure 2.5. Energy and concentration spectrum	7
Figure 2.6. Summary of mesomixing and micromixing sub processes.....	13
Figure 2.7. Competitive reactions	16
Figure 2.8. Interfacial tension	23
Figure 3.1. Typical solubility diagram.....	25
Figure 3.2. Influence of supersaturation on the nucleation rate	27
Figure 3.3. Crystallisation pathways.....	28
Figure 3.4. Driving forces behind the simple diffusion-reaction model of growth[9].....	30
Figure 3.5. Influence of mixing on local supersaturation and PSD.....	33
Figure 3.6. Formation of protein coated microcrystals (PCMCs)	34
Figure 4.1. Mixing scheme	39
Figure 4.2. Mixing process schematic	43
Figure 4.3. Energy balance	44
Figure 4.4. Pressure transducer locations.....	45
Figure 4.5. Major GC components	50
Figure 4.6. Sample calibration for methanol and acetone with ethanol internal standard.....	54
Figure 4.7. Chromatogram	54
Figure 4.8. Operational points on water/IPA/valine system solubility curve.....	58
Figure 4.9. Process flow diagram	59
Figure 4.10. Schematic diagram of the experimental set-up	61
Figure 4.11 Vertical projection of watertight cap (top) and side profile (bottom)	63
Figure 4.12. T-mixer dimensions	64
Figure 4.13. Operational points on water/IPA/valine system solubility curve.....	64
Figure 4.14. Process flow diagram	66
Figure 4.15. Total flowrate, mixers and formulations tested.....	67
Figure 5.1. Representation of the IEM Model.....	69
Figure 5.2. Representation of the IEM Model.....	71
Figure 5.3. Engulfment model	74
Figure 5.4. Two compartment model.....	78
Figure 5.5. Establishment of mixing zone	78

Contents

Figure 5.6. Four Compartment model.....	79
Figure 6.1. Dimensionless concentration at 1:1 volume ratio and 100ms mixing time	88
Figure 6.2. Dimensionless concentration at 3:1 volume ratio and 100ms mixing time	88
Figure 6.3. Dimensionless concentration at 1:3 volume ratio and 100ms mixing time	89
Figure 6.4. Dimensionless concentration at 10:1 Volume Ratio and 100ms mixing time	89
Figure 6.5. Fractional conversion vs. Damköhler number for different flow ratios	90
Figure 6.6. Fractional conversion vs. Damköhler number for different excess alkali	90
Figure 6.7. Profile for the engulfment model at 1:1 volume ratio	94
Figure 6.8. Profile for the engulfment model at 3:1 volume ratio	94
Figure 6.9. Profile for the engulfment model at 1:3 volume ratio	95
Figure 6.10. Profile for the engulfment model at 10:1 volume ratio	95
Figure 6.11. Fractional conversion vs. Da (engulfment).....	98
Figure 6.12. Fractional conversion vs. Da (Mixing half-life)	98
Figure 6.13. Fractional conversion vs. Da (90% mixed).....	99
Figure 6.14. Fractional conversion vs. Da for various alkali excesses	100
Figure 6.15. IEM model vs. engulfment time Damköhler number	102
Figure 6.16. IEM model vs. mixing half-life Damköhler number	103
Figure 7.1. 1:1, 3:1 and 10:1 Inlet Volumetric Flow Ratio	107
Figure 7.2. 1:1, 3:1 and 10:1 Total Volumetric Flow Ratio	108
Figure 7.3. Fractional Conversion vs. Alkali Stream Inlet Velocity.	109
Figure 7.4. Fractional conversion vs. energy dissipation rate	111
Figure 7.5. Regression ellipse plots	114
Figure 7.6. Transition from micromixing to mesomixing limiting behaviour	115
Figure 7.7. Fractional conversion vs. energy dissipation rate	116
Figure 7.8. Relationship between fractional conversion and mixing	117
Figure 7.9. Fractional conversion vs. energy dissipation rate (ignoring kinetic energy)	118
Figure 7.10. Fractional conversion vs. simplified energy dissipation rate	119
Figure 7.11. Energy Dissipation Rate vs. Inlet Velocity Cubed	121
Figure 7.12. Energy dissipation rate vs. inlet velocity cubed over jet diameter	121
Figure 7.13. Energy dissipation rate vs. outlet flowrate cubed.....	122
Figure 7.14. Energy dissipation rate vs. mixer pressure drop	123
Figure 7.15. Engulfment time vs. energy dissipation rate.....	125
Figure 7.16. Mixing half-life vs. energy dissipation rate.....	127
Figure 7.17. Mixing half-life gradient change.....	127
Figure 7.18. Probability of self-engulfment as a function of dimensionless time	129
Figure 7.19. 90% mixed time vs. energy dissipation rate.....	130

Contents

Figure 7.20. Regression ellipse plots for mixing time and fractional conversion	132
Figure 7.21. Modified composition fractional conversion	135
Figure 7.22. Modified composition mixing half-lives	135
Figure 7.23. Change in gradient of the mixing half-life at 1:1 and 3:1 with modified composition...	136
Figure 7.24. Influence of viscosity on mixing time at 1:1	137
Figure 7.25. Influence of viscosity on mixing time at 1:1	137
Figure 7.26. Fractional conversion 3:1 and 10:1 comparison	138
Figure 7.27. Fractional conversion at 3:1 and 1:3 flow ratios with no viscosity difference	140
Figure 7.28. Mixing half-life at 3:1 and 1:3 flow ratios with no viscosity difference	140
Figure 7.29. Fractional conversion for 3:1 and 1:3 flow ratios.....	141
Figure 7.30. Mixing half-life at 3:1 and 1:3 flow ratios	142
Figure 7.31. Fractional Conversion vs. Da	146
Figure 7.32. Fractional Conversion vs. ωDa	147
Figure 7.33. Corrsin relationship with 1% and 0.1% efficiency	150
Figure 7.34. Engulfment time with 2% and 0.1% efficiency	151
Figure 7.35 Comparison of timescales of mixing and residence	153
Figure 7.36. Regression ellipse plots	156
Figure 8.1. Solid Recovery after 90 Minutes	161
Figure 8.2. Turbidity of the samples after 1 minute and 30 minutes.....	163
Figure 8.3. Change in absorption with time	164
Figure 8.4. Time dependent solid recovery through 24mg/ml slice	164
Figure 8.5. Influence of flowrate on mean particle size	166
Figure 8.6. Particle Size Distributions at 24mg/ml	167
Figure 8.7. Obscuration vs. time	169
Figure 8.8. Radius of gyration vs. time	169
Figure 8.9. Laminated substructure caused by Kolmogorov scale segregation	171
Figure 8.10. Mixing Characterisation of a CIJ Mixer	172
Figure 8.11. Kolmogorov length scale in a CIJ mixer	172
Figure 8.12. F1 solid recovery	175
Figure 8.13. F1 net protein recovery.....	175
Figure 8.14. F1 filter rate.....	176
Figure 8.15. F1 in the vortex mixer (no Kenics) SEM 2000x magnification	177
Figure 8.16. F1 in the X mixer (no Kenics) SEM 2000x magnification	177
Figure 8.17. F2 solid recovery	178
Figure 8.18. F2 net protein recovery.....	178
Figure 8.19. F2 filter rate.....	179

Figure 8.20. F2 vortex mixer (no Kenics) SEM 2000x magnification	180
Figure 8.21. F2 X mixer (no Kenics) SEM 2000x magnification.....	180

List of Tables

Table 2.1. Variants of parallel reaction schemes	15
Table 2.2. Summary of the Bourne IV reaction scheme	17
Table 4.1. Reactions schemes	39
Table 4.2. Alcohol composition	42
Table 4.3. Summary of continuous mixers	49
Table 4.4. Calibration concentrations	52
Table 4.5. Calibration Concentration Ratios	53
Table 4.6. Chromatogram Areas	53
Table 4.7. Chromatogram Area Ratios	53
Table 4.8. Peak data	55
Table 4.9. Sample Calculation of the Fractional Conversion from GC Data	55
Table 4.10. Sample Calculation of the Fractional Conversion from GC Data	55
Table 4.11. Solution formulation	58
Table 5.1. Initial IEM conditions which correspond to the experiments (mmol/L).....	72
Table 5.2. Initial IEM conditions which correspond to the experiments in dimensionless form	73
Table 5.3. Summary of initial conditions.....	81
Table 5.4. Summary of Initial Conditions in Dimensionless Form	84
Table 6.1. Mixing Half-life Constants	96
Table 6.2. Mixing half-life constants comparison of mixing times and engulfment times	97
Table 6.3. Influence of volume ratio on fractional conversion.	102
Table 7.1. Power law fit of fractional conversion and energy dissipation rate	112
Table 7.2. Power law fit of fractional conversion and total energy dissipation rate	115
Table 7.3. Viscosity ratios and outlet viscosities (N.B. 1 cSt is $1 \times 10^{-6} \text{ m}^2/\text{s}$).....	134
Table 7.4. Estimate of percentage of total energy dissipation rate used by mixing	149
Table 7.5. Timescale analysis - mixer volume	154
Table 7.6. Timescale analysis - system volume	155
Table 8.1. Filtrate Turbidity and Filter Time as a function of filter time.....	163

Abstract

Mixing is a fundamental part of many processes in chemical engineering. In order for molecular processes to proceed there is an implicit requirement for molecular scale mixing. Many processes are so slow that they are effectively independent of mixing as mixing is fast relative to the process. However, for fast processes mixing can be the limiting step and for processes with competitive elements it can control product quality and distribution. Antisolvent crystallisation is one such process which is strongly influenced by mixing. The initial mixing controls the distribution of supersaturation which in turn controls the nucleation rate and hence many key parameters such as a particle size distribution. In order to understand antisolvent crystallisation and how the initial mixing influences nucleation it is important to first understand the mixing process itself. In this thesis mixing was measured and quantified by utilising a mixing sensitive competitive reaction scheme with well understood and well defined kinetics.

The reaction scheme that was chosen was the Bourne IV reaction scheme which has received considerable interest in the scientific literature as a means to quantify and characterise the mixing performance of rapid continuous mixers. The original scheme has some inherent limitations in terms of ranking mixers operating under the conditions commonly encountered in industrial applications; namely the 1:1 flow ratio and the lack of a difference in the physical properties of the streams. This original scheme has been extended in a systematic way to incorporate differences in the flow ratio and physical properties. The results have been analysed in conjunction with a model capable of allowing fair comparison between the flow ratios. Several continuous mixers of various sizes including an impinging jet mixer and a vortex mixer have been characterised over a variety of mixing conditions.

The antisolvent precipitation of valine in a confined impinging jet mixer was explored and analysed in conjunction with the mixing characterisation data allowing depth to be added to the analysis of standard crystallisation experiments. It is demonstrated that the initial mixing (over the first second) controls many of the key parameters in antisolvent crystallisation which underlines the importance of designing and scaling the initial mixing process correctly. It is also demonstrated

that this is true even when samples are subjected to additional shear over long timescales.

The vortex mixer characterised here was utilised in an industrial scale pilot trial and the results contrasted with those obtained using an “off the shelf” cross mixer. This work underlines that controlling the initial mixing step has strong industrial relevance and is one of the single most important parameters in the process design of antisolvent crystallisation processes.

Table of Nomenclature

<i>Symbol</i>	<i>Definition</i>
A	Area
A_{AM}	Dimensionless concentration of A in A Zone
B_{BM}	Dimensionless concentration of B in B Zone
c	Fraction of the energy dissipation utilised for mixing
C	Concentration
$\langle C \rangle$	Average concentration
$C_{A,i}$	Acid concentration in zone i
$C_{B,i}$	Base concentration in zone i
$C_{D,i}$	Dimethoxypropane concentration in zone i
C_{eq}	Equilibrium Concentration
C_{i0}	Initial concentration of i
$C_{i,im}$	Concentration of i in zone i
D	Molecular diffusion coefficient
Da	Damköhler number
D_{AM}	Dimensionless concentration of D in A Zone
D_{BM}	Dimensionless concentration of D in B Zone
D_T	Turbulent diffusion coefficient
E	Rate of engulfment
g	Order of crystal growth process
J	Nucleation rate
K	Power law pre-factor between Y and ϵ
k_B	Boltzmann constant
KE	Kinetic energy
k_d	Mass transfer coefficient of diffusion
k_i	Rate constant of reaction i
K_{omt}	Overall mass transfer coefficient
k_t	Mass transfer coefficient of surface integration
L_s	Length scale of segregation

Table of Nomenclature

<i>Symbol</i>	<i>Definition</i>
m	Mass flow rate or mass
m_v	Molecular volume
N	Wavenumber
P	Probability of engulfment
P_e	Parameter characterising mass transfer between X_{Am} and X_{Bm}
PE	Pressure energy
Q	Volumetric Flowrate
Q_B	Batch Feedrate
r	Radius
r_c	Critical radius
r_i	Rate of reaction of i
S	Segregation index
Sc	Schmidt Number
S_{sat}	Supersaturation
t	Time
T	Temperature
t_μ	IEM Characteristic mixing time
u	Local velocity
V	Volume
X_A	Volume fraction of A
X_a	Pure unmixed volume fraction of A
X_b	Pure unmixed volume fraction of B
X_{Am}	Volume fraction of A rich mixing zone
X_{Bm}	Volume fraction of B rich mixing zone
X_m	Volume of mixing zone ($X_{Am} + X_{Bm}$)
X_{A0}	Initial volume fraction of A
X_{B0}	Initial volume fraction of B
Y	fractional conversion

Greek symbols

<i>Symbol</i>	<i>Definition</i>
α	Volume fraction IEM
β	Dimensionless constant
γ	Interfacial energy
ΔG	Change in free energy
ε	Energy dissipation rate
λ_k	Kolmogorov length scale
λ_b	Batchelor timescale
μ	Dynamic viscosity
μ_p	Chemical potential
ν	Kinematic viscosity
ν_k	Kolmogorov velocity
ρ	Density
τ	Characteristic time
τ_k	Kolmogorov timescale
τ_s	Characteristic inertial-convective mixing time
τ_d	Characteristic timescale for turbulent dispersion
τ_e	Characteristic engulfment time
τ_b	Batchelor timescale
τ_c	Corrsin mixing time
t_ω	eddy turnover time
Ψ	Constant to extract c
ω	Constant between experimental results and engulfment model

1 Introduction

The manner in which fluids are mixed can have a considerable impact on many processes. Examples include product distribution for fast and complicated reactions or particle size distribution, product morphology and kinetics in crystallisation.[1]

A Damköhler number can be defined to assess the mixing sensitivity of a process:

$$Da = \frac{\tau_{mixing}}{\tau_{process}} \quad (1.1)$$

Processes exhibit sensitivity when the Damköhler number approaches or is greater than unity (i.e. mixing occurs on a timescale similar to or greater than that of the process itself). Therefore, in slow processes mixing is not an important processing parameter as the time required for mixing will be less than the time required for the process and molecular homogeneity is achieved long before the process can occur which results in the process occurring uniformly throughout the fluid.

In the case of fast and simple reactions then mixing only influences the kinetics. However, in many complex reaction systems there are often undesirable side reactions which result in the formation of by-products and reduce product yield in addition complicating separation processes. Obviously, the most desirable way to deal with by-product formation is by the addition of a catalyst to enhance the selectivity of the desired reaction. However, as this reaction speeds up it may reach a point where it becomes mixing controlled.[1–4]

It is easy to see how this can lead to a situation where a fast main reaction can be in competition with one or more slower side reactions, which are afforded the opportunity to react when the local stoichiometry is unbalanced. There are two scenarios, one where the mixing time (τ_{mix}) is much less than the characteristic reaction time of the slow reaction (τ_r) and the other where it is comparable or faster. In the first case, as the system approaches homogeneity, the yield of the slow reaction is undetectable as there is a local stoichiometric balance. When the mixing time (τ_{mix}) is comparable to characteristic reaction time of the slow reaction (τ_r),

segregation occurs and local stoichiometric inequality exists. In these segregated pockets the slow reaction occurs resulting in detectable conversion.

The selectivity that parallel chemical reactions exhibit can be exploited to create a scale to “measure” mixing.[5–7] If each characteristic mixing time results in a unique distribution of products then this distribution of products can be used for evaluating the effectiveness of mixing devices. There are various incarnations which are sensitive over different timescales and each has inherent advantages, disadvantages and limitations. In selecting the most appropriate, one has to consider an approximate timescale of the mixing process and compare this with reaction kinetics and then balance this with economic considerations and the availability of analytical equipment. In order to quantify the fast and efficient mixing offered by continuous static mixers a “slow” reaction that is relatively fast is required. This coupled with analytical equipment considerations made the Bourne IV reaction scheme the most appropriate choice for the mixing characterisation in this work.[6]

Crystallisation is also strongly influenced by mixing processes. Factors such as local and mean supersaturation as well as residence time have to be controlled and balanced with nucleation and growth kinetics in addition to secondary transfer processes such as aggregation and breakage to get the required final particle size distribution as well as control other important parameters.[8–10]

Supersaturation can vary locally within a crystalliser. In antisolvent crystallisation this can be because of spatial variations in mixing performance, in cooling crystallisation it can be because of thermal gradients or temperature segregation.

Classical nucleation theory assumes a homogeneous mixture with a uniform distribution of supersaturation. This assumption is only valid if the characteristic timescale of mixing is less than the characteristic timescale of the initial crystallisation. Often the assumption of mixing being fast with respect to crystallisation is based on macroscale observations where timescales are large with respect to mixing. However, microscale crystallisation events (such as nucleation or precursor formation) frequently have short timescales and therefore these events and consequently subsequent processes become sensitive to the initial mixing. In short -

in order to understand, control and optimise antisolvent crystallisation it is of critical importance to understand and control mixing.

There are two main subjects of interest in this thesis. Firstly the characterisation and quantification of turbulent mixing and secondly how turbulent mixing influences antisolvent crystallisation. The subjects of turbulent mixing and antisolvent crystallisation are introduced separately in Chapter 2 and Chapter 3 respectively.

Chapter 4 deals with the experimental methodology that was utilised during the course of this research. The methodology of the Bourne IV mixing characterisation reaction scheme is explained as are the modifications that were made to it along with the methodology of the crystallisation experiments.

In order to further analyse and explain the mixing characterisation results it was deemed necessary to employ a model of mixing and reaction. It was the aim that such a model would qualitatively agree with the experimental results and be quantitatively accurate to acceptable degree. Two models were considered, these were the interaction by exchange with the mean (IEM) model and the engulfment model. The background of these models is outlined in Chapter 5 and the results are shown in Chapter 6.

This then enabled depth to be added to the analysis of the mixing characterisation work. The results of the mixing characterisation experimentation are explored in Chapter 7. These results feed in to experiments which explored the influence of mixing on antisolvent crystallisation, the results of which are shown in Chapter 8.

2 Turbulent Mixing - Theory and Introduction

2.1 What is mixing?

In molecular scale processes, segregation is a measure of how well mixed a system is. Figure 2.1 illustrates the difference between the scale and intensity of segregation. Scale of segregation refers to the large scale breakup (macromixing and mesomixing) without molecular diffusion and intensity of segregation refers to concentration differences in segregated regions.[11]

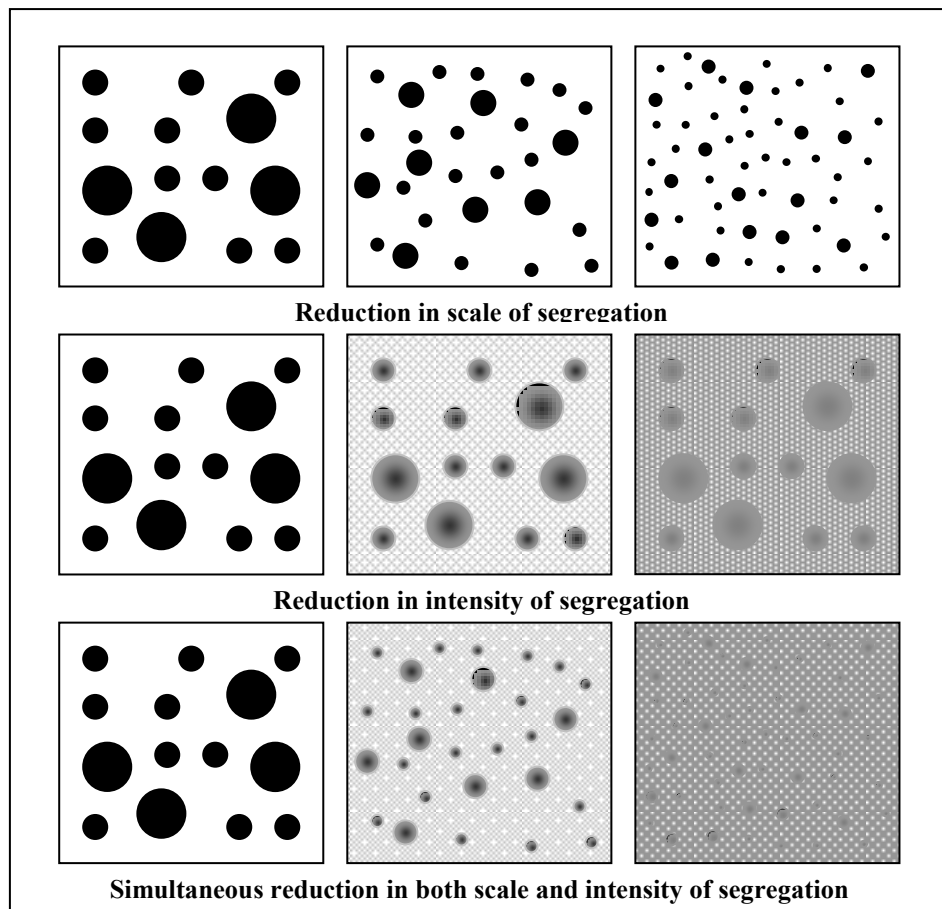


Figure 2.1. Segregation of mixing

Molecular diffusion is a requirement for the reduction of intensity of segregation under turbulent mixing conditions because even the smallest scales of turbulence are still gargantuan when compared to molecules. Typically, turbulence reduces the scale of segregation, whilst micromixing processes reduce both the scale and ultimately also the intensity at the smallest length scales. This reduction in scale

increases the interfacial area which in turn speeds up molecular diffusion. When there is no difference in segregation intensity on a molecular scale then the system can be considered to be completely mixed.

In practice, any probe measuring concentration would measure at a scale far above the molecular scale and so what may seem perfectly mixed on a process analytical basis could still be segregated on a smaller scale.

2.2 Turbulence and turbulent mixing

Although no precise definition of turbulence exists, it is characterised by the domination of viscous forces by inertial forces which results in local velocity fluctuations, rapid diffusion, fluctuating vortices and the dissipation of kinetic energy. These velocity fluctuations (Figure 2.2) efficiently transport momentum, making turbulent diffusion much more effective than molecular diffusion alone.[2]

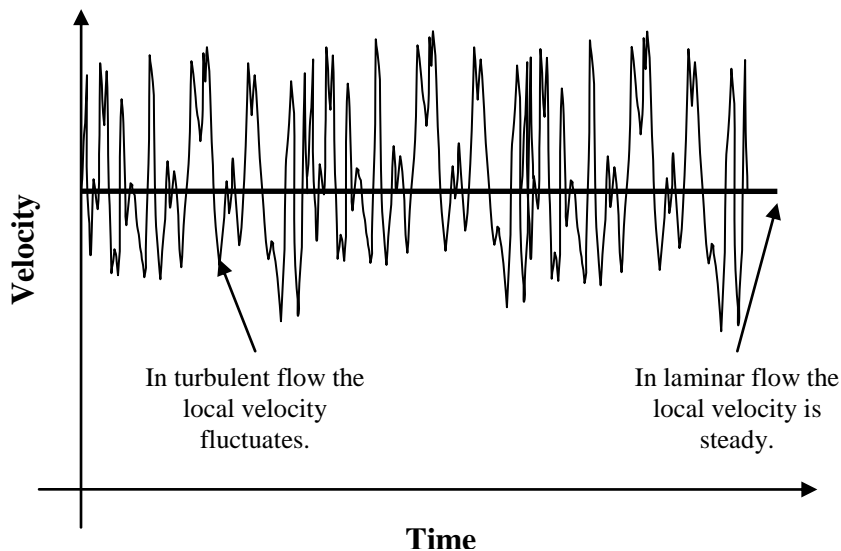
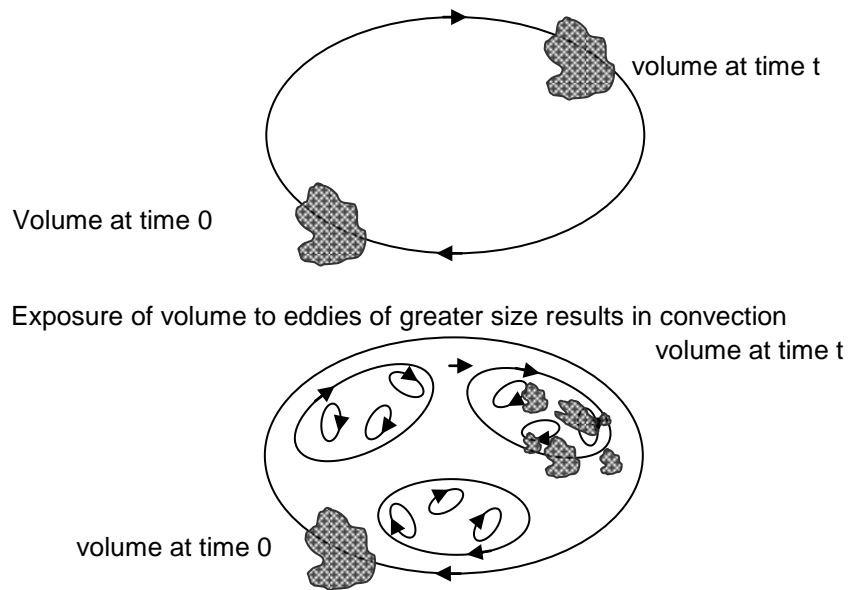


Figure 2.2. Eulerian view of local velocity

Consider firstly a fluid volume exposed to a turbulent flow of a second immiscible fluid with eddies of larger size than the volume (Figure 2.3 – top). The volume is simply transported through convection. However, when the eddies are of similar or smaller size than that of the volume (Figure 2.3 – bottom) then the volume is deformed, eroded and elongated by these eddies on multiple scales. As there is no molecular diffusion in this example (immiscible) the smallest scale of the drop size is

limited to the smallest scale of deformation – the Kolmogorov length scale. After a long time of exposure to turbulence the drop size distribution reaches equilibrium.[2]



Exposure of volume to eddies of similar or smaller size results deformation and breakage

Figure 2.3. Immiscible volume exposed to turbulent flow

Considering a fluid volume exposed to a turbulent flow of a second miscible fluid with eddies of greater or larger size than the volume (Figure 2.4). The turbulent flow contains a range of eddy length scales, ranging from the macroscale to the Kolmogorov length. Eddies that are smaller than that of the diffusing volume continually stretch, deform and distort it, resulting in concentration gradients which can then be smoothed by micromixing mechanisms. The lack of surface tension results in less breakage and therefore the diffusing volume is distributed in an irregular manner over a larger volume so that the concentration (averaged over the volume) decreases and the surface area (for molecular diffusion) increases.[12]

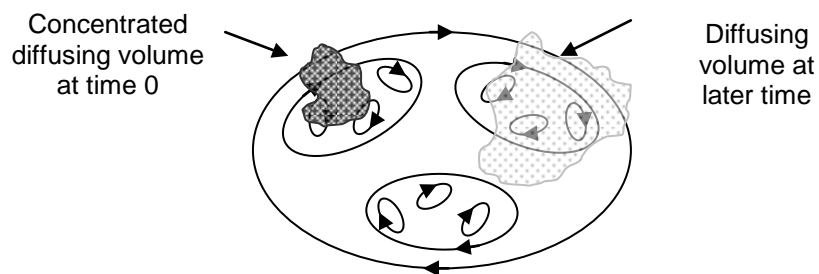


Figure 2.4. Diffusing volume exposed to turbulent flow

Although local velocity suffers from unpredictability, there is still an element of spatial structure. This structure consists of fluctuating vortices or “eddies”. These eddies range in size from the macroscale (vessel, pipe etc.) down to the Kolmogorov length. An energy spectrum characterises how the kinetic energy is distributed between length scales, a similar construction can be made to show how concentration fluctuates over a range of length scales.[12]

Large scale vortices draw their energy from bulk flow and then transfer it down to successively smaller scales until it reaches the smallest scale of turbulence (the Kolmogorov scale) where viscous forces begin to dominate. At the largest scale, the energy distribution is typically controlled by geometry and flow conditions (the integral scale). At the other extreme, the smallest length scales are orders of magnitude smaller and are isotropic. Between these extremes lies the inertial subrange. In this range the energy spectrum will be a function only of the length scale (N) and dissipation rate (ϵ) i.e. independent of viscosity.[12] Dimensional analysis allows the famous Kolmogorov 5/3 law to be defined:

$$E(N) = \beta \epsilon^{\frac{2}{3}} N^{-\frac{5}{3}} \quad (2.1)$$

where β is a constant with a value around 1, N is the wavenumber and ϵ the energy dissipation rate.

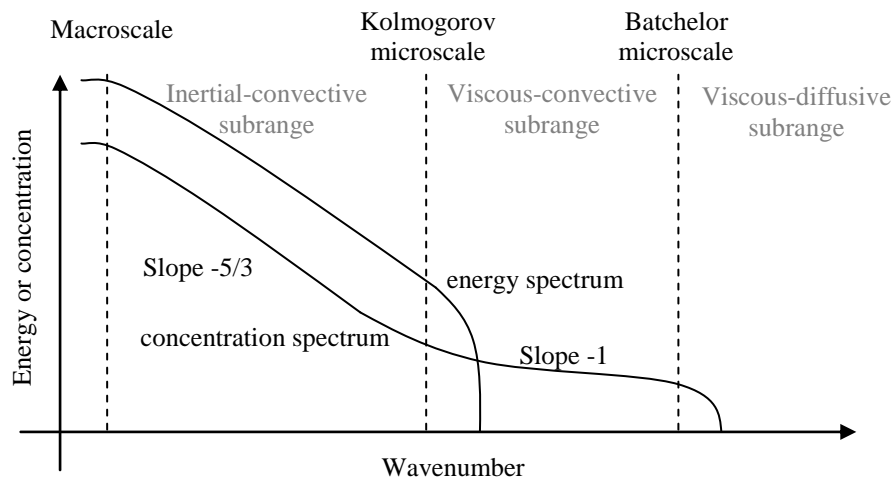


Figure 2.5. Energy and concentration spectrum

Figure 2.5 shows a typical energy and concentration spectrum. It is plotted against the wavenumber which is proportional to the inverse of the length scale. The

largest scales have the most energy and decay quickly after viscous force becomes significant around the Kolmogorov length.

Considering the concentration fluctuations allows three ranges to be defined; inertial-convective, viscous-convective and viscous-diffusive. In the inertial-convective subrange which lasts from the integral scale down to the Kolmogorov the fluid is deformed and broken up into smaller pieces reducing the scale of segregation.[13] In the viscous-convective subrange, which starts around the Kolmogorov length scale, laminar strain results in viscous deformation which further reduces the scale of segregation whilst molecular diffusion gradually becomes more significant as the Batchelor scale is approached. The viscous-diffusive subrange begins at this point and as the length scale decreases even further molecular diffusion rapidly reduces any concentration variance (segregation intensity).[4]

Kolmogorov proposed in 1941 that the smallest scales of turbulence depend only on the energy dissipation rate per unit mass ($\text{length}^2/\text{time}^3$) and kinematic viscosity ($\text{length}^2/\text{time}$).[14] Considering just a simple dimensional analysis produces the following scales:

Kolmogorov length scale	Kolmogorov time scale	Kolmogorov velocity scale
$\lambda_k = \left[\frac{\nu^3}{\varepsilon} \right]^{\frac{1}{4}} \quad (2.2)$	$\tau_k = \left[\frac{\nu}{\varepsilon} \right]^{\frac{1}{2}} \quad (2.3)$	$v_k = (\nu\varepsilon)^{\frac{1}{2}} \quad (2.4)$

Obviously, the relevant dynamic parameter (the energy dissipation rate) is an average value that is considered to be representative. In practice there will be spatial variations in this parameter resulting in local energy dissipation rates and hence spatial variation in segregation and consequently local reaction rates etc.

Mixing is considered over three length scales. At one extreme is macromixing which occurs on the largest scale of a vessel and includes mechanisms such as bulk convection whilst at the other extreme is micromixing which occurs in the viscous-convective (engulfment and deformation) or viscous-diffusive subrange (molecular diffusion). In between the two extremes lies mesomixing which reduces the length scale of segregation from the integral length scale to the Kolmogorov length scale and includes turbulent diffusion and inertial convection as its mechanisms. It occurs in the inertial regime. It particularly refers to the length scale of the feed stream.[3] Molecular processes require mixing on a molecular level to proceed (i.e.

micromixing) and although the processes occur simultaneously they complete top down (largest to smallest scale), consequently any of these processes can be the rate limiting step than controls mixing. In a small continuous mixer where the dimensions of the mesoscale (i.e. feed scale) is approximately the same dimensions of the vessel then macroscale mixing is not considered.[15]

The timescale for inertial-convective mesomixing was suggested by Corrsin [16]:

$$\tau_s = 2.04 \left(\frac{L_s^2}{\varepsilon} \right)^{\frac{1}{3}} \quad (2.5)$$

This represents the time required to reduce the largest concentration fluctuation L_s from the integral length scale down to the Kolmogorov microscale in the inertial regime (notice no dependence on the viscosity). When the inlet forms a strong jet a reasonable estimate of the length scale of segregation is the inlet radius. When a strong jet is not formed the length scale of segregation is estimated according to a volume element which either expands or contracts according to the velocity of the surrounding fluid.[3]

Another mesomixing mechanism called turbulent dispersion has also been identified. This occurs when a feed stream spreads out transversely, like a turbulent jet entering a larger volume. The timescale for turbulent dispersion is given by:[17]

$$\tau_D = \frac{Q_B}{uD_T} \quad (2.6)$$

Where Q_B is the feed stream flowrate, u is the local velocity and D_T is the turbulent diffusivity. It is more significant in larger mixers with a fast inlet flowrate relative to the surrounding velocity. The turbulent diffusivity is related to kinetic energy of turbulence and its dissipation rate.[4]

Micromixing occurs on a length scale around the order of the Kolmogorov length scale and below, in the viscous-convective and viscous-diffusive subrange. There are three mechanisms associated with microscale mixing, these are engulfment and deformation which reduce the scale of segregation further below the Kolmogorov scale and finally molecular diffusion which reduces the intensity of segregation.

Using a Lagrangian frame of reference in a Cartesian coordinate system, a fluid element below the Kolmogorov length is rapidly elongated in one direction causing thinning in the second direction and moderate increase in the third direction.[18] Long thin slabs are formed which increases interfacial area and accelerates molecular diffusion.

The thinning slabs formed by deformation become twisted due to vorticity and become embedded within the stretching vortices. Vortices around twelve times the Kolmogorov length are the most stable due to the balance of stretching and viscous dissipation.[19] The stretching of these energetically stable vortices draws in fluid from the environment in a process called “engulfment”.[20] This process is often the rate limiting step of the micromixing mechanisms and for fluids with Schmidt numbers (ratio of momentum diffusivity to molecular diffusivity) less than 4000 (in practice this means most low viscosity liquids) it can be used to model micromixing on its own.[21] The time constant for micromixing by engulfment is given by:[20]

$$\tau_E = 17.3 \left(\frac{\nu}{\varepsilon} \right)^{\frac{1}{2}} \quad (2.7)$$

Notice no dependence on the molecular diffusion.

Molecular diffusion, ultimately, is the method for the reduction of the concentration gradients. All other methods reduce the scale of segregation and increase the interfacial area both of which accelerate molecular diffusion. However, molecular diffusion is the process that reduces the intensity and results in homogeneity on a molecular level and allows any subsequent molecular level process (e.g. reaction or precipitation) to proceed.

The Batchelor microscale is characterised by the balance of the viscous convective and viscous diffusive transport properties in terms of timescales (t_k and t_b) but these have different length scales (λ_k and λ_b) due to different fluid properties (molecular diffusion coefficient D and viscosity ν).[22] The Batchelor microscale is the distance a molecule can move due to diffusion:

$$\lambda_b^2 = D \tau_b \quad (2.8)$$

This allows the Batchelor length scale to be expressed in the following way:

$$\tau_b = \tau_k = \left[\frac{\nu}{\varepsilon} \right]^{\frac{1}{2}} = \frac{\lambda_b^2}{D} \quad (2.9)$$

Substituting the following from the rearranged Kolmogorov length scale to eliminate the energy dissipation rate:

$$\varepsilon = \frac{\nu^3}{\lambda_k^4} \quad (2.10)$$

Gives:

$$\lambda_b = \left[\frac{D}{\nu} \right]^{\frac{1}{2}} \lambda_k \quad (2.11)$$

Substituting for the Schmidt number (Momentum diffusivity to molecular diffusivity):

$$\lambda_b = Sc^{-\frac{1}{2}} \lambda_k \quad (2.12)$$

i.e. the Batchelor scale is a small fraction of the Kolmogorov scale. This means that the smallest eddies (Kolmogorov length) are still enormous in comparison to the length scales associated with molecular diffusion and this highlights the importance of viscous-convective process in reducing the scale of segregation and subsequently accelerating the molecular mixing (diffusion) process.

The assumption of equating the time constants is that under constant energy dissipation the characteristic time for diffusion from the Batchelor microscale in turbulence is not more than the characteristic time for viscous-convective processes to reach the Batchelor microscale from the Kolmogorov scale.[23] At moderate Schmidt numbers (<4000) the characteristic time for engulfment is significantly higher than that for molecular diffusion.[20], [21], [24]

Corrsin considered the decay of concentration fluctuations in homogeneous turbulence at high Reynolds number.[16] The fluctuations were considered to follow an exponential decay from an initial average value to a value after some time[25]:

$$S_{i\tau} = S_{i0} \exp\left(\frac{-\tau}{\tau_c}\right) \quad (2.13)$$

Where S_i is the segregation index

$$S_i = (c_i - \bar{c}_i)^2 \quad (2.14)$$

The Corrsin mixing time (τ_c) is based on the reduction in segregation index from its initial value down to a factor of $1/e$ [16], [25]:

$$\tau_c = 2.04 \left(\frac{L_s^2}{\varepsilon} \right)^{\frac{1}{3}} + \frac{1}{2} \left(\frac{\nu}{\varepsilon} \right)^{\frac{1}{2}} \ln(Sc) \quad (2.15)$$

This equation is valid from for isotropic turbulence for liquids with a Schmidt number much greater than 1. The first term is a mesomixing term and the second term is micromixing term.

The time constants can be ranked to give an estimate of the likely rate limiting mixing mechanism. The mesomixing time decays as function of the energy dissipation rate to the power of $-1/3$ (see equation (2.5) or (2.6)) whilst the micromixing times decay as function of the energy dissipation rate to the power of $-1/2$ (equation (2.7)). This means the micromixing time decays at a faster rate than the mesomixing time which makes it possible for a mixer to be micromixing limited at low energy dissipation rates and mesomixing limited at higher energy dissipation rates. This is characterised by a viscosity dependence at low energy dissipation rates and an insensitivity to viscosity at higher energy dissipation rates.[26]

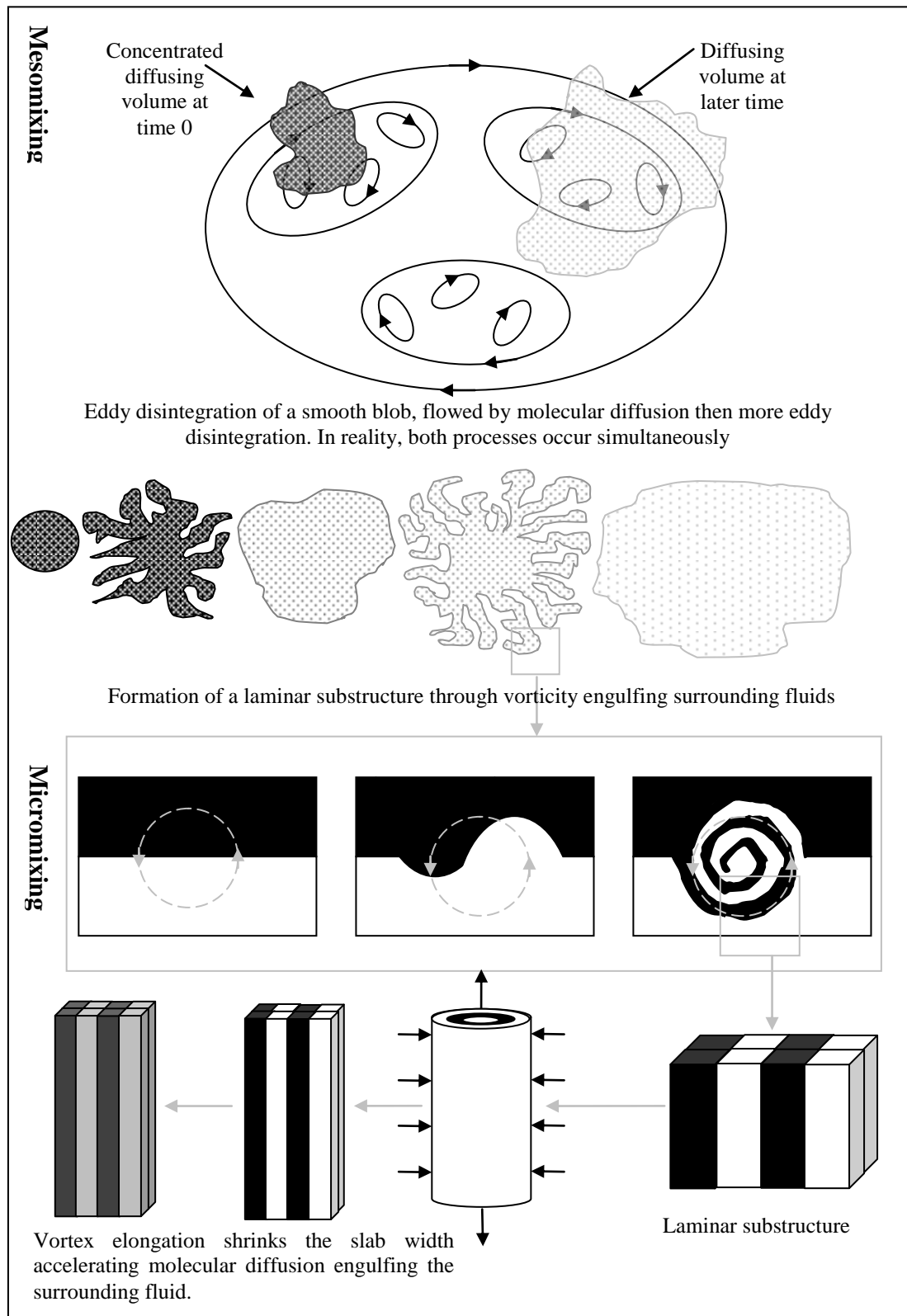


Figure 2.6. Summary of mesomixing and micromixing sub processes

Composite of ideas from presented by Bourne and Baldyga.[3], [4], [20], [27]

2.3 Mixing quantification using parallel reactions

The selectivity that parallel chemical reactions exhibit can be exploited to create a scale to “measure” mixing. If each characteristic mixing time results in a unique distribution of products then this distribution of products can be used for evaluating the effectiveness of mixing devices. This can either be done qualitatively in a “better” or “worse” way or quantitatively. A quantitative analysis would require information about the reaction mechanism and kinetics in order to construct a model which could then be used to calculate a theoretical relationship between mixing time and product distribution.

The basic premise involves competing a fast reaction that is mixing limited for a limiting reagent with a slow reaction that is limited by reaction kinetics. The kinetics of the reactions determine the range of mixing times to which the product distribution is sensitive. If the mixing is so fast that it can be considered instantaneous then the mixing limited reaction dominates and there is little or no conversion of the slower reaction – this fixes the lowest range of mixing times to the limit of detection of the analytical method. At the other end of the spectrum the sensitivity is limited when poor mixing results in a high fractional conversion of the slow reaction. The exact range of timescales to which the reaction product distribution is sensitive can be “tuned” by varying the reactant concentrations and hence reaction kinetics.

Competitive reactions were first proposed to “measure” mixing by Paul and Treyball[5] and have been developed extensively since, notably by Villermaux[7] and Bourne[6], [28]. There are various incarnations which are sensitive over different timescales and all have inherent advantages, disadvantages and limitations.

Broadly speaking there are two types of competitive reaction schemes; competitive parallel and the competitive consecutive. The main points and some examples are illustrated in Table 1. In the case of small continuous mixers mixing times from 1ms are attainable at the highest flowrates up to the order of a second at the lower flowrates. This range makes the Bourne IV reaction scheme the most sensible choice. The Villermaux reaction scheme can be used to evaluate mixing performance over a similar range[29] but there are concerns about the complex and not well understood kinetics of the this reaction.[30] Despite these concerns, the

Villiermaux reaction is widely utilised (particularly industrially) for mixing characterisation due to economic advantages over the other schemes. For small scale characterisation economics are less important.

	Parallel Competitive Reactions	Competitive Consecutive Reactions
General reaction scheme	$A + B \xrightarrow{k_1} R$ $D + A \xrightarrow{k_2} S$ Where $k_1 \gg k_2$	$A + B \xrightarrow{k_1} R$ $A + R \xrightarrow{k_2} S$ Where $k_1 \gg k_2$
Desirable Reagent characteristics	<ul style="list-style-type: none"> • Irreversible with few products (preferably two) and no side reactions. • Mechanism and kinetics are well known and understood • Routine, inexpensive and accurate analytical method • Solubility of reagents and products in solvent should be known and not exceeded in mixing • Safe and economical 	
Examples	Bourne III: Acid (A) and base (B) neutralisation which competes with the hydrolysis of ethylchloroacetate (D).[31]	
	Analytics	GC
	Time range	100-5000ms
	Pros	Easy to use
	Cons	Reactant instability
	Bourne IV: Acid (A) and base (B) neutralisation which competes for acid with the acid catalysed hydrolysis of dimethoxypropane (D) (DMP).[6]	
	Analytics	GC
	Time range	1-2000ms
	Pros	Easy to use and stable
	Cons	Handling of DMP
	Bourne I: Diazotised sulfanic acid (A) with 1-naphthol (B) to form mono-azo dye (R) competing with a reaction of R and A to form bis-azo (S). [28]	
	Analytics	UV
	Time range	65-5000ms
	Pros	Low concentration
Cons	Difficult to use	
Bourne II: Improved Bourne I reaction, blending 2-naphthol in the above scheme. [32]		
Analytics	UV	
Time range	30-5000ms	
Pros	Low concentration	
Cons	Difficult to use	
Villiermaux: Iodide/iodate.[7]		
Analytics	UV	
Time range	Complex kinetics make this more qualitative[30]	
Pros	Economical	
Cons	Complex kinetics	

Table 2.1. Variants of parallel reaction schemes

The Bourne IV reaction scheme is the only type considered in this thesis. It is of the competitive parallel reaction variety. An acid stream (A) is mixed with a stream containing base (B) and dimethoxypropane (D).

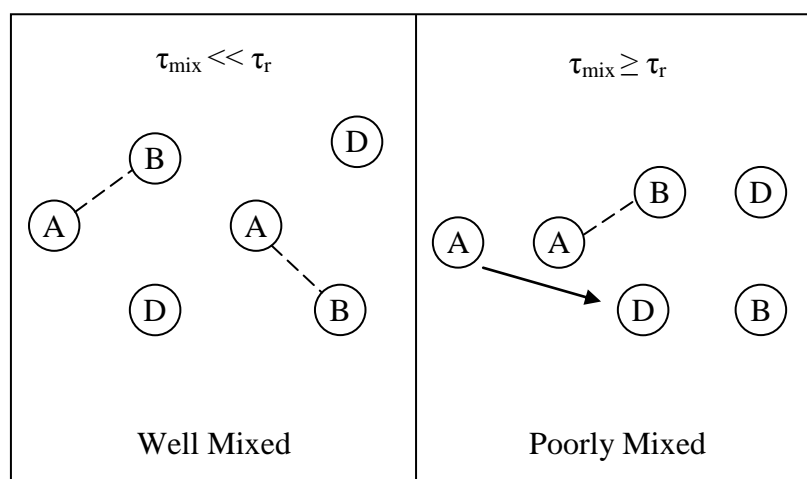


Figure 2.7. Competitive reactions

There are two scenarios (Figure 2.7), one where the mixing time (τ_{mix}) is much less than the characteristic reaction time of the slow reaction (τ_r) and the other where it is comparable or longer. In the first case, as the system approaches homogeneity, the yield of the slow reaction is undetectable as k_1 is much greater than k_2 .

When the mixing time (τ_{mix}) is comparable to characteristic reaction time of the slow reaction (τ_r), segregation occurs and local molar inequality exists. In these segregated pockets, any remaining acid and base react which will leave areas depleted in base and in these zones of base depletion the acid is free to react with the DMP via the slow reaction.

2.4 Bourne IV reaction scheme

This reaction scheme was developed by Bourne *et al.*[6] It has advantages due to its simple, safe operating procedures and simple analytical requirements (GC). It also has the advantage of reactions with well understood kinetics and mechanisms

which makes a quantitative analysis possible over the range of mixing times expected of continuous mixers.

It has been used, due to its mildly exothermic nature, to test if thermal segregation has a significant influence on local reaction rates. It was found that temperature segregation effects are negligible in this system which is adequately described by concentration segregation. This was found to be the case for both isothermal and adiabatic operation.[6] This should make modelling this reaction scheme relatively straightforward as any thermal effects can be safely ignored.

Acid Catalysed Hydrolysis of Dimethoxypropane (Bourne IV)													
Outline	Rapid neutralisation of a strong base and strong acid e.g.: $\text{HCl} + \text{NaOH} \xrightarrow{k_1} \text{H}_2\text{O} + \text{NaCl}$ $\text{A} + \text{B} \xrightarrow{k_1} \text{Products}$ Acid catalysed hydrolysis of dimethoxypropane: $\text{CH}_3\text{C}(\text{OCH}_3)_2\text{CH}_3 + \text{H}^+ (+ \text{H}_2\text{O}) \xrightarrow{k_2} \text{CH}_3\text{COCH}_3 + 2\text{CH}_3\text{OH} + \text{H}^+$ $\text{D} + \text{A} \xrightarrow{k_1} \text{Products}$												
Method	Acid stream mixed with a stream of DMP and base at volumetric flow ratio of 1:1 Molar ratio of 1.05:1:1 for NaOH:HCl:DMP DMP not contacted with any material with pH of less than 8 Analysed via gas chromatography Fast reaction: $k_1 = 1.4 \times 10^8 \text{ m}^3/\text{mol.s}$ $\Delta H = -55.8 \text{ kJ.mol}^{-1}$ Slow reaction $k_2 \approx 0.6 \text{ m}^3/\text{mol.s}$. Function of temperature and salt concentration.												
Solubility	<table border="1" style="width: 100%; border-collapse: collapse;"> <thead> <tr> <th></th> <th style="text-align: center;">Water</th> <th style="text-align: center;">Ethanol</th> </tr> </thead> <tbody> <tr> <td style="text-align: center;">DMP</td> <td style="text-align: center;">15g/l @ 20°C</td> <td style="text-align: center;">✓</td> </tr> <tr> <td style="text-align: center;">HCl</td> <td style="text-align: center;">✓</td> <td style="text-align: center;">✓</td> </tr> <tr> <td style="text-align: center;">NaOH</td> <td style="text-align: center;">✓</td> <td style="text-align: center;">✓</td> </tr> </tbody> </table> <p>N.B. The relatively low solubility of the dimethoxypropane in water explains why 25% by weight ethanol is added to both streams.</p>		Water	Ethanol	DMP	15g/l @ 20°C	✓	HCl	✓	✓	NaOH	✓	✓
	Water	Ethanol											
DMP	15g/l @ 20°C	✓											
HCl	✓	✓											
NaOH	✓	✓											
Pros	<ul style="list-style-type: none"> • Stable reactants and products • Easily quantified by gas chromatography • Well understood kinetics • No side reactions 												
Cons	<ul style="list-style-type: none"> • Difficulty in handling DMP, keep away from anything with a pH less than 8. In practice this means add the NaOH and mix before adding the DMP in solution preparation. 												

Table 2.2. Summary of the Bourne IV reaction scheme

Since the fast reaction is many orders of magnitude greater than the slow reaction and the fast reaction can be considered instantaneous with respect to the mixing, the characteristic reaction time, τ_r , can be expressed as the pseudo first order time constant of the slow reaction[4]:

$$\tau_r = \frac{1}{k_2 C_{HClO}} \quad (2.16)$$

Where C_{HClO} is the initial concentration of hydrochloric acid when mixed but with no reaction and k_2 is the rate constant of the slow reaction.

Mixing is quantified by the fraction of dimethoxypropane which reacts during mixing:

$$Y = 1 - \frac{C_D}{C_{D0}} \quad (2.17)$$

Johnson and Prud'homme used the Bourne IV reaction scheme to characterise the mixing performance of a confined impinging jet (CIJ) mixer and to develop a scaling relationship.[15] Johnson and Prud'homme assumed that the fractional conversion is entirely controlled by a Damköhler number with the mixing time controlled by the inlet velocity.

They found that the fractional conversion scaled with velocity to the power of 1.5 and using this relationship allowed them to define a Damköhler number by utilising the characteristic reaction time as defined by the kinetics. This Damköhler number was found to correlate well with the fractional conversion across a range of concentrations (reaction times). Furthermore, this correlation had an exponent of roughly 1, i.e., the fractional conversion is roughly proportional to the mixing time. Whilst this is strong evidence of the fractional conversion being roughly proportional to the mixing time it would be interesting to know over what range of concentrations and mixing conditions this linearity is applicable. One would intuitively think that non-linearity would creep in at the extreme fractional conversions associated with very good and very poor mixing.

From this a scaling relationship was built between all the key parameters including inlet velocity and kinematic viscosity in addition to geometrical parameters such as inlet diameter and confinement (chamber diameter) with all the constants and prefactors lumped into one universal constant.

The absolute mixing time was estimated from the residence time where outlet configuration had no influence on fractional conversion, this was then equated to the mixing time and was used to extract the constant for the scaling model. The constant was then used to define, in absolute terms, the mixing time in a CIJ mixer over a range of flowrates and geometrical differences.

One of the limitations of this work is that due to syringe pumps being used the maximum flowrates were relatively low. The CIJ characterised by Johnson *et al* has been studied using computational fluid dynamics (CFD) [33–35] and it has been shown that the Kolmogorov scaling exhibited in this work is a result of low flowrates. As the system becomes more turbulent, it is predicted to exhibit inertial limiting behaviour characterised by an independence from viscosity and a velocity dependence to the power of 1. Therefore it is likely that this scaling methodology is only applicable over low to moderate flowrates and would likely break down at high flowrates.

Liu and Fox employed computational fluid dynamics to calculate the fractional conversion of the Bourne IV reaction scheme as a function of flowrate in a confined impinging jet mixer.[33] This followed on from the work by Johnson and Prud'homme to experimentally characterise mixing in a CIJ mixer and uses CFD to model the mixing and compares these theoretical values with the Johnson results.

This work concluded that mixing in the impinging jet mixing is controlled at low flowrates by micromixing. At higher jet Reynolds numbers the model predicts inertial-range scaling not Kolmogorov range scaling.

Gavi *et al* used the same model as that deployed by Liu and Fox to understand the scaling of a CIJ mixer again using the Bourne IV test reaction scheme.[34] This work used the Damköhler number (mixing time calculated by CFD) as a scaling parameter and found excellent agreement across a range of characteristic reaction times. Marchisio *et al* showed again that the mixing time in a CIJ scales with the micromixing time at low flowrates but changes to mesomixing at higher flowrates, consistent with turbulent mixing theory.[35]

Siddiqui *et al* characterised mixing in a confined impinging jet reactor by experimentally measuring the total energy dissipation rate and compared this with CFD simulations and mixing characterisation using the Villermaux reaction

scheme.[36] They calculated the total energy dissipation rate by various methods including using micromixing data, pressure drop data, a mechanical energy balance and CFD and found broadly agreeable results between each method.

The CFD showed that the maximum rate of energy dissipation occurs, unsurprisingly, in the centre of the mixing chamber at the impingement point and that the maximum energy dissipation rate on a local level is around forty times that of the average. At high flowrates the CIJ operates with plug flow whilst at low flowrates it resembles a CSTR with dead volumes of low energy dissipation rate.

Liu *et al* used the Bourne IV reaction scheme coupled with CFD calculations to consider how mixing in a multi-inlet vortex mixer (MIVM) is influenced by inlet configuration and to compare it with mixing in a double inlet vortex mixer (DIVM).[37] Interestingly, they found no significant difference between the MIVM and DIVM, the MIVM was perhaps minimally better – this improvement was attributed to smaller length scales of segregation but this is unlikely to justify the additional complexity of manufacture.

The Bourne IV scheme was modified by concentration in Liu's work by keeping molar flowrates constant but changing the concentrations to allow different volumetric flow ratios which then allowed different configurations of inlet flows in the MIVM. Interestingly, it was concluded that these effects were minimal and it was largely insensitive to inlet configuration. However, this fails to take account of the effects concentration may have on fractional conversion. Concentrating reactants would influence local kinetics and therefore the fractional conversion is not a fair way to compare and it could be that in the context of mixing time there could be a difference.

Lindenberg *et al* used the Bourne IV reaction scheme and computational fluid dynamics (CFD) to compare mixing in a wide angled Y mixer and double inlet vortex mixer.[38] They also used a method similar to Liu *et al* to allow volumetric flow ratios to be investigated by using a concentration modification.

The fractional conversion as a function of average inlet Reynolds number in the vortex mixer was found to be very similar regardless of the flow ratio, but this does not account for any possible relationship between fractional conversion and mixing time which could be affected by local concentration. CFD results showed that

the slow reaction was confined to the acid zone which decreased as the acid was concentrated but this was largely offset by increasing reaction rate for the range of flowrates considered. When these effects are compensated for there was still little to distinguish the mixing time of the 1:1, 2:1 and 5:1 flow ratio systems. The effect of flow ratio on the performance of the Y mixer was not considered but it was concluded that the flow ratio did not strongly influence mixing in the vortex mixer – this was controlled by the average inlet velocity.

The vortex mixer was compared with the Y mixer and it was found that as a function of average inlet velocity the vortex mixer performed better than the Y mixer but as a function of pressure drop there was little difference at low pressure drop before the vortex mixer outperformed the Y mixer at high pressure drop. It is difficult to know what a fair comparison is geometrically, the inlet diameters of the mixers are the same but the vortex mixer has a large mixing chamber resulting in a greater mixer volume. It would be interesting to know if as a function of total energy dissipation rate there was still a discrepancy between the mixers. This volume difference between mixers also means that in this work the vortex mixer with larger residence times and smaller mixing times often accomplished mixing within the mixer but the Y-mixer required the outlet to complete mixing.

Lindenberg *et al* followed this work with an accompanying paper exploring the influence of viscosity on mixing in a vortex and Y-mixer.[39] The viscosity was modified using a polymer additive (hydroxypropyl methylcellulose) in the basic stream in a small weight fraction (less than 2%) which modified the viscosity ratio between the two inlets by up to a factor of 12. The mixers were observed to go from a region where viscosity has an effect on mixing time at low flowrates to region in which it had little. From a region with a micromixing dependence to one of mesomixing. The Y-mixer had an unusual relationship with viscosity which was attributed to viscosity causing asymmetrical mixing which resulted in improved radial exchange of fluid elements. The vortex mixer behaved in the expected way, with increased viscosity making mixing more difficult in the viscosity sensitive range. It is unclear to what extent this is an effect of high viscosity ratio or just high viscosity. A scaling relationship was also proposed which followed a similar procedure to the work undertaken by Johnson and Prud'homme for the CIJ mixer but

with the constant determined from the CFD calculations, this provided acceptable agreement with the experimental data.

Gillian and Kirwan used the Bourne IV reaction scheme to characterise the mixing performance of Y,T and CIJ mixers at a flow ratio of 1:1 over a range of characteristic reaction times (by varying the reactant concentrations) and viscosity ratios (by the addition polyethylene glycol).[40] The engulfment model of micromixing as developed by Baldgya[20] was utilised in order to provide a theoretical relationship between the fractional conversion and micromixing time and although no concentration modifications were made to investigate the effect of volume ratio on mixing this method could be adapted to compensate for concentration effects. They used this relationship to convert the fractional conversion to mixing time and then attempted to apply a Corrsin style mixing relationship to correlate the data, which provided a reasonable fit but as did a pure micromixing or pure mesomixing style model so it was concluded that both mechanisms had a role to play.

They concluded that the CIJ, Y and T mixers of similar size had comparable mixing performance at a flow ratio of 1:1 and equal inlet viscosities. They also concluded that there was no significant viscosity influence in a CIJ mixer, especially at high flowrates and that the Y mixer was largely unaffected also.

Wang *et al* used a similar method using Polyethylene glycol (PEG) as the viscosity modifying agent to characterise how the inlet viscosity ratio influences mixing in a confined impinging jet mixer.[41], [42] They reported difficulty in achieving mixing when the inlet viscosity ratio was around 3 but again it is difficult to distinguish between the influence of high viscosity ratio and just high viscosity. This was attributed to difficulty in droplet break up.

The interfacial tension that exists between two immiscible fluids is a well-known phenomenon which results because of a difference in intermolecular interactions.[43]

In the bulk of a liquid each molecule is pulled in all directions equally, resulting in a net force of zero. At the surface the molecules are pulled inwards as they are more attracted to the bulk molecules than those of the neighbouring medium. Therefore all the surface molecules are subject to an inward force (balanced

by incompressibility) resulting in a driving force to minimise the surface area (Figure 2.8). Another way of imagining it is taking the surface molecules to be in a higher energy state than the bulk molecules, therefore for the liquid to minimise its number of boundary molecules and therefore its surface area.



Figure 2.8. Interfacial tension

This surface minimisation results in a surface assuming the smoothest shape that it can. Any increase in surface area requires work and consequently surfaces will resist (to a certain extent) the creation of new interfaces.

The mixing of miscible fluids is similar in initial moments of fluid contact to the mixing of immiscible fluids.[44–47] Breaking the fluid into small droplets is an important process to achieve rapid mixing.

Considering immiscible dispersions under laminar conditions, Taylor “experienced difficulty in bursting drops of a viscous fluid by a disruptive flow field in a surrounding fluid of considering less viscosity”. [48] Estimates of the dynamic viscosity ratio where this effect occurs vary from around 2.5 (dispersed/continuous) to 3.[41], [49] The scale of segregation, known as striation thickness, has been shown to be strongly influenced by the viscosity ratio when subjected to laminar shear.[50–52]. Such results were observed for laminar shear flow and no such limit has been observed for extensional flow.

Despite the solvents being entirely miscible it is possible that a microscale segregation exists because of the transient interfacial tension between phases.[53] In this instance, the molecules are well dispersed in one another instead of being molecularly mixed. Micromixing occurs over a longer length scale than it otherwise would which results in longer mixing times. This was termed a “quasi-emulsion” by Wang *et al.*

3 Antisolvent Crystallisation - Theory and Introduction

3.1 Crystallisation theory

Crystallisation is commonly used in the pharmaceutical and chemical industries for particle formation, purification or separation. Product requirements typically demand a product of specified crystal size distribution, polymorphism and morphology etc. Due to the wide variety and complexity of crystallisation processes there is no “off the shelf” solution for a process engineer to use in the design of a crystalliser.

Factors such as local and mean supersaturation as well as residence time have to be controlled and balanced with nucleation and growth kinetics in addition to secondary particle formation processes such as aggregation and breakage to get the required final particle size distribution as well as control other important parameters. [8], [9], [54]

3.1.1 Driving force for phase change

The driving force for crystallisation is supersaturation. Technically, this is the ratio of activity of solute in the metastable solution to the activity of the solute at equilibrium. In practice this is usually expressed as the ratio of solute concentration and the equilibrium concentration of the solute. Implicit in this is the assumption that activity coefficients of the supersaturated and equilibrium states are equal.

$$S_{sat} = \frac{C}{C_{eq}} \quad (3.1)$$

Supersaturation can be induced by a number of methods. Figure 3.1 shows a variety of ways it can be induced on a concentration-temperature solubility diagram. Evaporation, for example, increases the solute concentration beyond the saturation line and into the metastable zone which is thermodynamically less stable but due to low supersaturation has a low nucleation rate and eventually with more evaporation the system moves into the unstable labile region where spontaneous precipitation occurs. Cooling the solution again moves the solution into the supersaturated region towards the metastable limit. The addition of an “antisolvent” in which the solute is sparingly soluble (antisolvent crystallisation) reduces the solubility of the final

solution again inducing supersaturation. Antisolvent crystallisation is most useful when the solute is highly soluble in the solution, even at low temperatures, or exhibits thermal instability which renders cooling crystallisation and evaporative crystallisation unfeasible.[55] Depending on the process economics the antisolvent can be recovered and this may have economic advantages over the energy costs of evaporative crystallisation. Its main disadvantage is a strong sensitivity to the initial moments of mixing.[56]

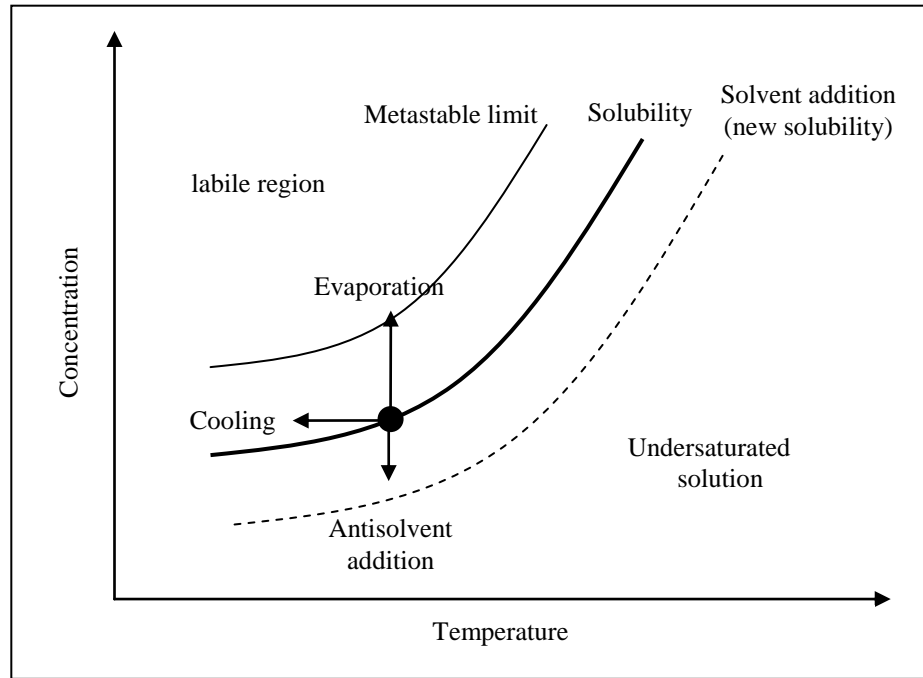


Figure 3.1. Typical solubility diagram

Supersaturation does not begin the crystallisation process directly. Instead, nuclei must form from a solid phase from the solute molecules. After formation these nuclei undergo transfer processes such as growth and aggregation. Supersaturation is reduced by nucleation or particle growth. The driving force for nucleation or growth can be expressed in terms of the chemical potential difference between the supersaturated state and the saturated state.[9]

$$\Delta\mu_p = \mu_{peq} - \mu_p \quad (3.2)$$

$$\mu_p = \mu_p^o + k_B T \ln C \quad (3.3)$$

$$\Delta\mu_p = -k_B T \ln(C / C_{eq}) \quad (3.4)$$

$$\Delta\mu_p = -k_B T \ln(S_{Sat}) \quad (3.5)$$

Where $^\circ$ denotes the reference state per molecule, μ_{eq} the equilibrium value, μ_p is the chemical potential, T is the absolute temperature, k_B is the Boltzmann constant and S is the supersaturation that is defined in equation (3.1).

3.1.2 Nucleation and growth

Nucleation is divided into two categories - primary and secondary nucleation. Primary nucleation itself is further divided into two categories - homogeneous nucleation and heterogeneous nucleation. Homogeneous nucleation occurs when nuclei form spontaneously from the solution and heterogeneous nucleation occurs when foreign substances act as a surface which reduces the energy barrier of a phase transition and consequently increases the rate of nucleation. In practice true homogeneous nucleation is rare at low supersaturation due to the high energy costs associated with the spontaneous creation of new surfaces. Secondary nucleation occurs due to breakage caused by fluid shear, crystal collision, wall collisions and impeller collisions.

Consider the simplified case of spherical nucleus of radius r nucleating in a homogeneous fashion from solution. Since the solution is supersaturated, the chemical potential change is negative, i.e. favouring phase change. This energy gain (ΔG_v) is reduced by the energy required to build a new surface (ΔG_s). The free energy change per molecule required to create or grow a particle is therefore:

$$\Delta G = \Delta G_v + \Delta G_s \quad (3.6)$$

$$\Delta G = -\left(\frac{4\pi r^3}{3m_v}\right)k_B T \ln(S_{sat}) + 4\pi r^2 \gamma \quad (3.7)$$

Where m_v is the molecular volume and γ is the interfacial free energy. At low supersaturation the rate of nucleation is low. Substituting in equation (3.5) gives:

$$\Delta G = \left(\frac{4\pi r^3}{3m_v}\right)\Delta\mu_p + 4\pi r^2 \gamma \quad (3.8)$$

As a function of the particle radius this function goes through a maximum. The radius corresponding to this maximum can be determined by taking the derivative of the free energy and setting it to zero.

$$r_c = \frac{2\gamma m_v}{\Delta\mu_p} \quad (3.9)$$

This radius is known as the critical radius and it represents the smallest particle size which is energetically stable. Particles smaller than this size are likely to dissolve due to the high surface energy. By substituting equation (3.9) into equation (3.7) the size of the energy barrier at the critical radius can be determined:

$$\Delta G_n = \frac{16\pi\gamma^3 m_v^2}{3\Delta\mu_p^2} \quad (3.10)$$

Common with all kinetic limited process, such as in the Arrhenius equation, the rate of a process is proportional to exponential of the negative of the height of the energy barrier of that process divided by $k_B T$:

$$J = A_p \exp\left(-\frac{\Delta G_n}{k_B T}\right) \quad (3.11)$$

Substituting equation (3.10) and equation (3.5) into equation (3.11) gives:

$$J = A_p \exp\left(-\frac{16\pi\gamma^3 m_v^2}{3k_b^3 T^3 [\ln(S_{Sat})]^2}\right) \quad (3.12)$$

Equation (3.12) shows how strongly the nucleation rate is dependent on the interfacial tension and supersaturation. Considering the nucleation rate as a function of just the supersaturation results in the following relationship (Figure 3.2):

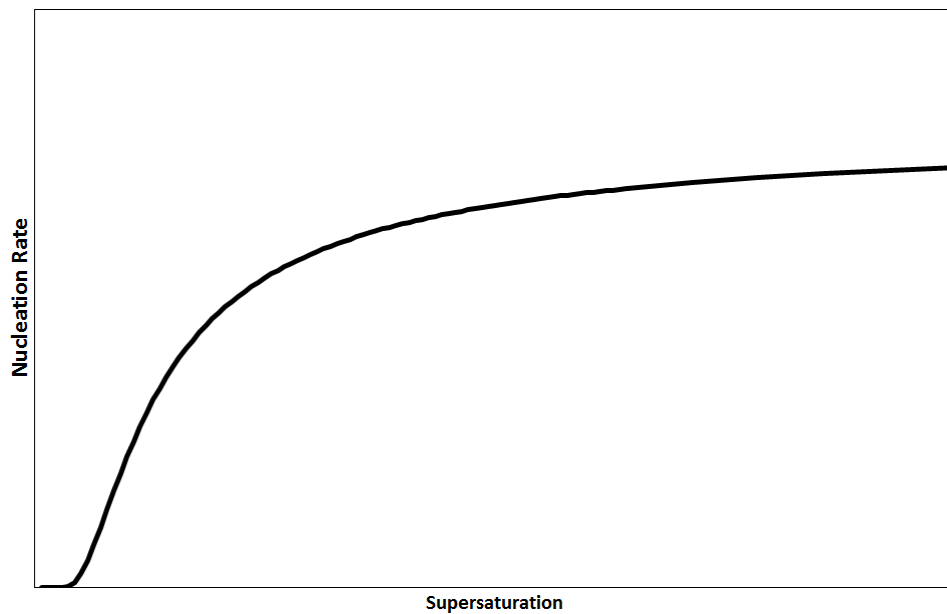


Figure 3.2. Influence of supersaturation on the nucleation rate

The model is compromised by a number of simplifications and assumptions, especially that the composition and structure of the nuclei is the same as the bulk crystalline phase. Nucleation is difficult to study since, due to the high surface energy, nuclei are often unstable and grow soon after formation. As the interfacial tension decreases and the supersaturation increases the critical particle size approaches the size of an individual molecule. This makes the distinction between bulk and surface energies less clear and the model breaks down.[57] As the critical particle size approaches the molecular scale, the system behaviour begins to resemble a spinodal decomposition.[58]

If the energy barrier associated with a phase transition to less ordered phase is less than that of the most stable then the crystallisation may proceed through a series of transitions. Oswald's Rule of Stages (Figure 3.3) predicts that an unstable system will not transform to its most stable state in a single step. Rather, crystallisation proceeds via the compositional and structural rearrangement of various amorphous precursors, crystalline intermediates and metastable crystals.

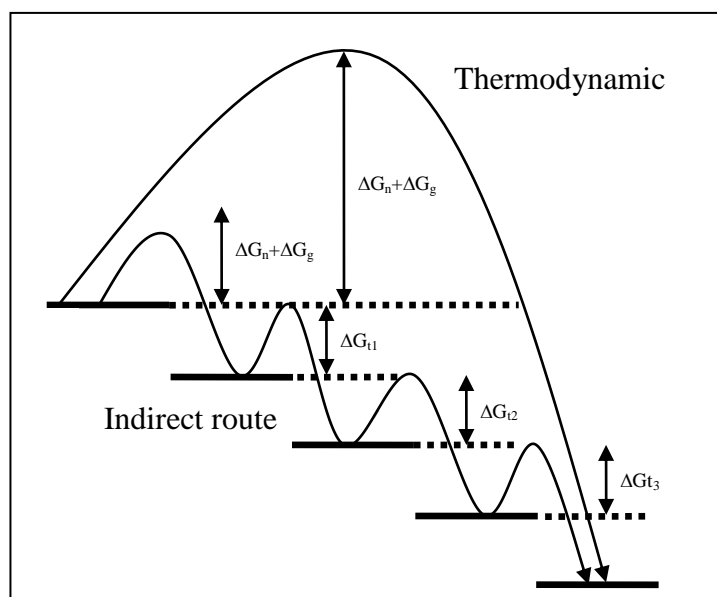


Figure 3.3. Crystallisation pathways

Ostwald's Rule of Stages (n – nucleation, g- growth and t-transition)[59]

Kinetics plays a critical role in the process, with different routes having different rates of nucleation and growth and even though some routes are thermodynamically more stable than others those with the fastest kinetics dominate as often the systems are non-equilibrium.[9]

Stable nuclei grow soon after formation. There are various proposed mechanisms for crystal growth but they can be broadly grouped into three groups – surface energy theories, adsorption layer theories and diffusion reaction theories.

Surface energy theories define the equilibrium morphology as the minimum of the sum of the products of the surface area of the exposed faces and the relative surface energies. This is known as Wulff's rule and means that crystal faces should grow in proportion to their respective surface energies, meaning that the faces with the highest surface energy grow fastest and vanish from the final morphology.[60]

Adsorption layer theories were first suggested by Volmer[61] and are based on the concept of an adsorbed layer of solute atoms on the surface of the crystal. When the solute encounters the crystal face they are not immediately integrated into the lattice, instead they lose one degree of freedom and can migrate over the surface of the crystal (surface diffusion).[9]

Diffusion-reaction theory (Figure 3.4) considers crystal growth to be a two-step process. Firstly, there is the diffusion of the solute molecule from the bulk solution to the supersaturated interface:

$$\frac{dm}{dt} = k_d A(C - C_i) \quad (3.13)$$

Where k_d is the mass transfer coefficient of the diffusion process, A is the surface area and C_i is the interfacial concentration. This is followed by a first order 'reaction' as the solute molecules integrate themselves into the lattice from the supersaturated film through the adsorption layer:

$$\frac{dm}{dt} = k_t A(C_i - C^*) \quad (3.14)$$

Where k_t is the mass transfer coefficient for surface integration and C^* is equilibrium concentration. Obviously, equations (3.13) and equation (3.14) are difficult to implement practically due to the difficulty in measuring the interfacial concentration C_i . It is much more convenient to consider the overall process.

$$\frac{dm}{dt} = K_{omt} A(C - C^*)^g \quad (3.15)$$

Where K_{omt} represents the overall mass transfer coefficient and g is the order of the crystal growth process.

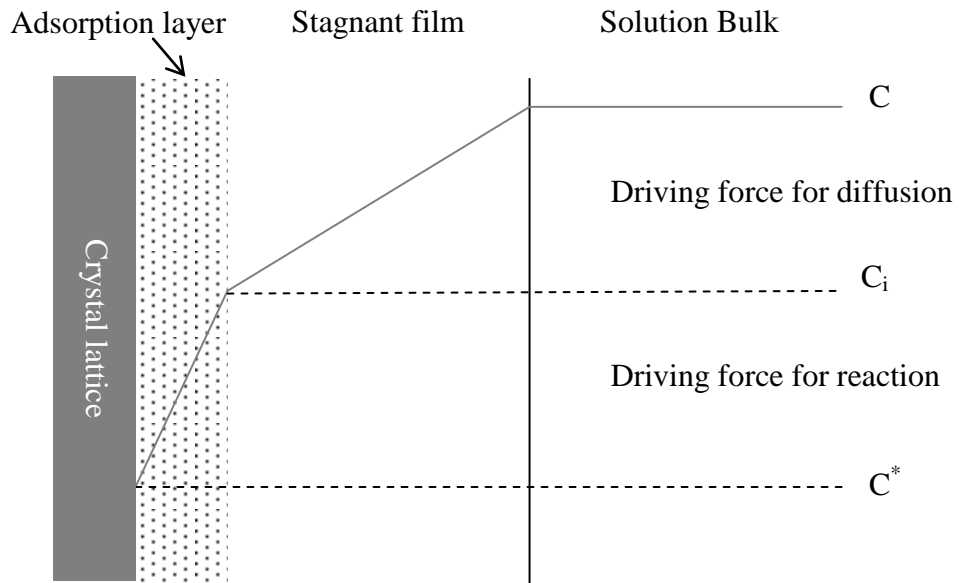


Figure 3.4. Driving forces behind the simple diffusion-reaction model of growth[9]

3.1.3 Secondary transfer processes

The particle number is an important parameter as it can control the final crystal size distribution. For a constant reduction in supersaturation, more nuclei will result in smaller particles and less nuclei in larger particles. Secondary transfer processes such as aggregation and Ostwald ripening act to reduce the particle number, which is undesirable if small particles are required. Secondary transfer processes are slower processes and therefore occur after particle formation.[35]

The rate of aggregation depends upon the collision frequency of particles and their collision efficiency. Collision mechanisms include Brownian motion (perikinetic aggregation) and fluid motions (orthokinetic aggregation) with perikinetic aggregation only active on the colloidal scale and orthokinetic aggregation dominant in vigorously agitated fluids. Not all collisions lead to an aggregate being formed, an efficiency is introduced to define the probability that a particle collision will result in particle aggregation. This efficiency takes account of viscous interactions and attractive and repulsive forces. [9], [57]

The zeta potential, which is the electric potential close the particle surface, can be measured and allows the repulsive forces to be estimated. The zeta potential acts to resist aggregation. A typical system is colloidally stable around a zeta potential of 25 mV (positive or negative), the larger the potential the more stable.

Ostwald ripening occurs when molecules in smaller particles join larger particles due to the lower surface to volume ratio of larger particles. This is because molecules on the surface of a particle are energetically less favourable than those in the bulk. Therefore as a system tries to minimize its overall energy (equilibrate), a particle on the edge of a smaller surface will tend diffuse through solution and add to the surface of the larger particle. Therefore larger particles have a tendency to grow larger at the expense of smaller particles which disappear.[62]

3.2 Mixing sensitivity in antisolvent crystallisation

Supersaturation can vary locally within a crystalliser. In antisolvent crystallisation this can be because of spatial variations in mixing performance, in cooling crystallisation it can be because of thermal gradients or temperature segregation.

Classical nucleation theory assumes a homogeneous mixture with a uniform distribution of supersaturation. This assumption is only valid if the characteristic timescale of mixing is less than the characteristic timescale of the initial crystallisation. Often the assumption of mixing being fast with respect to crystallisation is based on macroscale observations where timescales are large with respect to mixing. However, microscale crystallisation events (such as nucleation or precursor formation) frequently have short timescales and therefore these events and consequently subsequent processes become sensitive to the initial mixing.

In antisolvent crystallisation peaks in supersaturation occur in regions with high antisolvent content (low solubility). This occurs at the boundary layer between the solvent and antisolvent. Therefore, intuitively one would imagine that a mixing process that maximises the interfacial area between solvent and antisolvent would maximise local supersaturation and therefore nucleation.

Lince *et al* studied antisolvent precipitation of poly- ϵ -caprolactone (PCL) in a CIJ mixer using acetone as a solvent and water as an antisolvent.[63] They reported a decrease in particle size as a function of flowrate until a breakpoint was reached and further improvement in mixing resulted in little decrease in particle size. This was attributed to the timescale of mixing being less than the timescale of particle formation (i.e. Damköhler number less than 1). Johnson and Prud'homme studied the

precipitation of polybutylacrylate-*b*-polyacrylic acid in methanol water antisolvent again reported a breakpoint which attributed to a Damköhler number of 1.[64]

Marchisio *et al* studied the mixing influenced reaction precipitation of barium sulphate from solutions of barium chloride and sodium sulphate in a CIJ mixer.[35] These results were analysed in conjunction with CFD in order to establish the influence of characteristic mixing time on particle size. Again improved mixing reduced particle size until after some point no improvement was observed.

Schwarzer and Peukert also studied the influence of mixing on barium sulphate crystallisation this time in a T-mixer.[65] Again the particle size distribution was found to be strongly mixing sensitive, with narrower particle size distributions and particles of smaller size observed at high flowrates. Agglomeration was controlled by addition of adsorbing ions of barium which influenced the surface properties. The combination of controlled mixing and inhibited agglomeration (either by dilution or an additive) was necessary to form nanoparticles.

These results indicate that the initial mixing of fluids is one of the fundamental parameters in controlling particle nucleation and it is critical to ensure uniformity of mixing if uniformity is expected of particle product. The difficulty in scaling of mixing, between say a laboratory scale pilot and large scale production is an important problem to address for the processing industries. Furthermore, the thermodynamic theory outlined above assumes complete mixing before precipitation which is obviously wrong in many instances and therefore the thermodynamic explanation for nucleation and growth has to be considered as a theoretical model with obvious limitations that accounts for certain but not all behaviours. If one were to implement the method developed by Neilsen[66] and outlined in section 3.1.2 to estimate nucleation rates then one may obtain estimates which may differ widely to the observed rates due to mixing effects.[67]

Developing on these ideas leads to Figure 3.5. Considering perfect mixing (which would only occur in the slowest precipitations), where mixing is much faster than the fastest crystallisation event, then a homogeneous distribution of local supersaturation would occur with a value equal to the bulk supersaturation which would result in a homogeneous nucleation rate and consequently a narrow particle size distribution. This is implicitly assumed in the classical nucleation theory

outlined above. Now consider a real system, one where mixing is good (not perfect) and one where mixing is poor. Good mixing results in a sharp spike in supersaturation which results in a high nucleation rate which rapidly depletes the supersaturation. The result is a large number of small particles. Poor mixing on the other hand results in a wide distribution of supersaturation and results in the formation of a small number of large particles.

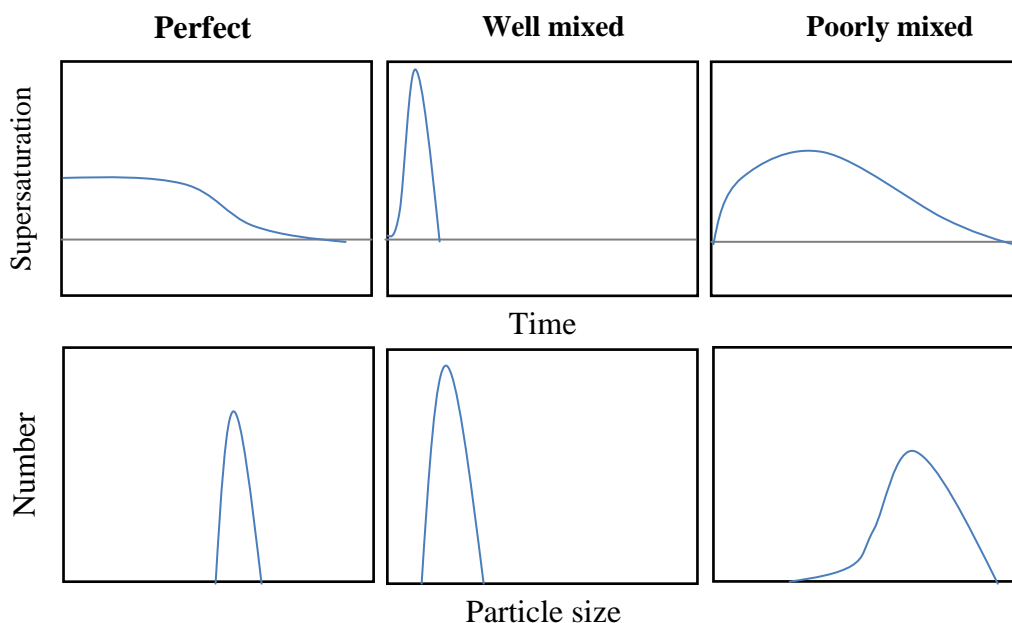


Figure 3.5. Influence of mixing on local supersaturation and PSD

Influence of mixing on supersaturation and particle size distribution for perfect mixing (where mixing is instantaneous with respect to crystallisation), for well mixed conditions where large peaks in supersaturation can be expected at the solvent-antisolvent interface and for poorly mixed conditions with a broader supersaturation and particle size distribution.

Wang *et al* studied the antisolvent precipitation of salicylic acid, methylparaben, butylparaben and glycine and reported that when a viscous solvent was added slowly to a non-viscous antisolvent in an agitated vessel or the fluids were mixed in equal flow ratios in a CIJ mixer an unusual phenomenon termed “quasi emulsion precipitation” occurred.[41], [42] Due to the interfacial tension between fluids in the initial moments of mixing when a viscous fluid was surrounded by a non-viscous fluid there a substantial difficulty in achieving rapid homogenised mixing was reported. In such circumstances rapid precipitation occurred at the interface, which further stabilised the interface and resulted in the formation of a metastable phase which exhibited substantial stability.

This indicates that mixing cannot only influence local supersaturation and local nucleation but it can also directly influence the crystallisation mechanism in certain circumstances opening up the possibility of non-classical particle formations routes due to intricacies of the fluid mechanics of mixing.

3.3 Formation of protein coated microcrystals (PCMCs)

Protein coated microcrystals (PCMCs) are prepared in a rapid co-precipitation of a therapeutic biomolecule with an excipient (Figure 3.6). The basic process involves the rapid mixing of an aqueous solution of the excipient (something like an amino acid) along with a buffer solution and the biomolecule (vaccine etc.) with an organic antisolvent resulting in a rapid precipitation which produces a product with a crystalline excipient core coated in the biomolecule.[68–70]

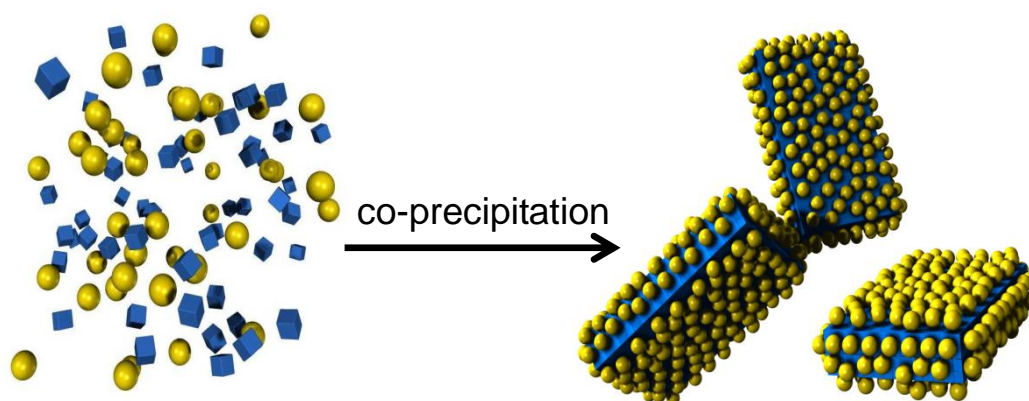


Figure 3.6. Formation of protein coated microcrystals (PCMCs)

Co-precipitation of excipient (blue) and the biomolecule (yellow).From [71]

The precipitation is thought to be more like a spinodal decomposition than classical nucleation and growth due to the high antisolvent ratio used (high supersaturation). As the precipitation is so rapid the biomolecule is protected from denaturing resulting in a stable solid product which has advantages over traditional liquid phase preparations like enhanced “shelf-life” and no requirement for refrigeration.[70] Further details can be found in Chapter 4.3.

3.4 Objectives of Investigation

The primary objective of investigation is to understand how the initial stages of mixing influence the nucleation and generation of crystalline material. The work will comprise two main components:

1. Understanding mixing processes
2. Using this understanding in a crystallisation environment

The first objective is to gain a qualitative and quantitative understanding of mixing processes. As antisolvent crystallisation typically occurs industrially with different solvents and high antisolvent ratios it is important that the experiments cover a range of conditions which include varying mixing ratios and physical properties. This will enable a qualitative picture of the mixing capabilities of various mixers under different condition to be built up. A quantitative understanding will require implementation of some modelling to compliment the qualitative understanding.

With this increased understanding of mixing processes and a quantitative understanding of how various mixers perform under different conditions, an investigation on how mixing influences the initial stages of crystallisation will be performed. The ultimate objective is gain some understanding of how the processing of Protein Coated Microcrystals (PCMCs) can be controlled, optimised and scaled by utilising mixing control.

4 Experimental Techniques and Methods

4.1 *Mixing characterisation*

The Bourne IV reaction scheme was utilised to carry out a comprehensive survey of various mixers including a confined impinging jet (CIJ) mixer, a vortex mixer and more conventional T and X mixers of different sizes ($\frac{1}{8}$ " and $\frac{1}{4}$ ") in a variety of different mixing conditions. This encompasses how flowrate, flow ratio (expressed as alkali stream to acid stream) and viscosity interact to influence the fractional conversion of the dimethoxypropane.

4.1.1 Objectives

The main objective of this work was to develop a method to move the original Bourne IV reaction scheme away from mixing fluids with the same physical properties in a 1:1 flow ratio towards mixing more typically encountered in real systems. Of particular interest is mixing in antisolvent crystallisation, which often involves mixing an organic stream with an aqueous stream at a volume ratio far from 1:1 and with an inlet viscosity ratio of around 2:1. The goal was then to use these modified schemes to characterise a range of mixers operating under a range of conditions.

Johnson *et al* concluded that in the original scheme the fractional conversion was controlled by the Damköhler number and that the fractional conversion was proportional to the mixing time.[15], [23] This is useful as it allows a lot of mixing analysis to be done with just the raw fractional conversion. It would be good to obtain some understanding of the limits to this relationship to help establish when it is sensible to use the fractional conversion in its raw unprocessed form. Is it linear across the whole range of fractional conversion (0 to 1) and what happens when the volume ratio is changed?

In order to accomplish this, a model will have to be developed and it will have to be capable of dealing with concentration and volume effects as well as standardising mixing to allow a fair comparison between flow ratios. This should be relatively straightforward as the kinetics are well defined, the hydrolysis reaction is confined to acid zone[38] and Baldyga *et al* have already determined that thermal

segregation plays no part.[6] The Interaction by Exchange with the Mean (IEM) and the Engulfment model are two methods often used for such a job. These are discussed in Chapters 5 and 6. Such a model should also be capable of predicting, with acceptable accuracy, the absolute mixing time associated with a fractional conversion.

The total energy dissipation rate can be calculated from experimentally accessible data.[36] If, as has been assumed[40], [72], this total energy dissipation is proportional to the energy dissipation rate in the bulk of the fluid then this total energy dissipation rate should be an effective means to correlate mixing. This will be tested for a range of mixers, flow ratios and viscosity ratios.

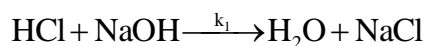
Wang *et al* reported a difficulty in mixing when the viscosity ratio was around 3, this phenomenon has been observed to occur when the viscous component occurs as the minor volume fraction.[41] It would be interesting to try to decouple the influence of high viscosity from high inlet viscosity ratio and to vary the volume ratio of the viscous component to see what influence this has.

Lindenberg *et al* concluded that a vortex mixer was unaffected by a change in flow ratio and that mixing was controlled by total flowrate.[38] It would be interesting to investigate if this is true at flow ratios beyond the maximum tested in that work (5:1) and if this is unusual for continuous mixers as only the vortex mixer was tested. Such a result would obviously be of interest in antisolvent crystallisation which often requires extreme flow ratios.

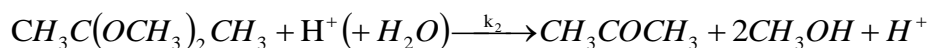
4.1.2 Bourne IV Reaction Scheme

A competitive reaction scheme which is fast enough for continuous reactors is a strong acid/base neutralisation competing for acid with the acid catalysed hydrolysis of dimethoxypropane (DMP) developed by Baldyga and Bourne, the so called Bourne IV reaction scheme.[6]

Rapid neutralisation of a strong base and strong acid:



Acid catalysed hydrolysis of dimethoxypropane:



The first reaction has a rate constant of the order of $k_1=1.4 \times 10^8 \text{ m}^3 \text{ mol}^{-1} \text{ s}^{-1}$ (i.e. instantaneous).[6] The second, slower reaction, can be simplified to a second order reaction due to the ubiquity of water in the system with a rate constant ($\text{m}^3 \text{ mol}^{-1} \text{ s}^{-1}$) given as a function of temperature and salt concentration[6]:

$$k_2 = 7.32 \times 10^7 \exp(-5556/T) 10^{(0.05434 - 7.07 \times 10^{-5} c_s)} \quad (4.1)$$

T is the temperature in Kelvin and C_s is the concentration of sodium chloride (mol/m^3), which was added to both reactant streams to ensure a moderate salt concentration always exists as the hydrolysis reaction has been found to accelerate with increasing salt content.[6] Since the fast reaction is many orders of magnitude greater than the slow reaction and the fast reaction can be considered instantaneous with respect to the mixing, the characteristic reaction time, τ_r , can be expressed as the pseudo first order time constant of the slow reaction:

$$\tau_r = \frac{1}{k_2 C_{HClO}} \quad (4.2)$$

Mixing timescales can be related to the fraction of DMP which reacted during mixing:

$$X = 1 - \frac{C_{DMP}}{C_{DMP0}} \quad (4.3)$$

Good mixing results in little segregation and therefore the fast reaction dominates and the fractional conversion of dimethoxypropane is low. Conversely, under poor mixing conditions, the fractional conversion of dimethoxypropane is substantial due to local molar inequality allowing the slow reaction to progress.

DMP (99%, Sigma Aldrich) and NaOH (1M or 2M standard solution diluted, Sigma Aldrich) in stream 1 were mixed with a second stream containing the hydrochloric acid (1M or 2M standard solution diluted, Sigma Aldrich). A molar ratio of 1.05:1:1 for NaOH:HCl:DMP was used to ensure that all H^+ ions were expended in the reaction upon completion of mixing (if H^+ was in excess then slow reaction would be free to progress until completion).

During solution preparation the DMP was not contacted with any material of pH less than 8 to prevent any hydrolysis. In practice this means adding the sodium hydroxide before the DMP. All solutions were prepared by weight and were

dissolved in a solution containing ethanol and water or just water (see Figure 4.1 and Table 4.1). The product distribution was then analysed by gas chromatography.

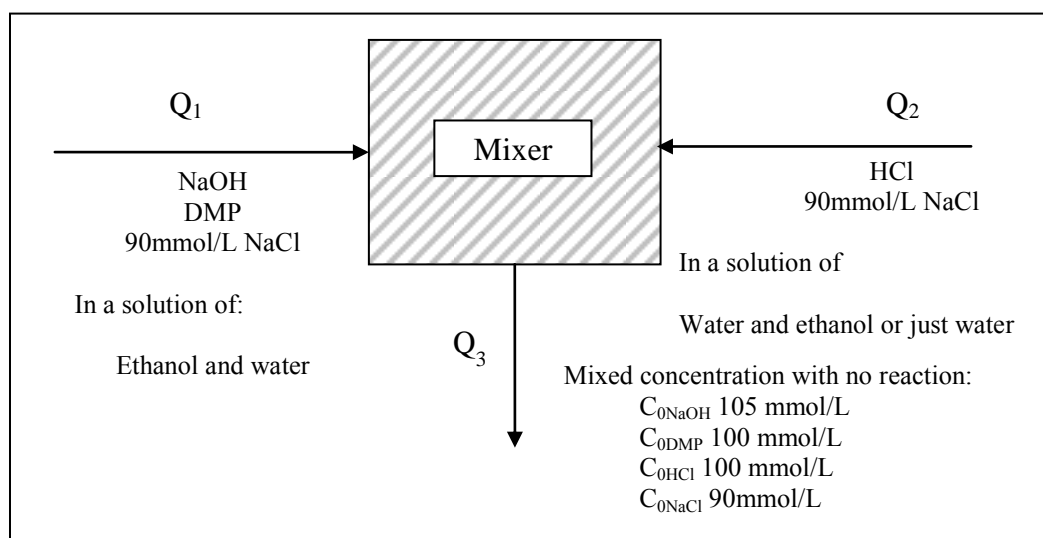


Figure 4.1. Mixing scheme

The NaOH and DMP are in stream one and the HCl in stream two. These two streams are mixed in a specified volumetric flow ratio which determines the concentration of the reactants. The concentrations are picked so that on mixing the concentrations of all reactant species is the same. The reactant species are dilute and the majority of the fluid is solvent. The solvent was originally 25% ethanol and 75% water by weight, with the alcohol added to address DMP solubility concerns. The composition of this carrier solution is modified in order to slightly change solution physical properties (see Table 4.1).

	Scheme	Flow ratio $Q_1:Q_2$	C_{NaOH}	C_{DMP}	C_{HCl}	Q_1 EtOH wt%	Q_2 EtOH wt%	Viscosity ratio ν_1/ν_2
1	Bourne IV Method	1:1	210	200	200	≈25%	≈25%	≈1
2	Modified Composition	1:1	210	200	200	≈50%	0%	≈2.7
3	Modified volume 3:1	3:1	140	$\frac{133.3}{3}$	400	≈25%	≈25%	≈1
4	Modified Volume 10:1	10:1	115.5	110	1100	≈25%	≈25%	≈1
5	Modified Composition & Volume 3:1	3:1	140	$\frac{133.3}{3}$	400	≈50%	0%	≈2.7
6	Modified Composition & Volume 10:1	10:1	115.5	110	1100	≈50%	0%	≈2.7
7	Reverse Composition 1:3	1:3	440	400	133.3	≈25%	≈25%	≈1
8	Reverse Modified Composition 1:3	1:3	440	400	133.3	≈50%	0%	≈0.35

Table 4.1. Reactions schemes

The inlet volumetric flow rates ranged from 50 ml/min to 600 ml/min in the ratio described in Table 4.1. Concentration of reactant species on mixing is the same in all schemes.

In scheme 1 (the original Bourne IV scheme) a mixture of 25% ethanol and 75% deionised water was used as solvent. The initial concentration of acid was 200 mmol/L.

As both reactant streams were blended with a solution containing (neglecting minor components) 75% water and 25% ethanol solution by weight it meant that there was little difference in the physical properties between streams, which is not representative of many real mixing processes. In scheme 2 reactant concentrations were the same as before but the solution was modified to create a difference in physical properties. The composition of stream 2 (acid stream) was pure water and for stream 1 (DMP and base stream) a blend of 50% ethanol and 50% water by weight. This ethanol content corresponds approximately to the maximum viscosity of an ethanol/water mixture and ensures the concentrations of all components upon mixing are identical.

Using the same ethanol content as the Bourne IV scheme (scheme 1), a concentration modification was added to allow different flow ratios to be evaluated (schemes 3 and 4). The starting concentrations were chosen so that molar flowrate of the reactant species in both streams was equal and so that on mixing, but with no reaction, the concentrations of all components would be equal (i.e. 25% wt ethanol with 105 mmol/L of NaOH, 100 mmol/L of DMP, 100 mmol/L of HCl and 90mmol/L NaCl). As the composition and concentrations of all components upon mixing is the same it is assumed that the reaction rate constant would not significantly altered and the only change to the kinetics would be an acceleration effect (due to increased acid concentration) competing with a decreased reaction volume.

Using the same carrier solutions as the modified composition scheme (scheme 2), a concentration modification was added to allow different flowrates to be evaluated (schemes 5 and 6). The starting concentrations were chosen so that molar flowrate of the reactant species in both streams was equal and so that on mixing, but with no reaction, the concentrations of all reactant species would be equal. The concentration of all reactant species is identical on mixing but there is a difference in final ethanol concentration (37.5% at 3:1 or 45.5% at 10:1 versus 25% ethanol by weight in the other runs). It is assumed that any kinetic effects brought on by a

change in ethanol content will be minimal in comparison to concentration, reaction volume and viscosity effects.

To check how sensitive the fractional conversion is to the local concentrations and reaction volumes, a modified volume approach was adopted but by concentrating the alkali stream instead of the acid stream so that the flowrate of the acid stream is three times that of the alkali stream. This is the case in scheme 7.

A modification to the composition of scheme 7 was made so that the concentration of the reactant species was identical but a viscosity difference was added. This has the effect of making the minor component viscous, unlike the other schemes where the major component is more viscous. Details on the physical properties can be found in Appendix 1.

4.1.3 Composition and Volume Modifications

Modified Volume

In the modified volume experiments the concentrations of all species upon mixing is identical in comparison to the original Bourne IV reaction scheme. All that changes is volume ratio and hence starting concentration (prior to mixing) of the acid. Local concentration of reactants can and does influence the kinetics of the slow reaction and to gain a quantifiable understanding of the extent of this two things were attempted. Firstly, an attempt to quantify mixing in terms of a standardised mixing time was made by using a suitable mixing model capable of estimating such effects. Secondly, both 3:1 and 1:3 experiments were conducted, these should behave in opposite ways and should hopefully be corrected by the model as mixing times should not differ for the same energy dissipation rate, physical properties, flow ratio and mixer.

Modified Composition

In the modified volume experiments at 1:1 the concentrations of all species upon mixing is identical in comparison to the original Bourne reaction scheme. All that changes is the solvent composition before mixing, after mixing this is identical to the original scheme. Therefore, this should have little effect of kinetics and should test for the influence of physical properties.

Modified Volume & Composition

In the modified volume experiments at ratios different to 1:1 the concentrations of all reactant species upon mixing is identical in comparison to the original Bourne reaction scheme. However, the concentration of alcohol is different in each of the configurations:

Scheme	Approximate Alcohol Weight% After Mixing
1:1 Bourne IV	25%
1:1 Modified Composition	25%
3:1 Modified Volume	25%
3:1 Modified Composition and Volume	37.5%
10:1 Modified Volume	25%
10:1 Modified Composition and Volume	45.5%
1:3 Modified Volume (Reverse)	25%
1:3 Modified Composition and Volume (Reverse)	12.5%

Table 4.2. Alcohol composition

If alcohol has a role in the slow reaction then the alcohol content could potentially influence the rate constant in a similar manner to how the salt does. No evidence of this was discovered in the literature but it cannot be definitively ruled out as a possible consequence. However, as the alcohol content changes both upwards and downwards for the Bourne IV composition it should be possible gain some inference on the likelihood of this by careful comparison of the experimental results.

The fast reaction should be unaffected. Whilst it is true that the additional ethanol will shift the equilibrium between sodium hydroxide and sodium ethoxide, sodium ethoxide is also strong base and should still react instantaneously with acid.[73], [74]

4.1.4 Mixing setup

Figure 4.2 shows the basic mixing setup. Pulse-free flow was obtained using micropump heads (GB series, suction shoe design gear pumps) magnetically coupled with a pump driver (Ismatec MCP-Z Standard). The pumps were calibrated for the desired flowrate and mixer using a water/ethanol solution prior to each run with ethanol content the same as that of the reaction scheme in question (see Table 4.1).

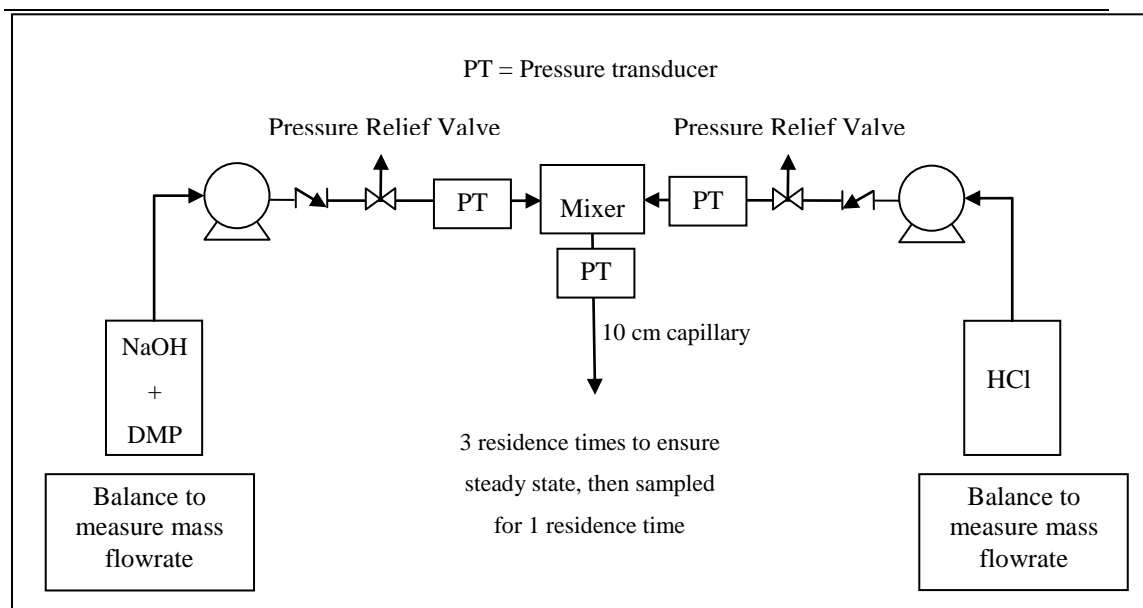


Figure 4.2. Mixing process schematic

The reactant solutions were maintained by water bath at $25^{\circ}\text{C}\pm 1^{\circ}\text{C}$. It is assumed that any heat loss prior to the run was negligible and therefore the inlet reactant temperature was also 25°C . During the reaction a small temperature rise (1 to 2°C) was recorded which was due to a combination of heat of reactions and turbulent energy dissipation. For the purposes of estimating the characteristic reaction time a temperature of 25°C was used.

For the $\frac{1}{4}$ " mixers all fittings were $\frac{1}{4}$ " Swagelok stainless steel with $\frac{1}{4}$ " (nominal external diameter) stainless steel piping throughout. For the smaller mixers ($\frac{1}{8}$ "T, $\frac{1}{8}$ "X, CIJ, vortex), all fittings were $\frac{1}{4}$ " Swagelok with $\frac{1}{4}$ " piping up to and including the inlet pressure transducers before going through a reducing union ($\frac{1}{4}$ " to $\frac{1}{8}$ ") and changing to $\frac{1}{8}$ " piping. After the mixer there is a 10cm stainless steel capillary to enable easy sampling and pressure measurement, the diameter of this capillary is $\frac{1}{4}$ " for the larger mixers and $\frac{1}{8}$ " for the smaller mixtures.

4.1.5 Determination of the total energy dissipation rate

Pressure transducers (PT) were used to estimate the pressure drop across the mixer (Figure 4.3). The pressure drop was then used to estimate the total energy dissipation rate.[36]

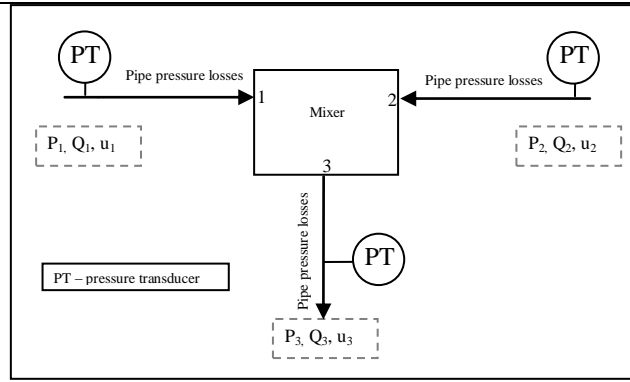


Figure 4.3. Energy balance

The energy dissipated should ideally be estimated from an energy balance (ignoring change in elevation) over the mixer volume (i.e. points 1, 2 and 3 in the figure above):

$$\Delta_{\text{Potential energy}} + \Delta_{\text{Kinetic energy}} + \Delta_{\text{Pressure energy}} = \text{total energy dissipated}$$

The potential energy was around 0.2% of the total energy and was considered negligible. The kinetic energy change was calculated from:

$$\Delta \text{KE} = \frac{m_1 u_1^2}{2} + \frac{m_2 u_2^2}{2} - \frac{m_3 u_3^2}{2} \quad (4.4)$$

And the pressure energy change calculated from:

$$\Delta \text{PE} = Q_3 \Delta P_{\text{Mixer}} \quad (4.5)$$

ΔP_{Mixer} was evaluated as an average of the pressure drop, weighted by the ratio of the volumetric flowrates.

Therefore the average total energy dissipation rate was estimated as:

$$\varepsilon_{\text{Total}} = \frac{Q_3 \Delta P_{\text{Mixer}} + \Delta \text{KE}}{\rho_3 V_{\text{mixer}}} \quad (4.6)$$

In practice, the pressures measured by pressure transducer were P_{T1} , P_{T2} and P_{T3} not P_1 , P_2 and P_3 . The pressure at points 1 and 2 were estimated by calculating the pressure drop using the Darcy–Weisbach equation with the Swamee–Jain approximation for Colebrook–White friction factor equation.[75], [76] The pressure P_{T3} was used without adjustment, but the mixer volume was modified to incorporate the volume between the mixer and transducer.

For the X mixers, which have 4 streams due to the divided flow, a similar approach was used but with an additional inlet stream.

Energy is lost through a variety of processes such as friction at surfaces and boundary layers as well as “mixing processes” which consume energy but do not contribute to reduce the concentration fluctuations, e.g., self-engulfment. It has been assumed that the energy dissipation rate that is utilised for mixing is a fraction of the total energy dissipation rate:

$$\mathcal{E}_{mixing} = c\mathcal{E}_{total} \quad (4.7)$$

This fraction (c) accounts for energy lost to non-mixing processes and would likely be different for each mixer and each flow ratio etc. This fraction has been estimated to be of the order of 1%. [3], [40]

The pressure is measured at 3 points using pressure transducers. These transducers were placed as close to the mixer inlet and outlet as possible but due to certain restrictions that were placed on the system by how the pressure transducers interfaced with the Swagelok system there was a capillary of several centimetres before the mixer inlet and after the mixer outlet (Figure 4.4).

An example of how the total energy dissipation rate was calculated is shown below. This corresponds to the vortex mixer operating at a flow ratio of 1:1 and with 25% ethanol feed streams (i.e. the original Bourne IV method – scheme 1).

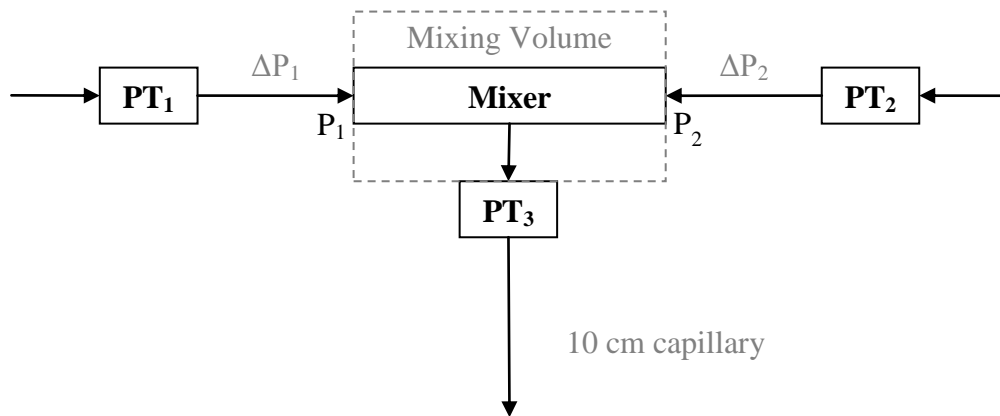


Figure 4.4. Pressure transducer locations

Experimental Techniques and Methods

The measured inlet pressures are shown (PT_1 and PT_2) as are the estimated pressure drops (ΔP_1 and ΔP_2). The pressure drop is around 8% of the total pressure.

Target Inlet Flowrate	PT_1 (mbar)	PT_2 (mbar)	ΔP_1 (mbar)	ΔP_2 (mbar)
50 ml/min	86.15	83.46	7.27	7.05
50 ml/min	87.22	83.66	7.26	6.97
100 ml/min	256.62	250.31	22.06	21.52
100 ml/min	258.25	254.79	22.18	21.88
200 ml/min	903.19	875.66	70.51	68.36
200 ml/min	910.70	887.69	70.23	68.46
400 ml/min	3551.43	3543.01	246.02	245.44
400 ml/min	3708.79	3837.46	245.80	254.33
600 ml/min	7363.15	7268.80	496.25	489.89
600 ml/min	7380.77	7306.87	491.45	486.53

The measured pressure (PT_1 and PT_2) minus the estimated pressure drop in the inlet capillaries (ΔP_1 and ΔP_2) provides an estimate of the pressure at the mixer inlet (P_1 and P_2). The outlet pressure drop (P_3) is used without adjustment but the mixing volume is adjusted to include the outlet capillary between the mixer and transducer. A mixer pressure drop can then be estimated by weighting the pressure drop by the relative volumetric flowrates (at 1:1 this is almost equal depending on how tightly the flowrates were controlled). This mixer pressure drop is then multiplied by the total volumetric flowrate in order to estimate the change in pressure energy over the mixer:

Experimental Techniques and Methods

Target Inlet Flowrate	P ₁ (mbar))	P ₂ (mbar))	P ₃ (mbar))	ΔP _{Mixer} (mbar))	Q ₃ ΔP _{Mixer} (Nm)
50 ml/min	78.88	76.41	32.99	44.38	0.00723
50 ml/min	79.96	76.697	35.61	42.47	0.00686
100 ml/min	234.56	228.79	93.55	137.30	0.04518
100 ml/min	236.08	232.91	96.37	137.25	0.04533
200 ml/min	832.68	807.29	319.81	497.33	0.32889
200 ml/min	840.46	819.23	323.89	503.01	0.33311
400 ml/min	3305.41	3297.57	1267.06	2021.96	2.74698
400 ml/min	3462.99	3583.13	1330.72	2179.75	3.04190
600 ml/min	6866.90	6778.91	2799.92	3997.68	8.08232
600 ml/min	6889.32	6820.34	2817.75	4011.50	8.19961

Utilising the mass flow rates and volumetric flowrates and the internal diameter outlined in Table 4.3 allows the change in kinetic energy over the mixer to be estimated:

Target Inlet Flowrate	V ₁ (m/s)	V ₂ (m/s)	V ₃ (m/s)	ΔKE (Nm)
50 ml/min	0.536	0.519	0.519	6.27E-05
50 ml/min	0.533	0.512	0.514	6.11E-05
100 ml/min	1.078	1.052	1.047	5.16E-04
100 ml/min	1.076	1.061	1.051	5.21E-04
200 ml/min	2.173	2.107	2.105	4.19E-03
200 ml/min	2.170	2.116	2.108	4.21E-03
400 ml/min	4.401	4.391	4.324	3.63E-02
400 ml/min	4.438	4.592	4.442	3.94E-02
600 ml/min	6.584	6.500	6.435	1.20E-01
600 ml/min	6.647	6.581	6.506	1.24E-01

This allows a total energy change (pressure plus kinetic energy as potential energy is negligible) which can be converted to total energy dissipation rate by using the outlet solution density and mixer volume:

Experimental Techniques and Methods

Target Inlet Flowrate	ΔTE (Nm)	Density (kg/m ³)	Volume (m ³)	Total Energy Dissipation Rate (W/kg)
50 ml/min	0.0073	961.5	3.37E-07	22
50 ml/min	0.0069	961.5	3.37E-07	21
100 ml/min	0.0457	961.5	3.37E-07	141
100 ml/min	0.0458	961.5	3.37E-07	141
200 ml/min	0.3331	961.5	3.37E-07	1027
200 ml/min	0.3373	961.5	3.37E-07	1040
400 ml/min	2.7833	961.5	3.37E-07	8580
400 ml/min	3.0813	961.5	3.37E-07	9499
600 ml/min	8.2019	961.5	3.37E-07	25283
600 ml/min	8.3232	961.5	3.37E-07	25657

N.B. The kinetic energy term was so small that it could be safely neglected if desired for a simplified energy dissipation rate just involving the pressure energy.

4.1.6 Mixers and mixing configurations

Various mixers (see Table 4.3) including T-mixers, X-mixers (with a split flow arrangement), a confined impinging jet mixer (CIJ) and a continuous double inlet vortex mixer and were evaluated. More mixer details can be found in Appendix 2.

Impinging jet mixers have the requirement of close to equal inlet momenta and as a result are constrained to roughly equal flowrates. This meant that it was not tested in the flow ratio modified schemes.

To overcome this limitation, a double inlet vortex mixer was made with inlets in a tangential arrangement. This allows the momentum from each stream to contribute independently and it is therefore possible to have one stream of low flowrate and the other of higher[37].

Experimental Techniques and Methods

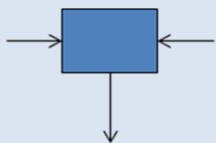
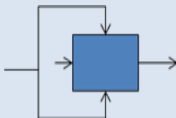

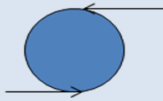
T Mixer	X Mixer	CIJ	Vortex
			
$\frac{1}{4}$ " & $\frac{1}{8}$ " OD Inlets and outlets all same dimensions $\frac{1}{4}$ " ID 4.8 mm $\frac{1}{8}$ " ID 2.3 mm	$\frac{1}{4}$ " & $\frac{1}{8}$ " OD Inlets and outlets all same dimensions $\frac{1}{4}$ " ID 4.8 mm $\frac{1}{8}$ " ID 2.3 mm	Inlet ID 1 mm Chamber 4.76 mm Outlet ID 2 mm	Inlet ID 1.4 mm Chamber 6 mm Outlet ID 2.8 mm
Mixer volume			
$\frac{1}{4}$ " 0.537 ml $\frac{1}{8}$ " 0.096 ml	$\frac{1}{4}$ " 0.537 ml $\frac{1}{8}$ " 0.096 ml	0.447 ml	0.217 ml
System volume (mixer and outlet capillary)			
$\frac{1}{4}$ " 2.999 ml $\frac{1}{8}$ " 0.458 ml	$\frac{1}{4}$ " 2.999 ml $\frac{1}{8}$ " 0.458 ml	0.809 ml	0.579 ml

Table 4.3. Summary of continuous mixers

4.1.7 Run procedure

The system was purged and calibrated for the exact system setup (i.e. mixer, flow ratio, carrier composition). The reactant solution (kept at 25°C in a water bath) was charged and processed for at least three residence times before two samples of approximately one residence was taken. There was no difference between samples which indicated that reaction and hence mixing was complete within the residence time. This was capped and refrigerated to limit any product evaporation or the thermal decomposition of the DMP before analysis could take place. This was a precaution, analysis has shown samples are stable for at least 1 month after mixing has completed and left the sample basic. Analysis was always completed within 24 hours. Each run was repeated and every sample was analysed by GC twice and averaged for each run.

4.1.8 Gas chromatography

Gas chromatography (GC) is a common analytical technique utilised to identify and quantify chemical compounds that can be vaporised without sample degradation. The separation of compounds occurs due to the interaction of the sample with the

stationary phase (column), different interactions have a different strength and consequently the compounds in the sample elute at different retention times based on the strength of these interactions. [77–81]

GC can be broken into three distinct sections; injection port, analytical column and a detector (Figure 4.5). The injection port vaporises the sample and dilutes it with inert carrier gas, the analytical column separates the compounds and the detector, usually a flame ionisation detector (FID) or thermal conductivity detector (TCD), quantifies the amount of analyte as it elutes. A brief overview of these components and specific information regarding calibration and sample calculations are shown below.

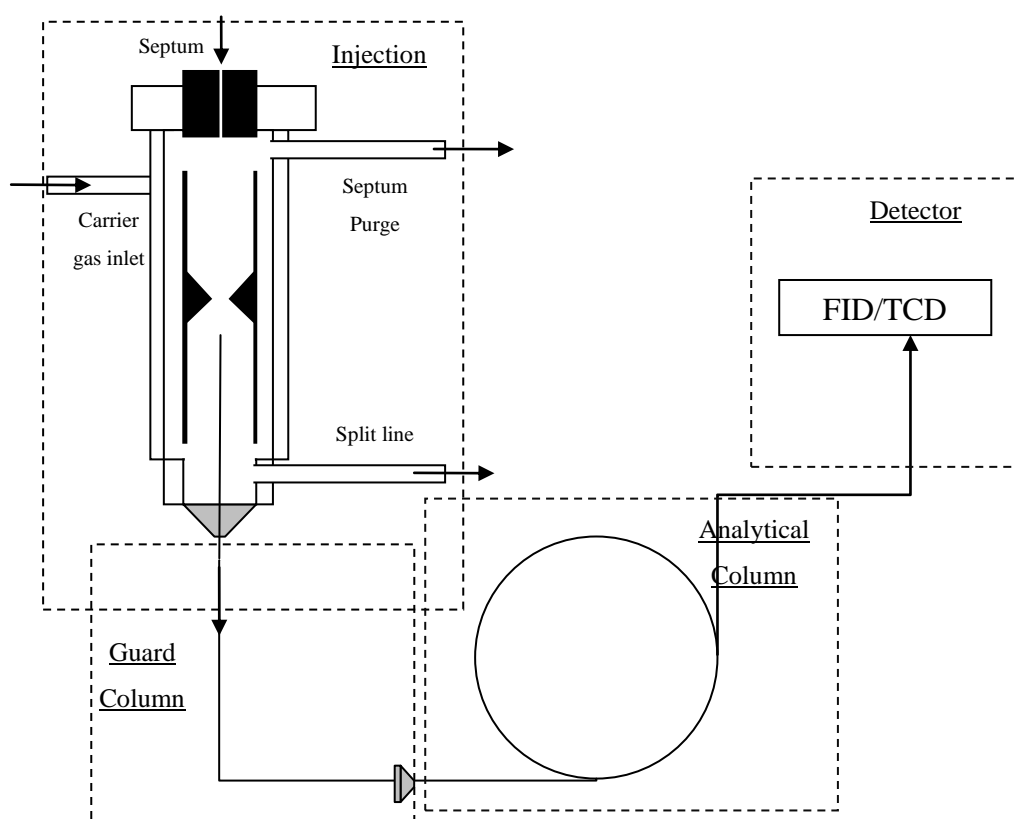


Figure 4.5. Major GC components

The main components include the injection port, guard column, analytical column and detector.

Injection Port, Column and Detector

The sample is injected into the injection port through a septum and exposed to a high temperature, which is selected to vaporise the sample and depends on the volatility of the sample (temperatures of around 200 °C are common). The carrier gas

(or mobile phase – usually helium) then carries either the whole sample (splitless) or a set fraction (split injection) of the sample into the column. Sample concentration determines whether it is best to inject in a split or splitless fashion. The higher the concentration the more it is diluted with a higher split ratio to prevent column overloading.

The analytical column is located in an oven which is maintained at a constant temperature. There are two main types of analytical column, a packed column and a capillary column.

A packed column is a column somewhere between 1-2m in length and about 2-4mm in internal diameter that is packed with a fine inert particulate material and coated in the stationary phase. The nature of the stationary phase controls the intermolecular attractions and different stationary phases are designed for separating different types of compounds.

A capillary column is a long narrow column between 20-80m in length but only microns in diameter. The column is coated in a stationary phase and again different stationary phases are designed for separating different types of compounds. It is also possible to get a guard column, which is a shorter (up to 20m) length of column which is placed before the analytical column and is made up of the inert support material without the active coating. This is designed to protect the analytical column from any low volatile materials that may be difficult to vaporise. The guard column does not contribute to the separation but protects the analytical from non-volatile components. The guard column is cut down in 10cm as part of regular system of general maintenance which involves replacing liners and septa every 50 or so injections.

Column temperature is a balance between short retention times, which occur at high temperature and compromise on separation between compounds (and therefore possibly have poor peak resolution), and long retention times which occur at low temperature and provide good separation of compounds but increase the analytical time.

The most common type of detector for organics is a flame ionisation detector (FID). An FID detector works by burning a hydrogen/air flame which pyrolyses

producing electrons and positively charged ions. These ions are then exposed to a potential difference and the resulting current is then measured as a function of time.

Run Settings

The samples were analysed by gas chromatography using a Shimadzu 2014 gas chromatograph with manual injection. A 10m guard column was used to protect the analytical column (30m RTX1301) from non-volatiles. An injection volume of 2 μ L was used with a split ratio of 100:1 and a column temperature of 60°C. Ethanol was used as an internal standard. Fractional conversion was quantified on the basis of the amount of methanol produced with the amount produced from acetone used for an additional internal consistency check.

Calibration was carried out periodically and standard solutions were injected each day before analysis to ensure the accuracy of the calibration curve. Each sample was measured twice by GC and averaged, so all data points represent the average fractional conversion based on two injections.

Calibration

An example of the construction of a calibration line for ethanol, acetone and methanol is shown below. Calibration took place on a regular basis and a standard solution was always injected before any analytical runs took place to check system performance against the calibration master curve.

Four standard aqueous solutions with approximately constant ethanol concentration (ethanol was used as an internal standard) but with different acetone and methanol concentrations were prepared.

	Concentration g/ml				
	1	2	3	4	5
Ethanol	0.2760	0.2401	0.2451	0.2421	0.2469
Acetone	0.0159	0.0100	0.0082	0.0051	0.0006
Methanol	0.0189	0.0119	0.0098	0.0032	0.0007

Table 4.4. Calibration concentrations

In order to utilise the ethanol concentration (which is a known quantity in the experimental runs, fixed by solution preparation and flow ratios) as an internal

standard one simply creates a dimensionless concentration by dividing the concentration of the components of interest by the ethanol concentration.

	Concentration Ratios				
	1	2	3	4	5
Ace/Eth	0.0576	0.0416	0.0336	0.0210	0.0023
Meth/Eth	0.0686	0.0496	0.0401	0.0133	0.0028

Table 4.5. Calibration Concentration Ratios

The standard solution is then injected into the GC using the same procedure and operating conditions that is used for the analysis of experimental runs. The compounds elute after a retention time and the FID detector provides a chromatogram with peak areas:

	Area				
	1	2	3	4	5
Methanol	708,297	489,191	399,894	88,501	18,508
Ethanol	14,124,556	13,776,419	14,176,328	13,980,180	14,012,069
Acetone	736,824	567,706	469,716	166,790	17,314

Table 4.6. Chromatogram Areas

As before with the concentrations, one simply divides the area by the ethanol area to create an area ratio:

	Area Ratios				
	1	2	3	4	5
Meth/Eth	0.0501	0.0355	0.0282	0.0104	0.00217
Ace/Eth	0.0522	0.0412	0.0331	0.0196	0.00203

Table 4.7. Chromatogram Area Ratios

The concentration and area ratios can now be plotted and a relationship between the quantities can be determined (Figure 4.6):

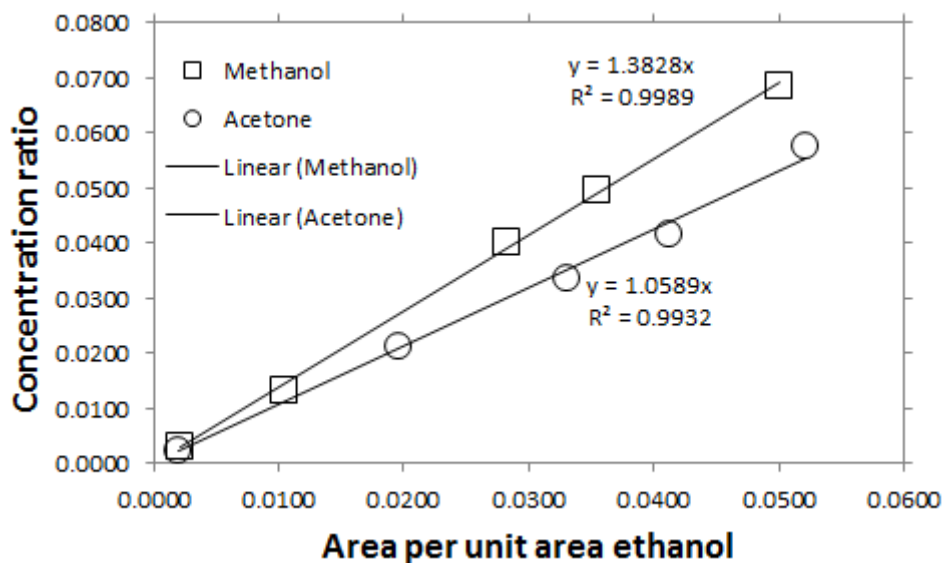


Figure 4.6. Sample calibration for methanol and acetone with ethanol internal standard

Therefore, to quantitatively analyse a sample, one simply injects the solution into the GC and notes the areas of the peaks, dividing the area of the component to be quantified (methanol and acetone) by the internal standard peak area (ethanol).

The dimensionless concentration is then read off the chart or calculated using the calibration relationship and then converted to a real concentration by multiplying by the concentration of the internal standard (ethanol) which is a known quantity.

Sample Calculation

A sample set of results is shown for the vortex mixer operating with a 1:1 volumetric flow ratio mixing two streams with similar physical properties (i.e. the original Bourne IV scheme) and an inlet flowrate of 50ml/min (Figure 4.7).

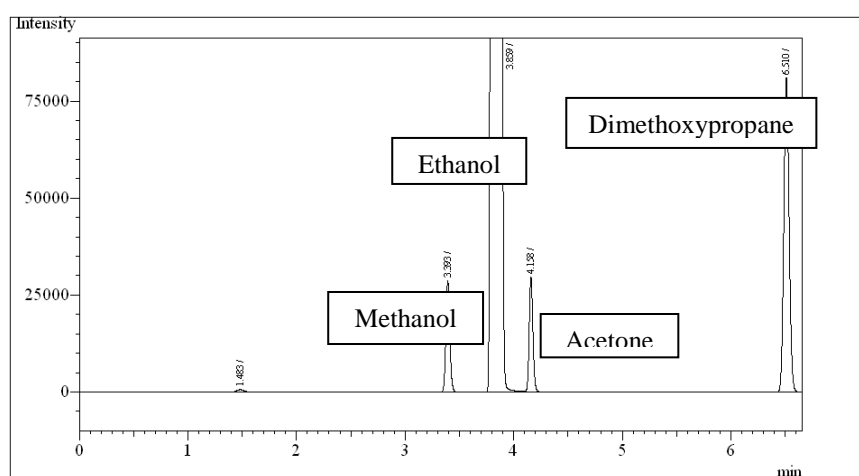


Figure 4.7. Chromatogram

The samples elute in order of their volatility with methanol having the shortest retention time and the DMP the longest. The areas of the peaks are shown below.

Peak#	Ret.Time	Area	Height
1	1.483	2829	618
Methanol 2	3.393	70930	28332
Ethanol 3	3.859	14496070	4355288
Acetone 4	4.158	70385	29193
DMP 5	6.510	273994	80473
Total		14914208	4493904

Table 4.8. Peak data

The methanol and acetone peaks (peaks 2 and 4 respectively) are then converted to an ethanol area ratio by the dividing by the ethanol peak area (peak 3). This area ratio is converted to a dimensionless concentration using the calibration data constructed before. The ethanol concentration is known due to knowing the ethanol concentration of both inlet streams and measuring the inlet flow rates, this concentration is used to convert from a dimensionless concentration to a real concentration of analyte.

	Ethanol Area Ratio	Dimensionless Concentration	Ethanol Concentration g/L	Analyte Concentration g/L
Methanol	0.004893	0.006766	232.7	1.5744
Acetone	0.004855	0.005279	232.7	1.2256

Table 4.9. Sample Calculation of the Fractional Conversion from GC Data

This is converted to a molar concentration. The original concentration of DMP is 100 mmol/L or 0.1mol/L. For every mole of dimethoxypropane that reacts two moles of methanol and 1 mole of acetone are produced. Therefore, the fractional conversion can be determined on both a methanol basis and acetone basis.

	MW	Molarity mol/L	Fractional Conversion
Methanol	32	0.0492	0.24
Acetone	58	0.0211	0.21

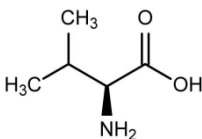
Table 4.10. Sample Calculation of the Fractional Conversion from GC Data

The gas chromatography conditions were optimised on the basis of methanol and therefore this is the value that is used for the reported fractional conversion as

this peak was found to be the most reproducible. However, the fractional conversion on an acetone basis was always calculated and compared with the methanol as an additional check. Where a significant difference occurred the analysis was either repeated or if consistently different it was taken as an indication of reduction in performance and routine replacement of consumable components was carried out.

4.2 Mixing influenced precipitation of valine

Two different experimental setups were used to consider how mixing influences the precipitation of valine from an aqueous solution using isopropanol as an antisolvent. These experiments consider two very different types of mixers and flow ratios. The first concerns itself with mixing in a confined impinging jet mixer at a flow ratio of 1:1 and the second considers semi-batch crystallisation at an 8:1 (antisolvent: solvent) ratio. The objective of these experiments was to draw attention to the similarities, differences, advantages and problems between the intensification offered by a continuous micromixer such as the CIJ mixer and the more traditional semi batch crystalliser.

Valine	Deionised Water	Isopropanol	50% v/v Water/IPA	11% v/v Water/IPA
	Valine solubility ≈70 mg/ml	Valine solubility ≈ 0 mg/ml	Valine solubility 14 mg/ml	Valine solubility ≈ 0.6 mg/ml
Solute	Solvent	Antisolvent	CIJ experiments outlet	Closed loop experiments Outlet

4.2.1 Mixing influenced precipitation of valine in a confined impinging jet mixer

Mixing was carried out in the same CIJ mixer as the mixing characterisation work and at a 1:1 (solvent:antisolvent) volumetric flow ratio. The equilibrium solubility of valine in 50% by volume water/isopropanol at a temperature of 25°C was measured using NMR by Jawor-Baczynska and found to be 14.5mg/ml.[82] These experiments were carried out at room temperature with a slightly lower solubility which has been estimated gravimetrically to be 14mg/ml. The full solubility diagram from the water/valine/isopropanol system is shown in Figure 4.8 and the operating points of the CIJ experiments shown. Bulk supersaturation ranged from 1.14 to 2 and inlet flowrates ranged from 50ml/min to 700ml/min.

The solid recovery was measured at a fixed interval in time (90 minutes). This allowed the creation of a contour map of the solid recovery as a function of inlet flowrate (mixing) and bulk solute concentration (supersaturation) at a 1:1 flow ratio

which then enabled the identification of a solute concentration that was particularly sensitive to mixing (24mg/ml).

This concentration (24mg/ml) of valine was then selected for a time dependent study to quantify the kinetics of the process and how mixing controls it. This involved measurement of the solid recovery as a function of time, spectrophotometry, particle sizing by laser diffraction and the mixing characterisation work from the previous chapters.

The specified amount of valine was added to the solvent (deionised water) and left to dissolve on a magnetic stirrer for several hours. After dissolution, the solvent was filtered using 0.45 μm Millipore filters to remove any undissolved valine or insoluble impurities.

Concentration when mixed	Bulk supersaturation when mixed
16 mg/ml	1.14
20 mg/ml	1.42
24 mg/ml	1.71
28 mg/ml	2.00

Table 4.11. Solution formulation

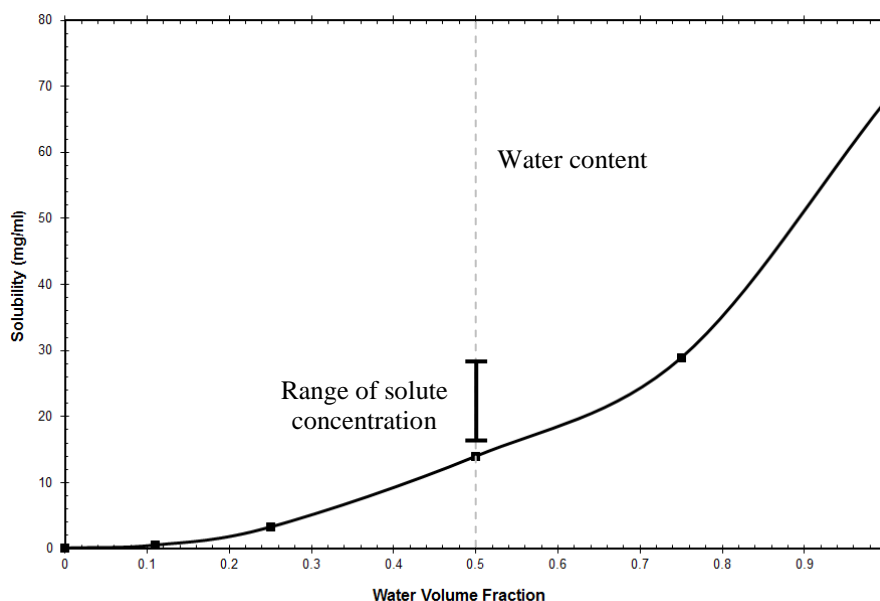


Figure 4.8. Operational points on water/IPA/valine system solubility curve

Points on chart a combination of those measured by Jawor-Baczynska[82] and those estimated gravimetrically.

Figure 4.9 shows the basic mixing setup. Pulse free flow was obtained using micropump heads (GB series, suction shoe design gear pump) magnetically coupled

with a pump driver (Ismatec MCP-Z Standard). The pumps were calibrated for the desired flowrate using water and isopropanol as calibrants prior to each run. All fittings, piping and the CIJ mixer were constructed of stainless steel.

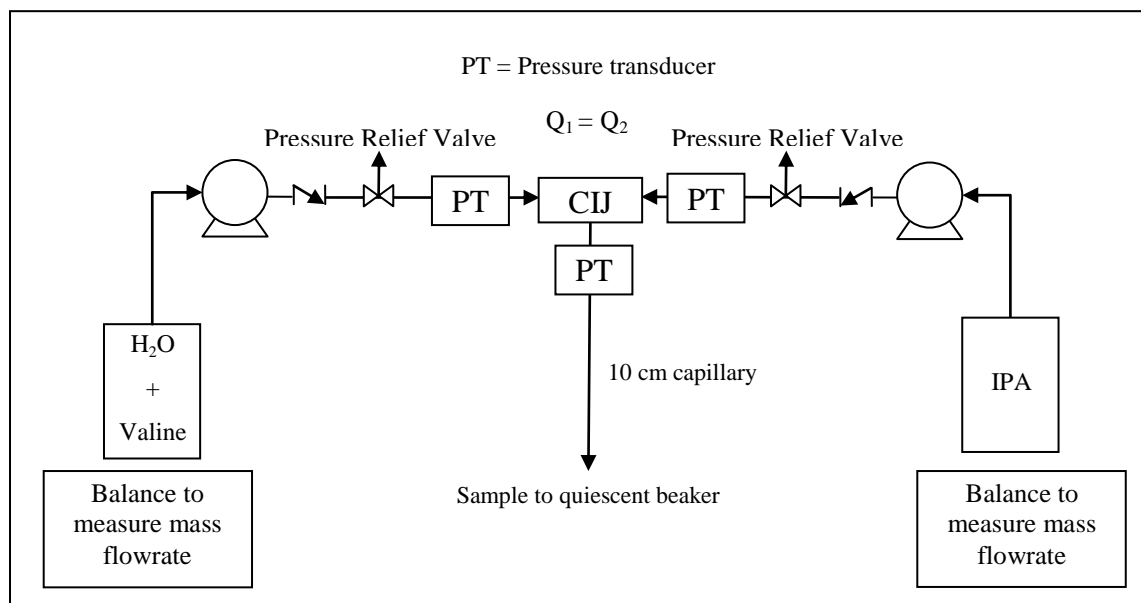


Figure 4.9. Process flow diagram

The system was calibrated with water and isopropanol for the required flowrates to ensure that the flow ratio was maintained within 1% of the target. Prior to every run the system was purged for several residence times using warm water to clear the lines and dissolve any residual crystals within the system volume.

The antisolvent and solvent solutions were charged and processed for at least three residence times before a sample of 200ml (for gravimetric analysis) and a smaller sample (for spectrophotometric analysis) were taken into quiescent beakers.

The flowrate was measured using a balance to measure the mass difference and calculate the mass flowrate which can readily be converted to volumetric flowrate by the density of the solutions. All calculations used mass difference, mass fractions and mass flowrates as their basis not their volume equivalents.

Pressure transducers were placed before and after the mixer to measure the pressure drop across the mixer which can be translated to a total energy dissipation rate if flowrates, physical properties and the mixer dimensions are known.[36]

After 90 minutes, the 200ml sample was filtered. The crystal residue remaining in the beaker was rinsed with mother liquor and added to the filtration in order to minimise crystal loss to glassware. The filter cake was then dried and weighed in

order to estimate the mass of crystals formed and this was compared to the equilibrium value to create a solid recovery percentage.

A small sample was also immediately placed in a UV spectrophotometer to analyse the absorption as a function of time. Mother liquor was used as a reference and a wavelength of 248nm was used. This was carried out for solute concentrations ranging from 16 mg/ml to 28 mg/ml and flowrates ranging from 50 ml/min to 700 ml/min.

For a valine concentration of 24 mg/ml, a concentration determined to be very mixing sensitive, time dependent solid recovery was also carried out using the same method as before but changing the time of filtration. Laser diffraction was also used to measure the particle size distribution at different times.

Samples for laser diffraction were diluted by a factor of six using mother liquor to quench growth after a specified period of time. The amount of mother liquor had to strike a balance to ensure that the growth was adequately suppressed but that the obscuration was such that a reasonable signal strength is obtained but not so high that multiple scattering became an issue. A dilution factor of 6 was chosen.

4.2.2 Closed loop semi-batch crystallisation

Another set of experiments were carried out at the Swiss Federal Institute of Technology in Zurich. These utilised different experimental equipment to the other experiments and involved a semi-batch system at a high antisolvent ratio. This involved the premixing of an antisolvent and solvent in a T-mixer before ejection of the mixed solution into an agitated vessel containing more antisolvent. The experiment was designed to operate in a vessel sealed from the environment to minimise the liquid/air interface. An analytical loop was attached which withdrew a sample of fluid into a particle sizer and then back into the vessel (Figure 4.10).

Firstly, an aqueous valine solution was prepared by adding a specified mass of valine to a specific volume of deionised water and allowing it to agitate on a magnetic stirrer for a few hours. The valine solution and the pure isopropanol were filtered using 0.45 μm Milipore filter.

The pumping loop between the agitated vessel and the Mastersizer (particle sizer), approximately 50ml in volume, was filled with filtered isopropanol in order to

eradicate air from the system. The vessel was then filled with 700ml of filtered isopropanol. 100ml of both the filtered water/valine and filtered isopropanol solutions were then fed into a T-mixer by syringe pumps and mixed in a capillary which led to the agitated vessel (400 rpm) containing 700ml of filtered isopropanol (see Figure 4.10).

The maximum flowrate that could be comfortably calibrated and controlled by both syringe pumps was 100ml/min. The low flowrate conditions correspond to this flowrate (i.e. a total volumetric flowrate of 200ml/min and flow ratio of 1:1). In order to move towards a well-mixed high flowrate system the syringe pumps were used in a mode which maximised the flowrate. This was not controllable and resulted in a total flowrate of 550 ml/min through the capillary and into the vessel. It also was not balanced, each syringe pump unfortunately had a slightly different flowrate. Therefore, two experiments were carried out. Both had the same final composition but during the injection one experiment had a higher antisolvent flowrate and one a higher aqueous flowrate. The results were averaged to get a best estimate of the results expected at 1:1 and the individual results were taken as the limits of uncertainty.

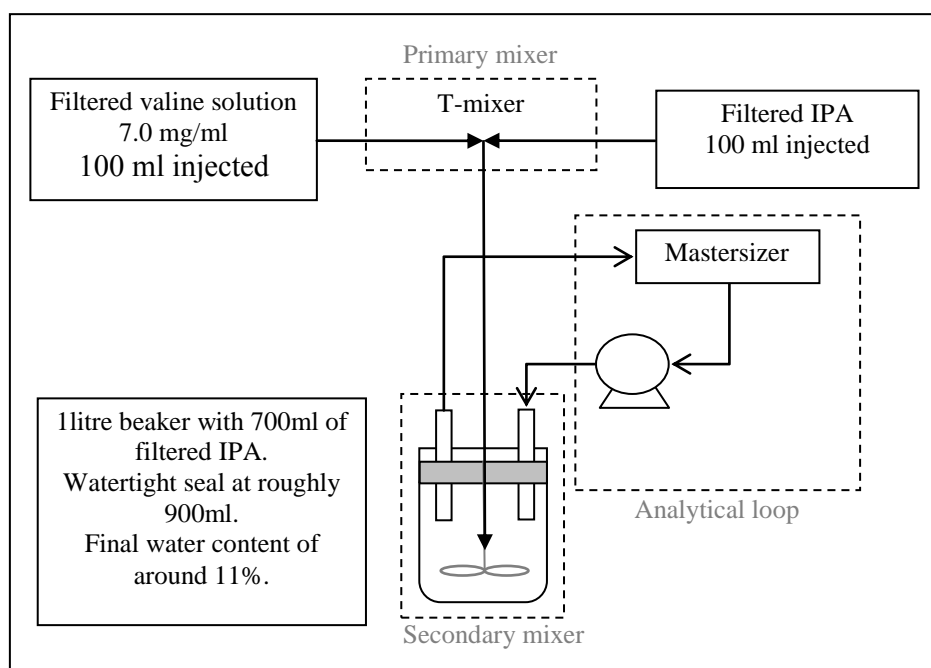


Figure 4.10. Schematic diagram of the experimental set-up

The isopropanol/water/valine solution was then drawn from an outlet pipe and through the Malvern mastersizer and back into the agitated vessel in a continuously recirculating closed analytical loop.

A plastic cap with holes drilled into it (see Figure 4.11 top) provided a watertight seal at roughly 900ml (700ml + 100ml +100 ml). The central hole was filled by a hollow metal cylinder which doubled as the entry point for the impeller shaft and an overflow. This central cylinder sits flush to the underside of the cap. A capillary hole sat immediately in front of the impeller shaft hole and the capillary exit location was fixed just above the bottom of the Rushton impeller (Figure 4.11 bottom). The inlet and outlet fittings are in a fixed position about half way down the capillary (Figure 4.11 bottom).

All fittings were made watertight with an O-ring which forced, after injection via the capillary, the liquid and any remaining air through the overflow, resulting in a very small liquid/air interface equal to the surface area difference between the shaft inlet and the shaft itself. The T-mixer (Figure 4.12) consisted of a 1mm inlet and outlet followed by a 1mm wide capillary that is 20cm in length.

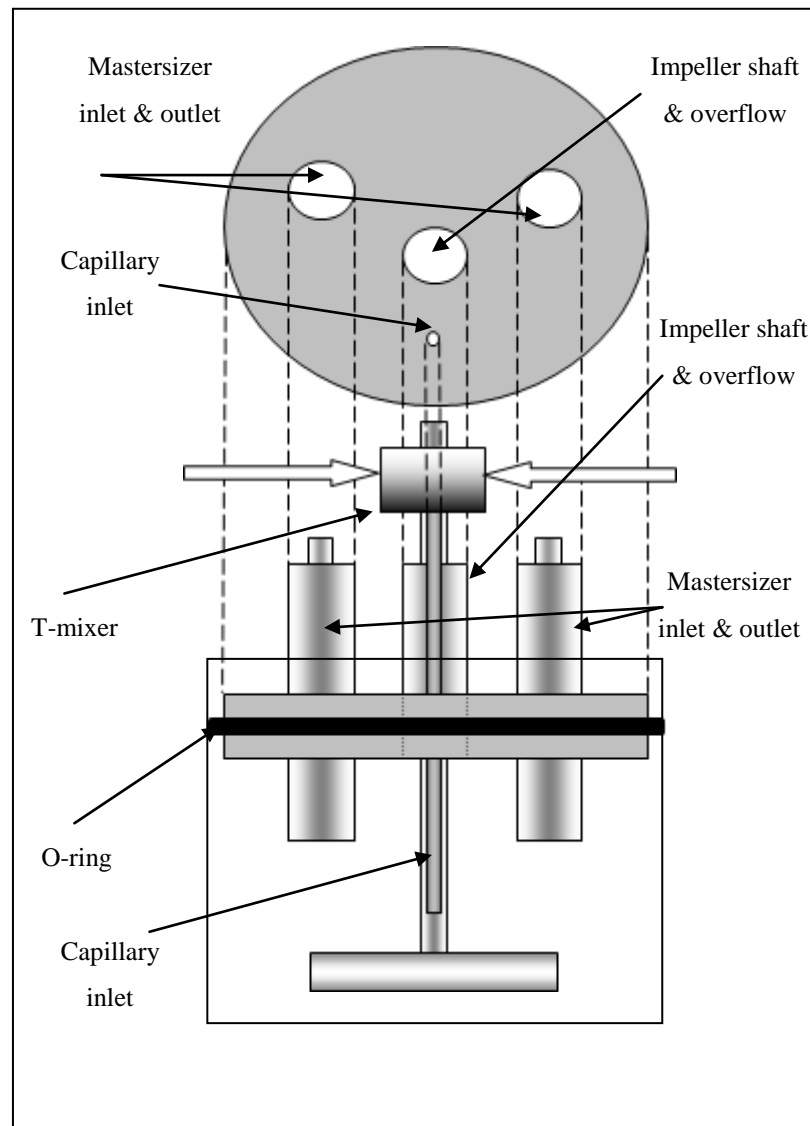


Figure 4.11 Vertical projection of watertight cap (top) and side profile (bottom)

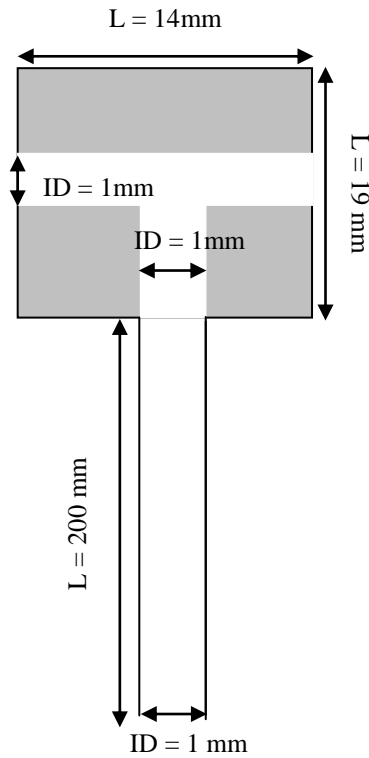


Figure 4.12. T-mixer dimensions

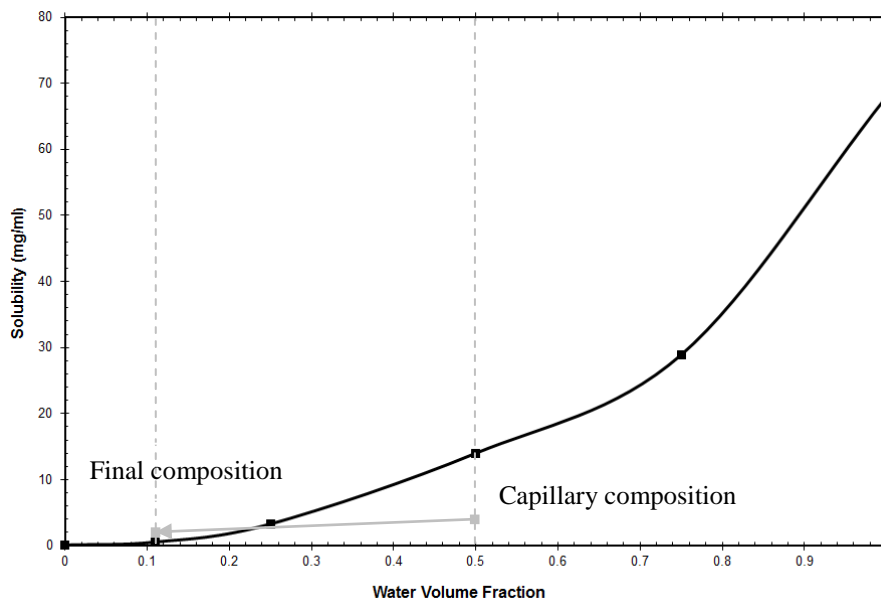


Figure 4.13. Operational points on water/IPA/valine system solubility curve

Figure 4.13 shows the operational points on a water/valine/isopropanol solubility diagram. Initially, after premixing in the T-mixer (primary mixer), the solution was undersaturated. As the solution exited into the closed vessel (secondary

mixer) and analytical loop, which were both prefilled with isopropanol, the injected volume gradually increased in isopropanol content whilst the solute concentration decreased.

4.3 Testing the vortex mixer in commercial applications

The final set of crystallisation experiments was an industrial case study of a mixing sensitive process. The aim was to quantify how mixing in a vortex mixer or a X mixer at an extreme flow ratio influenced the production of protein coated microcrystals (PCMCs). The vortex mixer, which has been characterised to be a better mixer than the X mixer at extreme flow ratios, was tested to see if this characterised mixing superiority translated into process improvements in a real industrial process which involves considerable formulation complexity in comparison to the more controlled water/valine/isopropanol system.

These experiments were conducted using two different formulations developed by Xstalbion Limited for the production of protein coated microcrystals (PCMCs). The exact formulations have been hidden for confidentiality reasons but this omission is of little significance as the only purpose of the experiments was to compare the vortex mixer with the X mixer. Both formulations required a flow ratio of 19:1. Extreme flow ratios were found to favour the vortex mixer (chapter 7). The mixers were tested both with and without a Kenics static mixer immediately downstream of the primary mixer (Figure 4.14). The effect of flowrate was not investigated. A total flowrate of 200ml/min was chosen as this provided a sensible operation time for the production of around a litre of product, increasing the flowrate would obviously provide intensification benefits but the operational timescale would reduce which was deemed to be undesirable. Therefore, the challenge was to gain acceptable product quality at low to moderate flowrates.

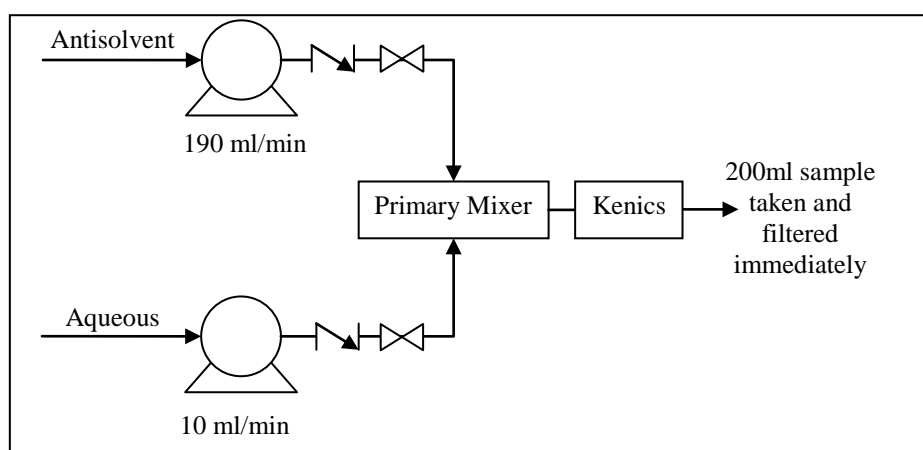


Figure 4.14. Process flow diagram

Experimental Techniques and Methods

In this set of experiments the flowrate was always 190 ml/min in the antisolvent stream and 10 ml/min in the solvent. All that was investigated was the influence of the primary mixer with and without a secondary mixer (Kenics mixer).

Prior to the run the pumps were calibrated for the desired flowrate and mixer with the antisolvent (2-methyl-1-propanol) and water. After initialisation the pumps were run for approximately 3 residence times before a sample of approximately 200ml was taken.

Mixer	F1	F2
Vortex	200 ml/min	200 ml/min
Vortex + Kenics	200 ml/min	200 ml/min
1/8" X	200 ml/min	200 ml/min
1/8" X+Kenics	200 ml/min	200 ml/min

Figure 4.15. Total flowrate, mixers and formulations tested

Two formulations were tested. These were designated F1 (high protein content with a fast crystallising excipient) and F2 (high protein content with a slow crystallising excipient).

F1	
<i>High protein content with a fast crystallising excipient</i>	
Protein	38.2 mg/ml
Buffers and excipients	36.3 mg/ml
TPL	51.3%
Solvent:	2M1P

F2	
<i>High protein content with a slow crystallising excipient</i>	
Protein	23.9 mg/ml
Buffers and excipients	25.7 mg/ml
TPL	48.2%
Solvent:	2M1P

The mass of the antisolvent, solvent and sample were measured before and after each run and the mass flowrates calculated. All calculations were based on mass, mass fractions and mass flowrates. The solid recovery, net protein recovery (NPR) and filter rate were then compared across all the mixers

The solid recovery was calculated from the mass of solid deposited on the filter paper and the measured mass in the solution (from mass fraction of solids). For the purposes of these calculations any losses and any residual solubility of the mother liquor were assumed to be negligible.

The NPR represented a component balance of the protein that coated the excipient, expressed as a percentage of the initial amount. This was calculated using UV spectrophotometry to determine the concentration of a reconstituted solution of the filter cake.

The average filtration time was calculated by measuring the duration of filtration and dividing the filtrate volume by this duration. Common with all constant pressure filtrations, the instantaneous filter rate reduced with time as the thickness of the filter cake built. This was not monitored or measured. SEM images were taken of the samples after filtration.

All these data were then collated and compared for both mixers and analysed in conjunction the theory outlined in Chapter 3 in addition to the results presented in Chapter 7.

5 Micromixing Reaction Models

The main objective was to deploy a model that could, with acceptable accuracy, convert the fractional conversion to an estimated mixing time. Such a model would have to standardise the mixing time to allow for fair comparison and would have to account for concentration and volume effects to allow comparison between different flow ratios.

Two models of micromixing which have been commonly used in previous literature have been considered. These are the Interaction by Exchange with the Mean model (IEM) and the Engulfment model (sometimes referred to as the E-model). The E-model assumes engulfment is the rate limiting step (valid for liquids at moderate Schmidt numbers – less than 4000) and hence ignores the deformation and diffusion aspects of micromixing which are considered in the more involved EDD model (engulfment, deformation and diffusion model).

5.1 Interaction by exchange with the mean (IEM model)

Interaction by the exchange with the mean (IEM) is a simple mixing model proposed and developed by Costa and Trevissoi[83] and Villermaux[29], [84] which can be used to estimate, with acceptable accuracy, the fractional conversion of a parallel reaction when mass is exchanged between two streams at a known rate.

For the case of mixing two streams the concentration of each species (k) is evaluated in two zones (Figure 5.1):

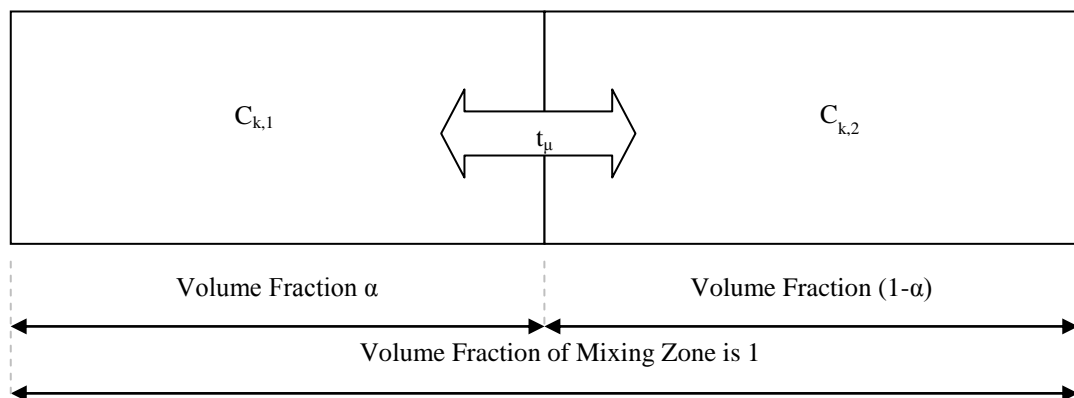


Figure 5.1. Representation of the IEM Model

If there is no back mixing and plug flow is assumed, the IEM equations are simply the interaction of the streams in their relative proportion.[29] The model utilises the whole volume as the reaction zone and the concentration of each species at a specified time is considered constant across each zone and the zones exchange mass.[85] For the mixing two fluids, there are two equations for each chemical species - one for each zone:

$$\frac{dC_{k,1}}{dt} = \frac{\langle C_k \rangle - C_{k,1}}{t_\mu} + R_{k,1} \quad (5.1)$$

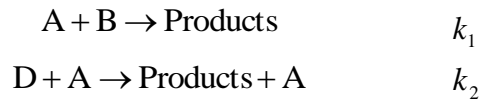
$$\frac{dC_{k,2}}{dt} = \frac{\langle C_k \rangle - C_{k,2}}{t_\mu} + R_{k,2} \quad (5.2)$$

$$\langle C_k \rangle = \alpha C_{k,1} + (1 - \alpha) C_{k,2} \quad (5.3)$$

Where $R_{k,1}$ and $R_{k,2}$ are the change in concentration due to reaction of species k in streams 1 and 2, $C_{k,1}$ and $C_{k,2}$ are the concentrations of species k in streams 1 and 2, α is the volume fraction of stream 1, $\langle C_k \rangle$ is the average concentration of species k and t_μ is the characteristic time for the exchange of mass between zone 1 and zone 2 (i.e. the mixing time).

To relate the mixing time to the fractional conversion, one first assumes a value of the characteristic time and then solves the system of differential equations.[29] The procedure is then repeated for a new mixing time and so on until the fractional conversion is solved for a range of associated mixing times.

The Bourne IV reaction scheme involves the acid catalysed hydrolysis of dimethoxypropane (D) competing for acid (A) with a strong base (B). The dimethoxypropane and alkali are in stream 1 and the acid is in stream 2. The rate constant of the fast reaction (k_1) is many orders of magnitude larger than (k_2). It can be represented as:



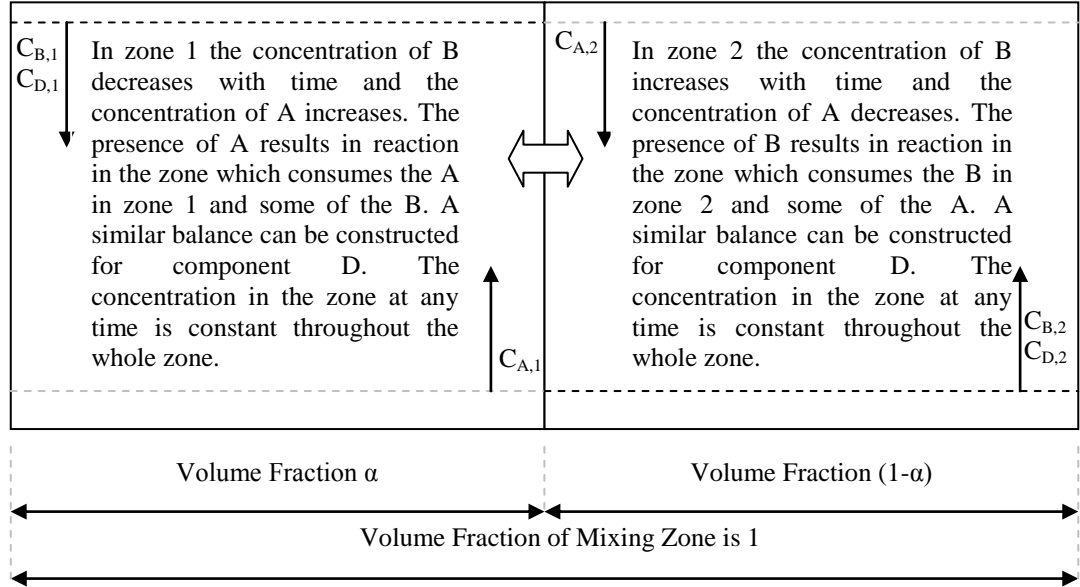


Figure 5.2. Representation of the IEM Model

The IEM model partitions the fluid to be mixed into two regions and mass is exchanged between the regions. The concentration of a species is constant through the whole region (i.e. mass transfer within a region is fast in comparison to mass transfer between regions) and the whole volume is utilised as a mixing volume.

In the case of dimethoxypropane hydrolysis competing for acid (the catalyst) with a strong base neutralisation there are three reactant species which interact across two zones. This results in six ordinary differential equations (ODEs) which are readily solved numerically by a backward differentiation formula (BDF) method. A BDF approach was required because of the stiffness created by the large variation in time constants between the slow and fast reactions. One could easily make the fast reaction instantaneous with respect to mixing which would allow us to define the rate of reaction independent of k_1 which would resolve the stiffness issue and allow another family of numerical methods such as a fixed step Runge-Kutta to solve the systems of equations.

B and D (the alkali and dimethoxypropane) are in zone 1 whilst the acid (A) is in zone 2.

The six ODEs are formed as follows:

$$\frac{dC_{B,1}}{dt} = \frac{\langle C_B \rangle - C_{B,1}}{t_\mu} - k_1 C_{B,1} C_{A,1} \quad (5.4)$$

The first term governs the mass transfer between the zones and the second term the consumption due to reaction in zone 1. Substituting in the expression for average concentration and simplifying:

$$\frac{dC_{B,1}}{dt} = \frac{\alpha C_{B,1} + (1-\alpha)C_{B,2} - C_{B,1}}{t_\mu} - k_1 C_{B,1} C_{A,1} \quad (5.5)$$

$$\frac{dC_{B,1}}{dt} = \frac{(1-\alpha)(C_{B,2} - C_{B,1})}{t_\mu} - k_1 C_{B,1} C_{A,1} \quad (5.6)$$

The equations for the other streams and components are:

$$\frac{dC_{B,2}}{dt} = \frac{(\alpha)(C_{B,1} - C_{B,2})}{t_\mu} - k_1 C_{B,2} C_{A,2} \quad (5.7)$$

$$\frac{dC_{A,1}}{dt} = \frac{(1-\alpha)(C_{A,2} - C_{A,1})}{t_\mu} - k_1 C_{A,1} C_{B,1} \quad (5.8)$$

$$\frac{dC_{A,2}}{dt} = \frac{(\alpha)(C_{A,1} - C_{A,2})}{t_\mu} - k_1 C_{A,2} C_{B,2} \quad (5.9)$$

$$\frac{dC_{D,1}}{dt} = \frac{(1-\alpha)(C_{D,2} + C_{D,1})}{t_\mu} - k_2 C_{D,1} C_{A,1} \quad (5.10)$$

$$\frac{dC_{D,2}}{dt} = \frac{(\alpha)(C_{D,1} - C_{D,2})}{t_\mu} - k_2 C_{D,2} C_{A,2} \quad (5.11)$$

Which can be solved given the following initial conditions:

$$C_{B,1}(0) = C_{B0}, C_{B,2}(0) = 0, C_{A,1}(0) = 0, C_{A,2}(0) = C_{A0}, C_{D,1}(0) = C_{D0}, C_{D,2}(0) = 0$$

Where C_{K0} indicates the initial concentration of K. The initial conditions used to model the different alkali volumetric flowrates of the experiments are:

Alkali:Acid	$C_{B,1}$	$C_{B,2}$	$C_{A,1}$	$C_{A,2}$	$C_{D,1}$	$C_{D,2}$	α
1:1	210	0	0	200	200	0	0.5
3:1	140	0	0	400	133.33	0	0.75
1:3	420	0	0	133.33	400	0	0.25
10:1	115.5	0	0	1100	110	0	0.909

Table 5.1. Initial IEM conditions which correspond to the experiments (mmol/L)

Which is converted into dimensionless form by normalising by the initial concentration at 1:1 flow ratio (i.e. 200 mmol/L).

Alkali:Acid	$C_{B,1}$	$C_{B,2}$	$C_{A,1}$	$C_{A,2}$	$C_{D,1}$	$C_{D,2}$	α
1:1	1.05	0	0	1	1	0	0.5
3:1	0.7	0	0	2	0.66	0	0.75
1:3	2.1	0	0	0.66	2	0	0.25
10:1	0.58	0	0	5.5	0.55	0	0.909

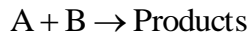
Table 5.2. Initial IEM conditions which correspond to the experiments in dimensionless form

The calculations were carried out in dimensionless form.

5.2 The engulfment model (E-model)

A brief overview of this method is given here, for full details consult “Turbulent Mixing and Chemical Reactions” by Baldyga and Bourne.[20] If the Schmidt number (defined as the ratio of the rate of momentum diffusion (μ/ρ) to molecular diffusion (D)) is less than 4000 then engulfment can be reasonably assumed to be the rate limiting micromixing mechanism and hence micromixing can be modelled on this step alone.[4], [20], [21], [24], [85]

Consider the following simple instantaneous reaction, such as a strong acid/alkali neutralisation:



Where B is added in a very small volume fraction in comparison to A (Figure 5.3).

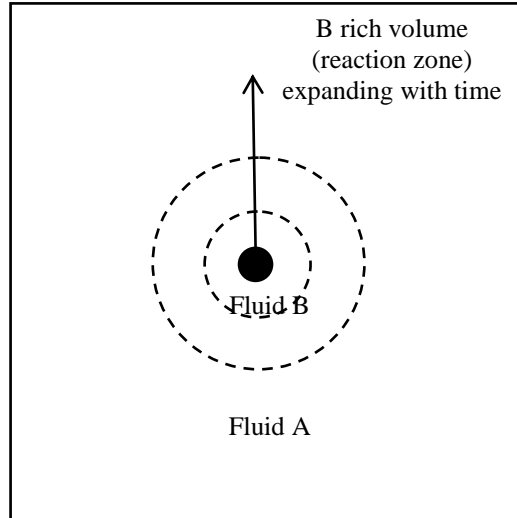


Figure 5.3. Engulfment model

The reaction zone grows with time at a rate proportional to the engulfment rate (E)[20]:

$$\frac{dV_m}{dt} = EV_m \quad (5.12)$$

Where the mixing volume (V_m) is very much smaller than the total volume

$$V_m(0) \ll V_T \quad (5.13)$$

A mole balance of B in this growing region:

$$\frac{d(V_m C_B)}{dt} = EV_m \langle C_B \rangle + r_B V_m \quad (5.14)$$

Where $\langle C_B \rangle$ is the concentration of B in the local environment with the first term on the right hand side equal to the rate of addition of B in the region by engulfment and the second terms is the generation or consumption of B due to reaction in the expanding reaction zone. Diffusion is considered to be rapid relative to engulfment so C_B is considered to be constant across the zone. Substituting equation (5.12) into equation (5.14) and using the product rule gives:

$$\frac{d(C_B)}{dt} = E(\langle C_B \rangle - C_B) + r_B \quad (5.15)$$

$$E \approx 0.058 \left[\frac{\varepsilon}{\nu} \right]^{\frac{1}{2}} \quad (5.16)$$

An analogous equation can be written for the other component (component A) in the expanding reaction zone B:

$$\frac{d(C_A)}{dt} = E(\langle C_A \rangle - C_A) + r_A \quad (5.17)$$

On first glance this equation (5.17) may appear to be remarkably similar to the equivalent IEM equation (5.4) and in many respects it is. However, the difference is not just the different parameters (E and τ_μ), it is that the engulfment model is formed due a combination of equations (5.12), (5.14) and (5.16). This crucial difference means that the engulfment model has a growing reaction zone whilst the IEM model which utilises the whole volume for reaction. Additionally, the parameter E (equation (5.16)) is related to the kinematic viscosity and the energy dissipation, giving the model a physical grounding. This grounding relates to the mixing process of engulfment in the viscous-convective range which is often the rate limiting step of the micromixing mechanisms. The IEM model has less physical basis and the time that characterises the exchange the mass between the zones is often assumed to be the Corrsin mixing time, which has a significant inertial-convective component which feels a little inconsistent for a micromixing model. [21], [24], [85]

Assuming instantaneous reaction, the concentration of A in reaction zone B is always zero and the rate of change of the concentration of A with respect to time in this zone would also be zero. Therefore, one can derive a reaction rate that would satisfy the condition of instantaneous reaction with respect to mixing:

$$\frac{d(C_A)}{dt} = 0 = E(\langle C_A \rangle - C_A) + r_A \quad (5.18)$$

$$C_A = 0 \quad (5.19)$$

$$\therefore r_A = E\langle C_A \rangle = EC_{A0} = r_B \quad (5.20)$$

Which can be substituted into equation (5.15) to give:

$$\frac{d(C_B)}{dt} = -E(C_{A0} + C_B) \quad (5.21)$$

Which can then be integrated and solved, given the initial conditions.

This methodology is valid only for those with very small volume fractions of the B rich solution. If the volume B is no longer insignificant, then the assumptions made in the model above no longer hold and self-engulfment occurs which does not

contribute to mixing but consumes energy. Therefore the previous methodology overestimates reaction rates when the B rich zone is relatively large. To adjust for this, an engulfment probability, P, is added[20]:

$$\frac{dV_m}{dt} = EPV_m \quad (5.22)$$

A mass balance of B in this growing region:

$$\frac{d(V_m C_B)}{dt} = EPV_m \langle C_B \rangle + r_B V_m \quad (5.23)$$

Which after treatment by the product rule and substitution as before becomes:

$$\frac{d(C_B)}{dt} = EP(\langle C_B \rangle - C_B) + r_B \quad (5.24)$$

The probability of self-engulfment is estimated from the volume fraction of the B rich region (X_B), therefore the probability of engulfment is estimated as:

$$P = 1 - X_B \quad (5.25)$$

The evolution of the B rich reaction zone is a fraction of the total volume and is determined by dividing (5.22) by V_T and substituting (5.25):

$$\frac{dX_B}{dt} = E(1 - X_B)X_B \quad (5.26)$$

$$X_B(0) = X_{B0} \quad (5.27)$$

The concentration of B in this zone is:

$$\frac{d(C_B)}{dt} = E(1 - X_B)(\langle C_b \rangle - C_b) + r_b \quad (5.28)$$

and A in zone B:

$$\frac{d(C_A)}{dt} = E(1 - X_B)(\langle C_A \rangle - C_A) + r_a \quad (5.29)$$

Given that the reaction is instantaneous and A cannot exist in the B region, i.e.

$$\frac{d(C_A)}{dt} = 0 \quad (5.30)$$

$$C_A = 0 \quad (5.31)$$

$$r_b = r_a \quad (5.32)$$

Then:

$$r_b = r_a = -E(1 - X_B)(C_A) \quad (5.33)$$

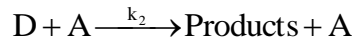
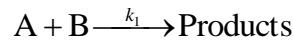
$$\frac{d(C_B)}{dt} = -E(1 - X_B)(C_B + C_{A0}) \quad (5.34)$$

$$C_b(0) = C_{b0} \quad (5.35)$$

Equations (5.26), (5.16) and (5.34) make up the system of equations along with some initial conditions. These equations still assume that the minor component has a small volume fraction in comparison to the larger component. This assumption has been shown to be valid for a volume ratio greater than 10.[20] As the experimental volumetric flow ratios considered are 1:1, 3:1 1:3 and 10:1 a more complex formulation based on this method was chosen as the most appropriate.

5.3 Comparable volume engulfment

Comparable volume engulfment, based on the unequal volume formulation described above, was outlined by Baldgya in “Turbulent mixing and chemical reactions”[20] but has also been utilised successfully by Gillian and Kirwan to model the Bourne IV reaction scheme at 1:1.[40] The Bourne IV reaction scheme involves the acid catalysed hydrolysis of dimethoxypropane (D) competing for acid (A) with a strong base (B). The rate constant of the fast reaction (k_1) is many orders of magnitude larger than (k_2), so much so that the neutralisation reaction can be considered instantaneous to mixing:



The model is a four compartment model after one eddy lifetime as explained below. During the first eddy lifetime the model initialises. Initially, the two streams are entirely segregated into two unmixed pure volumes, volume A (V_{A0}) and volume B (V_{B0}) with volume fractions (X_{A0} and X_{B0}) which take up the whole volume (Figure 5.4). The subscript K0 represents the initial volume/fraction/concentration in the K zone.

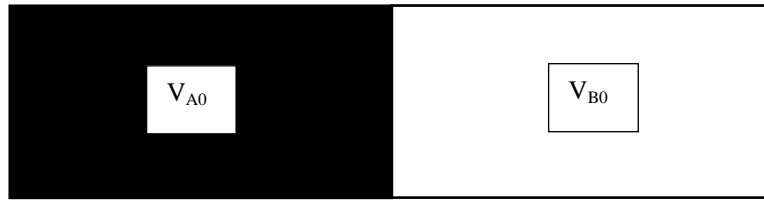


Figure 5.4. Two compartment model

Two compartment model showing the initial conditions at time=0

$$X_{A0} = \frac{V_{A0}}{V_{B0} + V_{A0}} \quad (5.36)$$

$$X_{B0} = \frac{V_{B0}}{V_{A0} + V_{B0}} \quad (5.37)$$

$$X_{A0} + X_{B0} = 1 \quad (5.38)$$

During the first eddy turnover time a mixing zone is established (Figure 5.5) for a mixed volume V_m and pure unmixed volumes V_a and V_b :

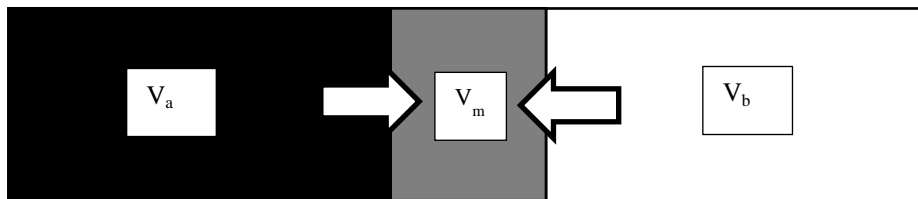


Figure 5.5. Establishment of mixing zone

Creation of a mixing zone during one eddy turnover time (τ_w). The arrows indicate mixing by engulfment.

The change in volume of the mixing zone is proportional to the engulfment rate and the probability of self-engulfment, as before:

$$\frac{dV_m}{dt} = EPV_m \quad (5.39)$$

Considering mixing of fluid A into fluid B, then the probability of self-engulfment is X_{A0} . Then equation (5.39) can be rewritten as:

$$\frac{dV_m}{dt} = EV_T X_{A0} X_{B0} \quad (5.40)$$

$$V_m(0) = 0 \quad (5.41)$$

The mixing volume is equal to the total volume multiplied by the volume fraction of the mixing zone:

$$V_m = V_T X_m \quad (5.42)$$

Therefore, dividing equation 5.40 through by the total volume allows an expression for the change in the mixing volume with respect to time to be developed:

$$\frac{dX_m}{dt} = EX_{A0}X_{B0} \quad (5.43)$$

$$X_m(0) = 0 \quad (5.44)$$

This needs to be addressed in order to solve the systems of equations. To do this, the model is solved after one eddy turnover time where a four compartment model exists.

After one eddy turnover time, a four compartment model exists with the two pure component zones (X_a and X_b) as before but now separated by an expanding mixing zone (X_m) which itself is divided into an A rich zone (X_{am}) and a B rich zone (X_{bm}) (Figure 5.6).

The A rich mixing volume X_{am} interacts with its pure mixing zone (X_a) and with the B rich mixing zone X_{bm} . X_{bm} interacts with X_{am} and the pure B zone X_b .

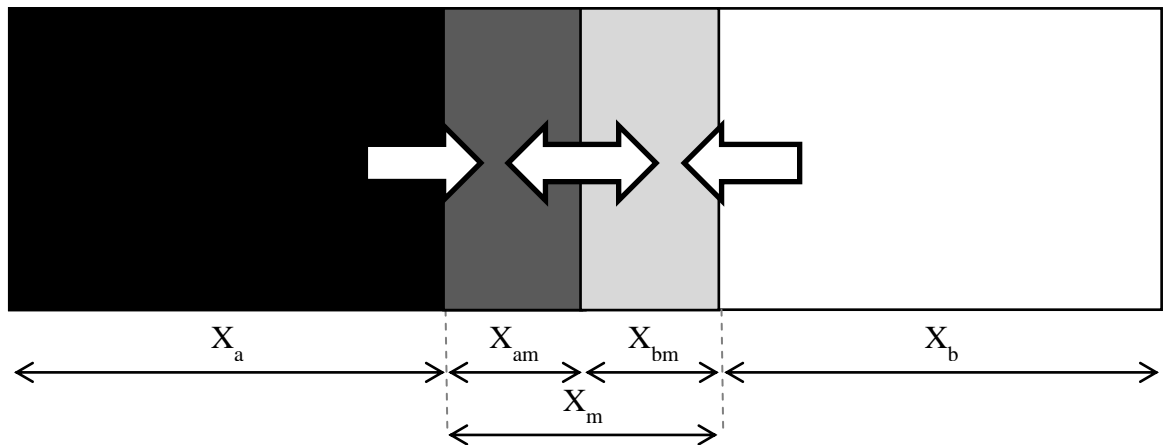


Figure 5.6. Four Compartment model

Four compartment model created after one eddy turnover time (τ_w). The arrows indicate mixing by engulfment.

Initially, at zero time, the mixing zone does not exist and the whole volume is occupied by the pure A zone (X_a) and the pure B zone (X_b). Therefore, the sum of the initial volume fractions ($X_{A0} + X_{B0}$) is one. During the first eddy turnover time a

mixing zone is established according to the relationship defined in equation (5.43) and by separating the variables and integrating between volume fractions of 0 and X_{m0} and times of 0 and the eddy turnover time:

$$\int_0^{X_{m0}} dX_m = EX_{A0}X_{B0} \int_0^{t_\omega} dt \quad (5.45)$$

$$X_{m0} = EX_{A0}X_{B0}t_\omega \quad (5.46)$$

The eddy turnover time (t_ω) is equal to $\ln 2/E$. [21] Substituting this into equation (5.46) gives:

$$X_{m0} = X_{A0}X_{B0} \ln 2 \quad (5.47)$$

Therefore the discontinuity has been addressed. Equation (5.47) allows the initial conditions (at 1E) for the four compartment model to be specified as long as the flow ratios are known. Before considering the further development of this model, the initial conditions corresponding to the experimental conditions of 1:1, 3:1, 1:3 and 10:1 are calculated using equation (5.47).

At 1:1 mixing, the volume fraction of the A rich zone is equal to the B rich which is equal to 0.5. Therefore:

$$X_{m0} = EX_{A0}X_{B0}t_w \quad (5.48)$$

$$X_{m0} = \frac{\ln 2}{4} = 0.1733 \quad (5.49)$$

$$X_{m0} = X_{Am0} + X_{Bm0} \quad (5.50)$$

$$X_{Am0} = X_{Bm0} = 0.0866 \quad (5.51)$$

At 3:1 mixing, the volume fraction of the B rich zone is equal to three times the A rich. Therefore, B is 0.75 and A is 0.25:

$$X_{m0} = EX_{A0}X_{B0}t_w \quad (5.52)$$

$$X_{m0} = 0.13 \quad (5.53)$$

$$X_{m0} = X_{Am0} + X_{Bm0} \quad (5.54)$$

$$X_{Bm0} = 3X_{Am0} \quad (5.55)$$

$$X_{Bm0} = 0.0975, X_{Am0} = 0.0325 \quad (5.56)$$

At 1:3 mixing, the volume fraction of the B rich zone is equal to one third of the A rich. Therefore, B is 0.25 and A is 0.75:

Micromixing Reaction Models

$$X_{m0} = EX_{A0}X_{B0}t_w \quad (5.57)$$

$$X_{m0} = 0.13 \quad (5.58)$$

$$X_{m0} = X_{Am0} + X_{Bm0} \quad (5.59)$$

$$X_{Bm0} = \frac{X_{Am0}}{3} \quad (5.60)$$

$$X_{Bm0} = 0.0325, X_{Am0} = 0.0975 \quad (5.61)$$

At 10:1 mixing, the volume fraction of the B rich zone is equal to ten times the A rich. Therefore B is 0.909 and A is 0.0909

$$X_{m0} = EX_{A0}X_{B0}t_w \quad (5.62)$$

$$X_{m0} = 0.0826 \quad (5.63)$$

$$X_{m0} = X_{Am0} + X_{Bm0} \quad (5.64)$$

$$X_{Bm0} = 10X_{Am0} \quad (5.65)$$

$$X_{Am0} = 0.07513, X_{Bm0} = 0.007513 \quad (5.66)$$

The initial conditions for the experimental conditions are:

Alkali:Acid	C _{B,Bm0}	C _{B,Am0}	C _{A,Bm0}	C _{A,Am0}	C _{D,Bm0}	C _{D,Am0}	XB _{m0}	X _{Am0}
1:1	210	0	0	200	200	0	0.0866	0.0866
3:1	140	0	0	400	133.33	0	0.0975	0.0325
1:3	420	0	0	133.33	400	0	0.0325	0.0975
10:1	115.5	0	0	1100	110	0	0.0751	0.0075

Table 5.3. Summary of initial conditions

At this stage ($t=t_w$), molecular scale mixing (and hence reaction) has not occurred. X_{m0} consists of two zones, one which is rich in A and one which is rich in B. Introducing a probability for self-engulfment ($P = 1 - X_m$), yields:

$$\frac{dX_m}{dt} = EX_m(1 - X_m) \quad (5.67)$$

$$X_m(0) = X_{m0} \quad (5.68)$$

Which can be integrated and solved for any time, t:

$$X_m(t) = \frac{X_{m0}e^{Et}}{1 - X_{m0}(1 - e^{Et})} \quad (5.69)$$

$X_m(t)$ is divided into consists of two zones which evolve in time by exchanging mass with other zone and their pure unmixed compartment:

$$\frac{dX_{Bm}}{dt} = EX_{B0}X_m(1 - X_m) + EP_eX_{Bm}X_{Am} \quad (5.70)$$

$$\frac{dX_{Am}}{dt} = EX_{A0}X_m(1 - X_m) - EP_eX_{Bm}X_{Am} \quad (5.71)$$

The first term is the fresh feed incorporation and the second term is the interaction between the mixing zones. The P_e term controls the interaction between the A and B rich zones. Its value is either 1 or -1. It determines whether the mixed fluid becomes part of the A rich zone (A_m) or B rich zone (B_m) upon mixing. It depends upon the concentrations of A and B in the mixing zone. If the concentration of A in the mixing zone is greater than B then P_e is -1 and if B is greater than A then P_e is 1.

Physically, what this means is that if there is more A than B upon mixing then the A rich region grows, this volume for growth comes from the B rich zone (see the equations (5.70) and (5.71) with P_e equal to -1). If there is more B then the B grows at the expense of the A zone (P_e is 1).

The evolution of concentration can also be defined in a similar way:

$$\begin{aligned} \frac{d(C_{B,Bm}X_{Bm})}{dt} &= EX_{B0}X_m(1 - X_m)C_{B0} \\ &- E\left(\frac{1 + P_e}{2}\right)X_{Bm}X_{Am}C_{A,Am} - E\left(\frac{1 - P_e}{2}\right)X_{Bm}X_{Am}C_{B,Bm} \end{aligned} \quad (5.72)$$

In this case, the first term represents the change in concentration due to the incorporation of fresh B from the unmixed B zone. The second terms represents the loss of B due to reaction with A (which is considered instantaneous, due to large rate constant) if B is engulfing A (P_e is 1). The third term deals with the situation where B is engulfed (P_e is -1) where B is lost to the A zone. At each time step, P_e has a fixed value so therefore either the second or third term equals zero depending on the value of P_e .

Equation (5.72) can be simplified using the product rule and substituting the expression for dX_{bm}/dt (equation (5.70)):

$$\begin{aligned} \frac{d(C_{B,Bm})}{dt} &= \frac{EX_{B0}X_m(1-X_m)}{X_{Bm}}(C_{B0} - C_{B,Bm}) \\ &+ EX_{Am}\left(-\left(\frac{1+P_e}{2}\right)C_{A,Am} - \left(\frac{1-P_e}{2}\right)C_{B,Bm} - P_e C_{B,Bm}\right) \end{aligned} \quad (5.73)$$

Notice how if P_e is -1 then the second term in equation (5.73) equals zero. P_e is -1 when A engulfs B, this affects the volume of B_m but not the concentration. In this circumstance, the concentration is only influenced by the incorporation of fresh feed. If P_e is 1 (B engulfs A) then the concentration is influenced by fresh feed incorporation and reaction.

Equation (5.73) can be rewritten in a dimensionless form, using $t^*=Et$ as a dimensionless time and dividing the concentrations by C_{B0} (i.e. $B_{Bm}=C_{B,Bm}/C_{B0}$):

$$\begin{aligned} \frac{d(B_{Bm})}{dt^*} &= \frac{X_{B0}X_m(1-X_m)}{X_{Bm}}(1 - B_{Bm}) \\ &+ X_{Am}\left(-\left(\frac{1+P_e}{2}\right)A_{Am} - \left(\frac{1-P_e}{2}\right)B_{Bm} - P_e B_{Bm}\right) \end{aligned} \quad (5.74)$$

An analogous equation can be written for A in the A rich zone A_m

$$\begin{aligned} \frac{d(A_{Am})}{dt^*} &= \frac{X_{A0}X_m(1-X_m)}{X_{Am}}(A_0 - A_{Am}) \\ &+ X_{Bm}\left(-\left(\frac{1-P_e}{2}\right)B_{Bm} - \left(\frac{1+P_e}{2}\right)A_{Am} + P_e A_{Am}\right) \end{aligned} \quad (5.75)$$

The concentration of A in zone B_m is always zero (assumed instantaneous reaction). Likewise the concentration of B in zone A_m is always zero.

This leaves an expression for the concentration of D in zones A_m and B_m to be determined. For D in zone B this involves no reaction as the fast reaction dominates to the extent that there is no A available long enough to catalyse the dimethoxypropane reaction.

$$\begin{aligned} \frac{d(D_{Bm})}{dt^*} &= \frac{X_{B0}X_m(1-X_m)}{X_{Bm}}(D_0 - D_{Bm}) + \\ &X_{Am}\left(-\left(\frac{1-P_e}{2}\right)D_{Bm} + \left(\frac{1+P_e}{2}\right)D_{Am} - P_e D_{Bm}\right) \end{aligned} \quad (5.76)$$

For the concentration of D in reaction zone A the reaction of dimethoxypropane has to be considered. The first term in equation (5.77) is the D gained from zone B ($P_e=-1$), the second term is D lost to zone B ($P_e=1$) and the last term is D lost to reaction in

zone A. Applying the product rule and substituting (5.70) into equation (5.77) gives equation (5.78) which can then be transformed into dimensionless units (equation (5.79)):

$$\frac{d(C_{D,Am} X_{Am})}{dt} = E \left(\frac{1-P_e}{2} \right) X_{Am} X_{Bm} C_{D,Bm} - E \left(\frac{1+P_e}{2} \right) X_{Am} X_{Bm} C_{D,Am} - k_2 C_{A,Am} C_{D,Am} \quad (5.77)$$

$$\frac{d(C_{D,Am})}{dt} = \frac{E X_{A0} X_m (1-X_m)}{X_{Bm}} (-C_{D,Am}) + E X_{Bm} \left(\left(\frac{1-P_e}{2} \right) C_{D,Bm} - \left(\frac{1+P_e}{2} \right) C_{D,Am} + P_e C_{D,Am} \right) - k_2 C_{A,Am} C_{D,Am} \quad (5.78)$$

$$\frac{d(D_{Am})}{dt^*} = \frac{X_{A0} X_m (1-X_m)}{X_{Bm}} (-D_{Am}) + X_{Bm} \left(\left(\frac{1-P_e}{2} \right) D_{Bm} - \left(\frac{1+P_e}{2} \right) D_{Am} - P_e D_{Am} \right) - \frac{k_2 C_{A0}}{E} A_{Am} D_{Am} \quad (5.79)$$

The initial conditions used to model the experimental conditions is summarised in dimensionless form in Table 5.4.

Alkali:acid	B _{Bm0}	B _{Am0}	A _{Bm0}	A _{Am0}	D _{Bm0}	D _{Am0}	X _{Bm0}	X _{Am0}
1:1	1.05	0	0	1	1	0	0.0866	0.0866
3:1	0.7	0	0	2	0.67	0	0.0975	0.0325
1:3	2.1	0	0	0.67	2	0	0.0325	0.0975
10:1	0.577	0	0	5.5	0.55	0	0.0751	0.0075

Table 5.4. Summary of Initial Conditions in Dimensionless Form

The resulting six dimensionless ODEs are then solved for a variety of different energy dissipation rates (Engulfment rates) by a fixed step Runge-Kutta method. Notice how only the equation for the dimethoxypropane in the acid rich mixing zone (D_{Bm}) depends on the engulfment rate – all other equations are independent of the engulfment rate (mixing) in dimensionless time.

6 Micromixing Reaction Models - Results and Discussion

The main objective of the implementation of a mixing model was to convert the fractional conversion, which in the literature is often assumed to be proportional to the mixing time, to an estimated absolute mixing time. Such a model would have to agree qualitatively with the experimental observations of the influence of local concentration on fractional conversion as outlined in Chapter 7.

6.1 IEM results

Figure 6.1 to Figure 6.4 show the dimensionless concentration profiles averaged over the whole volume as a fraction of the initial average concentration of acid at 1:1 (i.e. 100 mmol/L) for volumetric flow ratios of 1:1, 3:1, 1:3 and 10:1 as a function of dimensionless time (t/t_{μ}) when mixing occurs with a characteristic time (t_{μ}) of 100ms. Expressing the concentration in this manner means that reduction of the dimensionless concentration from its initial value (1.0) is entirely due to reaction. If mixing was perfect, and there was no segregation, then the neutralisation reaction would dominate and the DMP would not react resulting in a final dimensionless DMP concentration of 1. The main advantage of formulating the concentrations in this way is that the acid concentration profile can now be considered an indicator of mixing completion from complete segregation (dimensionless concentration of 1) to perfectly mixed (dimensionless concentration of 0).

The alkali is in slight excess in the resulting mixture. This results in some residual base upon completion of the neutralisation reaction which is a requirement to terminate the DMP reaction upon conclusion of the mixing.

Considering first the 1:1 volumetric flow ratio (Figure 6.1). The concentrations decrease with time from their initial values. This reduction is caused entirely by reaction due to the dimensionless concentration being formulated as a volume average. The fractional conversion of the slow reaction is also plotted and for these conditions it levels out at about 0.6. After the depletion of acid at around a dimensionless time of 4 the slow reaction terminates and so the concentrations of DMP and alkali stabilise at this point.

The dimensionless concentration profiles for 3:1 (Figure 6.2), 1:3 (Figure 6.3) and 10:1 (Figure 6.4) all with a characteristic mixing time of 100ms are also shown. Differences between these profiles represent the effect, as predicted by the IEM model, that local concentration will have on fractional conversion and are not representative of different characteristic mixing times. This highlights the importance of separating mixing and concentration effects if a fair comparison is to be made between fractional conversion and mixing time.

Figure 6.5 shows how the Damköhler number (mixing time divided by reaction time – see equations (4.1) and (4.2) for the definition of reaction time) influences the fractional conversion at flow ratios of 1:1, 3:1, 1:3 and 10:1 if modelled according to the IEM model. As the characteristic reaction time is constant, a higher Damköhler number represents poorer mixing and poorer mixing means more segregation and more opportunity for the slow dimethoxypropane reaction to react in the acid zone and so a higher fractional conversion. This was expected.

The effect of volume fraction is also shown in Figure 6.5. This represents the weakness of the IEM model, as will be demonstrated in Chapter 7, it does not deal effectively with deviations from 1:1 mixing ratios.[85] In the IEM model the whole volume is a reaction volume, therefore it underestimates segregation effects at flow ratios that deviate from about 1:1. This only manifests itself at moderate to high Damköhler numbers (poor mixing) where it significantly overestimates how big the reaction volume is resulting in the model predicting significantly reduced fractional conversion in flow schemes when the acid is concentrated and increased fractional conversion when the alkali is concentrated. This is due to the relative volume fractions, which in the IEM model is the same as the reaction zones. Concentrating the acid makes most of the reaction volume basic which suppresses the DMP reaction as it is confined to the acidic zone. Concentrating the alkali stream has the opposite effect.

The asymptotical value at poor mixing is influenced by the excess of alkali (Figure 6.6). A greater excess of alkali results in a lower fractional conversion, which is expected as it would preferentially react with the acid reducing the amount available to catalyse the DMP. This highlights an important source of error that could be present in the experimental data. The excess of alkali is set to 5%, this is largely

an insurance to ensure residual basicity upon mixing and to make sure that the DMP reaction terminates after mixing completes. However, as the fractional conversion is very sensitive to the alkali excess it is important that the flow ratio is controlled tightly. The flow ratio was not allowed to vary from the target by more than 1% in any of the experiments.

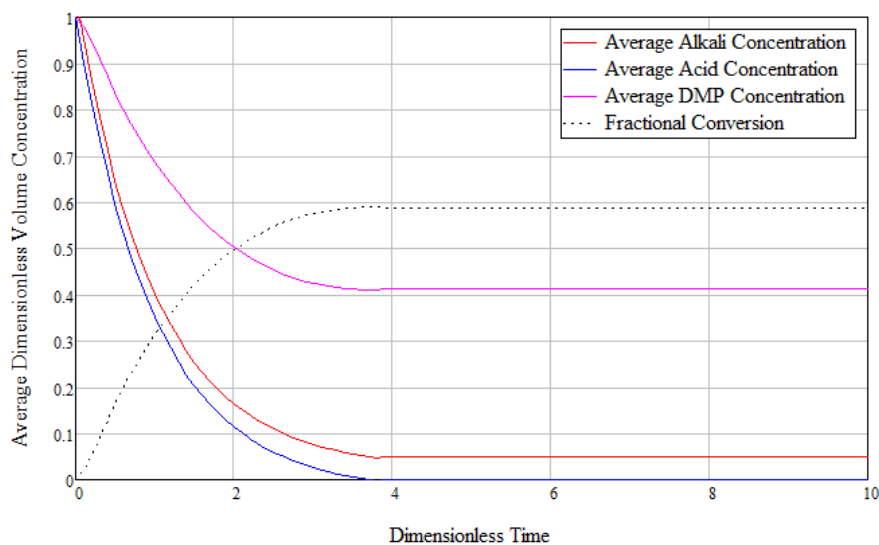


Figure 6.1. Dimensionless concentration at 1:1 volume ratio and 100ms mixing time

Concentration profile of reactant species as a functions of dimensionless time (t/t_μ) at a 1:1 volume ratio and a characteristic mixing time (t_μ) of 100ms. The acid concentration reduces to zero, the system remains basic upon exhaustion of the acid and the DMP is the only reactant species whose final concentration is dependent upon the mixing time. This calculation is repeated for many different characteristic mixing times to determine the fractional conversion associated with a range of characteristic mixing times.

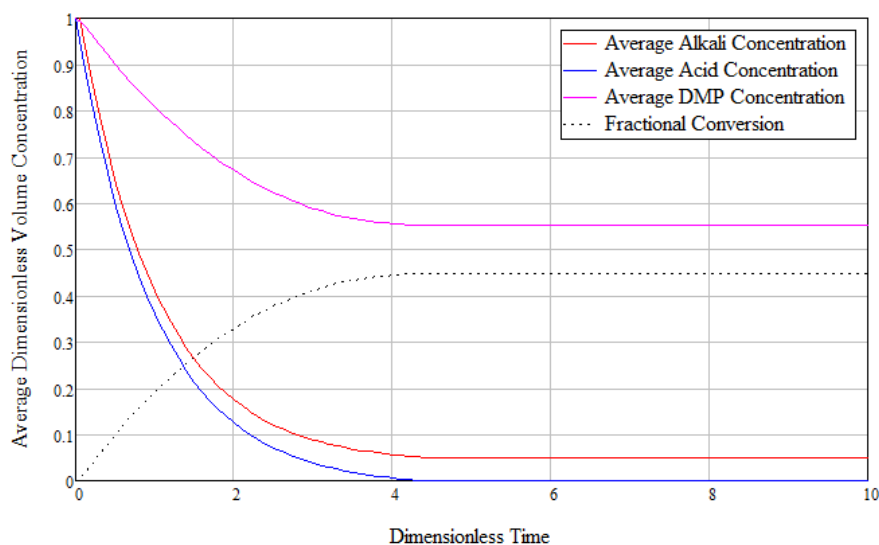


Figure 6.2. Dimensionless concentration at 3:1 volume ratio and 100ms mixing time

Concentration profile of reactant species as a functions of dimensionless time (t/t_μ) at a 3:1 volume ratio and a characteristic mixing time (t_μ) of 100ms. The acid concentration reduces to zero, the system remains basic upon exhaustion of the acid and the DMP is the only reactant species whose final concentration is dependent upon the mixing time. This calculation is repeated for many different characteristic mixing times to determine the fractional conversion associated with a range of characteristic mixing times.

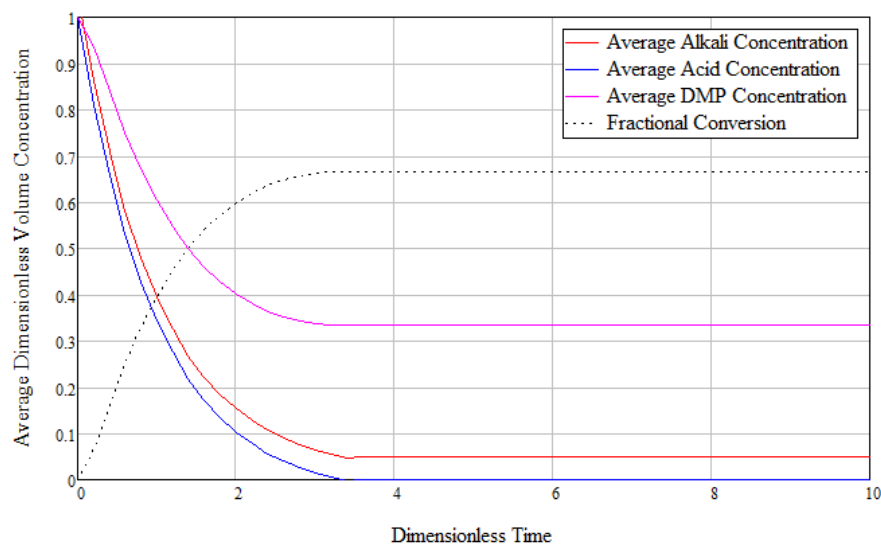


Figure 6.3. Dimensionless concentration at 1:3 volume ratio and 100ms mixing time

Concentration profile of reactant species as a functions of dimensionless time (t/t_μ) at a 1:3 volume ratio and a characteristic mixing time (t_μ) of 100ms. The acid concentration reduces to zero, the system remains basic upon exhaustion of the acid and the DMP is the only reactant species whose final concentration is dependent upon the mixing time. This calculation is repeated for many different characteristic mixing times to determine the fractional conversion associated with a range of characteristic mixing times.

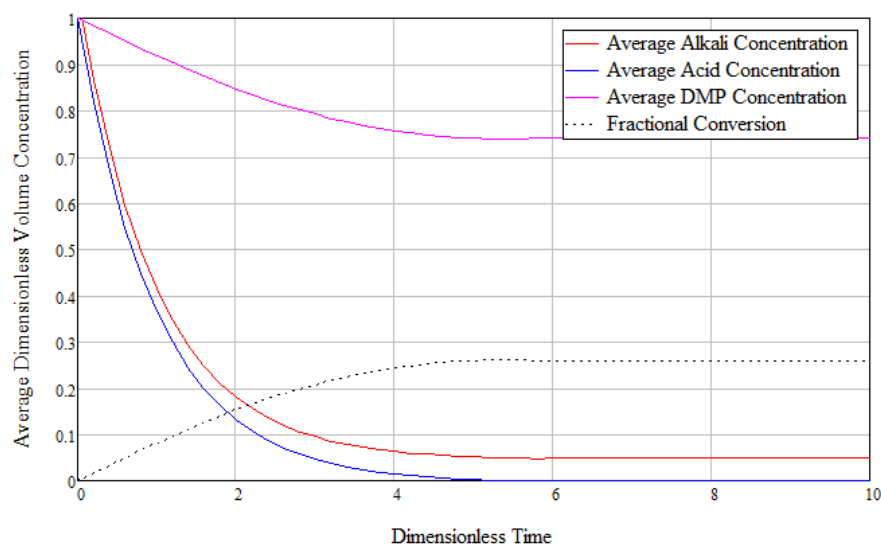


Figure 6.4. Dimensionless concentration at 10:1 Volume Ratio and 100ms mixing time

Concentration profile of reactant species as a functions of dimensionless time (t/t_μ) at a 10:1 volume ratio and a characteristic mixing time (t_μ) of 100ms. The acid concentration reduces to zero, the system remains basic upon exhaustion of the acid and the DMP is the only reactant species whose final concentration is dependent upon the mixing time. This calculation is repeated for many different characteristic mixing times to determine the fractional conversion associated with a range of characteristic mixing times.

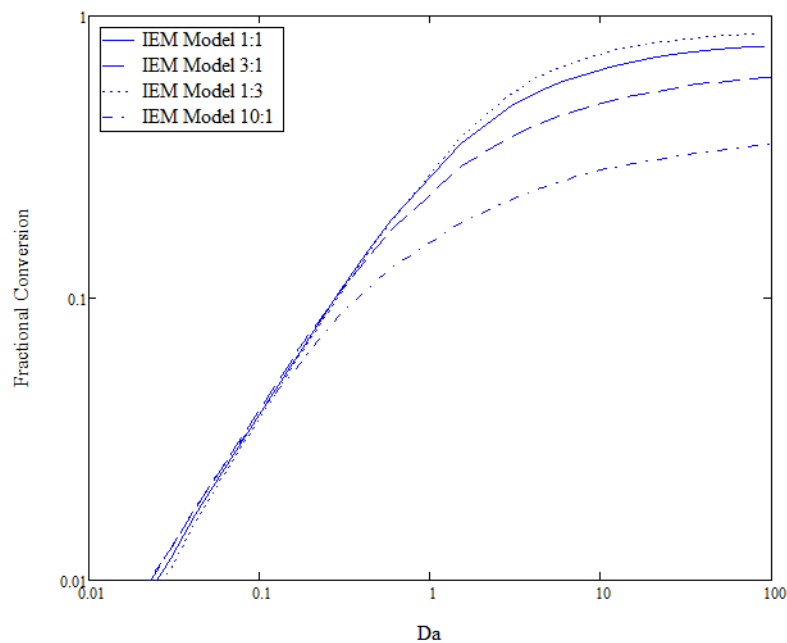


Figure 6.5. Fractional conversion vs. Damköhler number for different flow ratios

The Damköhler number is defined as t_H/t_r , the characteristic reaction time in all cases is 16.7ms and was evaluated using equations 4.1 and 4.2. A larger Damköhler number represents poorer mixing.

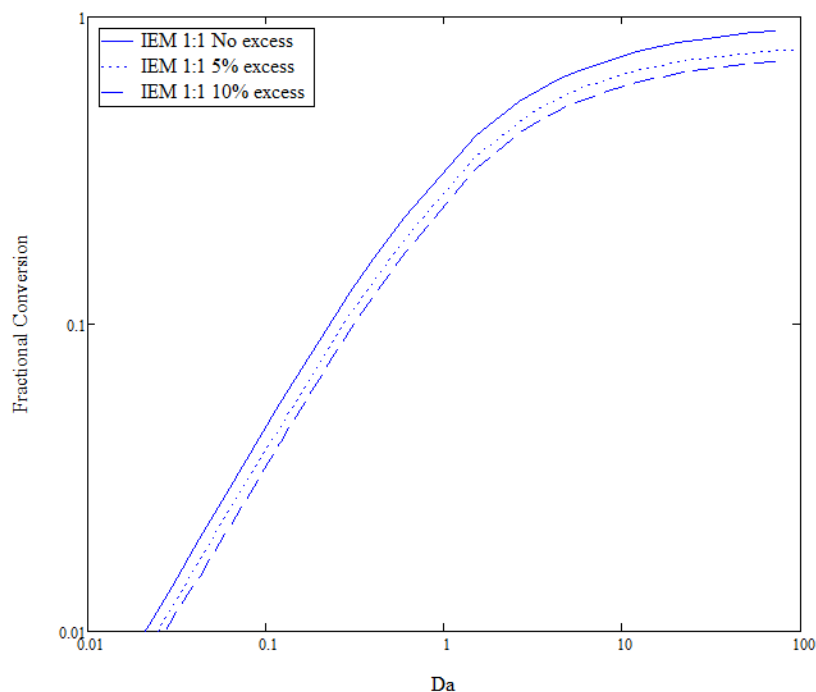


Figure 6.6. Fractional conversion vs. Damköhler number for different excess alkali

The Damköhler number is defined as t_H/t_r , the characteristic reaction time in all cases is 16.7ms and was evaluated using equations 4.1 and 4.2. A larger Damköhler number represents poorer mixing.

6.2 Comparable volume engulfment results

The reactant profiles are shown for 1:1 (Figure 6.7), 3:1 (Figure 6.8), 1:3 (Figure 6.9) and 10:1 (Figure 6.10) flow ratios (alkali:acid) and an energy dissipation rate of 1 W/kg (and engulfment time of around 24ms in this system, as defined by equation (2.7)). The concentration of acid, alkali and DMP are expressed as a fraction of the initial amount of acid and averaged through the whole volume. These are shown as a function of dimensionless time. The volume fraction of the alkali rich zone (B_m), the volume fraction of the acid rich zone (A_m) and the fractional conversion are also shown on the profiles.

The alkali is in 5% excess therefore as a fraction of the acid concentration the starting value of alkali is 1.05. The amount of DMP is equal to the amount of acid therefore both the acid and the alkali have an initial dimensionless concentration of 1 (see Table 5.4). Presenting it in this way means that if mixing and no reaction occurred, the dimensionless concentrations of base, acid and DMP would be 1.05, 1 and 1 respectively. This is convenient as the neutralisation is instantaneous with respect to mixing and therefore the amount of acid left shows how complete the mixing is from 1 (not started) to 0 (complete).

Since the kinetics of the neutralisation reaction are limited only by the mixing, the profile of the acid and the base are controlled entirely by the energy dissipation rate which in turn controls the engulfment rate. Therefore, in dimensionless time, the profile of the acid and alkali is independent of the energy dissipation rate (obviously, the energy dissipation rate controls how time is converted to dimensionless time so it is still dependent in real time). In dimensionless time, only the DMP concentration profile is sensitive to mixing (see Chapter 5.3). It takes one engulfment time for the mixing zones to be established, which is why the reaction profiles (Figure 6.7-Figure 6.10) begin after 1 engulfment (see section 5.3).

Due to the excess of base, two things happen. Firstly, the amount of base levels out at 0.05 (5% excess). Secondly, the residual base causes the entire volume to become alkali rich therefore the volume fraction of the alkali rich region (B_m) tends to 1 with the acid rich region (A_m) tending to 0 unlike in the IEM model where the volumes are fixed.

Figure 6.7 shows the profile of the reactant species at a 1:1 volumetric flow ratio and an energy dissipation rate of 1 W/kg. Notice how the volume fractions A_m and B_m are initially the same (see section 5.3) and both increase with time due to incorporation of the fresh feed. However, the alkali rich volume (B_m) increases at a quicker rate than the acid rich volume (A_m). This is due to the excess of alkali consuming part of the acid rich region and making it part of the alkali rich region (see section 5.3 with $P_e = 1$). At about 6 engulfments the rate of fresh feed incorporation is equal to the loss to the alkali rich zone and after this point the acid rich zone shrinks and the conversion of DMP begins to tail off. After 8 engulfments the mixing zone occupies the whole volume.

Also marked on the graphs is the mixing “half-life” (50% acid conversion) specified as a number of engulfments. This is useful because the characteristic reaction time of the slow reaction is also its half-life therefore it is sensible to use a Damköhler number that compares the half-lives of both mixing and reaction. The mixing half-life can be specified because, as mentioned earlier, the reactants are quantified in such a way that the deviation from the initial value is entirely due to reaction and the kinetics of the fast reaction are dependent upon the mixing alone. As the reactant profiles of the acid and alkali are the same in dimensionless time, regardless of the energy the dissipation rate, then the value extracted is a constant number of engulfments required to progress the mixing to 50% completion. It should also be remembered that the mixing process requires 1 engulfment time to initialise (see section 5.3), which explains why the graphs start at 1. This can then be converted to a real time by the relationship between the engulfment time and the energy dissipation rate. Similarly, the value at 90% mixed is also marked.

Changing the flow ratios changes the local concentrations and the initial starting conditions used to solve the equations. This is apparent in the subsequent graphs corresponding to 3:1 (Figure 6.8), 1:3 (Figure 6.9) and 10:1 (Figure 6.10). The initial conditions are tabulated in Table 5.4.

At 3:1 (Figure 6.8) initially the volume fraction of the acid zone is less than the volume fraction of the alkali zone and again both rise due to fresh feed incorporation. However, this time the acid rich zone grows quicker than the alkali rich zone due to the high concentration of acid (see section 5.3 with $P_e = -1$). This is accompanied by

a rapid reduction in the amount of DMP as both the expanding reaction zone and higher concentrations are favourable for the slow reaction. This continues until about 4 engulfments when the concentrations equalise and P_e switches from predominately -1 to predominantly 1 due the alkali excess and then the alkali zone begins grow at the expense of the acid zone. This reduces the rate of the slow reaction but it continues steadily until the rate of fresh feed incorporation of acid is equal to the rate of loss to the alkali rich zone at the maximum at about 6 engulfments, the mixing zone occupies the whole volume after 8 engulfments and then both the acid volume fraction the rate of the slow reaction drop off to zero. The mixing half-life occurs at about 6 engulfments.

The opposite happens when the alkali stream is concentrated (Figure 6.3). This means that the initial volume fraction of the acid rich zone (A_m) is greater than the alkali rich zone (B_m) (see Table 5.4). This concentrated alkali zone ensures that the alkali zone increases rapidly in the initial stages which prevents any DMP finding its way into the acid rich zone until about 4 engulfments and therefore there is no conversion of the DMP. After 4 engulfments the concentrations begin to equalise and so the P_e can switch between -1 and 1. At this point both zones are still growing but with the alkali zone growing faster due to the slight excess of alkali before the acid zone reaches its maximum due to the balance between fresh feed incorporation and loss to the alkali zone at about 6 engulfments which slows the rate of the reaction of the DMP. Interestingly, the difference between fractional conversion at 3:1 and 1:3 is due to the local concentrations and reaction volumes, it is not a reflection on the mixing differences. This is reflected in the fact the mixing half-life for 1:3 is the same as at 3:1 – 6 engulfments. This illustrates the importance of deploying a model that correctly handles local concentration issues.

The 10:1 scheme is just like a more extreme version of the 3:1 scheme explained above. The mixing half-life is about 7 engulfments.

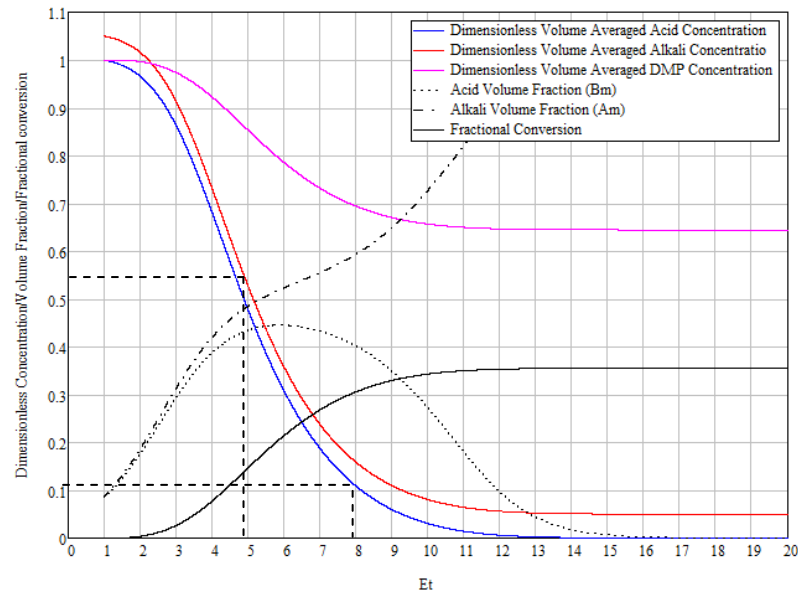


Figure 6.7. Profile for the engulfment model at 1:1 volume ratio

Energy dissipation rate is equal to 1 W/kg. Values of dimensionless volume at $Et=1$ are equal to 0.0866 for the alkali and 0.0866 for the acid (see chapter 5.3 for details). Dimensionless acid and alkali concentrations are dependent only on the dimensionless time (Et) but the DMP concentration is also dependent on the energy dissipation rate. Establishment of the mixing zone takes $1E$, which explains why $1 Et$ represents the initial value (see chapter 5.3 for details).

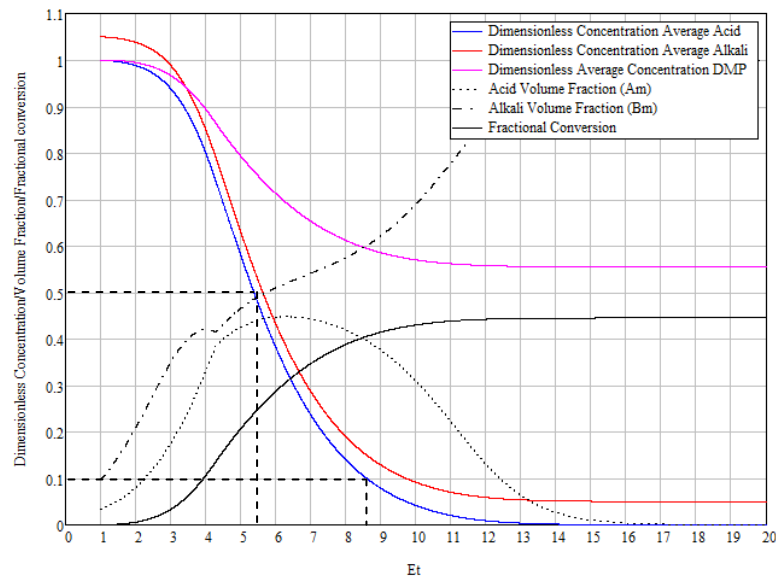


Figure 6.8. Profile for the engulfment model at 3:1 volume ratio

Energy dissipation rate is equal to 1 W/kg. Values of dimensionless volume at $Et=1$ are equal to 0.0975 for the alkali and 0.0325 for the acid (see chapter 5.3 for details). Dimensionless acid and alkali concentrations are dependent only on the dimensionless time (Et) but the DMP concentration is also dependent on the energy dissipation rate. Establishment of the mixing zone takes $1E$, which explains why $1 Et$ represents the initial value (see chapter 5.3 for details).

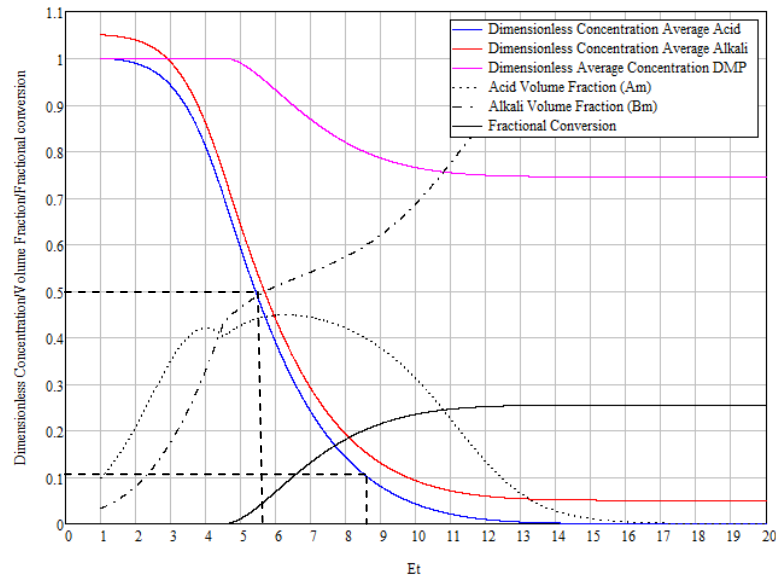


Figure 6.9. Profile for the engulfment model at 1:3 volume ratio

Energy dissipation rate is equal to 1 W/kg. Values of dimensionless volume at $Et=1$ are equal to 0.0325 for the alkali and 0.0975 for the acid (see chapter 5.3 for details). Dimensionless acid and alkali concentrations are dependent only on the dimensionless time (Et) but the DMP concentration is also dependent on the energy dissipation rate. Establishment of the mixing zone takes 1E, which explains why 1 Et represents the initial value (see chapter 5.3 for details).

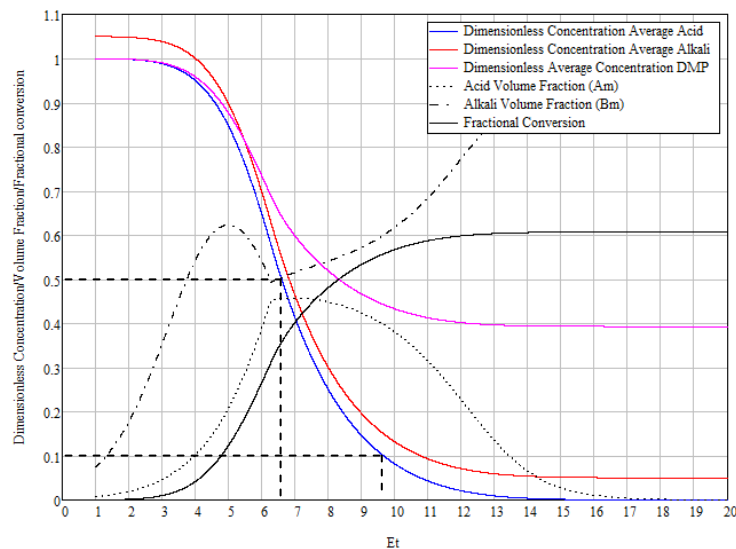


Figure 6.10. Profile for the engulfment model at 10:1 volume ratio

Energy dissipation rate is equal to 1 W/kg. Values of dimensionless volume at $Et=1$ are equal to 0.07513 for the alkali and 0.007513 for the acid (see chapter 5.3 for details). Dimensionless acid and alkali concentrations are dependent only on the dimensionless time (Et) but the DMP concentration is also dependent on the energy dissipation rate. Establishment of the mixing zone takes 1E, which explains why 1 Et represents the initial value (see chapter 5.3 for details).

Flow Ratio (Alkali: Acid)	Number of Engulfments for 50% Mixed	Number of Engulfments for 90% Mixed
1:1 Volume Ratio	5	8
3:1 Volume Ratio	6	9
1:3 Volume Ratio	6	9
10:1 Volume Ratio	7	10

Table 6.1. Mixing Half-life Constants

N.B. the total number of engulfments is equal to the value from the reactant profiles above plus one. This is due to the engulfment model starting after 1 engulfment as described in section 5.3.

Calculating the above reactant profiles many times over a range of engulfment rates allows the fractional conversion as function of the Damköhler number to be plotted. This Damköhler number is expressed purely as a function of the engulfment rate (Figure 6.11), as a function of the Damköhler number standardised to equivalent mixing conditions using the mixing half-life (Figure 6.12) and as a function of the Damköhler number standardised to equivalent mixing conditions using 90% mixed times (Figure 6.13).

Let us consider, firstly, fractional conversion for flow ratios of 1:1, 3:1, 1:3 and 10:1 expressed purely as a function of the engulfment rate (Figure 6.11). Taking the acid concentration as being representative of mixing, this approach is unstandardised and provides unfair comparison between the different flow ratios. Measuring it in this way implies that the mixing time would be constant regardless of the flow ratios. Clearly this is not the case, the acid stream takes more engulfments to completely be depleted of acid as the flow deviates from 1:1. This is due to the reaction volume ($X_m = X_{bm} + X_{am}$) decreasing as the flowrate deviates from 1:1 (i.e. the mixing volume at 10:1 is less than that at 3:1 which is less than at 1:1 so the streams are more segregated). As the flowrate deviates further from 1:1 the mixing volume (X_m) decreases and therefore more engulfments are required to complete mixing. This is summarised nicely in Table 6.2. The number of half-lives taken increases with deviation from 1:1 flow ratio and the fractional conversion varies quite considerably.

Particularly interesting is the comparison between 3:1 and 1:3 flow ratios. If you take essentially the same fluids (reactant species are minor components) and mix in the same way with the same energy dissipation rate then the mixing would be identical. This is the case with mixing half-lives of 6 engulfments for both the 3:1 and 1:3 flow ratios. However, the fractional conversion between these conditions

varies considerably. This is a concentration effect and not a mixing effect. Clearly mixing has to be standardised to provide fair comparison and correct for bias caused by concentration and volume.

Flow Ratio (Alkali: Acid)	Fractional Conversion with $\varepsilon = 1$ W/kg	Number of Engulfments for 50% conversion
1:1 Volume Ratio	0.37	5
3:1 Volume Ratio	0.43	6
1:3 Volume Ratio	0.26	6
10:1 Volume Ratio	0.61	7

Table 6.2. Mixing half-life constants comparison of mixing times and engulfment times

The mixing half-life (50% conversion) constant has been used to standardise the mixing and smooth out concentration effects which should allow the conversion of the fractional conversion in the subsequent experiments to an estimated mixing time (Figure 6.12). This mixing time now corresponds to the same degree of mixedness after removing the volume effects that cause the mixing half-life to increase as the flow ratio becomes more extreme. Now, all that is left is the influence that concentration has on the fractional conversion. Considering Figure 6.12 it is apparent that concentrating the acid has increased the fractional conversion whilst concentrating the alkali has decreased the fractional conversion. This is the opposite effect to that predicted by the IEM (Chapter 6.1).

This reaction scheme has been modelled by Gillian and Kirwan for a 1:1 flow ratio using a comparable volume engulfment model.[40] These results were used as a benchmark to verify the successful implementation of the model at 1:1 flow ratio. Gillian and Kirwan extracted a constant to standardise mixing from a model which considered mixing without reaction to value of 95% completion. However, this choice of constant and indeed those utilised in this is arbitrary in nature work and just shifts the data left or right. The important point is the shape of the curve and the asymptotical value which is the same in both works as expected. When the same standardisation constant is used the conversion curves are the same, indicating the successful implementation at 1:1. The results are also shown for 90% complete mixing (Figure 6.13) which just shifts the conversion curves further to the right (i.e., higher Damköhler number).

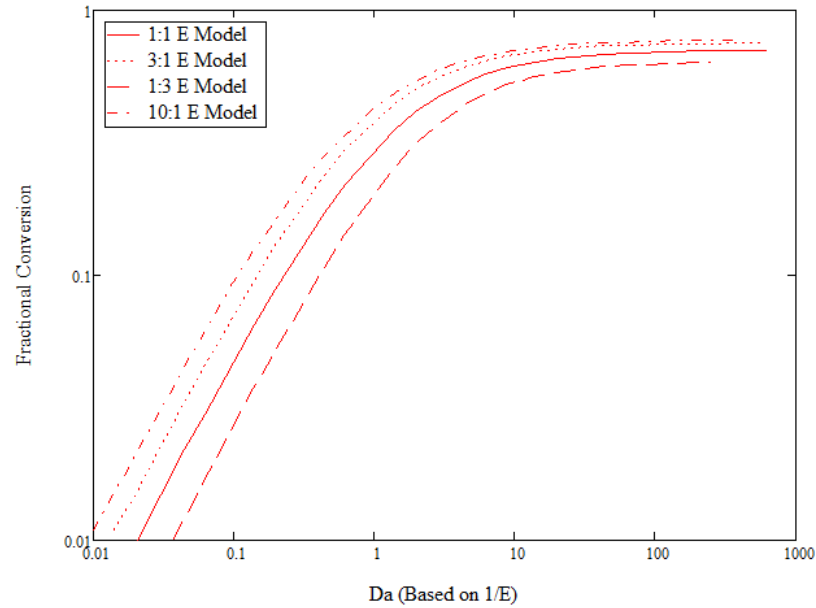


Figure 6.11. Fractional conversion vs. Da (engulfment)

An engulfment rate is chosen and the six ODEs are solved for that engulfment rate yielding a fractional conversion. This is repeated over a range of engulfment rates. Da based on one over the engulfment rate multiplied by the characteristic reaction time of the slow reaction ($1/(E \cdot \tau_R)$).

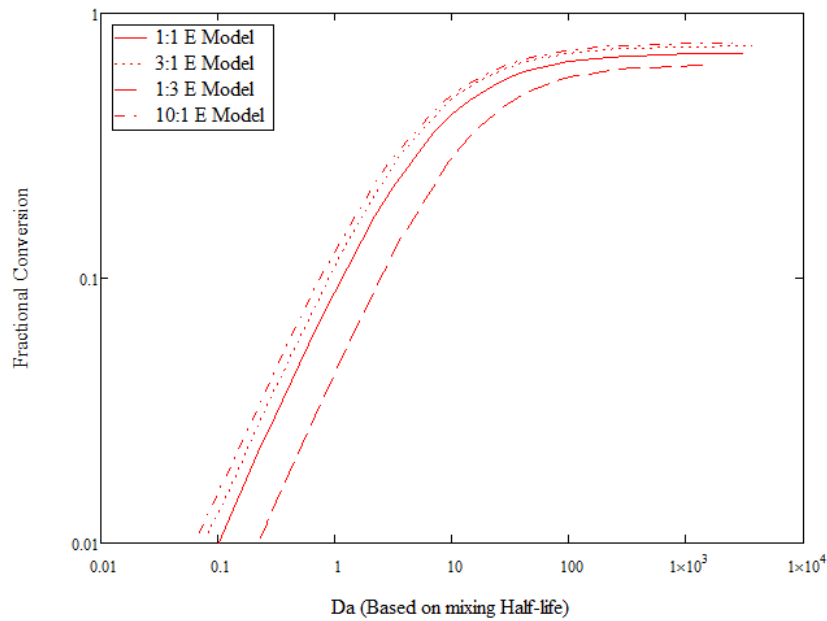


Figure 6.12. Fractional conversion vs. Da (Mixing half-life)

An engulfment rate is chosen and the six ODEs are solved for that engulfment rate yielding a value fractional conversion. This is repeated over a range of engulfment rates. Da is based on the mixing half-life which is one over engulfment rate multiplied by the half life constant and then divided by the characteristic reaction time of the slow reaction ($k_{\text{half-life}}/(E \cdot \tau_R)$).

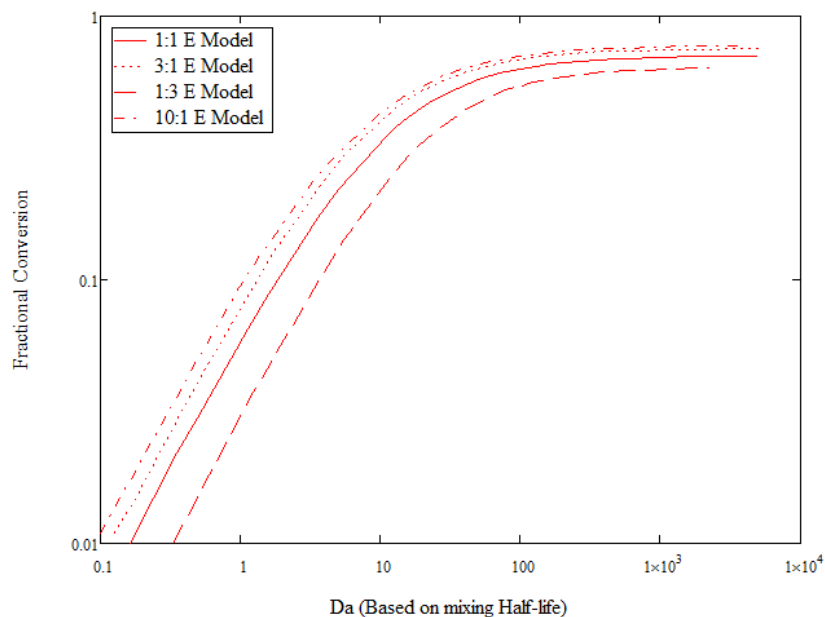


Figure 6.13. Fractional conversion vs. Da (90% mixed)

An engulfment rate is chosen and the six ODEs are solved for that engulfment rate yielding a value fractional conversion. This is repeated over a range of engulfment rates. Da is based on the mixing half-life which is one over engulfment rate multiplied by the half life constant and then divided by the characteristic reaction time of the slow reaction ($k_{90\%} / (E \cdot \tau_R)$).

The theoretical asymptotical value of fractional conversion under poor mixing conditions (high Damköhler number) for a parallel competitive reaction scheme with a catalysed second reaction is reported to be 1.0.[3] Figure 6.14 shows the influence of alkali excess on this asymptotical value. It is obvious from this that the theoretical value of 1.0 is only obtained when the acid and alkali are present in perfectly balanced stoichiometry. As the alkali excess concentration increases the asymptotical value of fractional conversion decreases.

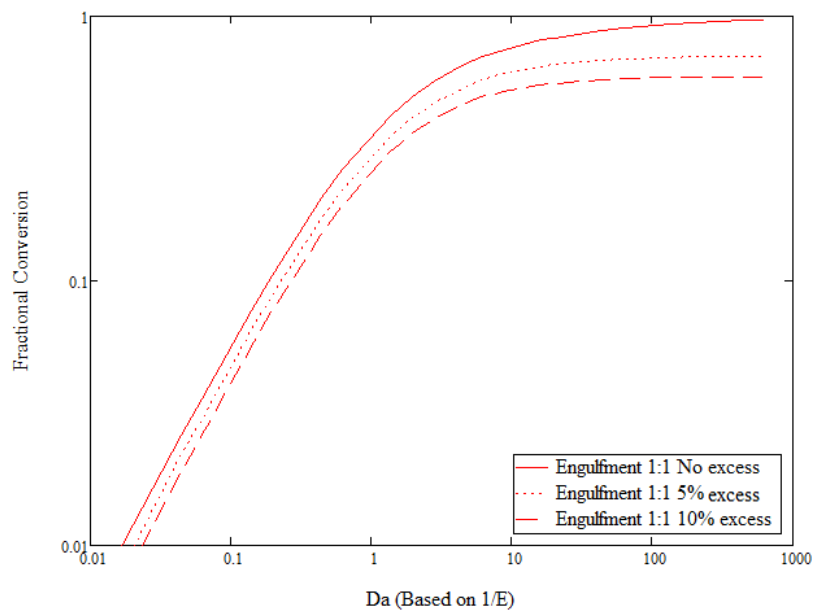


Figure 6.14. Fractional conversion vs. Da for various alkali excesses

Influence of alkali excess on the fractional conversion as a function of the Damköhler number defined as $1/(E \cdot \tau_R)$.

6.3 Comparison of the IEM and E-model results

The IEM model is adequately characterised by the characteristic mixing time (t_μ) alone, which was varied over a range of times and the corresponding equations solved which allowed the fractional conversion versus Damköhler number chart to be constructed over a range of Damköhler numbers for 1:1, 3:1, 1:3 and 10:1 flow ratios. This is adequate because in the IEM model the entire volume is the mixing volume and therefore the fast reaction is almost entirely unaffected by the volume effects. Therefore, as can be seen in section 6.1, if an analogous mixing constant defined by 50% acid consumption were to be extracted from the charts its value would be close to 1 in all instances. Therefore, the selected mixing time is assumed to be adequate in capturing the kinetics of the mixing process for the IEM model. The results of the engulfment model were shown both in its unadjusted form and the form corrected by the mixing half-life and these corresponding values of conversion were then compared with the IEM values (Figure 6.15 and Figure 6.16).

The absolute values are not considered important with regards to this comparison, as it is not immediately clear exactly what a fair way to standardise the

characteristic mixing times between both models would be. Instead, model quality will be judged qualitatively with respect to whether the model deals effectively with the volume ratio changes and how it compares in this respect to experimental observations, i.e. does it capture the essence of the observed phenomenology?

The volume ratio has a more dramatic effect on the fractional conversion of the IEM model than on the engulfment model. This is due to the reaction volumes in the IEM being fixed to their initial volumes whilst in the engulfment model the reaction volumes change with time, growing from an initially small volume. This means that using the IEM for the 1:3 system the acid volume (DMP hydrolysis reaction zone) is always $\frac{3}{4}$ s of the volume and it does not shrink with time, just gradually reduces in concentration until there is no acid left. Therefore in the 1:3 system the IEM model predicts a higher fractional conversion than that which would be obtained with the identical mixing time in the 3:1 system as in this system only $\frac{1}{4}$ of the volume is taken up by the acid volume.

With the engulfment model the reaction volumes grow with time but also concede volume to one another based on the local concentrations at each timestep. The net effect of this is acceleration of the DMP reaction in the 3:1 scheme due to the acid concentration and a delay in the start of the hydrolysis of the DMP in the 1:3 reaction due to the alkali concentration.

As shown in the experimental results section (Chapter 7) and summarised in Table 6.3 the engulfment model agrees with the phenomenology observed in the experimental data but the IEM model shows the opposite trend. In the experimental data, concentrating the alkali stream (1:3 volume) results in a lower fractional conversion than mixing in an identical way but with a concentrated acid stream (3:1 volume). Therefore, the engulfment model was chosen as the most appropriate model with which to analyse the experimental data, especially at flow ratios different from 1:1.

	Fractional conversion		
	IEM Model	Engulfment Model	Experimental Observation
3:1	Lower	Higher	Higher
1:3	Higher	Lower	Lower

Table 6.3. Influence of volume ratio on fractional conversion.

IEM and Engulfment model relative fractional conversions chosen by general observation. Experimental values chosen by comparing results at 3:1 and 1:3 in the same mixer operating with the same total energy dissipation rate which should result in an identical mixing time.

The IEM model is in good agreement with the results obtained using the E-model at 1:1 with respect to asymptotical value and shape. Therefore, considering there is some degree of uncertainty in the positioning of the curves on the horizontal axis it is proposed that the IEM model would also provide acceptable results at flow ratios close to 1:1.

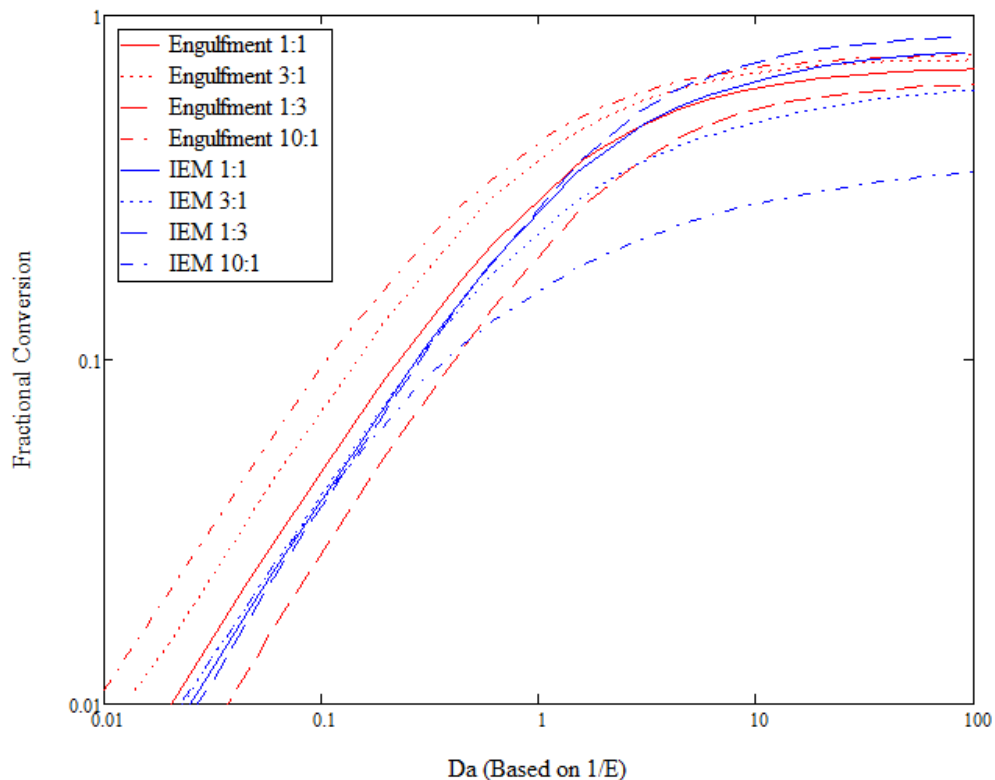


Figure 6.15. IEM model vs. engulfment time Damköhler number

The Damköhler number is defined as a mixing time divided characteristic reaction time (16.7 ms for the slow reaction). For the engulfment model the mixing time is defined by the uncorrected engulfment time ($1/E$). The IEM model just uses the characteristic time (t_p) which characterises mixing adequately as the IEM utilises the whole volume as a reaction zone and therefore the acid/base reaction is not influenced by the volume fractions.

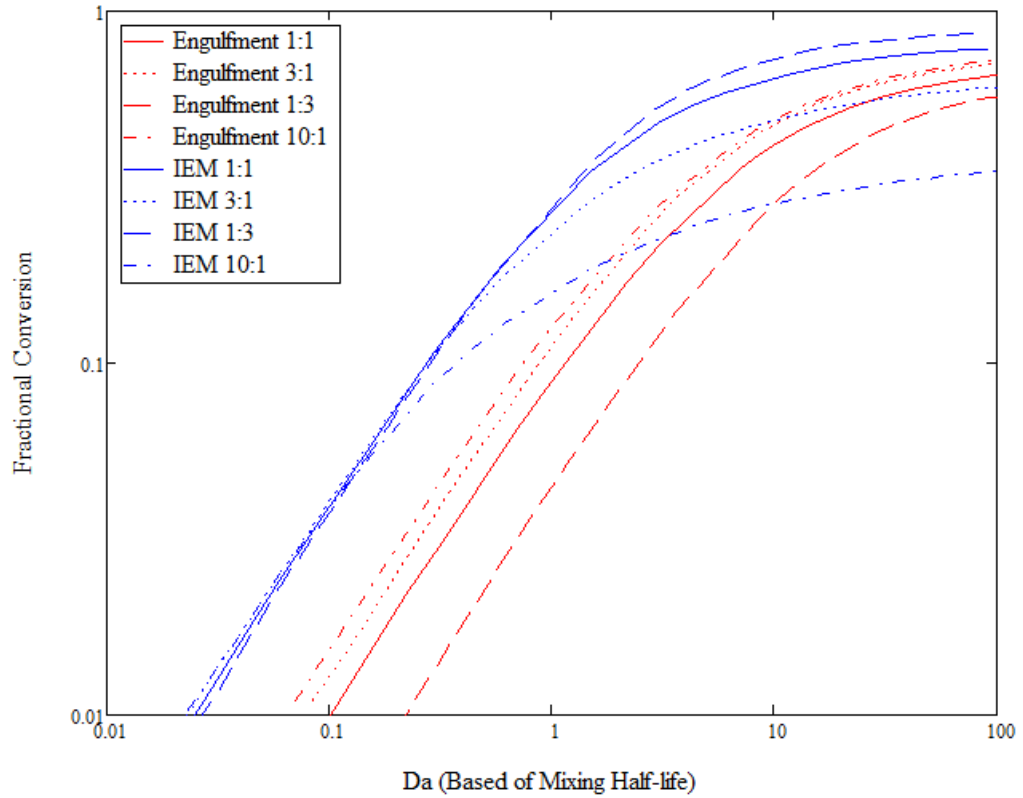


Figure 6.16. IEM model vs. mixing half-life Damköhler number

The Damköhler number is defined as a mixing time divided characteristic reaction (16.7ms for the slow reaction). For the engulfment model the mixing time is defined by using the mixing half-life constants to standardise mixing whilst the IEM model just uses the specified characteristic time (t_{μ}) which characterises mixing adequately as the IEM utilises the whole volume as a reaction zone and therefore the acid/base reaction is not influenced by the volume fractions.

6.4 Modelling conclusions

Two different models (IEM and Engulfment) have been utilised to model the fractional conversion of the acid catalysed hydrolysis of dimethoxypropane in competition for acid with a strong alkali and how mixing influences the product distribution.

These were deployed in order to gain an insight into the influence of local concentration on fractional conversion and to quantify with acceptable accuracy the link between the fractional conversion and a physical mixing time. The advantage of such models is that they have the potential to be implemented widely as they are formulated from material balances coupled with simple reaction kinetics and solved using standard numerical techniques. These are within in the grasp of the typical process engineer, unlike something like computational fluid dynamics (CFD) which undoubtedly provides significantly more insight but requires a high degree of specialism to implement effectively.

The engulfment model has been found here, as well as by other researchers[85], to agree qualitatively with experimental observations of how concentration and volume influence reaction rates and conversion but the IEM has been found to deal poorly with changes in the flow ratio. Therefore, the engulfment model was chosen as a model to analyse the experimental data with. The IEM model appears to provide acceptable results at flow ratios around 1:1 and considering its inherent simplicity it may even be a preferable formulation under those conditions.

The engulfment model has been standardised by way of a mixing half-life and 90% mixed time to ensure concentration effects are removed from the fractional conversion when it is translated to a mixing time and therefore a fair comparison between mixers operating under different flow ratios can be made, free from the concentration bias which influences the fractional conversion data.

7 Mixing Characterisation – Results and Discussion

The Bourne IV reaction scheme was utilised to carry out a comprehensive survey of various mixers including a confined impinging jet (CIJ) mixer, a vortex mixer and more conventional T and X mixers of different sizes ($\frac{1}{8}$ " and $\frac{1}{4}$ ") in a variety of different mixing conditions. This study encompasses how flowrate, flow ratio (expressed as acid stream to alkali stream) and viscosity interact to influence the fractional conversion (a parameter closely related to the mixing time) in these mixers and how this fractional conversion can be correlated and predicted.

The fractional conversion is then converted to an absolute mixing time using the theoretical treatment developed in Chapters 5 and 6. This enables further analysis including estimating a mixing efficiency in addition to making comparisons between the mixing time and the residence time which is useful in determining whether a mixer achieves solution homogeneity or not.

7.1 Relative mixing performance of various continuous mixers

7.1.1 Effect of flowrate and flow ratio

Figure 7.1 shows the fractional conversion of the slow reaction as function of the flowrate of alkali stream. For the smaller mixers (CIJ, vortex, $\frac{1}{8}$ " T and X), an increase in volumetric flowrate results in a decrease in the fractional conversion of the dimethoxypropane which indicates better mixing as would be expected. This decrease follows a power law relationship with inlet volumetric flowrate – this is indicated by a linear relationship on a log-log chart with a gradient equal to the exponent of the power law and the y-intercept equal to the prefactor.

The larger mixers ($\frac{1}{4}$ "X and $\frac{1}{4}$ "T) have a plateau region before entering a power law region indicative of mixing improvement with increasing flowrate, as would be expected with the onset of a turbulent mixing mechanism. The plateau could be caused by a laminar mixing mechanism. Assuming this, the onset of turbulent behaviour in these mixers is around an inlet flowrate of 200 ml/min.

At a flow ratio (alkali stream to acid stream) of 1:1 (black) there is surprisingly little difference in the mixing performance of the smaller mixers. The vortex mixer is the best but this small improvement in performance is unlikely to justify additional manufacturing complexity and fabrication costs in practical applications. In such circumstances it is likely that a T or X of similar size would give comparable mixing performance and would usually be the sensible choice due to the inherent simplicity of these devices. It is also unclear how the CIJ and vortex mixer should be directly compared with $\frac{1}{8}$ " mixers. They have a smaller inlet size but then enter into a mixing chamber of greater diameter. They have been grouped together on the basis of mixer performance rather than any geometrical based similarity. None the less, flowrate and mixer size control most of mixing process at 1:1, while all other parameters such as mixer internals/geometry have a weaker influence.

At a flow ratio of 3:1 (red) the story is similar to that of 1:1 (black). Similar sized mixers produce similar mixing performance for a given flowrate. As a function of alkali flowrate the mixing performance at 3:1 is worse than at 1:1, this is because at constant alkali inlet flowrate, the total flowrate at 3:1 is less as it is the acid stream that makes up the smaller stream.

The vortex mixer becomes substantially better than the other mixers at a flow ratio of 10:1 (blue). This is interesting as previously the mixing performance was controlled almost entirely by approximate inlet size and flowrate. The vortex mixer has demonstrable advantages in terms of more efficient mixing at flow ratios from somewhere between 3:1 and 10:1 and above and when coupled with the work undertaken by Lindenberg *et al* this estimate can be improved to between 5:1 and 10:1 and above.[38]

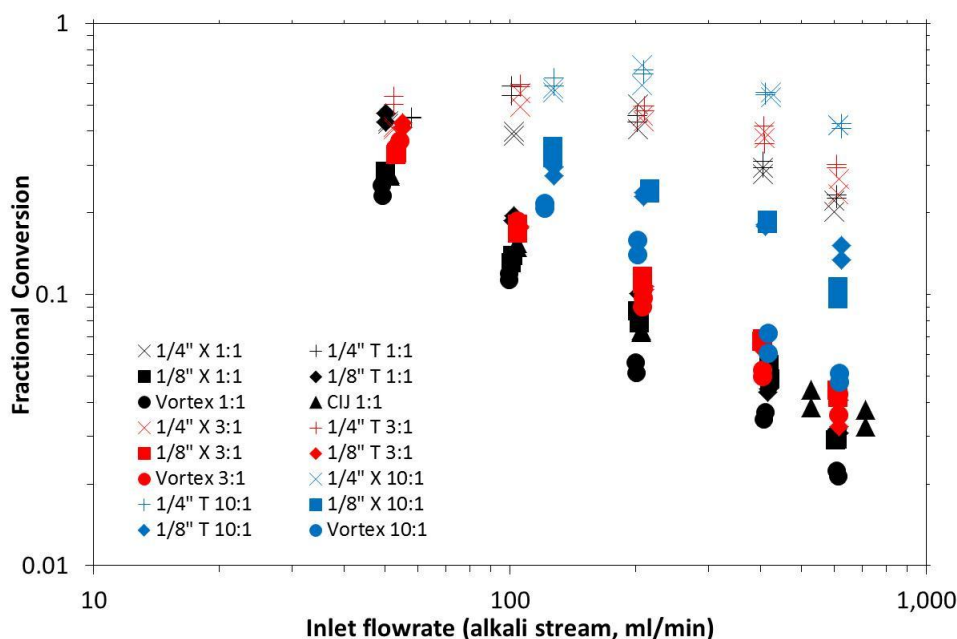


Figure 7.1. 1:1, 3:1 and 10:1 Inlet Volumetric Flow Ratio

The alkali inlet flowrate is the same regardless of the flow ratio as it is the acid flowrate that reduces as flow ratio deviates from 1:1 (except for the 1:3 ratio which for simplicity is not being considered until later in the chapter). Therefore, although the alkali stream inlet flow rate is the same across all flow ratios, the total flowrate is not the same and as result there is unlikely to be much in the way of correlation between different flow ratios. In other words, whilst alkali inlet flowrate may correlate well with the fractional conversion, it is due to a relationship with another parameter which fundamentally controls mixing.

Figure 7.2 shows the fractional conversion for all the mixers for flow ratio (alkali:acid) of 1:1 (black), 3:1 (red) and 10:1 (blue) as a function of the total flowrate through the mixer. Interestingly, the performance at 1:1 (black) and 3:1 (red) seem to correlate well with the total flowrate for both the larger mixers (black and red plateau and then power law region) and the smaller mixers. However, comparing just on the basis of fractional conversion may not allow for fair comparison as concentration effects are neglected (see below).

As the flowrate deviates further from 1:1, the vortex mixer provides better performance with respect to other mixers. At 10:1 the vortex mixer has broken from the pack and holds its performance as a function of total volumetric flowrate whilst other mixers provide poorer performance.

When comparing the 1/4" and 1/8" mixers, again very different behaviour is observed. Clearly, something other than volumetric flowrate will have to be used in order to explain the change of mixing times that happens with different mixers, flow ratios and different flowrates.

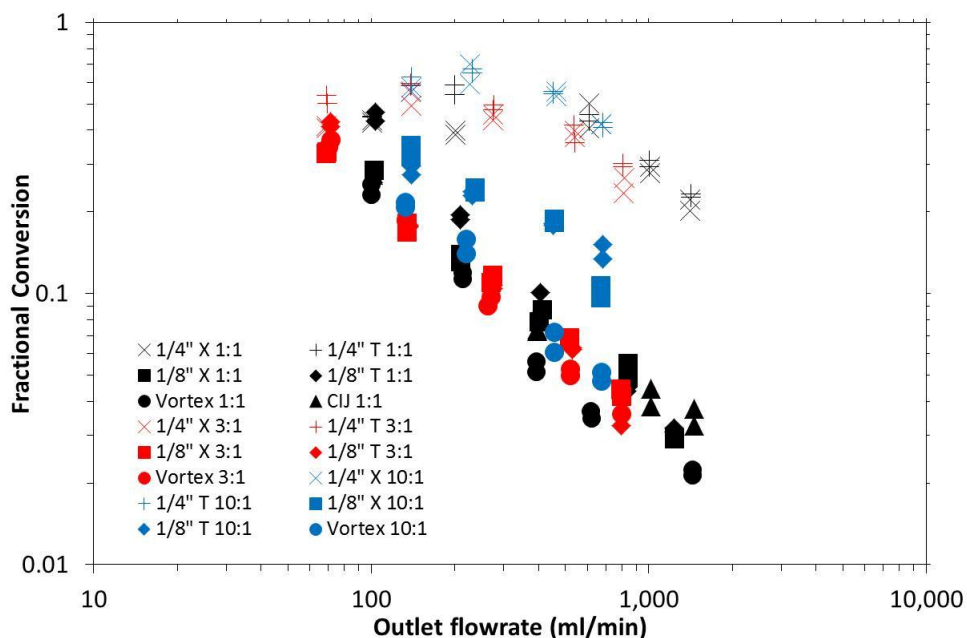


Figure 7.2. 1:1, 3:1 and 10:1 Total Volumetric Flow Ratio

It would be sensible to think that there may be some degree of correlation between the mixers and the inlet velocity due to the dependence of kinetic energy on velocity and its widespread application in the literature. Again there is good correlation for individual mixers (Figure 7.3) but there is poor correlation between mixers of different size (CIJ and Vortex, vs. 1/8"X and 1/8"T vs. 1/4"X and 1/4"T). Therefore, one could easily use velocity when estimating how flowrate would be likely to change mixing time, but little can be predicated from this about mixers of different sizes (scaling), different flow ratios or different geometries.

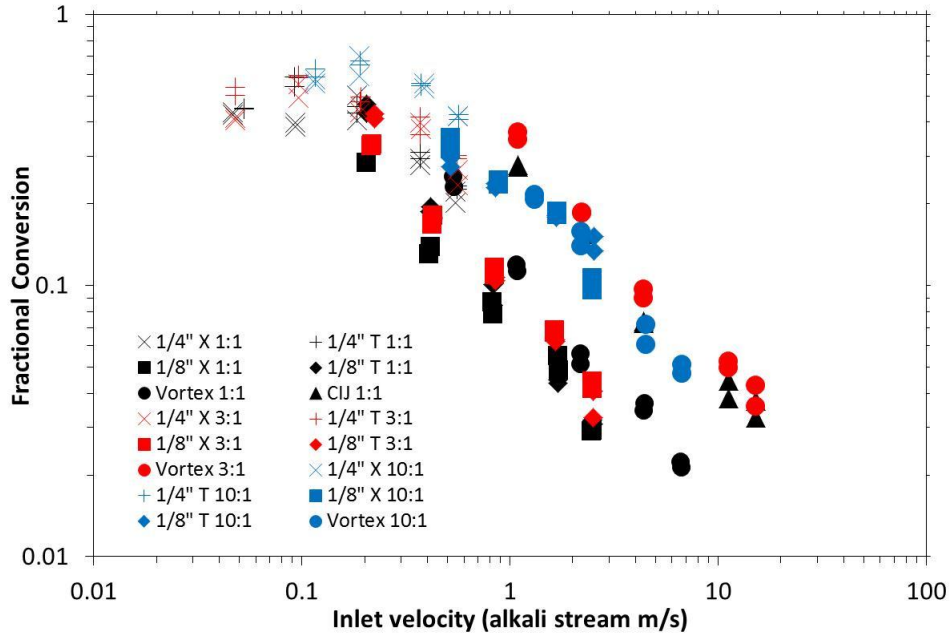


Figure 7.3. Fractional Conversion vs. Alkali Stream Inlet Velocity.

Obviously, the fundamental variable controlling mixing is the local energy dissipation rate in the fluid bulk. This is not possible to measure directly. However, it is possible to measure the pressure drop over the mixer and from this calculate the total energy dissipation rate. Assuming there is a strong relationship between this total energy dissipation rate and the local energy dissipation rate utilised for mixing then there should be a strong correlation between total energy dissipation and mixing time and hence fractional conversion.

7.2 Total energy dissipation rate

The total energy dissipation rate can be calculated from an energy balance over the mass of fluid that occupies the mixer volume. Energy is lost through a variety of processes such as friction with surfaces and boundary layers as well as “mixing processes” which consume energy but do not contribute to the reduction of concentration fluctuations, e.g., self-engulfment.[40], [72] It has been assumed that the energy dissipation rate that is utilised for mixing is a fraction of the total energy dissipation rate:

$$\mathcal{E}_{mixing} = C\mathcal{E}_{total} \quad (7.1)$$

The fraction accounts for energy lost to non-mixing processes and could be expected to be different for each mixer and each flow ratio etc. This fraction has been estimated to be of the order of 1% [40], [86]. If this relationship holds then one would expect the following:

$$\tau_m = f(\varepsilon_{mixing}) \quad (7.2)$$

$$\therefore \tau_m = f(\varepsilon_{total}) \quad (7.3)$$

$$X = f(\tau_m) \quad (7.4)$$

$$\therefore X = f(\varepsilon_{total}) \quad (7.5)$$

Therefore, assuming the above relationship holds, the total energy dissipation rate which can be experimentally obtained should correlate with the fractional conversion and mixing time and it should be better than the inlet flowrate, total flowrate or velocity when comparing between mixers and flow ratios. The above assumption has been tested and the relationship between flowrate/velocity and energy dissipation rate has also been considered.

An example of how the total energy dissipation rate was calculated is shown in section 4.1.5. The method was taken from the mechanical energy balance approach of Siddiqui *et al.* [36]

7.2.1 Correlation with energy dissipation rate

The total energy dissipation rate is an effective means to correlate the fractional conversion. Figure 7.4 shows the dependence of fractional conversion on the energy dissipation rate of various mixers at a flow ratio of 1:1 (black), 3:1 (red) and 10:1 (blue) but with the same compositions (25% ethanol) and hence similar physical properties in both mixing streams.

Equal volumetric flow ratio (1:1 – black) correlates well with energy dissipation rate. The vortex mixer (black circles) is possibly slightly below the others but considering an average error of around ± 0.03 ranging from about ± 0.07 at low flowrates to about ± 0.01 at high flowrates it is not significant.

At 3:1 all the mixers correlate with total energy dissipation rate and interestingly they also correlate with the mixers at 1:1. However, this does not yet take into effect the influence of local concentrations on fractional conversion.

At 10:1 there are two categories of mixers. The vortex mixer (blue circles) deviates from the other mixers and approaches the performance as a function of the energy dissipation rate of the other mixers at 1:1 and 3:1. This is interesting as previously it seemed that energy dissipation rate was the parameter with the strongest influence on mixing, all other parameters (geometry, inlet diameter, velocity etc.) had little or no impact. The vortex mixer is a superior mixer than the other mixers at a ratio of 10:1, it appears that it translates a higher fraction of its total energy dissipation into mixing than the other mixers. The vortex mixer at 10:1 is slightly off the curve of the mixers at 1:1 and 3:1.

There is also good agreement between the same mixers of a different size. The plateau region of the 1/4" mixers leads into a power region which overlaps with the lower end of the power law region of the smaller mixers (1/8").

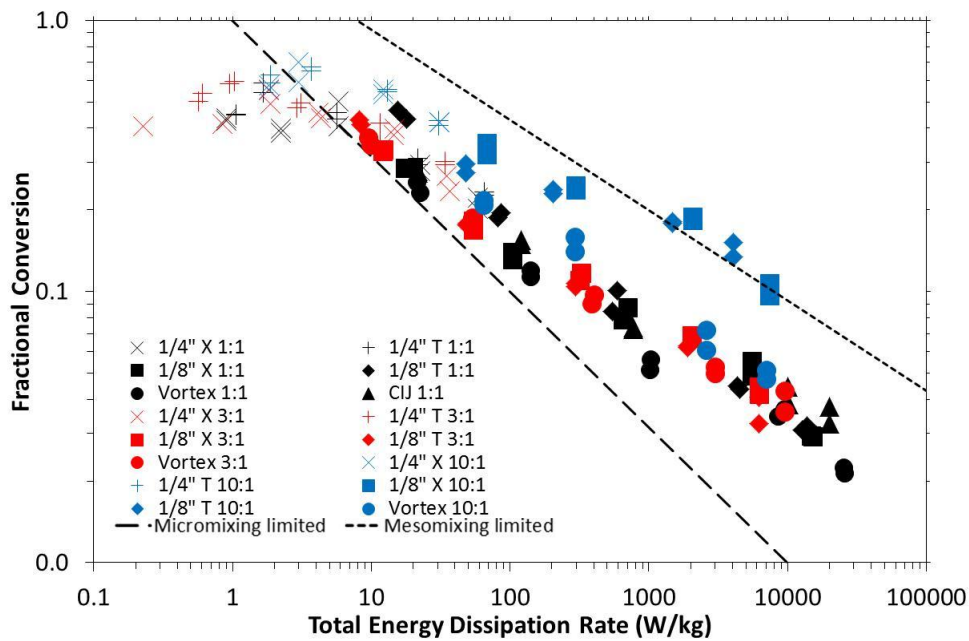


Figure 7.4. Fractional conversion vs. energy dissipation rate

1:1 (black), 3:1 (red) and 10:1 (blue) mixing in a 25% by weight ethanol stream

A least squares fit can be carried out to determine the gradient (exponent) and y-intercept (prefactor) that best fits the data to a power law. The power law prefactors (K), exponents (X) and coefficients of determination (R^2) for the global minima of the data fits are shown below (Table 7.1).

When fitted to a mixing time the exponents should indicate something about the mixing process, i.e. whether it is mesomixing or micromixing limited (or even

somewhere in between). A gradient of -0.5 is indicative of micromixing limited behaviour whilst a gradient of -0.33 indicates mesomixing limited behaviour. A gradient between the two indicates that both processes are significant and the process is best described by a model that considers both elements (e.g. a Corrsin style model).

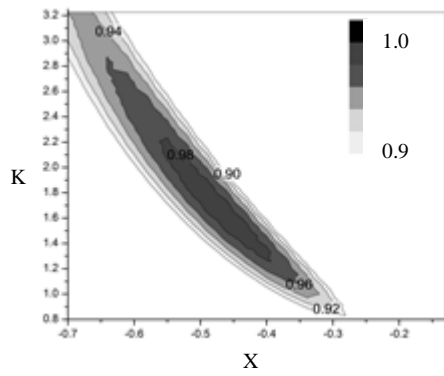
When fitted to the fractional conversion the relationship between fractional conversion and mixing time has to be considered. Ignoring this momentarily, the global minimum of the fit is summarised below:

$Y=K\varepsilon^X$	$\frac{1}{8}''$ X	$\frac{1}{8}''$ T	Vortex	CIJ
1:1 B				
K	0.771	1.656	0.748	0.772
X	-0.349	-0.468	-0.369	-0.337
R ²	0.993	0.997	0.997	0.998
3:1 B				
K	0.745	0.977	0.796	-
X	-0.335	-0.405	-0.355	-
R ²	0.994	0.995	0.998	-
10:1 B				
K	0.837	0.506	0.753	-
X	-0.216	-0.147	-0.299	-
R ²	0.977	0.987	0.99	-

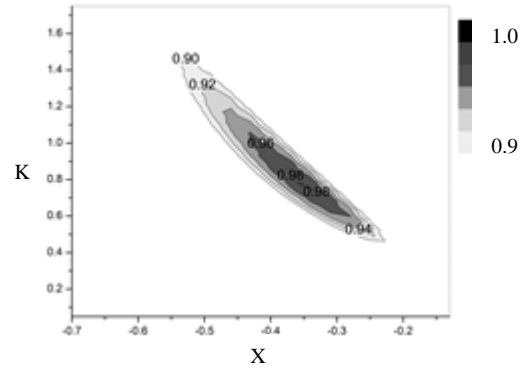
Table 7.1. Power law fit of fractional conversion and energy dissipation rate

A problem inherent in regression is that although it is straightforward to determine a “best fit” and the corresponding exponent and prefactor, this can be misleading. There is likely to be a range of X and K values which combine over a two dimensional parameter space and result in a good fit.

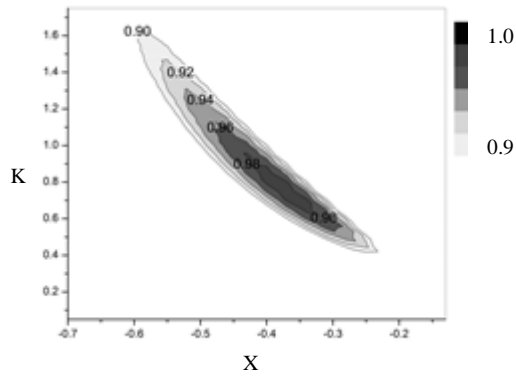
To consider the joint dependency of these values, regression ellipse plots were constructed by creating a 2D space from about 1000 points over a range of K and X values around the global minimum values. A fit of these 1000 points to the data for each mixer and flow ratio results in a coefficient of determination for each point. The ellipse plot simply shows the range of values where the K-X space has a coefficient of determination that is greater than or equal to 0.9 (i.e. a region with reasonable fit, not just the point corresponding to the global minimum). These plots are shown in Figure 7.5.



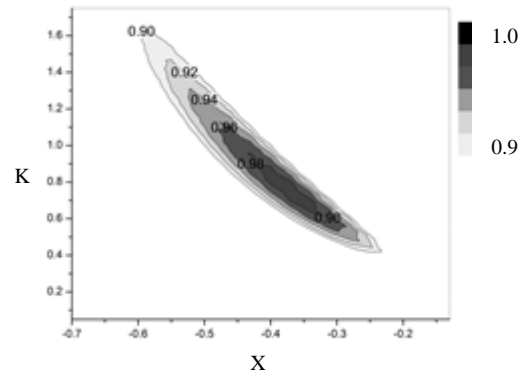
a) 1/8" T 1:1 Bourne



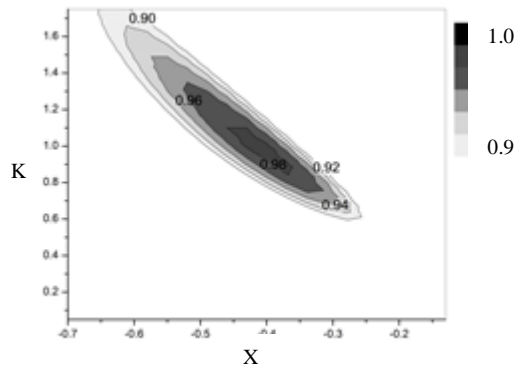
b) 1/8" X 1:1 Bourne



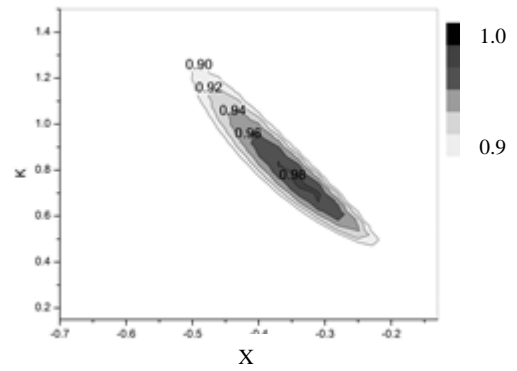
c) Vortex 1:1 Bourne



d) CIJ 1:1 Bourne



e) 1/8" T3:1 Bourne



f) 1/8" X 3:1 Bourne

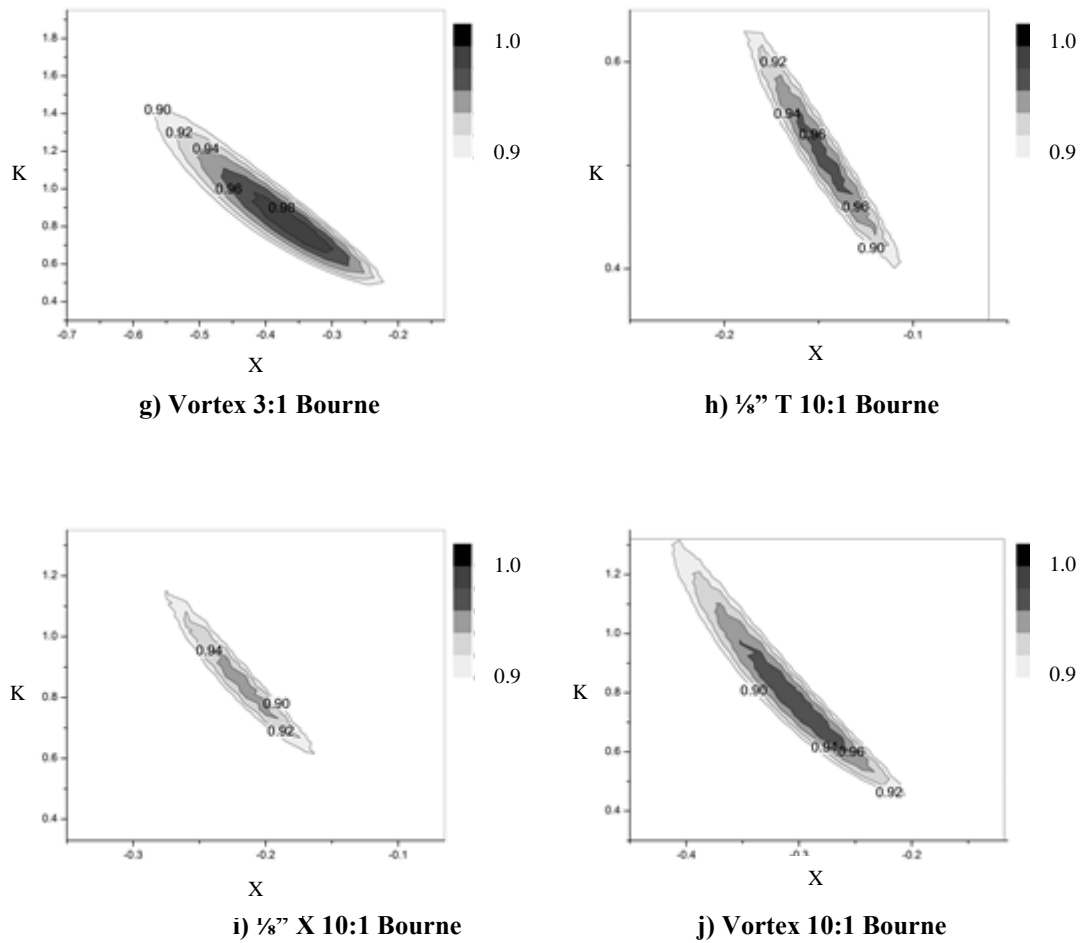


Figure 7.5. Regression ellipse plots

A range of values with reasonable fit were extracted from the graphs and vary about the global minimum with varying degrees of asymmetry. This highlights the difficulty in definitively putting an exponent that characterises the relationship between fractional conversion/mixing time and therefore ultimately making a judgement about what mixing processes are likely to be limiting.

Instead, a range of values with a good fit would be statistically more meaningful. A value of 0.98 has been arbitrarily chosen for 1:1 and 3:1 flow ratios and 0.95 for 10:1. The reason for this reduction is that at 10:1 the data is less reproducible than at 1:1 and 3:1 and therefore there is more scatter. The range of values that provide a good fit are shown in Table 7.2:

$Y=K\varepsilon^X$	$\frac{1}{8}''$ X	$\frac{1}{8}''$ T	Vortex	CIJ
	1:1 B			
X_{upper}	-0.37	-0.56	-0.44	-0.44
X_{lower}	-0.33	-0.39	-0.32	-0.31
X_{best}	-0.35	-0.47	-0.37	-0.34
	3:1 B			
X_{upper}	-0.37	-0.46	-0.42	-
X_{lower}	-0.30	-0.36	-0.30	-
X_{best}	-0.34	-0.42	-0.36	-
	10:1 B			
X_{upper}	-0.24	-0.16	-0.35	-
X_{lower}	-0.19	-0.13	-0.25	-
X_{best}	-0.23	-0.15	-0.30	-

Table 7.2. Power law fit of fractional conversion and total energy dissipation rate

Another difficulty is that while the exponents of mesomixing and micromixing are different, systems have a tendency to move from micromixing limited at low flowrates (energy dissipation rates) to mesomixing limited at high flowrates (energy dissipation rates). When an exponent is between that expected of mesomixing and micromixing, this might be caused by mixing within a transition region where both processes are important or it could also be caused by regression transgressing both regimes resulting in a best fit not differentiating between the behaviours (Figure 7.6 and Figure 7.7).

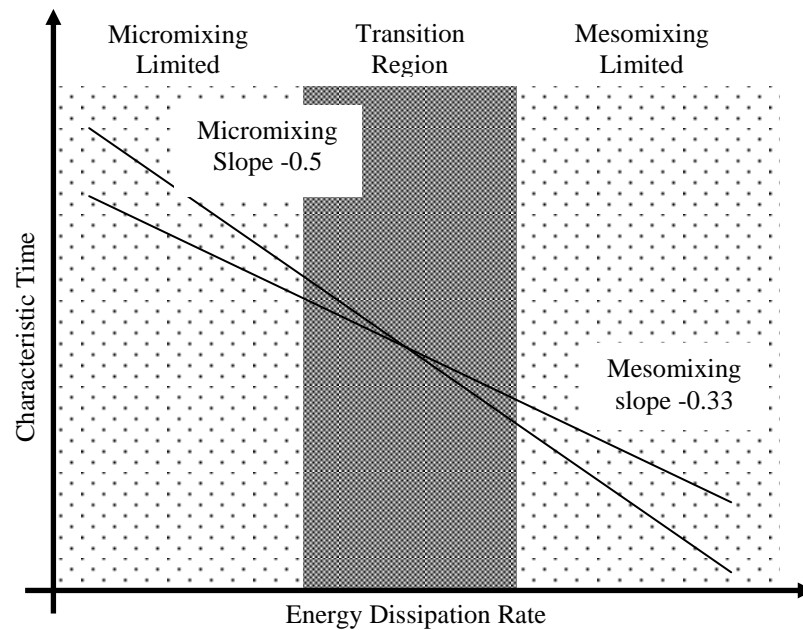


Figure 7.6. Transition from micromixing to mesomixing limiting behaviour

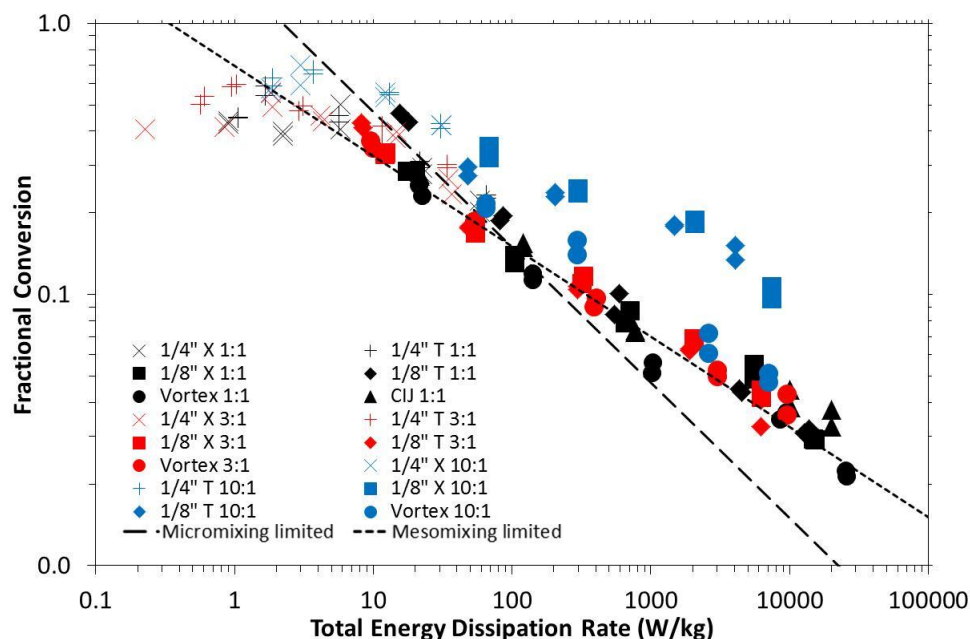


Figure 7.7. Fractional conversion vs. energy dissipation rate

1:1 (black), 3:1 (red) and 10:1 (blue) mixing in a 25% by weight ethanol stream

Therefore, there is a degree of subjectivity involved in determining which mechanism is rate limited over a specific set of experimental data. None the less, generalisations can be made. As can be seen, there is a tendency at 1:1 for the system to transition from a region with a micromixing dependency at low flowrates to a region with a strong mesomixing dependency at higher flowrates. The 10:1 results showed no evidence of a micromixing dependency over any of the tested flowrates. Perhaps the micromixing region at 10:1 exhibits micromixing behaviour at flowrates below those tested. In general, for regression over the whole range of tested flowrate at 1:1 the figures are lower than those of 3:1 which are in turn lower than those of 10:1. The values at 10:1 are smaller in absolute value than would be expected of mesomixing performance and turbulent mixing theory. However, the vortex mixer retains its mixing performance better than the other mixers.

The increase in mixing time as the volume ratio increases to a level below that expected of mesomixing in turbulent mixing theory implies that the relationship between fractional conversion and mixing time may not be as simple as previously assumed, especially in the modified volume ratio systems.

The theoretical relationship between the fractional conversion and mixing half-life, as calculated in chapter 6, is shown for a reduced range of Damköhler numbers corresponding to good mixing conditions (low Damköhler numbers) in Figure 7.8.

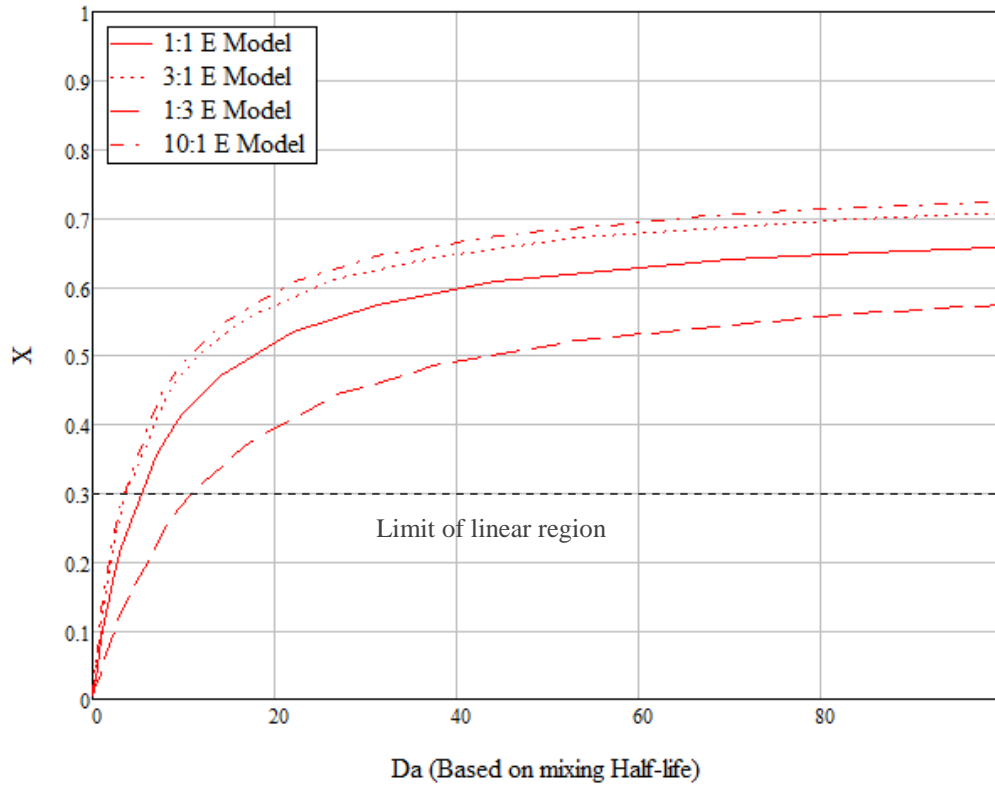


Figure 7.8. Relationship between fractional conversion and mixing

The relationship between fractional conversion and mixing time (Da is proportional to mixing time) is approximately linear at low mixing times. This linear region lasts until a fractional conversion of around 0.3 and less at 10:1

Considering this theoretical limitation between the fractional conversion and mixing time, one could imagine that the exponents of the smaller mixers at 1:1 and 3:1, with many points within the linear region, would compare well with the equivalent mixing time regressions but the 10:1 data would compare less well. This possibly explains the smaller absolute value (less steep) of the exponents at 10:1.

Considering just the 1:1 and 3:1 experiments and assuming for a moment that the fractional conversion is proportional to the mixing time, which is predicated to be the case for a fractional conversion less than 0.3 which encompasses most of the points for the smaller mixers, it appears that both micromixing and mesomixing processes are important with micromixing more significant at 1:1 than 3:1.

7.2.2 Alternative energy dissipation formulations

The total energy dissipation was defined according to an energy balance over the mixing volume. In this formulation the potential energy was deemed negligible and so the total energy dissipated was based on the pressure energy and the kinetic energy (see section 4.1.5). However, a simplified formulation that considers only the pressure energy can be constructed.[36], [40], [72] Results of using this formulation are shown in Figure 7.9. Comparing this with Figure 7.4 reveals the contribution of the kinetic energy is minimal and it would be safe to use the simplified formulation that considers only the contribution of pressure energy.

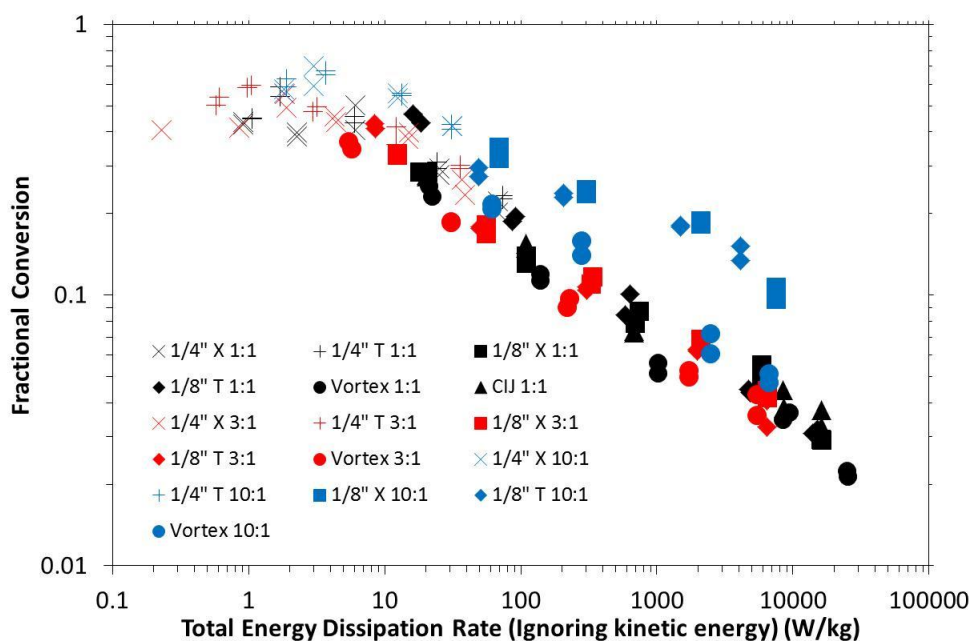


Figure 7.9. Fractional conversion vs. energy dissipation rate (ignoring kinetic energy)

1:1 (black), 3:1 (red) and 10:1 (blue) mixing in a 25% by weight ethanol stream. Simplified energy dissipation rate calculated ignoring the influence of kinetic energy.

One of the unsatisfactory aspects of the experimental setup was the location of the pressure transducers. This meant that the total pressure drop had a pressure drop contribution caused by friction in the pipe before the mixer built in to it and so the pressure transducers overestimated the pressure drop in the mixer. To overcome this, the pressure drop caused by the pipe was estimated by the methods described in section 4.1.5 and this additional pressure drop was factored in.

This was done in order to get an estimate of the true total energy dissipation rate over the mixer. However, one of the criticisms that could be aimed at such a

formulation is that the removal of the pre-mixer pressure drop is another processing step than removes the total energy dissipation rate even further from its unadjusted pressure drop measurement. To prove that this had no bearing on the results, a formulation was made which neglected the contribution of kinetic energy and used the uncorrected raw pressure drop data – this is shown in Figure 7.10. It shows that using the uncorrected pressure does not influence the observed correlation it simply shifts the data very slightly to higher energy dissipation rate.

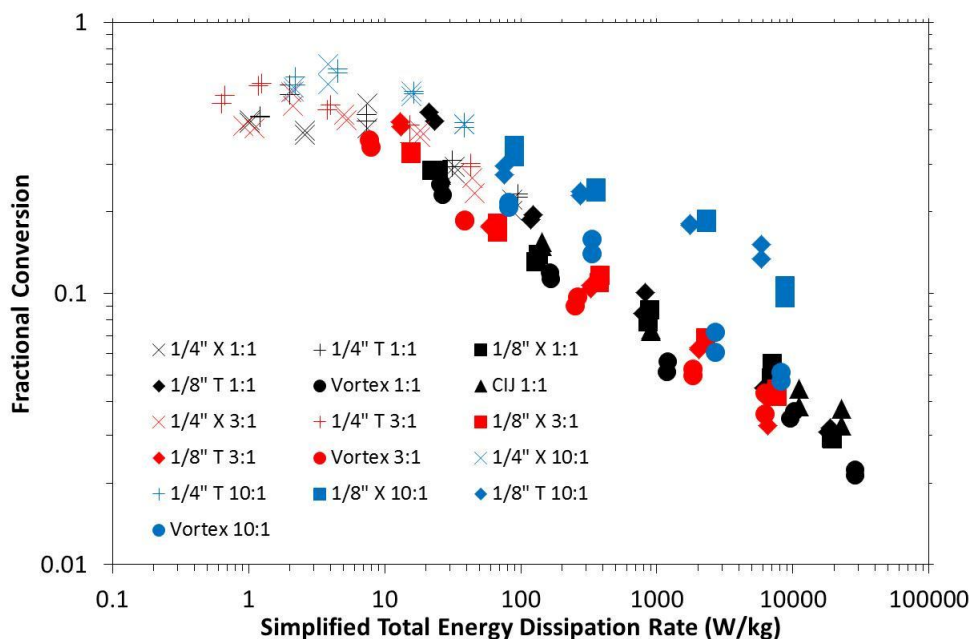


Figure 7.10. Fractional conversion vs. simplified energy dissipation rate

1:1 (black), 3:1 (red) and 10:1 (blue) mixing in a 25% by weight ethanol stream. Simplified energy dissipation rate calculated ignoring both the kinetic energy contribution and the pressure drop before entering the mixer.

For the purposes of this work the definition of the total energy dissipation rate used in all other sections is the one described in section 4.1.5, which includes kinetic and pressure energy terms and corrects for pre-mixer pressure loss. This was chosen as it is thought to more accurately reflect the energy dissipation rate of the mixer. However, it is apparent from Figure 7.9 and Figure 7.10 that any of the other definitions could have been chosen as well.

7.2.3 Generation of energy dissipation rate by mixer

The good correlation between total energy dissipation rate and fractional conversion, which is proportional to mixing time at low and moderate fractional

conversion, allows analysis of the less satisfactory correlations between fractional conversion and flowrate/velocity by considering how each of the mixers generate energy dissipation as a function of flowrates and velocities. This is useful for gaining an understanding of the differences between mixers and testing some of the assumptions made about the influence of energy dissipation rate and velocity commonly used by other researchers.[15], [40]

In turbulent flow, the pressure drop is proportional to the velocity squared. Therefore, given that pressure energy is proportional to the pressure drop multiplied by the flowrate it is reasonable to assume that the energy dissipation rate would be proportional to the velocity cubed. Figure 7.11 shows the relationship between inlet velocity cubed and the total energy dissipation rate. It reveals that for each mixer operating at one flow ratio the gradient is around one, indicating that the cubed relationship between velocity holds within a reasonable degree of accuracy as expected. This is useful when considering how energy dissipation rate changes within a mixer and defined system (physical properties, flow ratios etc.) but cannot divulge any further information on its own. However, it has been considered with other variables as part of a scaling methodology such as the momentum diffusion in a CIJ mixer proposed by Johnson *et al* with considerable success. [15]

Gillian and Kirwan assumed that the velocity cubed divided by the characteristic length scale of segregation, which they took as the diameter of the inlet, as proportional to the total energy dissipation rate.[40] This relationship is shown in Figure 7.12. It demonstrates a better propensity to scale between the same mixers of a different size but again poor correlation between mixers of different geometry and different flow ratios. It is also more difficult to define a characteristic length scale of segregation for the vortex mixer or the CIJ due to the complex geometry involved in the change in diameter from inlet to mixing chamber.

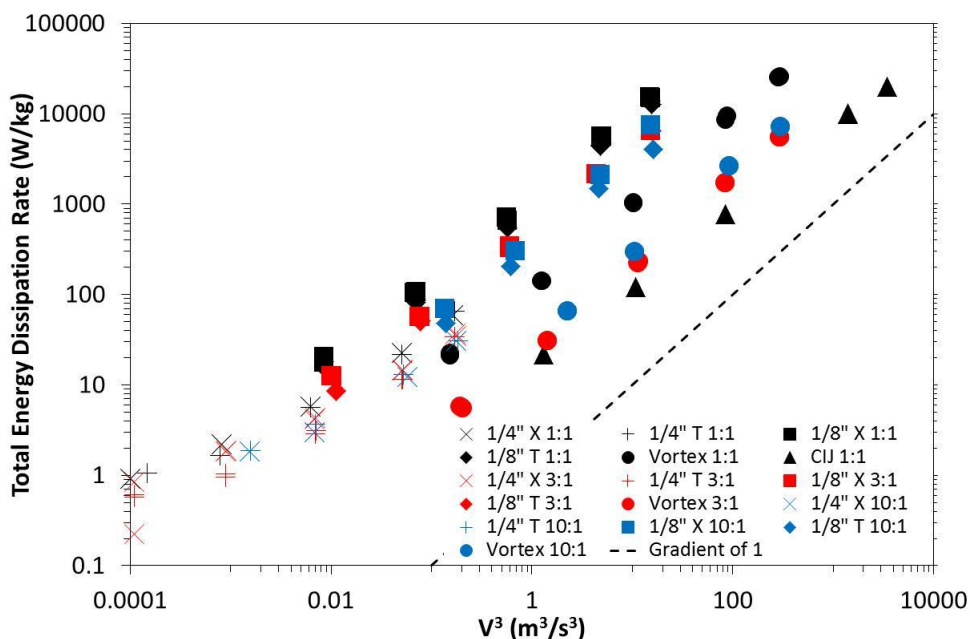


Figure 7.11. Energy Dissipation Rate vs. Inlet Velocity Cubed

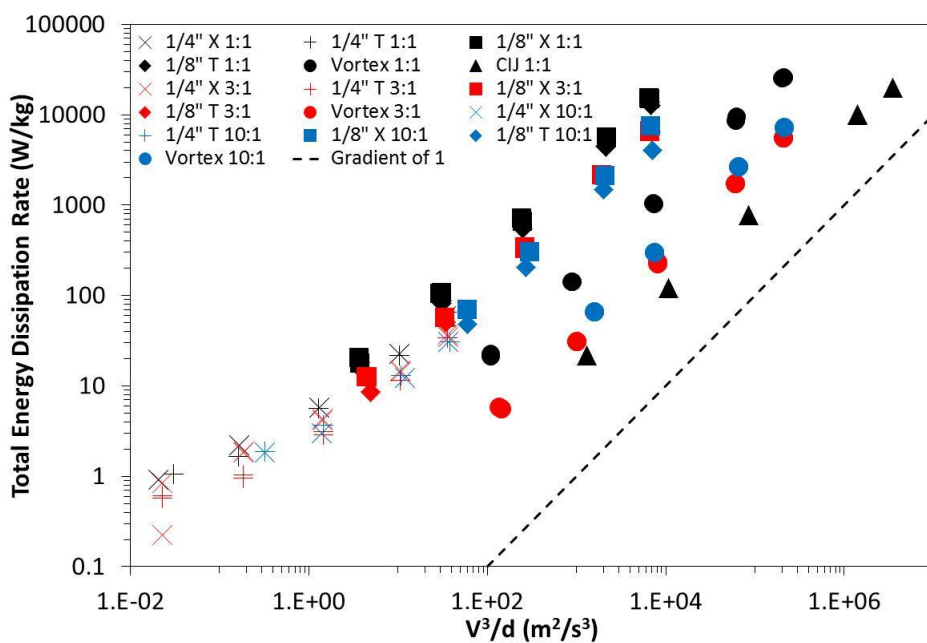


Figure 7.12. Energy dissipation rate vs. inlet velocity cubed over jet diameter

The poor agreement between flow ratios in section 7.1 was partially improved previously by moving from inlet flowrate to an outlet flowrate. This is due to the other inlet, which within the confines of our dataset is the inlet with the small volume fraction and hence a lower velocity. Therefore, the inlet velocity on both sides are unequal as the flow ratio deviates from 1:1. This explains why the correlation is

better as function of the total flowrate and it provides fairer comparison between different flow ratios.

As a function of the total flowrate cubed (Figure 7.13), there is a better correlation with fractional conversion in two distinct groups – large and small mixers. This explains why the graphs of fractional conversion against total volumetric flowrate also form into two distinct groups at 1:1 and at 3:1. The vortex mixer appears to provide the highest energy dissipation rate as a function of total volumetric flowrate, although there is not much difference between the mixers. If the same flowrate is put through a similarly sized mixer, a similar total energy dissipation rate and similar mixing performance would be expected.

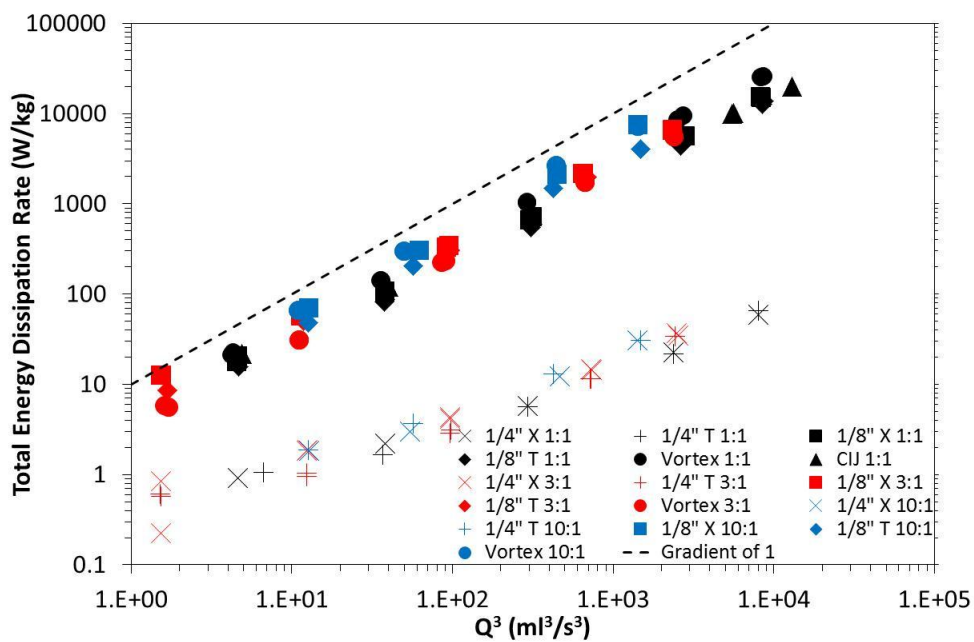


Figure 7.13. Energy dissipation rate vs. outlet flowrate cubed

Obviously the total energy dissipation rate is dependent on the pressure drop and so there ordinarily would not be much benefit in plotting them. However, such a plot highlights an important difference between the mixers (Figure 7.14). The CIJ and vortex mixer, despite their smaller inlet diameter, have a larger internal volume. This is due to the relatively large mixing chamber. Therefore the same pressure drop in a CIJ or vortex mixer results in a smaller energy dissipation rate than in the other mixers.

This is not to say that they are less efficient, for that to be considered properly one would have to consider the fraction of the total energy dissipation that is utilised by the mixing process. This will be explored in more detail later.

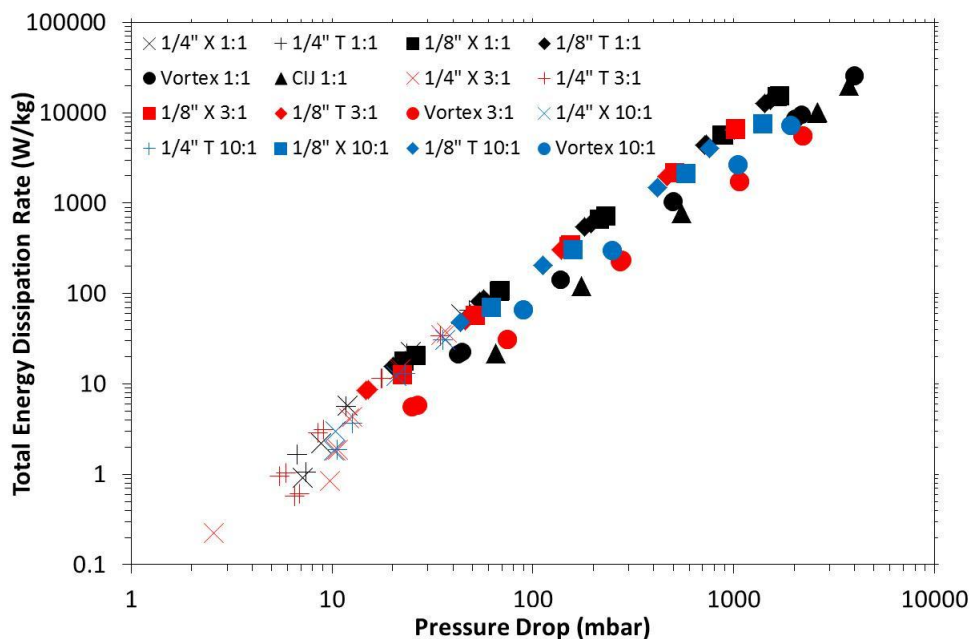


Figure 7.14. Energy dissipation rate vs. mixer pressure drop

This explains why although there is excellent correlation between energy dissipation rate and pressure drop and hence mixing time, it is important to take account of the dissipation volume. An increased dissipation volume reduces energy dissipation but increases residence time which is often desirable (section 7.6). Figure 7.13 shows that for the smaller mixers, the energy dissipation at constant flowrate is around the same which indicates that the pressure drop for the CIJ and vortex mixer must be larger. This was noted during the experiments and was assumed to be evidence of the superiority of mixing in these devices, which aside from the vortex mixer at 10:1, was not really the case after taking into account the dissipation volume and fractional conversion.

7.3 Estimation of an absolute mixing time

The fractional conversion is some unique function of the Damköhler number. The concentration of reactant species determines the characteristic reaction time, which in turn determines the range of mixing times to which the parallel reactions are sensitive. This can be tuned by varying the concentration, controlled at the upper

limit by the concentration, as high concentrations (fast reactions) are “blind” to poor mixing and good mixing is limited at the other end by the sensitivity of the analytics.

This has not been attempted in these experiments, where the reactant concentration (on mixing) has always been constant with the emphasis on methods by which the mixing process can be manipulated and compared on the same “reaction scale”. Ultimately, the 100 mmol/L concentrations provide a sensible reaction rate for the fast and efficient mixing expected of a continuous mixer. For poorer mixers (such as the ¼” ones, or even batch mixers) it may make sense to decrease the reactant concentration in order to recalibrate the mixing times which the process is sensitive to. For those mixers that are much poorer (or much better) it may be necessary to change reaction scheme to get the required sensitivity. Ultimately, it depends on the timescale of the process of interest what concentrations or reactions make the sensible choice for the estimation of mixing times.

Using the fractional conversions, the characteristic reaction times and the theoretical curves obtained in Chapter 6, the graph of fractional conversion vs. total energy dissipation rate (Figure 7.4) can be converted to a theoretical mixing time. Those shown below include engulfment time vs. total energy dissipation rate (Figure 7.15), mixing half-life vs. total energy dissipation rate (Figure 7.16) and also 90% mixed time vs. total energy dissipation rate (Figure 7.19).

Figure 6.11 shows the relationship between fractional conversion and Damköhler number as calculated by the E-model using the raw unstandardised engulfment time. Considering a vertical line on Figure 6.11 (constant Damköhler number) the same engulfment Damköhler number is attributed to a higher fractional conversion at 3:1 and higher still at 10:1. This is due to the higher acid concentration increasing the rate of reaction in the acid rich zone and volume effects making mixing less efficient for constant energy dissipation rate which slows mixing and increases segregation. This means that an equivalent fractional conversion occurs at 3:1 at a lower engulfment Damköhler number than in the 1:1 system.

If this definition of mixing time is used to define the theoretical relationship between fractional conversion and Damköhler number then when the experimental fractional conversion is transformed to a theoretical mixing time we get Figure 7.15. Using this model predicts that for the same energy dissipation rate the 3:1 flow ratio

has a lower mixing time than the 1:1 flow ratio and vortex mixer at 10:1 is also better than all the 1:1 mixers. This is obviously not realistic and is an effect of concentration and volume - not an effect of better or worse mixing.

The engulfment rate which determines the engulfment time is dependent only on the kinematic viscosity and energy dissipation rate. Using this to define a mixing time is misleading when comparisons are made between different flow ratios. The more extreme the flow ratio, the smaller the mixing zone. As the flow ratio deviates from 1:1 it takes more engulfments or more energy to complete mixing to the same extent. This is not considered in defining the engulfment time as no effort is made to control what the mixing time actually means with respect to the intensity of segregation.

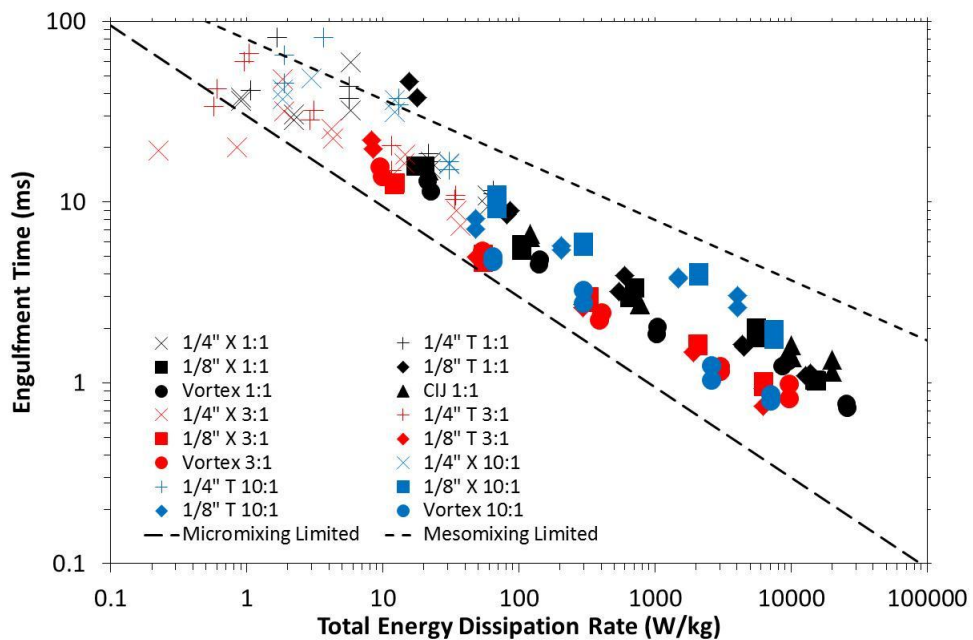


Figure 7.15. Engulfment time vs. energy dissipation rate

The engulfment time is determined from a cubic spline interpolation of the theoretical points obtained from the engulfment model with the experimental points. This allows a value of the Damköhler number, based on engulfment time, to be estimated and this is then multiplied by the characteristic reaction time of the slow reaction to provide an estimate of the mixing time based on the engulfment time.

Fractional conversion is not a measure of mixing degree, it is a measure of segregation history and as such it is sensitive to how fluids are mixed (concentration, volume etc.) in addition to how quickly they are mixed. As the neutralisation reaction is mixing controlled, the reactant concentration of this reaction is directly related to

mixing progress. This can be used to standardise mixing by utilising the concentration profiles averaged out over the entire volume as discussed in Chapter 6. Any value on the y-axis could be used to standardise the mixing progress but two values have been chosen. First a half-life, at 50% acid consumption, which is useful for defining a characteristic mixing time and second at 90% acid consumption which is used to estimate the time of the entire mixing process. This properly standardised mixing provides a fair comparison and also more importantly feasible results.

Consider, firstly, the half-life (Figure 7.16) which provides a neat definition of the Damköhler number as the characteristic reaction time of a second order reaction is also a half-life. The mixing times of the 1:1 and 3:1 mixing flowrates both correlate well with each other as a function of total energy dissipation rate with 10:1 some way off other than the vortex mixer which holds its performance relative to the 3:1 and 1:1 data.

This is again due to concentrations effects. Standardised to the half-life of the fast reaction, the same fractional conversion theoretically corresponds to longer mixing time at 10:1 in comparison to the 3:1 or 1:1 flow ratios. When the concentration is changed to modify the flow ratios, two things happen but in opposite directions. Firstly, the reaction volume decreases in size which slows down the reaction and secondly the concentration within this reduced zone increases (to keep molar flowrates the same) which has the effect of accelerating the reaction.

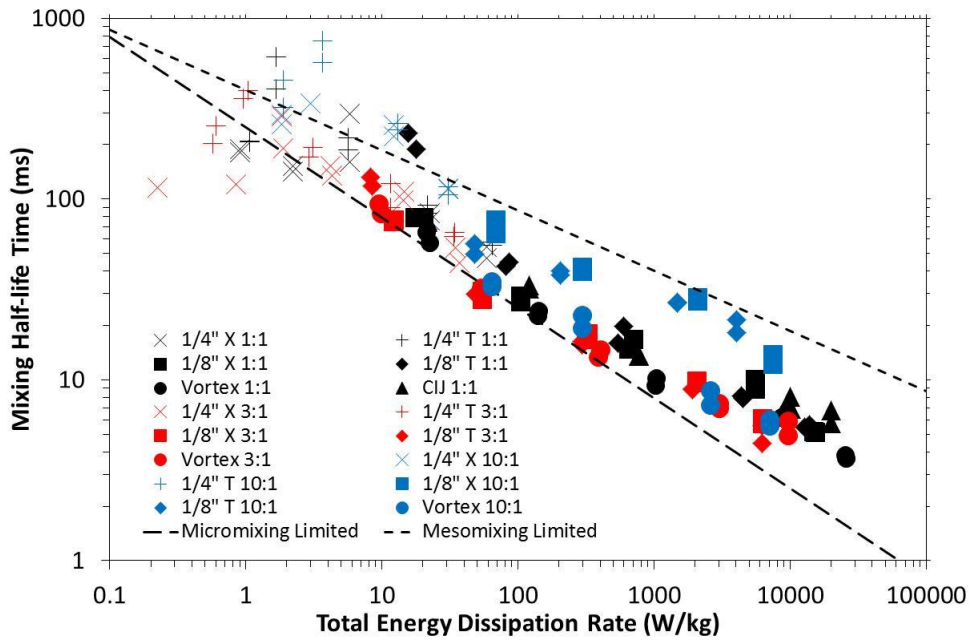


Figure 7.16. Mixing half-life vs. energy dissipation rate

Mixing half-life time is determined from a cubic spline interpolation of the theoretical points obtained from the half-life engulfment model with the experimental points. This allows a value of the Damköhler number, based on mixing half-life, to be estimated and this is then multiplied by the characteristic reaction time of the slow reaction to provide an estimate of the mixing time based on the mixing half-life.

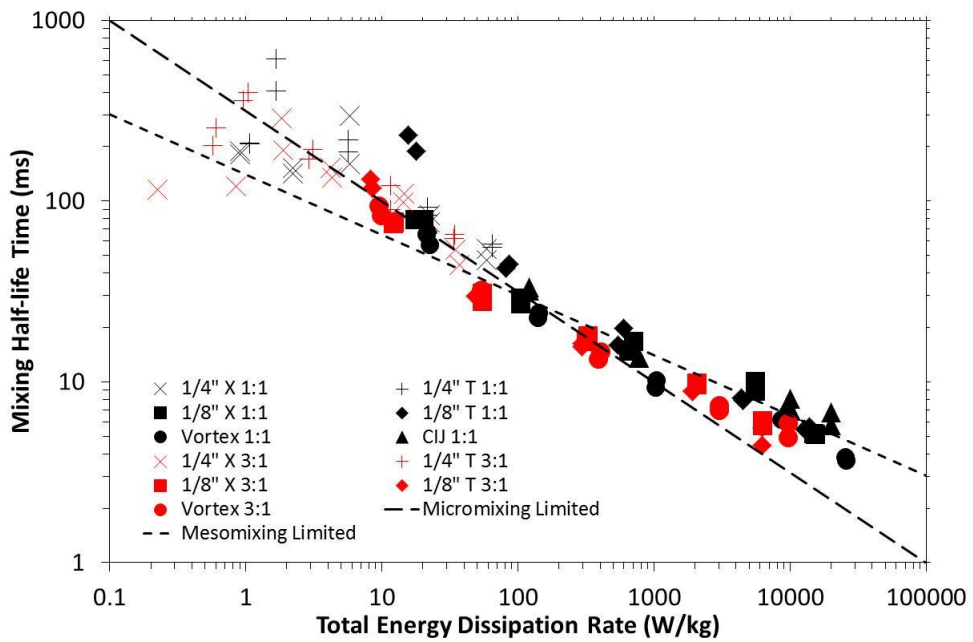


Figure 7.17. Mixing half-life gradient change

Change in gradient at 1:1 and 3:1. From a region with a micromixing dependency to a region without.

The overlap of the 1:1 and 3:1 mixers is a real effect when the concentration influence is adjusted for, but the 10:1 data shifts. The characteristic mixing time ranges from hundreds of milliseconds at low flowrates (50 ml/min – larger mixers) to a few milliseconds at high flowrates (600ml/min) for both the 1:1 and 3:1. At 10:1 the vortex mixer is clearly the best with its characteristic mixing time ranging from around 30 milliseconds (120 ml/min) to about 10 milliseconds (600 ml/min) but other mixers range from around 80 milliseconds (120ml/min) to about 15 milliseconds (600ml/min). Again there is significant change in the gradient at 1:1 and 3:1, from a micromixing region (gradient -0.5) through a transition region and into a mesomixing region (gradient -0.33).

The data is indicating that changing the volumetric flow ratio from 1:1 to 3:1 has no effect on the mixing time. This is counterintuitive. Changing the flow ratio changes the probability of self-engulfment, or physically for the same energy dissipation rate the fluid is more likely to consume energy without contributing to mixing. This should cause an increase mixing time. This is backed up by considering the mixing half-life constants in Table 6.1 which show that for 1:1 the half-life constant is 5 and for 3:1 it is 6. Figure 7.18 shows the probability of self-engulfment for the engulfment model as a function of dimensionless time for 1:1, 3:1 and 10:1. So from a combination of Figure 7.18 and Table 6.1 it can be surmised that moving the volume fraction from 1:1 to 3:1 does adversely affect the mixing time. As the experimental data shows that mixing is largely unaffected by the change from 1:1 to the 3:1, the question that remains is to quantify the reduction in mixing performance that would be theoretically expected given the known issues with the model and then compare this with the sensitivity expected of the experimental technique and the error associated with it.

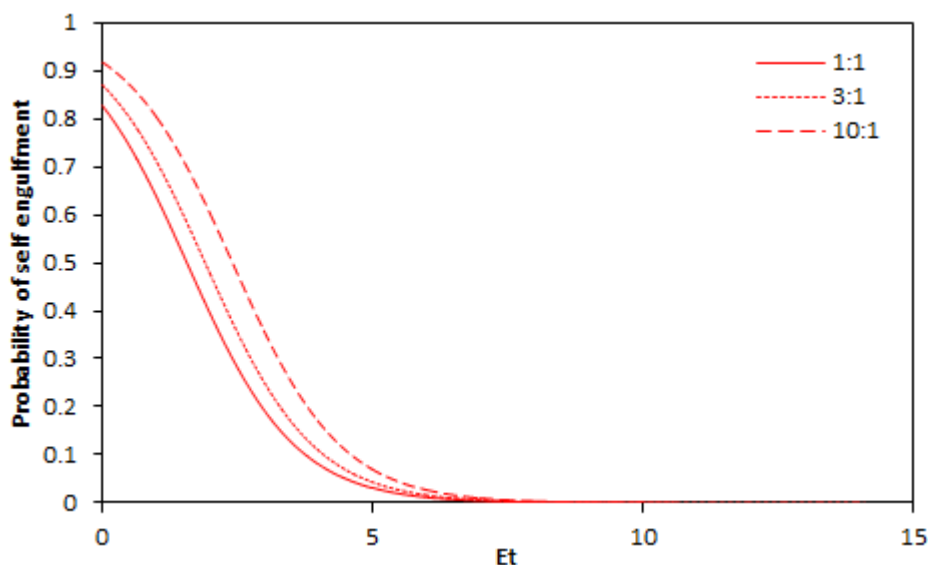


Figure 7.18. Probability of self-engulfment as a function of dimensionless time

The probability of self-engulfment is equal to one minus the mixing volume. The probability is shown as function of dimensionless time for flow ratios of 1:1, 3:1 and 10:1. The area under each curve is 15.2 (1:1), 23.5 (3:1) and 45.2 (10:1)

The error associated with the fractional conversion is around ± 0.03 , this is a combination of experimental and analytical error. This figure comes from a wide analysis over a range of flowrates and before averaging the multiple GC runs, it is a generally representative figure. The error reduces (in absolute size) as the mixing improves and is larger at 10:1 than at 1:1 and 3:1. The ± 0.03 figure would translate into around 8ms. This would decrease to about 2ms at high flowrates and increase to 30ms at low flowrates.

Considering the tightness of the 1:1 and 3:1 data, it seems reasonable to suggest that data within a range of ± 30 ms at low flowrate, around ± 10 ms at moderate energy dissipate rates and ± 5 ms at high energy dissipation rate would not be noticeably outliers.

So the question remains what sort of time scale difference could theoretically be expected by changing from 1:1 to 3:1 and whether or not the experimental error could mask this? Considering the change in half-life constant from 5 to 6 suggests an increase of mixing time of around 1 engulfment. Considering Figure 7.15, it is observed the engulfment time is around 10ms at low total energy dissipation rate, 5ms at moderate total energy dissipation rate and 1ms a high total energy dissipation

rate, which would not be very noticeable, i.e. within the region of outliers or within the expected accuracy of the experiments and model. 10:1 on the other hand would provide an increase in characteristic mixing time of around 20ms, 10ms and 2ms at low, moderate and high total energy dissipation rate which is definitely within the accuracy level that could be reasonable expected. Therefore it is concluded that the mixing is likely affected slightly by the change from 1:1 to 3:1 but not hugely and the sensitivity and accuracy of the experimental technique is not sufficient enough to capture this.

The 90% mixed time (Figure 7.19) is defined in the same way as the half-life and its values and trends are just a time shifted version of the half-life values. The estimated mixing completion times range from several hundred milliseconds at low flowrates (50 ml/min) to around 10 milliseconds at high flowrates (600ml/min) for both the 1:1 and 3:1. At 10:1 the vortex mixer completes mixing in a time ranging from around 50 milliseconds (120 ml/min) to about 10 milliseconds (600 ml/min) but other mixers range from about 100 milliseconds (120ml/min) to about 20 milliseconds (600ml/min).

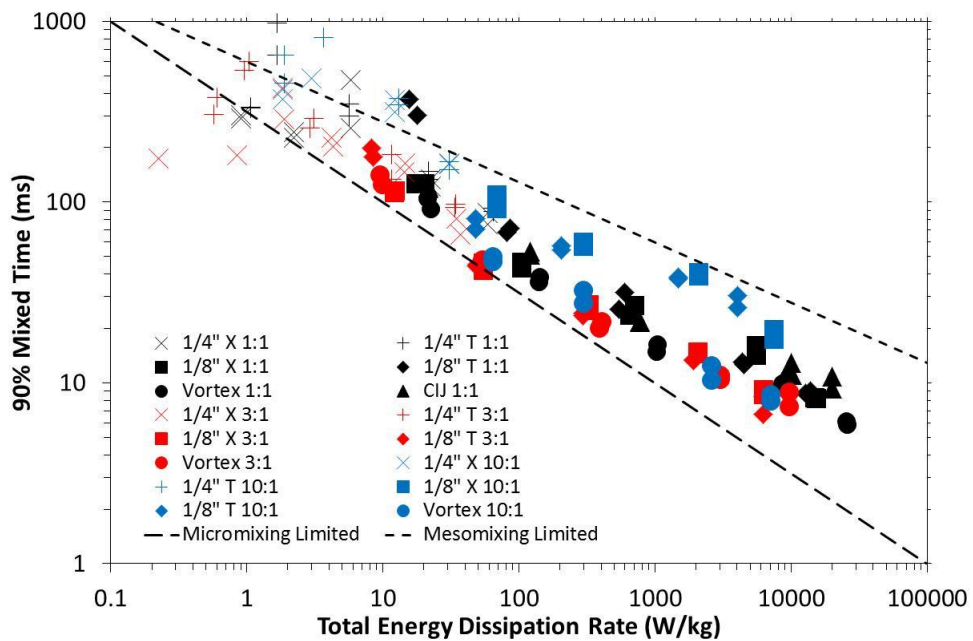
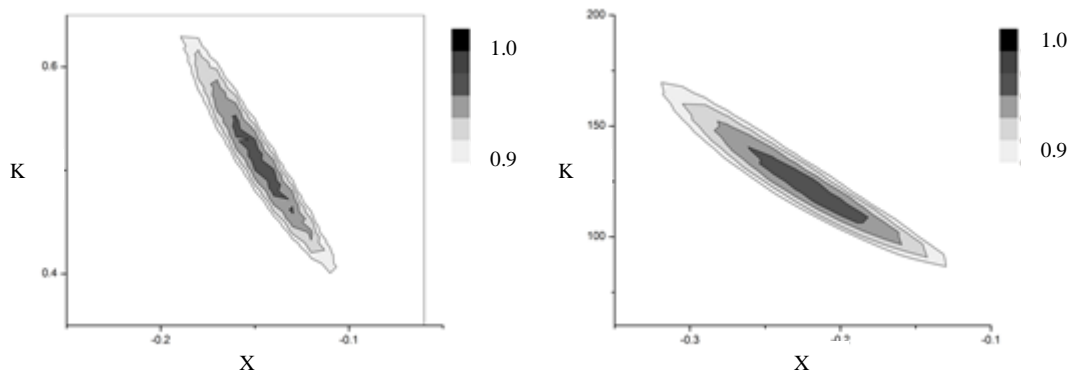


Figure 7.19. 90% mixed time vs. energy dissipation rate

The 90% time is determined in the same fashion as the mixing half-life except the constant is defined at 90% volume averaged acid consumption not 50%. Therefore, it is a simply a “time shifted” version of the half-life.

From the gradient lines on Figure 7.19, it is clear that the gradient at 1:1 and 3:1 lies somewhere between -0.5 and -0.33 which is in good agreement with the results obtained from a regression of the fractional conversion in Section 7.2.1. Therefore, the result of micromixing and mesomixing both being significant processes is further reinforced.

The 10:1 data was considered to be affected by non-linearity in the relationship between fractional conversion and mixing time and so an exponent value was found not to be representative of the actual mixing process. Converting the fractional conversion to a mixing time, defined as an engulfment time (Figure 7.15), mixing half-life (Figure 7.16) or 90% mixed time (Figure 7.19) should overcome this problem. Visually, from gradients marked on the chart these chartd, the 10:1 data is now consistent with the other data and the kink that existed previously at a fractional conversion above 0.2 has been straightened out. This is caused by the non-linearity (see Figure 7.8). This is also confirmed by comparing the regression plots from the fractional conversion with those from the mixing half-life at 10:1 (Figure 7.20), which confirm the shift to a lower exponent, consistent with turbulent mixing theory, as denoted by X on the charts below.



a) 10:1 1/8" T fractional conversion

b) 10:1 1/8" T mixing time

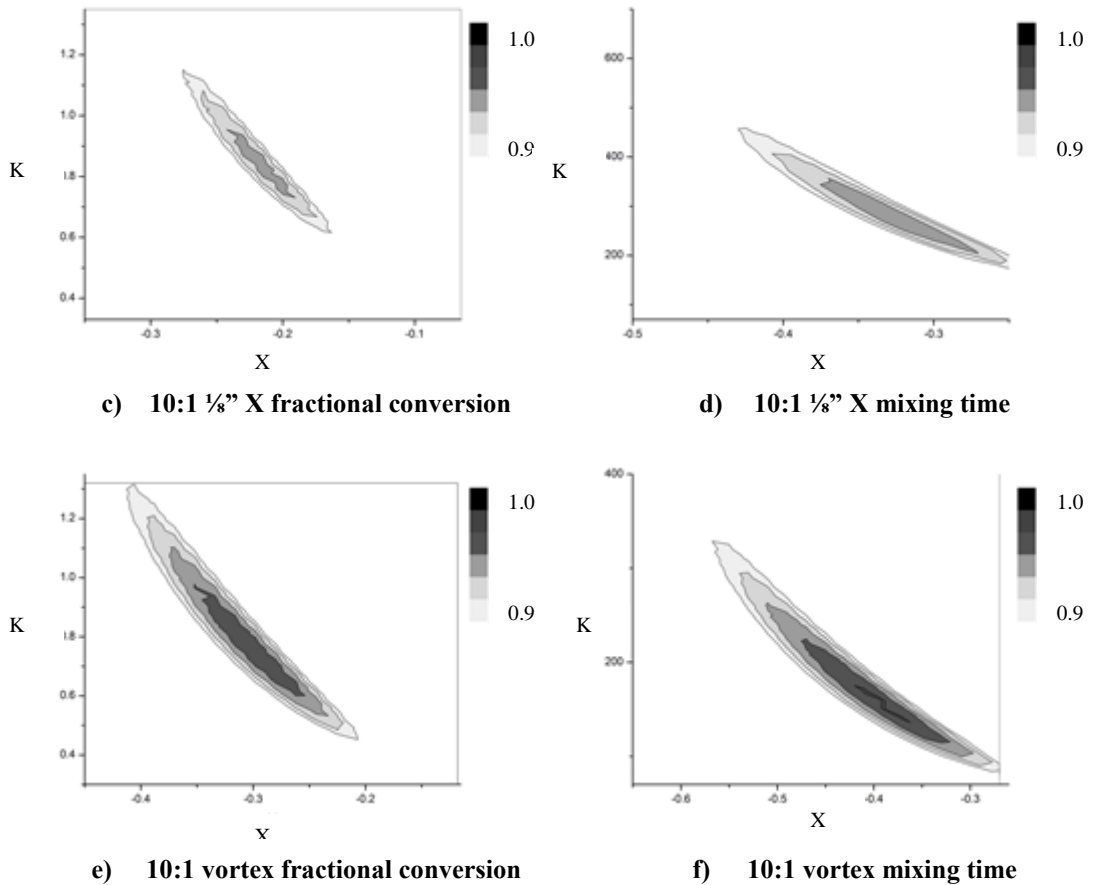


Figure 7.20. Regression ellipse plots for mixing time and fractional conversion

Aside from the vortex mixer, the system at 10:1 seems to be mainly in the mesomixing regime.

7.4 Comparison of estimated mixing times with literature

Johnson and Prud'homme[15] estimated the mixing time in a CIJ style mixer with an inlet diameter of 500 μ m by varying outlet configurations and finding a point where the system transitioned from the outlet having an effect on fractional conversion to not having an effect. This point was taken as the onset of completion within the mixer and then the mixer residence time was taken as the mixing time. This allowed the constant in a scaling theory to be determined which allowed the mixing time over a range of flowrates to be estimated as a function of inlet flowrate for different sized mixers. In terms of absolute mixing time, Johnson and Prud'homme estimated the mixing time to be around 30 milliseconds at inlet

Reynolds number of 500 and to single digit milliseconds at Reynolds numbers of 4000. This compares well with the figures for the CIJ in this thesis which predicts 50 milliseconds at an inlet Reynolds number of 500 and around 10 milliseconds at 4000.

Gillian and Kirwan[40] used a combination of the Bourne IV reaction and the comparable volume engulfment model as proposed by Baldyga and Bourne[20] to estimate the mixing time in a range of mixers at a 1:1 flow ratio. The mixing times estimated by Gillian and Kirwan ranged from around a millisecond at high flowrates ($\approx 800\text{ml/min}$) to up to a second at low flowrates ($\approx 10\text{ml/min}$) for similar sized mixers and a similar range of flowrates.

Falk[29] utilised the Villermaux reaction scheme[7] coupled with the IEM mixing model to estimate the mixing time of various micromixers. Whilst none of the mixers are directly comparable to the results of this these due to channel size and diversity of the mixers tested it shows a reasonable estimate of the mixing times that can achieved in continuous mixers from around 100ms to about 1ms over a range of total energy dissipation rates of 1 to 10,000 W/kg. The range of both estimated mixing times and total energy dissipation rate are consistent with the estimates in this study.

Marchisio *et al* utilised CFD to estimate the mixing time associated with mixing in a CIJ mixer over a range of flowrates for inlet diameters of 1mm and 2mm.[35] For the 1mm inlet diameter the estimated mixing times ranged from around 20 milliseconds at a Reynolds number of 500 down to around 4 milliseconds at a Reynolds numbers of 2000. This again compares relatively well to the results in this thesis.

7.5 Viscosity and volume fractions

The kinematic viscosities (dynamic viscosity/density) of both inlet streams from the previous section are all around 2 centistokes ($2 \times 10^{-6} \text{ m}^2/\text{s}$). There is no viscosity difference between the measured inlet streams and consequently the outlet streams are also around 2 centistokes. This is not reflective of many processes, such as antisolvent crystallisation, which involve the mixing of streams which have different physical properties.

The schemes with modified composition (MC) (as outlined in chapter 4.1) were designed to provide a viscosity difference between the inlet streams. The acid stream solvent is pure water and the alkali stream solvent is 50% ethanol/water.

Scheme	Acid Inlet Viscosity cSt	Alkali Inlet Viscosity cSt	Viscosity Ratio Acid/alkali	Outlet Viscosity cSt
1:1	2.00	1.87	0.94	1.90
3:1	1.82	1.92	1.05	1.85
1:3	1.84	2.10	1.15	1.89
10:1	1.82	1.92	1.05	1.88
1:1 MC	0.91	2.52	2.77	1.93
3:1 MC	0.91	2.41	2.64	2.24
1:3 MC	0.90	2.64	0.34	1.35
10:1 MC	0.95	2.43	2.56	2.33

Table 7.3. Viscosity ratios and outlet viscosities (N.B. 1 cSt is $1 \times 10^{-6} \text{ m}^2/\text{s}$)

The fractional conversion as a function of the energy dissipation rate is shown in Figure 7.21 for the modified schemes with a viscosity difference for 1:1, 3:1 and 10:1 flow ratio. Again the gradients for 1:1 and 3:1 are somewhere between -0.5 and -0.33 but at 10:1 they are less than -0.33 in absolute value.

The fractional conversion can also be converted to a mixing time as before. The mixing half-lives are shown in Figure 7.22. This adjusts the gradient in the 10:1 flow ratio back into a range consistent with turbulent mixing theory.

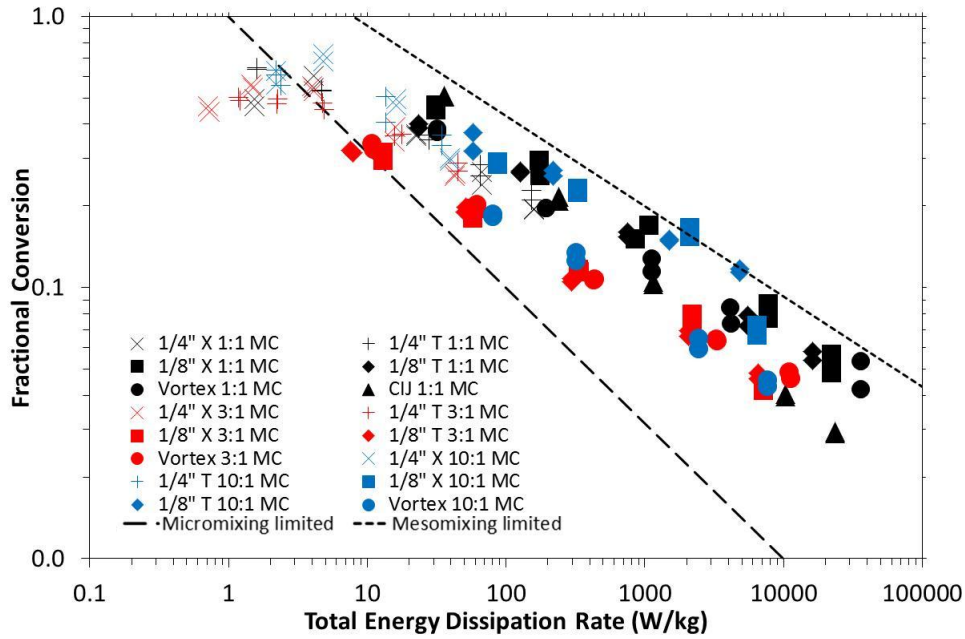


Figure 7.21. Modified composition fractional conversion

Fractional conversion vs. total energy dissipation rate for the modified composition scheme with an inlet kinematic viscosity ratio of around 2.5. This should be compared with Figure 7.4 which has an inlet viscosity ratio of around 1.0. For 1:1 (black) the outlet viscosity is the same in both graphs as the outlet composition is identical. The 3:1 (red) and 10:1 graphs have slightly higher outlet viscosities in the modified formulation than in the original formulation but the results appear to be largely independent of viscosity at 3:1 and 10:1.

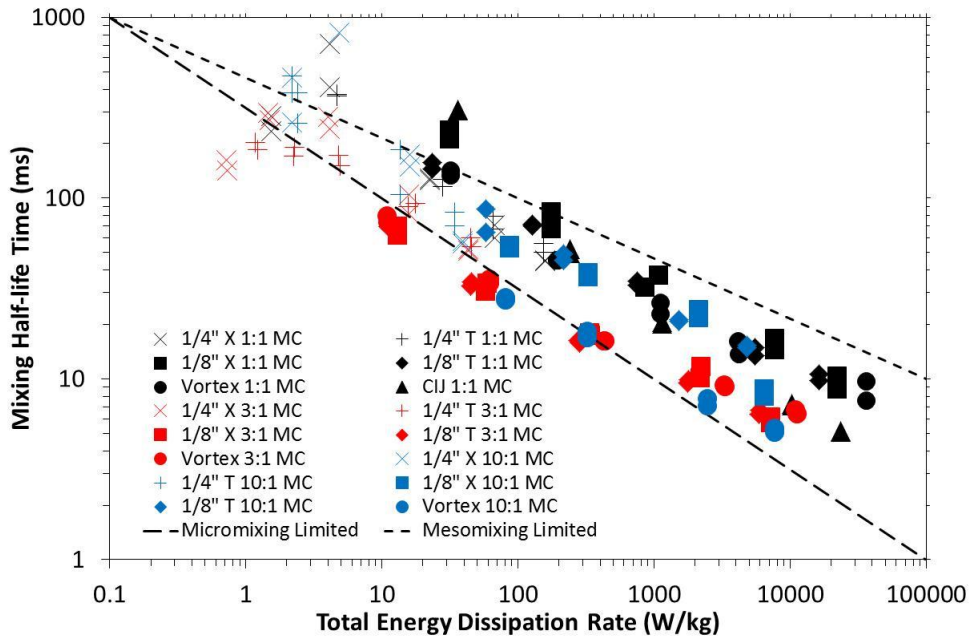


Figure 7.22. Modified composition mixing half-lives

Fractional conversion translated into a mixing half-life using the same method as before and as outlined in Chapter 6. This is for a flow ratio of 1:1 (black), 3:1 (red) and 10:1 (blue) for the modified composition with an inlet viscosity difference.

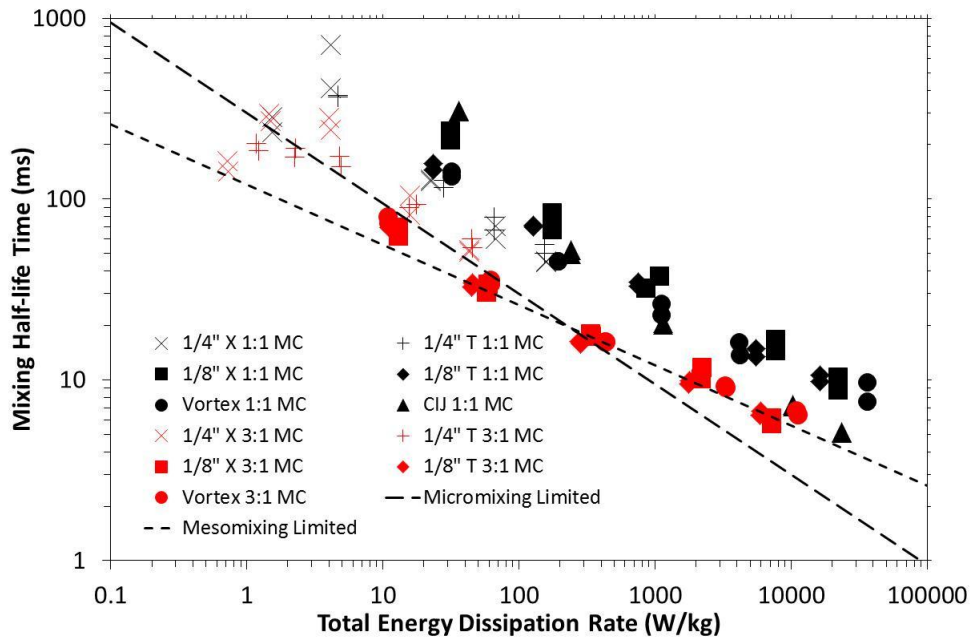


Figure 7.23. Change in gradient of the mixing half-life at 1:1 and 3:1 with modified composition

Fractional conversion translated into a mixing half-life using the same method as before and as outlined in Chapter 6. This is for a flow ratio of 1:1 (black) and 3:1 (red) for the modified composition with an inlet viscosity difference.

Figure 7.24 and Figure 7.25 shows the influence of a viscosity ratio of around 2.7 (grey) in comparison to a viscosity ratio of 1 (black) for a flow ratio of 1:1. In each case the outlet viscosity is constant as the outlet solution composition is the same.

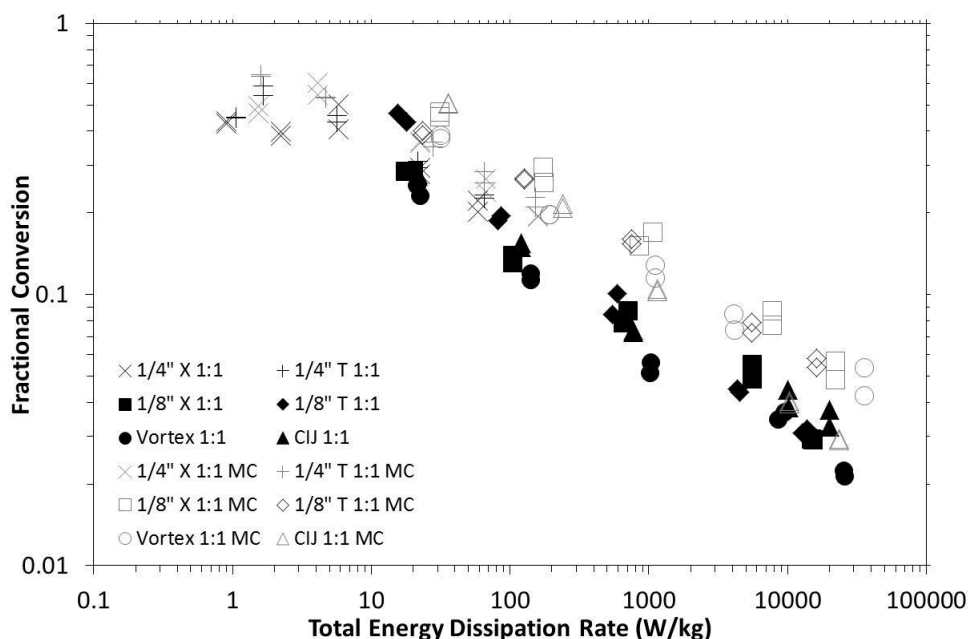


Figure 7.24. Influence of viscosity on mixing time at 1:1

Fractional conversion at 1:1 flow ratio for the modified scheme (grey) with an inlet viscosity ratio of around 2.75 and the original Bourne IV scheme (black) with a viscosity ratio of around 1.

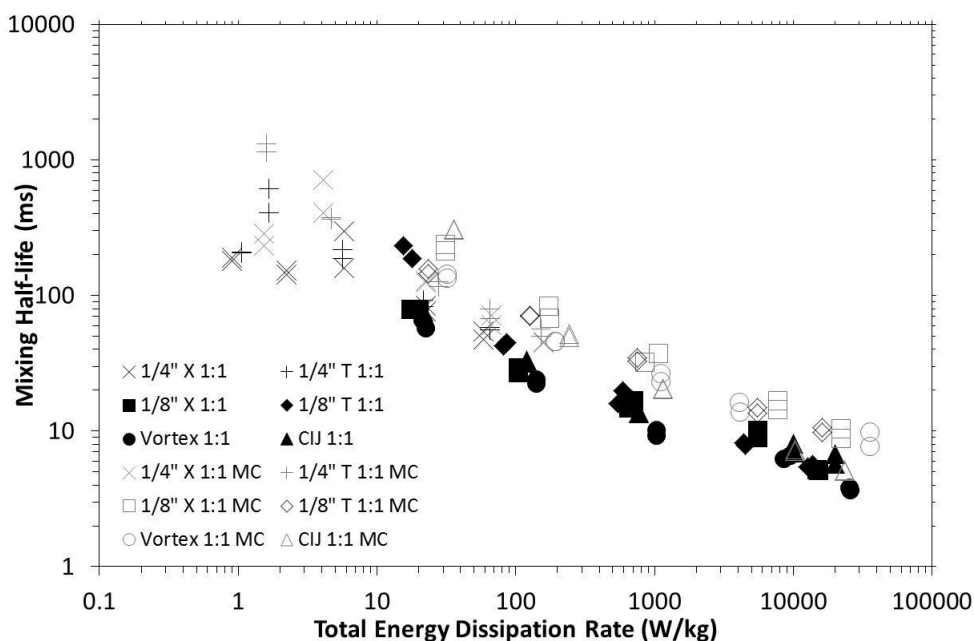


Figure 7.25. Influence of viscosity on mixing time at 1:1

Fractional conversion at 1:1 flow ratio for the modified scheme (grey) with an inlet viscosity ratio of around 2.5 and the original Bourne IV scheme (black) with a viscosity ratio of around 1.

Previous attempts at the modification of solvent physical properties have taken the approach of using a high viscosity polymer additive added in low concentrations

to increase the viscosity of one solution without significantly changing the solvent compositions.[15], [39–41] However, this increases both the viscosity ratio and the final outlet viscosity making it hard to draw distinction between the effect of an inlet viscosity difference and the effect of high overall viscosity.

Our approach, at 1:1, changes the viscosity ratio but keeps the outlet (mixed) viscosity constant. Figure 7.24 and Figure 7.25 show that at 1:1 the increased viscosity ratio increases the mixing time. However, the modified composition 3:1 and 10:1 runs are similar to the original 3:1 and 10:1 runs. This is highlighted in Figure 7.26 which shows the mixing half-life as a function of the total energy dissipation rate for 3:1 (red) and 10:1 (blue) for the original scheme with no inlet viscosity difference (solid) and the modified scheme with a viscosity difference (open).

Independence of fractional conversion (or mixing time) to viscosity differences is evidence of operation within the inertial regime. Figure 7.26 shows that changing the viscosity ratio so that the minor stream is less viscous and the major stream more viscous has little or no influence on the fractional conversion at 3:1 and 10:1.

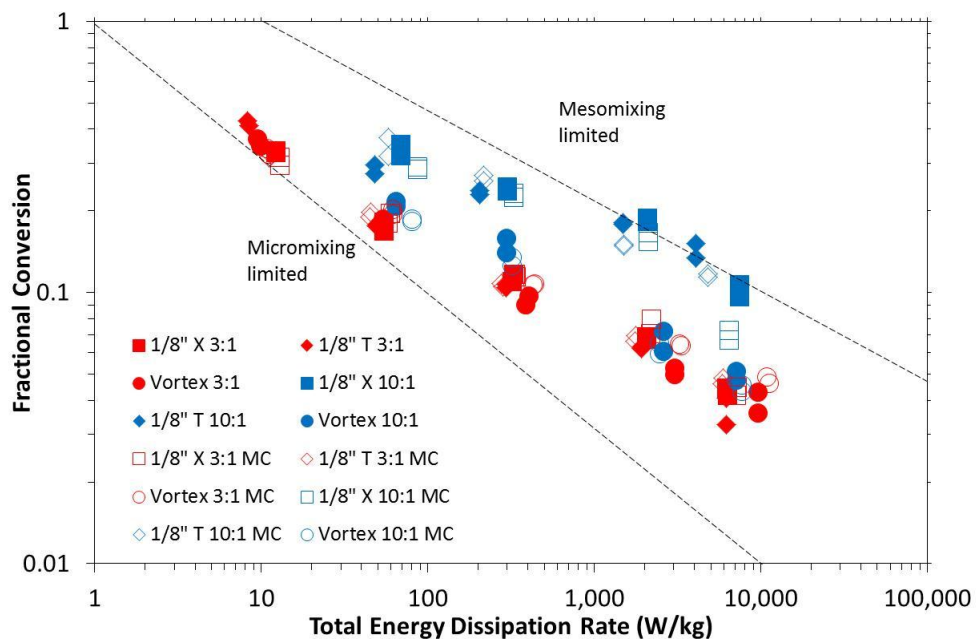


Figure 7.26. Fractional conversion 3:1 and 10:1 comparison

Comparison between the original carrier composition (solid) with an inlet viscosity ratio of 1 and the modified composition (open) with an inlet viscosity ratio of around 2.7 for a volumetric flowrate of 3:1 (red) and 10:1 (blue). The effect of viscosity appears to be minimal for these flowrates and viscosities.

In order to experimentally determine the influence of local concentration, the experiments were repeated at a flow ratio of 1:3 (alkali:acid) and these values were then compared with those of 3:1 (alkali:acid). This was carried out for experiments with and without a viscosity difference.

Obviously, for the 1:3 run without a viscosity difference the same mixing performance would be expected as the 3:1 system. If you mix the same fluids, in the same mixer with the same intensity then the mixing time should be the same. For the comparison of the 3:1 and 1:3 experiments with equal inlet viscosities the reaction is sensitive to which stream is concentrated but the mixing is not (reactant species are dilute). Therefore the mixing time should be same for a given energy dissipation rate and any fractional conversion difference is due to local concentration effects.

This is shown in Figure 7.27, where it is apparent that concentrating the alkali stream (blue) has reduced the fractional conversion in comparison to concentrating the acid stream (red). This is in agreement with the theoretical relationship between fractional conversion and mixing time explored in Chapter 6 which predicted that the concentrated alkali inhibits the acid catalysed hydrolysis.

When this theoretical relationship is employed to standardise mixing according to a mixing half-life (Figure 7.28) then the influence of concentration reverse. This is taken as some degree of validation of the engulfment model utilised to estimate the theoretical relationship between fractional conversion and energy dissipation rate. The model is at least able to account for the direction of local concentration effects and to a reasonable degree also the magnitude although it has overestimated the concentration effect but considering the level of accuracy expected the results can be considered to be in adequate agreement.

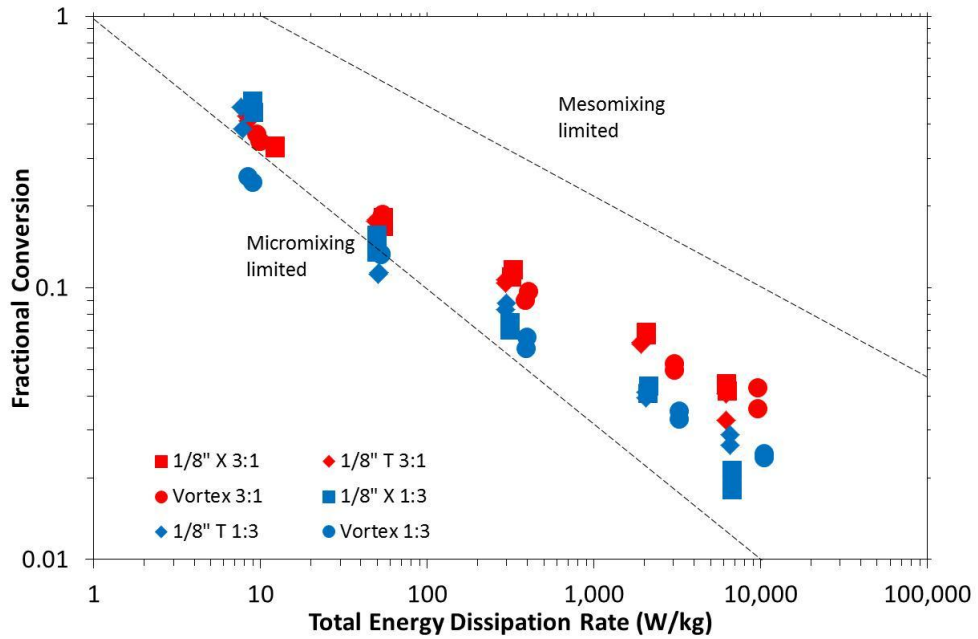


Figure 7.27. Fractional conversion at 3:1 and 1:3 flow ratios with no viscosity difference

Fractional conversion at 1:3 is substantially less than the fractional conversion at 3:1. The physical properties are the same and if the same fluids are mixed in the same mixer with the same intensity the mixing time should be identical. Therefore, this has to be a concentration rather than mixing effect.

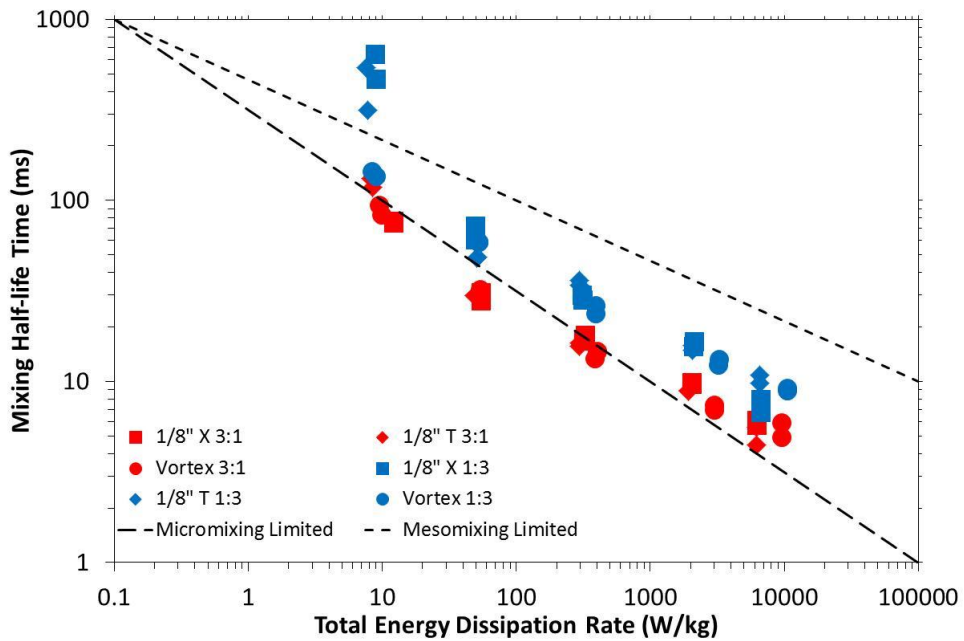


Figure 7.28. Mixing half-life at 3:1 and 1:3 flow ratios with no viscosity difference

When converted to mixing half-life the difference between the 3:1 and 1:3 largely disappears. This is taken as some validation of the engulfment model to predict behaviour caused by local concentration. Note that the logarithmic scale hides some discrepancy at low energy dissipation rate.

So now that the model has been validated and local concentration effects can be accounted for, the influence of viscosity can be considered under both 3:1 conditions and 1:3 conditions. In the modified composition scheme at 3:1 the major stream is more viscous, but at 1:3 the minor stream is more viscous. This means that the outlet viscosity is higher at 3:1 than 1:3 conditions

The effect of viscosity was considered before at 3:1 and it was concluded that at 3:1 the system was independent of the viscosity difference that could be expected of a real system (ratio $\approx 2-3$). At 1:3 this clearly is not the case. Figure 7.29 shows the fractional conversion and Figure 7.30 the mixing half-life as a function of the total energy dissipation for both 3:1 (red) and 1:3 (blue) for mixing without a viscosity difference (solid) and with a viscosity difference (open).

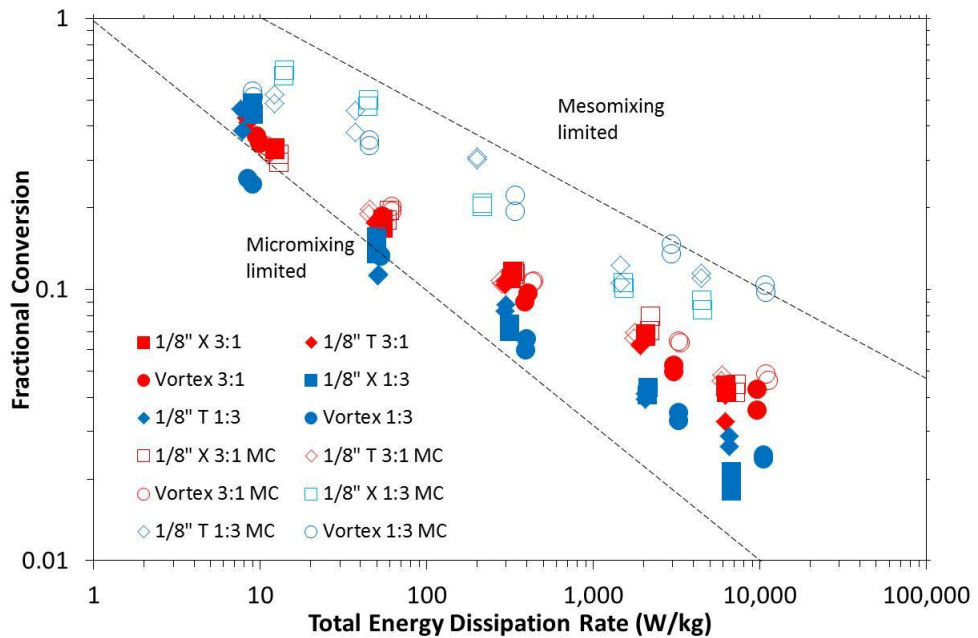


Figure 7.29. Fractional conversion for 3:1 and 1:3 flow ratios

The modified composition experiments (MC) have a viscosity ratio of around 2.5 whilst the others have a viscosity ratio of 1. In the 3:1 experiments the large stream is more viscous and in the 1:3 experiments the small stream is more viscous.

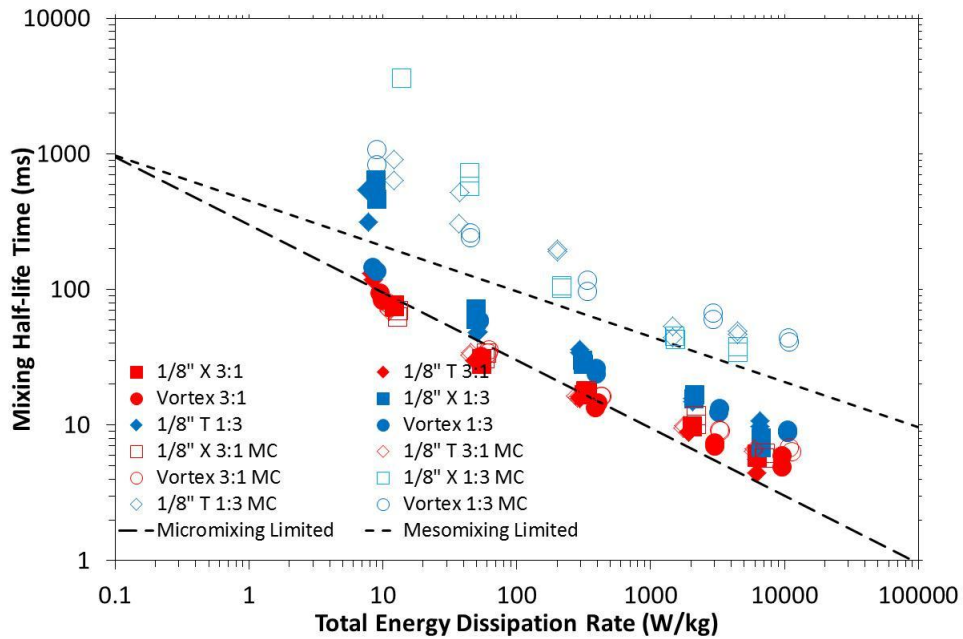


Figure 7.30. Mixing half-life at 3:1 and 1:3 flow ratios

The modified composition experiments (MC) have a viscosity ratio of around 2.5 whilst the others have a viscosity ratio of 1. In the 3:1 experiments the large stream is more viscous and in the 1:3 experiments the small stream is more viscous

The 1:3 modified viscosity experiments (open blue symbols) lie off the trend followed by the other points, even further off once the theoretical relationship is utilised, although it has been established above that this overestimates concentration effects slightly. The difference between these points and those of the 3:1 experiments with a viscosity difference (open red symbols) is that in the 1:3 experiments the viscous stream makes up the smaller stream but in the 3:1 experiments the viscous stream is the majority. Making the minor component more viscous has impeded mixing.

At first glance these experimental results appear contradictory. At 3:1 the results were the same regardless of whether there was an inlet viscosity difference or not. In isolation this could be taken as some qualitative evidence that mixing is limited by inertial scale processes but that is inconsistent with the data at 1:3 where the viscosity has a significant effect of the mixing process. However, unlike the 1:1 system, the 3:1 system shows no dependency on viscosity. Either the 3:1 to system is in the inertial regime or the viscosity effects in the 3:1 systems are so minor that they have little influence on the mixing process? Conversely, this would then mean that

because the 1:3 does exhibit a viscous dependency then either the viscosity change transitions the system to a micromixing limited system or the viscous effects are somehow more significant in the 1:3 setup than the 3:1.

An examination of the gradients of fractional conversion and total energy dissipation rate and mixing half-life and total energy dissipation rate reveals a relationship that, at low flowrates, is consistent with a micromixing dependency (gradient ≈ -0.5). These gradients transition to mesomixing behaviour (gradient ≈ -0.33) at high flowrates, consistent with the observations of the 1:1 systems and turbulent mixing theory.

This seems to rule out the first idea of the 3:1 system being entirely in the inertial regime and the composition adjustment for the 1:3 modified system causing the mixing process to become micromixing limited. This leaves precise nature of the viscosity difference in the 1:3 modified system being more relevant to the mixing process than the 3:1 modified system which has no influence on the mixing performance when compared with the 3:1 or 1:3 system without the viscosity difference.

Considering laminar flow, Mohr equated the shear stress in two components being mixed in different proportions and derived from the definition of Newtonian viscosity that the ratio of the shear rates must be equal to the ratio of the viscosities.[52] The ratio of the striation thickness to the initial striation thickness was then shown to be directly related to the ratio of the viscosity of the component present in a small volume fraction to that of the large. Furthermore, it was stated that when the viscosity ratio of the minor component is less than that of the major component the “ratio of viscosities is taken as unity...because the minor component can never be deformed more rapidly than the matrix of the major component”.[52]

The mixing of miscible fluids in initial moments of fluid contact is similar to the mixing of immiscible fluids.[44–47] Considering immiscible dispersions, again in laminar shear flow, Taylor “experienced difficulty in bursting drops of a viscous fluid by a disruptive flow field in a surrounding fluid of considerably less viscosity”.[48] The mechanism for this stability is not likely to be because of a viscosity difference, it is more likely to be caused by the presence of an interfacial tension, or Kortaweg stress, which relaxes with time as the concentration equalises

across the interface. Estimates of the dynamic viscosity ratio (dispersed/continuous) where this effect occurs vary from around 2.5 to 3.[41], [49] In the 1:3 system with modified composition, since the small volume fraction (the viscous phase) is likely to be the dispersed phase and the viscosity ratio is around this threshold ($\mu_{\text{dispersed}}/\mu_{\text{continuous}} = 2.75$) this system is likely to exhibit some stability due and therefore molecular diffusion may have to occur over a longer length scale. In the 3:1 system with modified composition the viscosity ratio of the small volume fraction to the large ($\mu_{\text{dispersed}}/\mu_{\text{continuous}} = 0.38$) is less than one but as Mohr suggested this would be rounded up to 1 due to the inability of the small component to be deformed more rapidly than the large component making the predicted rate of striation thinning the same as the 3:1 or 1:3 systems without the viscosity difference ($\mu_{\text{dispersed}}/\mu_{\text{continuous}} = 1$). This provides some tentative explanation for the behaviour assuming that the mixing in the viscous-convective range behaves in a similar manner in both systems.

7.6 Fraction of total energy utilised for mixing

7.6.1 Correlation with the Corrsin mixing time

Under certain conditions the mixing exhibits micromixing limited behaviour and at others mesomixing limited behaviour. Therefore, a sensible option for modelling of the mixing process should consider both elements. One such model is the well-known Corrsin mixing model[16]:

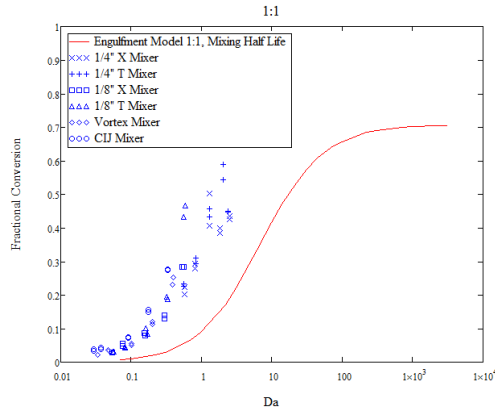
$$\tau_c = 2.04 \left(\frac{L_s^2}{\varepsilon} \right)^{\frac{1}{3}} + \frac{1}{2} \left(\frac{\nu}{\varepsilon} \right)^{\frac{1}{2}} \ln(Sc) \quad (7.6)$$

The first term is the mesomixing time, characterised by a length scale of segregation and energy dissipation rate whilst the second term is the micromixing term characterised by the kinematic viscosity, molecular diffusion coefficient and the energy dissipation rate.

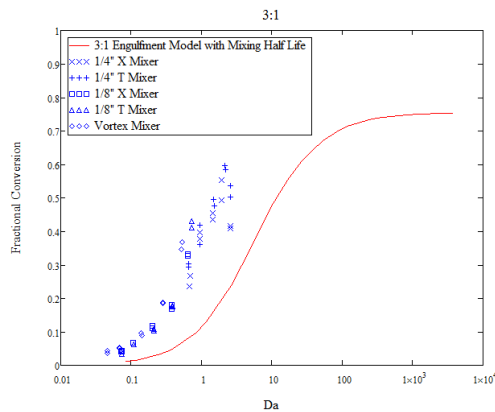
The total energy dissipation rate for experimental data along with an estimate of the length scale of segregation (based on the mixer inlet diameter divided by two) and the molecular diffusion coefficient can be used to determine a Corrsin Damköhler number, defined as:

$$Da_{\text{Corrsin}} = \frac{2.04 \left(\frac{L_s^2}{\varepsilon} \right)^{\frac{1}{3}} + \frac{1}{2} \left(\frac{\nu}{\varepsilon} \right)^{\frac{1}{2}} \ln(Sc)}{\tau_R} \quad (7.7)$$

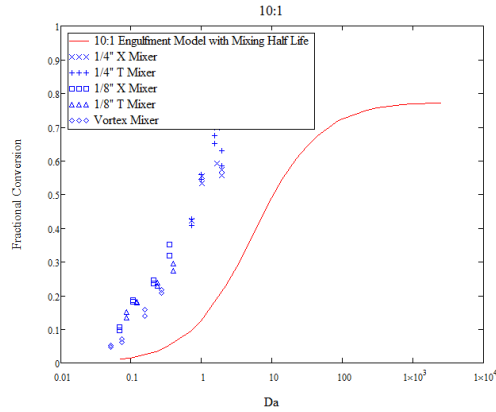
The fractional conversion obtained by experiment, each with an associated Corrsin Damköhler number, can then be compared with the theoretical values as calculated in Chapter 6. This is shown in Figure 7.31 for flow ratios of 1:1 (a), 3:1 (b) and 10:1 (c).



(a) Comparison of experimental and theoretical results at 1:1



(b) Comparison of experimental and theoretical results at 3:1



(c) Comparison of experimental and theoretical results at 10:1

Figure 7.31. Fractional Conversion vs. Da

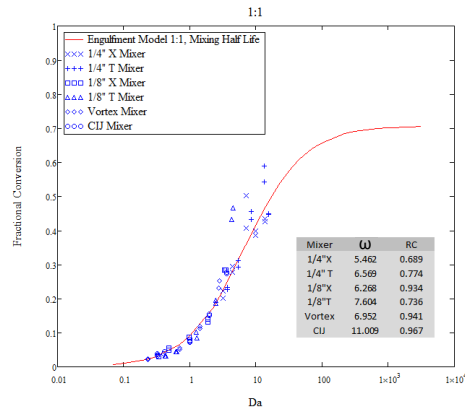
Fractional conversion as a function of the Damköhler number defined as the Corrsin mixing time divided the characteristic reaction time (blue) and with the theoretical line (red) calculated from the mixing half-life.

A constant can be defined to account for differences between models:

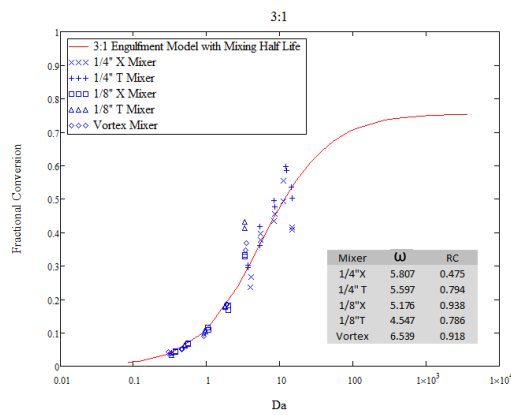
$$Da_{\text{corrsin}} = \frac{\omega \left(2.04 \left(\frac{L_s^2}{\varepsilon} \right)^{\frac{1}{3}} + \frac{1}{2} \left(\frac{\nu}{\varepsilon} \right)^{\frac{1}{2}} \ln(Sc) \right)}{\tau_R} \quad (7.8)$$

This constant (ω) can then be determined from a least squares fit of the data. This is shown in Figure 7.32 with the values of the constant ω and the values of the coefficients of determination (RC) for each mixer.

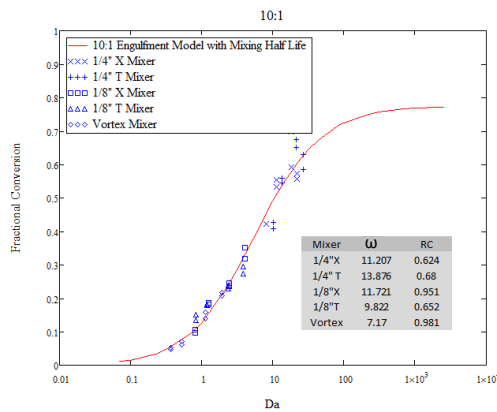
The large mixers at low flowrates (high Damköhler number) fall off the trend, perhaps due to laminar mixing behaviour, but all other points provide a reasonable agreement. An inherent disadvantage of a least squares fit is that due to their larger contributions to the residual error, points with larger values are given more weight in comparison to those a low values. This could be adjusted for by using a logarithmic version of a least squares but was not attempted due to the reasonably good fit obtained without it. This explains why the points can be slightly off the curve at low Damköhler number.



(a) Least squares fit at 1:1



(b) Least squares fit at 3:1



(c) Least squares fit at 10:1

Figure 7.32. Fractional Conversion vs. ωDa

As before but with a least square fit to determine the constant. Values of the constant (ω) and the coefficient of determination (R^2) are shown in the chart.

If it is assumed that a constant is required in order to correct for the fraction of the total energy dissipation rate that it is utilised by the bulk for mixing, then this fraction could be extracted by a similar method. However, in order to successfully extract some quantitative information one has to consider what the exact relationship between the mixing half-life as defined previously and the Corrsin mixing time is.

The Corrsin mixing time is based on the reduction segregation from its initial value down to a factor of 1/e[16], [25]:

$$S_i = S_{i0} \exp\left(\frac{-\tau}{\tau_c}\right) \quad (7.9)$$

To make an approximate equivalency between the Corrsin time and the mixing half-life, the magnitude of segregation initially and finally has to be considered. The mixing half-life occurs at 50% acid consumption. S_i is defined as the concentration fluctuations around a mean value squared:

$$\frac{S_i}{S_{i0}} = \frac{(c_i - \bar{c}_i)^2}{(c_{i0} - \bar{c}_{i0})^2} \quad (7.10)$$

Initially, the volume averaged acid concentration is 100mmol/L and at 50% mixed it is 50 mmol/L. The concentration of acid in the alkali rich zone is always zero (neutralisation is instantaneous with respect to mixing) therefore $c_i = c_{i0} = 0$. This leaves:

$$\frac{S_i}{S_{i0}} = \frac{50^2}{100^2} \quad (7.11)$$

$$\frac{S_i}{S_{i0}} = 0.25 \quad (7.12)$$

$$0.25 = \exp\left(\frac{-\tau}{\tau_c}\right) \quad (7.13)$$

$$\tau = 1.386\tau_c \quad (7.14)$$

If it is assumed that the same fraction of the total energy dissipation rate is utilised for mixing in both the micromixing and mesomixing terms then the following equation can be constructed:

$$\text{Da}_{\text{corssin}} = \frac{1.386 \left(2.04 \left(\frac{L_s^2}{c\varepsilon} \right)^{\frac{1}{3}} + \frac{1}{2} \left(\frac{\nu}{c\varepsilon} \right)^{\frac{1}{2}} \ln(Sc) \right)}{\tau_R} \quad (7.15)$$

Which can be written as:

$$\text{Da}_{\text{corssin}} = \frac{1.386 \left(2.04 \left(\frac{1}{c} \right)^{\frac{1}{3}} \left(\frac{L_s^2}{\varepsilon} \right)^{\frac{1}{3}} + \frac{1}{2} \left(\frac{1}{c} \right)^{\frac{1}{2}} \left(\frac{\nu}{k\varepsilon} \right)^{\frac{1}{2}} \ln(Sc) \right)}{\tau_R} \quad (7.16)$$

A new constant, ψ , can be defined:

$$\psi = \left(\frac{1}{c} \right)^{\frac{1}{3}} \quad (7.17)$$

Then the term from the micromixing expression can be written as:

$$\left(\frac{1}{c} \right)^{\frac{1}{2}} = \psi^{\frac{3}{2}} \quad (7.18)$$

Substituting these in gives:

$$\text{Da}_{\text{corssin}} = \frac{1.386 \left(2.04\psi \left(\frac{L_s^2}{\varepsilon} \right)^{\frac{1}{3}} + \frac{1}{2} \psi^{1.5} \left(\frac{\nu}{\varepsilon} \right)^{\frac{1}{2}} \ln(Sc) \right)}{\tau_R} \quad (7.19)$$

A least squares fit as before allowed a value of ψ to be extracted and this was then converted to c . This provides the following as an estimate of the percentage of the total energy dissipation utilised by the mixing process:

	$\frac{1}{4}''X$	$\frac{1}{4}''T$	$\frac{1}{8}''X$	$\frac{1}{8}''T$	Vortex	CIJ
1:1	2.1	1.3	1.4	0.9	1.1	0.6
3:1	2.0	1.9	2.5	3.5	1.6	-
10:1	0.3	0.2	0.3	0.4	1.1	-

Table 7.4. Estimate of percentage of total energy dissipation rate used by mixing

This method estimates that the fraction of the total energy dissipation rate utilised by the mixing process is around 1% at 1:1, 2% at 3:1 and a fraction of a percent at 10:1.

Figure 7.33 shows the mixing half-life as a function of the energy dissipation rate with the Corrsin mixing relationship shown with 1%, and 0.1% of the total

energy dissipation rate used for mixing. This uses a length scale of segregation of 2mm (approximately the length scale for the smaller mixers) and the relationship between the Corrsin mixing time and the mixing half-life (1.386) was used as a prefactor as before.

The shows graphically, that at 1:1 and 3:1 the mixing efficiency is around 1% and at 10:1 it is around 1% for the vortex and 0.1% for the other mixers.

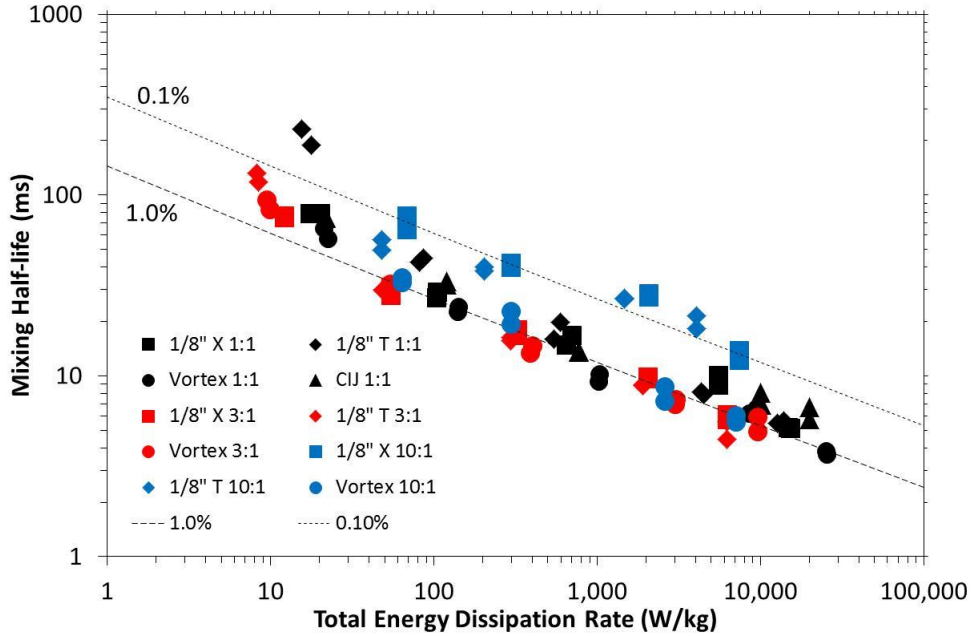


Figure 7.33. Corrsin relationship with 1% and 0.1% efficiency

Corrsin mixing relationship with a representative length scale of segregation of 2mm and Schmidt number and kinematic viscosity around that of the systems.

7.6.2 Correlation with engulfment time

Another, simpler way, of estimating the fraction of the total energy dissipation rate utilised by the mixing process would be to translate the fractional conversion to a theoretical engulfment time using the relationship theoretically determined in Chapter 6 (and used to construct Figure 7.15) and then to consider the fraction of the total energy dissipation rate that equates the engulfment as calculated by equation (2.7) with this engulfment time:

$$\tau_E = 17.3 \left(\frac{v}{c\epsilon_{total}} \right)^{\frac{1}{2}} \quad (7.20)$$

Lines corresponding to 2% of the total energy dissipation rate and 0.1% of the total energy dissipation rate are shown in Figure 7.34. This shows, again, that only a

small fraction of the total energy dissipation is utilised by the total energy dissipation rate. The main flaw in this methodology is, that as shown in section 7.2 and 7.3, the mixing is not entirely limited by the process of engulfment, especially at 10:1. This should be obvious when comparing the gradients. Regardless, it provides a quick and easy approximation which agrees broadly with the figure provided by the Corrsin model.

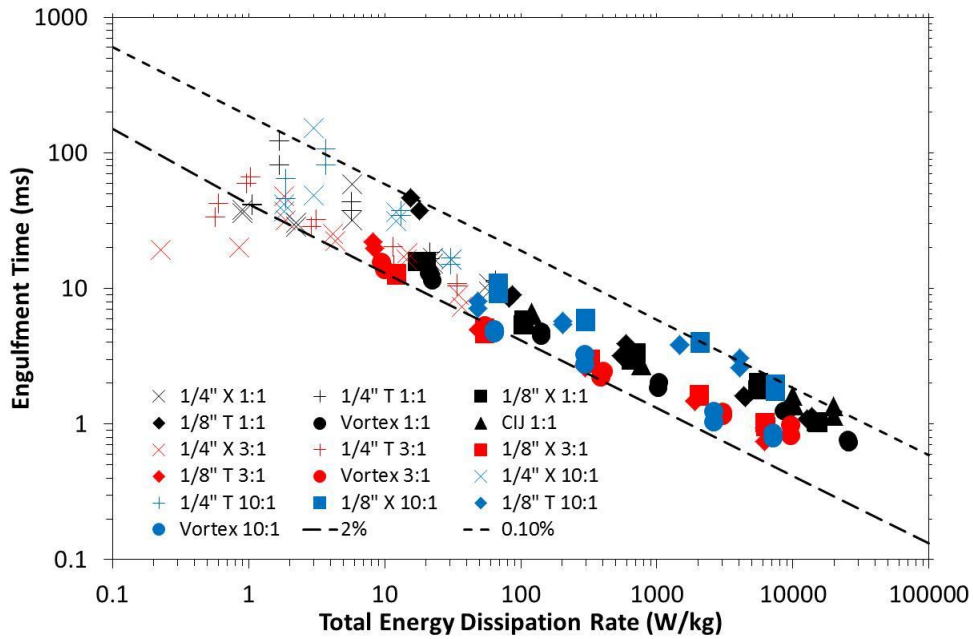


Figure 7.34. Engulfment time with 2% and 0.1% efficiency

The theoretical relationship between the engulfment time and fractional conversion, as determined in Chapter 6 and utilised in creation of Figure 7.15, can be used to estimate the fraction of the total energy dissipation rate that is used by the mixing process.

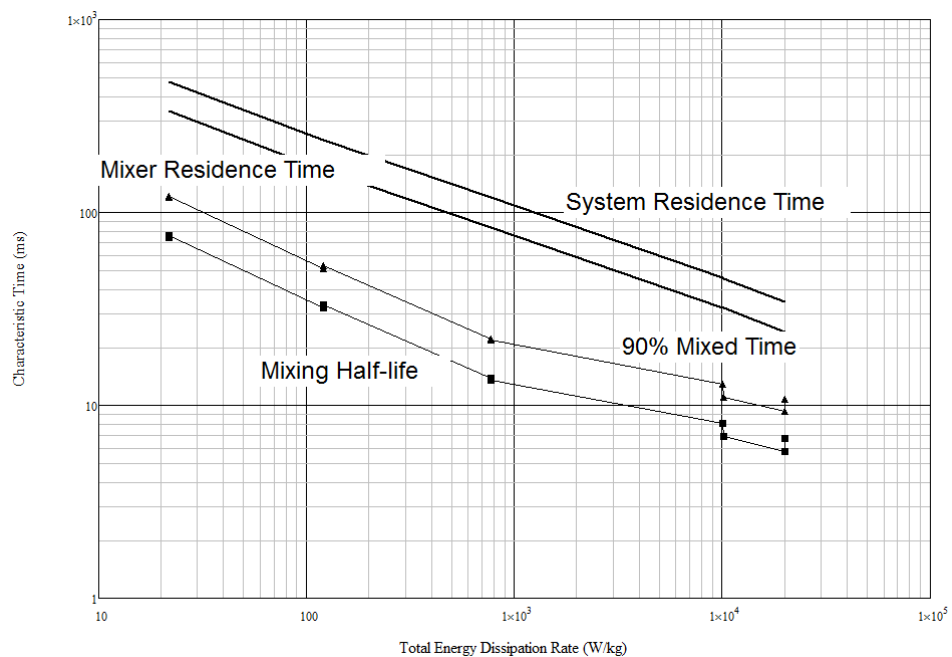
7.7 Comparison of mixing and residence timescales

Now that an estimate of the absolute mixing time has been achieved it is sensible to compare the timescales of the mixing process with the residence time in the mixer itself and within the system which is defined as the mixer plus an outlet capillary. Comparing it with the mixer timescale indicates whether or not the mixer itself successfully completes mixing. This is useful to know as in many applications it is desirable to achieve homogeneity as quickly as possible to remove mixing as a variable in the subsequent process. This section aims to provide an indicative measure of whether this is possible in these mixers and mixing conditions.

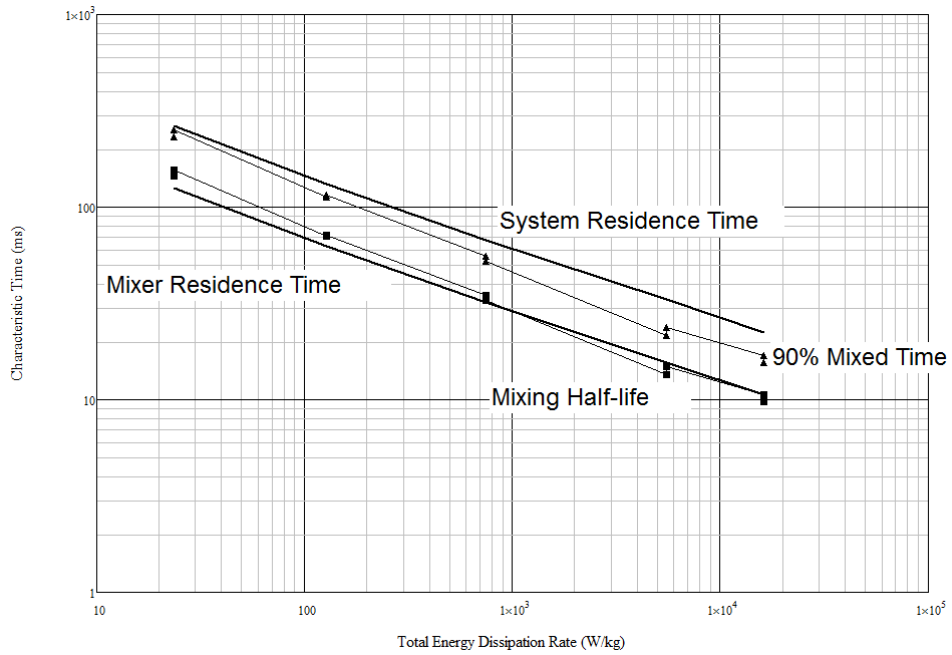
Two residence times have been defined. In our setup, after the mixer, there was a short capillary to enable the pressure drop to be measured and the flow to be

directed to a container for sampling. The system residence time is the sum of the time in the mixer and in the capillary. It is important because if mixing is not complete within the system then mixing will be left to complete by molecular diffusion alone. It is predicted that if the mixing time is similar to or greater than the system residence time then this will be accompanied by an increase in data scatter and lower reproducibility. Another residence time, corresponding to the volume of the mixer itself, was also defined in order to establish if mixing was completed within the mixer itself.

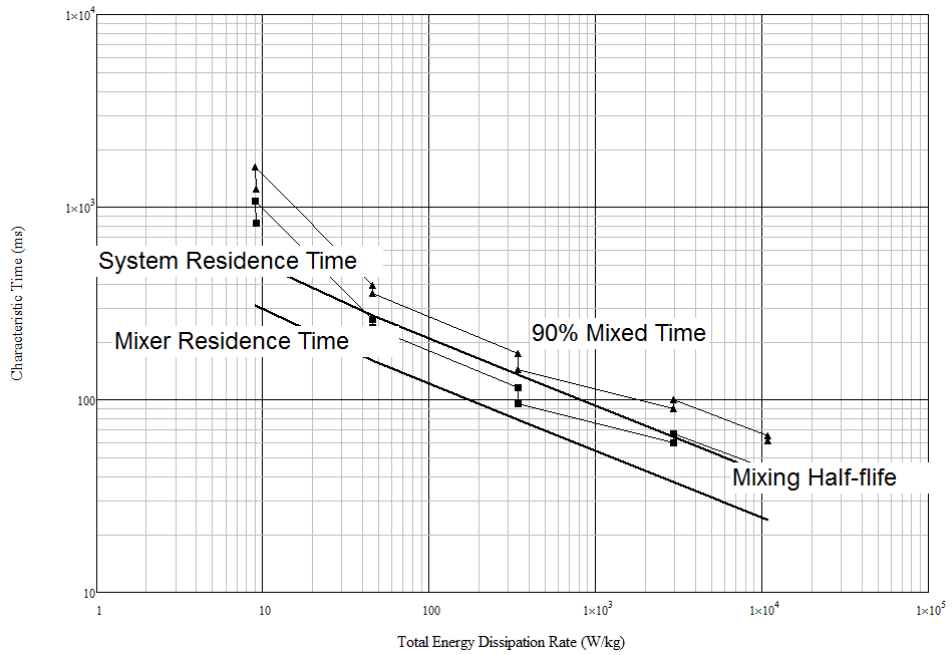
Three examples of the timescale comparison graphs are shown corresponding to conditions where mixing is easily completed (Figure 7.35 a), is completed within the system volume but the mixer itself struggles (Figure 7.35 b) and finally where neither the mixer nor system complete mixing (Figure 7.35 c). The results are then summarised for the mixer volume (Table 7.5) and system volume (Table 7.6) and the full graphical results are shown in the appendix.



(a) CIJ 1:1 no viscosity difference



(b) 1/8" X Mixer 1:1 with a viscosity difference



(c) 1/8" X Mixer 1:3 with a viscosity difference

Figure 7.35 Comparison of timescales of mixing and residence

First consider the 90% mixed time and the mixer volume (Table 7.5). No mixer successfully manages to mix the stabilised 1:3 MC system but the vortex mixer

successfully mixes all others and the CIJ successfully mixes at 1:1 both with and without a viscosity difference. However, the 1/8" X and T mixers struggle to complete mixing within the mixer residence time in many experiments and the 1/4" mixers fail to complete mixing within the mixer residence time in all instances.

After evaluating the performance of the mixers and estimating a mixing, there was found to be little difference in the estimated mixing time for the smaller mixers. The crucial difference is mixer volume. Due to the mixing chamber the CIJ and vortex mixer have inherently larger volumes and consequently they have a greater residence time which happens to be generally larger than the mixing time.

	CIJ	Vortex	1/8" X	1/8" T	1/4" X	1/4" T
1:1	✓	✓	Borderline	Borderline	✗	✗
3:1	n/a	✓	✓	✓	✗	✗
1:3	n/a	✓	Borderline	Borderline	✗	✗
10:1	n/a	✓	✗	✗	✗	✗
1:1 MC	✓	✓	✗	✗	✗	✗
3:1 MC	n/a	✓	✓	✓	✗	✗
1:3 MC	n/a	✗	✗	✗	✗	✗
10:1 MC	n/a	✓	Borderline	Borderline	✗	✗

Table 7.5. Timescale analysis - mixer volume

Obviously, with the addition of a sufficiently long capillary, any miscible fluids would eventually mix. The previous results were taken to mean that for simple operations the CIJ and vortex mixer could be utilised without additional precautions whilst the T and X mixers should always be deployed with additional residence time (i.e. an outlet capillary) if molecular scale mixing is a requirement for a subsequent process.

In comparing the 90% mixed time with the system residence time (Table 7.6), it is observed that the vortex mixer comes close to mixing the stabilised 1:3 system but both the small X and T still fail. The small T and X also struggle under 10:1 conditions. The larger T and X mixers struggle or fail in all instances. Obviously the solution is to use a longer capillary but that was not the objective of the analysis. The

objective was to identify when the system struggled to complete mixing before sampling in order to compare the scatter of data at these points.

	CIJ	Vortex	1/8" X	1/8" T	1/4" X	1/4" T
1:1	✓	✓	✓	✓	Borderline	Borderline
3:1	-	✓	✓	✓	Borderline	Borderline
1:3	-	✓	✓	✓	✗	Borderline
10:1	-	✓	✓	✓	✗	✗
1:1 MC	✓	✓	Borderline	Borderline	Borderline	Borderline
3:1 MC	-	✓	✓	✓	Borderline	Borderline
1:3 MC	-	Borderline	✗	✗	✗	✗
10:1 MC	-	✓	✓	✓	✗	✗

Table 7.6. Timescale analysis - system volume

The scatter of the mixing experiments which failed to complete mixing within the system is best considered by returning to the regression ellipse plots constructed previously in the chapter. These are shown for three conditions where mixing struggled to complete (Figure 7.36 a,b,c) and one where it completed within the system but not the mixer itself (Figure 7.36 d). The region of good fit (coefficient of determination > 0.9) between fractional conversion and energy dissipation is both larger in size and magnitude (darker) in the experiment where mixing is judged complete compared to those where mixing is incomplete. A system with good reproducibility would be expected to have less scatter and better correlation. Figure 7.36 illustrates the effect incomplete mixing can have on the fractional conversion and explains the larger error observed in the 1:3 system with the viscosity difference for all mixers and of the larger 1/4" mixers in general.

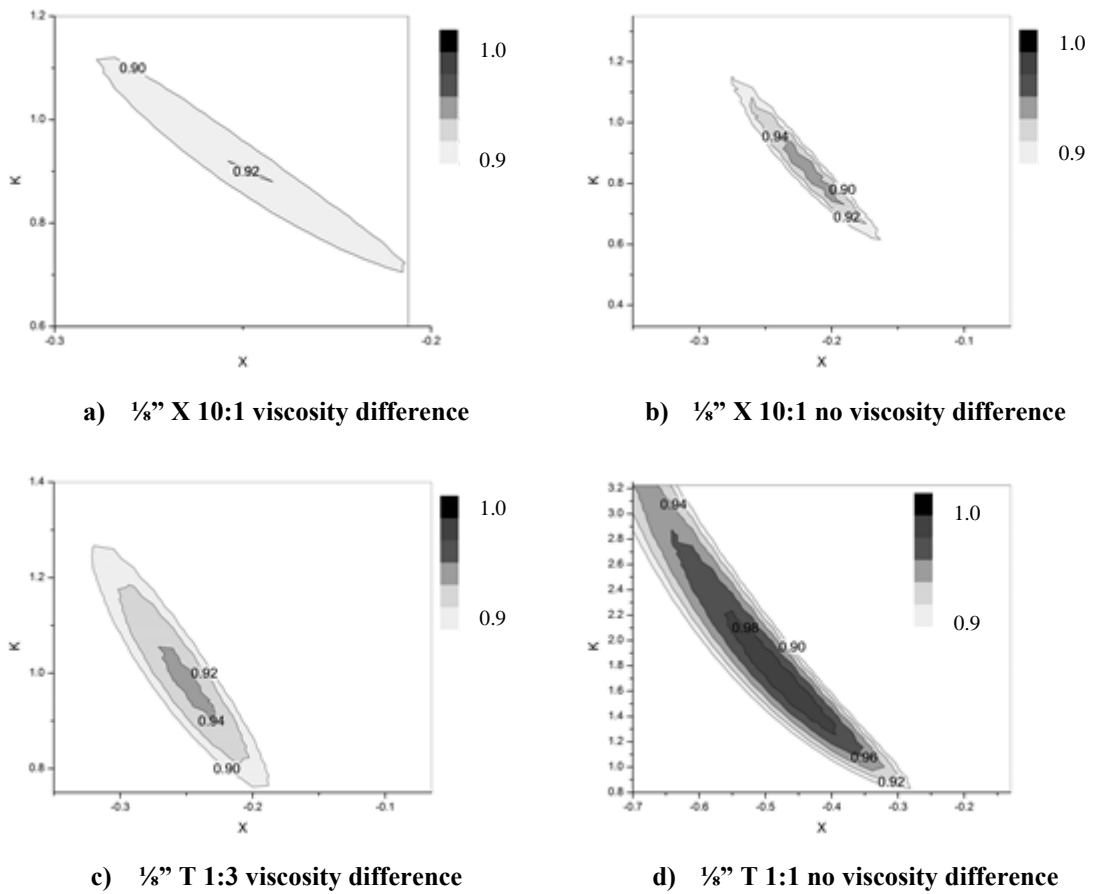


Figure 7.36. Regression ellipse plots

Regression ellipse plots for systems where the mixer struggled to complete mixing with the system volume (top left, top right and bottom left) compared to one where mixing was completed (bottom right).

7.8 *Mixing characterisation conclusions*

The Bourne IV competitive reaction scheme is a robust method for characterisation of mixer performance and can be easily extended to include volumetric flow ratios and the physical property differences that can be expected in common processing applications. However, the addition of volumetric flow ratios involves concentrating the reactants one of the streams which influences the local reaction rates. This requires a model in order to compensate for these effects and provide fair comparison about the flow ratios influence on the mixing time.

The engulfment model was employed and has been experimentally verified to predict with reasonable accuracy the direction and magnitude of these concentration effects. They can also provide, with acceptable accuracy, a well-defined estimate of the absolute mixing time. The IEM model was also utilised but it was found to deal poorly with the volumetric flow ratio changes. The advantages of such models over more advanced approaches like CFD is that they are relatively easy to implement using tools widely available to process engineers whereas CFD requires a degree of specialism.

The fractional conversion of dimethoxypropane has been found to have a linear relationship with mixing time until a fractional conversion of about 0.3. This is useful as it allows the interpretation of many mixing effects without the need to employ a time consuming model.

The total energy dissipation is a very effective means to correlate the mixing times, which implies the assumption often used in the literature of the total energy dissipation rate being proportional to the energy dissipation rate utilised for the mixing process is valid. The fraction of the total energy dissipation rate utilised for mixing has been estimated to around 1% at 1:1 and 2% at 3:1, the vortex mixer holds its performance of 1% at 10:1 but the efficiency of the other mixers (T and X mixer) reduce to around 0.3% at 10:1.

In continuous mixers, especially those operating at a flow ratio of 1:1, both micromixing and mesomixing parts of mixing were found to be important and therefore a Corrsin style mixing model is likely to be the most accurate. As the ratio changes from 1:1 micromixing becomes less important.

The vortex mixer and CIJ mixer can be employed directly as they are for simple mixing operations but a T and X mixer should always be used with a capillary. This is due to mixing chamber in the CIJ and vortex mixer ensuring a residence time which is greater than the mixing time. The vortex mixer is the best mixer but only marginally so at 1:1 and 3:1. Therefore it is expected that for most operations around a 1:1 flow ratio a T or X mixer with an outlet capillary would be sensible choice due to the inherent simplicity and low cost of these devices. At 10:1 the vortex mixer is substantially better than the others and would be advised for ratios greater than 3:1.

A stabilisation effect when the small stream is the more viscous stream has been noted. This is thought to be due to the difficulty in droplet breakup when a more viscous stream is surrounded by a less viscous majority phase. None of the mixers tested here was able to deal effectively with this. A practical example of such a system would be antisolvent precipitation of a solute from an organic solvent using an aqueous solution as the antisolvent.

8 Mixing Influenced Precipitation - Results and Discussion

If mixing and segregation have an underlying role in a process then this implies the characteristic timescale for the process is less than or comparable to the mixing timescale. A Damköhler number can be defined to assess the mixing sensitivity of a process:

$$Da = \frac{\tau_{Mixing}}{\tau_{Process}} \quad (8.1)$$

From this definition it is apparent that mixing is only important as Da approaches or is greater than unity (i.e. mixing occurs on a timescale similar to or greater than that of the process itself). Therefore, if a process exhibits a degree of mixing sensitivity then this implies that the process itself is fast with respect to mixing.

Chapter 7 outlined the mixing performance of various mixers, including the CIJ mixer which will be considered in section 8.1. This mixer was found to have a mixing time around 100ms at low flowrates (50ml/min) and around 10ms at high flowrates (700ml/min). It was also pointed out that this mixing time was significantly less than the residence time in the mixer.

Consequently, if an antisolvent crystallisation process exhibits mixing sensitivity then it can be considered likely that the timescale of nucleation or precursor formation is less than that of the mixing time.

8.1 Mixing influenced precipitation of Valine

Nucleation is the single most important parameter to control in a crystallisation process. Nucleation controls the number of particles that are formed and along with growth rate and duration as well as secondary transfer processes such as aggregation it controls the particle size distribution. For instance, if nanoparticles are desired then it is important to maximise the nucleation rate which maximises the number of particles formed and if growth is controlled and aggregation suppressed then the final particle size and distribution should be small. No attempt in this work is made to quantify or control the growth or aggregation. All that is studied is the influence of

the initial mixing, which in antisolvent crystallisation controls the nucleation step, on the crystallisation process.

8.1.1 Survey of mixing influenced solid recovery

Figure 8.1 shows the solid recovery (as a percentage of the equilibrium solid recovery,) after ninety minutes under quiescent conditions following the initial rapid mixing as a function of both solute content (supersaturation) and inlet flowrate (initial mixing). It is apparent that two regions exist, a region of fast kinetics at one extreme in the top right and a region of slow kinetics in the bottom left. Curving its way between these regions is a transition region with intermediate solid recovery. Metastability can be induced in this system either by poor mixing or low supersaturation.

The contour plot is constructed by linear interpolation of a fairly dense set of 20 points in the variable space. Although it demonstrates the regions with clearly different kinetics and how mixing and bulk supersaturation influence them, it does not clearly demonstrate how the transition between these regions occurs i.e. whether it is sudden or gradual as the linear interpolation between points implies.

Even at the poorest mixing conditions (low flowrate) mixing is complete within a hundred milliseconds. Mixing differs only in these first hundred milliseconds and therefore for the subsequent ninety minutes the conditions are the same, yet the difference in solid recovery can be seventy percent or more. This means that crystallisation is influenced and controlled by a process which occurs in a timescale of less than a second and therefore the initial mixing is the single most important parameter to control next to the bulk supersaturation.

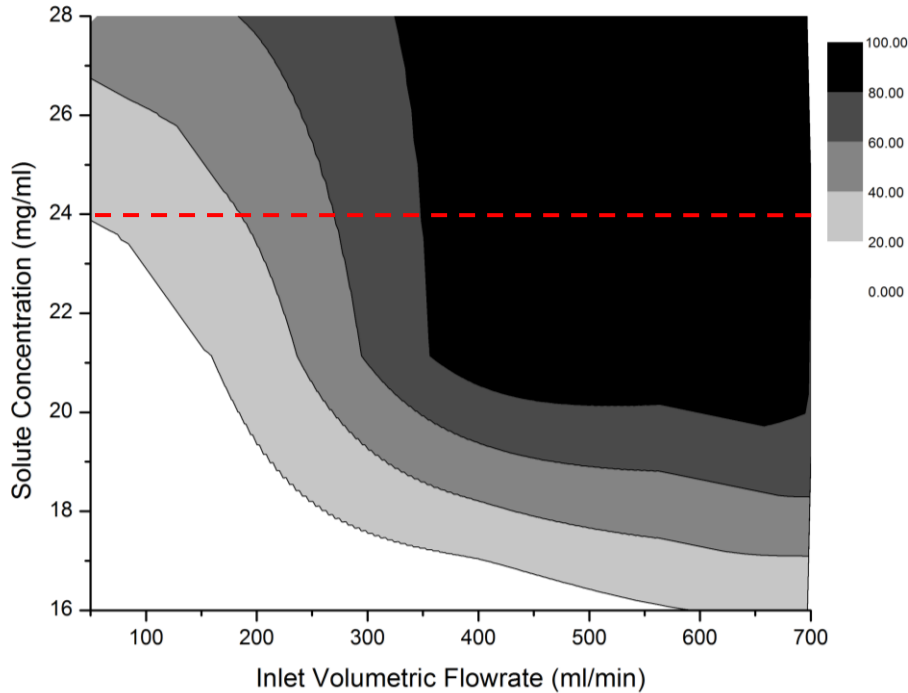


Figure 8.1. Solid Recovery after 90 Minutes

Solid recovery (as a percentage of equilibrium solid recovery) after 90 minutes as a function of the inlet volumetric flowrate (X axis) and solute concentration (Y-axis). The dashed red line shows the region through which time dependent analysis was carried out to gain a sense of the nature of transition and the influence of mixing on kinetics and particle size distribution.

8.1.2 Time dependent analysis

The 50ml/min and 200 ml/min samples were visibly different from the other solutions, with little turbidity resulting in a small number of distinct large particles forming. At higher flowrates the systems was very turbid. In between these extremes (300 ml/min) the systems was less turbid (Figure 8.2). After 30 minutes it was observed that crystals in the low flowrate samples almost entirely sedimented but in high flowrate samples crystals were still suspended in the solution. One explanation of this behaviour is that at low flowrates a few large crystals were generated and quickly sedimented but at high flowrates many small crystals were generated and stayed suspended for longer.

Interestingly, although the 50 ml/min and 200 ml/min solutions were not turbid, when filtered after a short interval, the filtrate was turbid. This was the case for growth periods up to 10 minutes or more for the 50 ml/min flowrate but the period where this phenomenon was observed reduced as the flowrate increased until

at higher flowrates it was not observed at all or occurred in a timescale smaller than 1 minute as summarised in Table 8.1.

Also as summarised in Table 8.1, when the turbid filtrate was observed it was also accompanied by a huge increase in filtration time (by as much as a factor of 10 for low flowrates filtered after a short period). As the growth period and/or the inlet flowrate increased (better mixing) the filtration speed increased to normal and the filtrate became clear.

The 50 ml/min sample looked visibly clear after 1 minute. However, the filtration was very slow (longer than 50 minutes) and it seemed as if the filter clogged and the filtrate was visibly turbid. This observation indicates that the sample solution was metastable and the filtration process triggered nucleation, clogged the filter to some extent and slowed down the filtration process.

The 700 ml/min sample on the other hand looked visibly turbid after 1 minute, the filtration was normal (less than 5 minutes) and the filtrate was clear. Apparently this sample passed through the window where filtration had a huge effect on the sample in less than 1 minute or such dependencies do not exist at all. This window is illustrated by the blue region in Figure 8.4.

The turbidity was monitored (Figure 8.3) as a function of both flowrate and solute concentration. At low solute concentration there was little or no absorption and this trend continued at low flowrates (50ml/min and 200ml/min) and high solute concentration. At the higher flowrates, as the system headed towards the high solid recovery region, a substantial absorption was recorded at solute concentrations from 20mg/ml with the best mixing (highest flowrate) peaking first. At 24mg/ml a flowrate of 300ml/min was tested and this showed much greater than absorption than the flowrates below it but nowhere near as high as the flowrates above it. 300 ml/min appears to be on the edge of a transition region between fast and slow kinetics, this transition can be seen in Figure 8.1, Figure 8.2, Figure 8.3 and Figure 8.4.

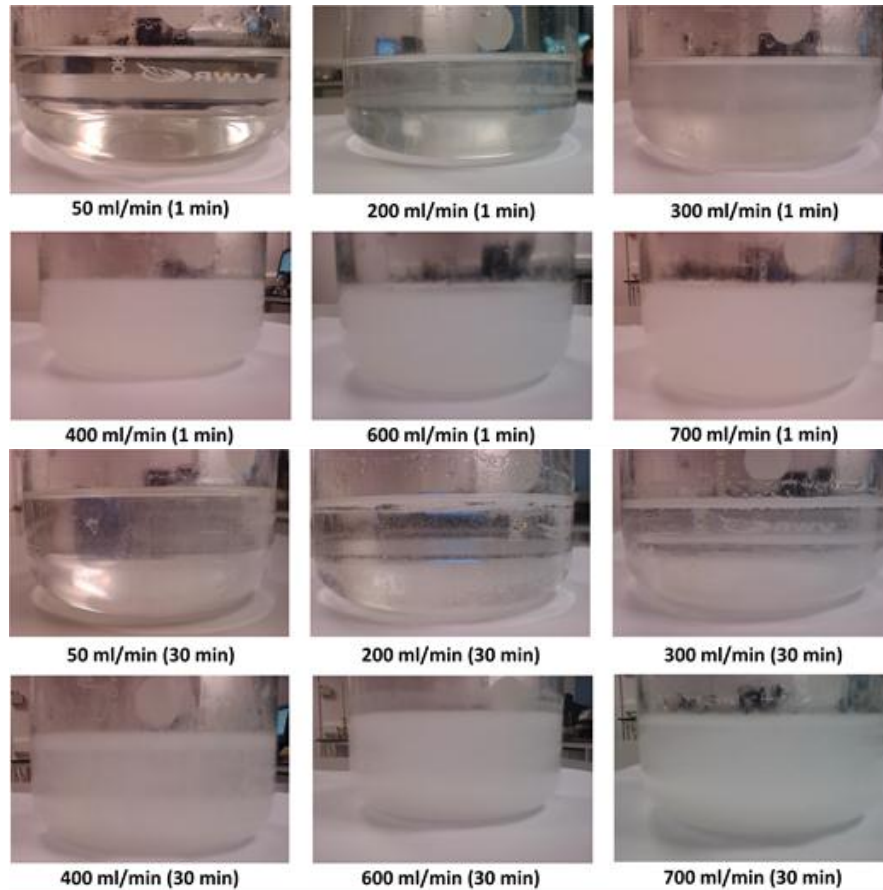


Figure 8.2. Turbidity of the samples after 1 minute and 30 minutes

Pictures of the 200ml samples before gravimetric analysis at a concentration of 24 mg/ml 1 minute after mixing (top two lines) and 30 minutes after mixing (bottom two lines) over a range of flowrates.

		1 min	5 min	10 min	30 min
50 ml/min	Filtrate	Turbid	Turbid	Turbid	Clear
	Filter Speed	Very Slow	Very Slow	Slow	Normal
200 ml/min	Filtrate	Turbid	Turbid	Clear	Clear
	Filter Speed	Very Slow	Slow	Normal	Normal
300 ml/min	Filtrate	Turbid	Clear	Clear	Clear
	Filter Speed	Very Slow	Normal	Normal	Normal
400 ml/min	Filtrate	Turbid	Clear	Clear	Clear
	Filter Speed	slow	Normal	Normal	Normal
600 ml/min	Filtrate	Clear	Clear	Clear	Clear
	Filter Speed	Normal	Normal	Normal	Normal
700 ml/min	Filtrate	Clear	Clear	Clear	Clear
	Filter Speed	Normal	Normal	Normal	Normal

Table 8.1. Filtrate Turbidity and Filter Time as a function of filter time

The filtrate is either turbid or clear. The filter time is normal, slow or very slow. Normal indicates a filter time of less than 5 minutes, slow of the order of 20 minutes and very slow of the order of 50 minutes.

Mixing Influenced Precipitation - Results and Discussion

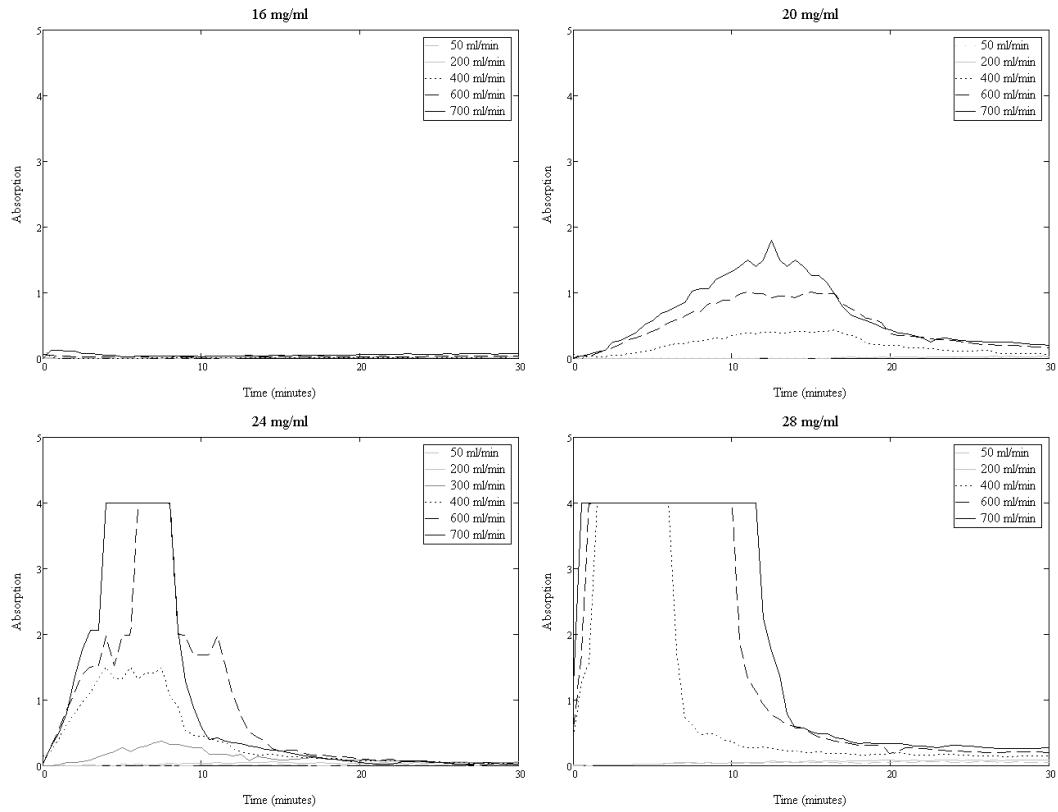


Figure 8.3. Change in absorption with time

UV absorption as a function of time at a wavelength of 248nm for different inlet flowrates and concentrations

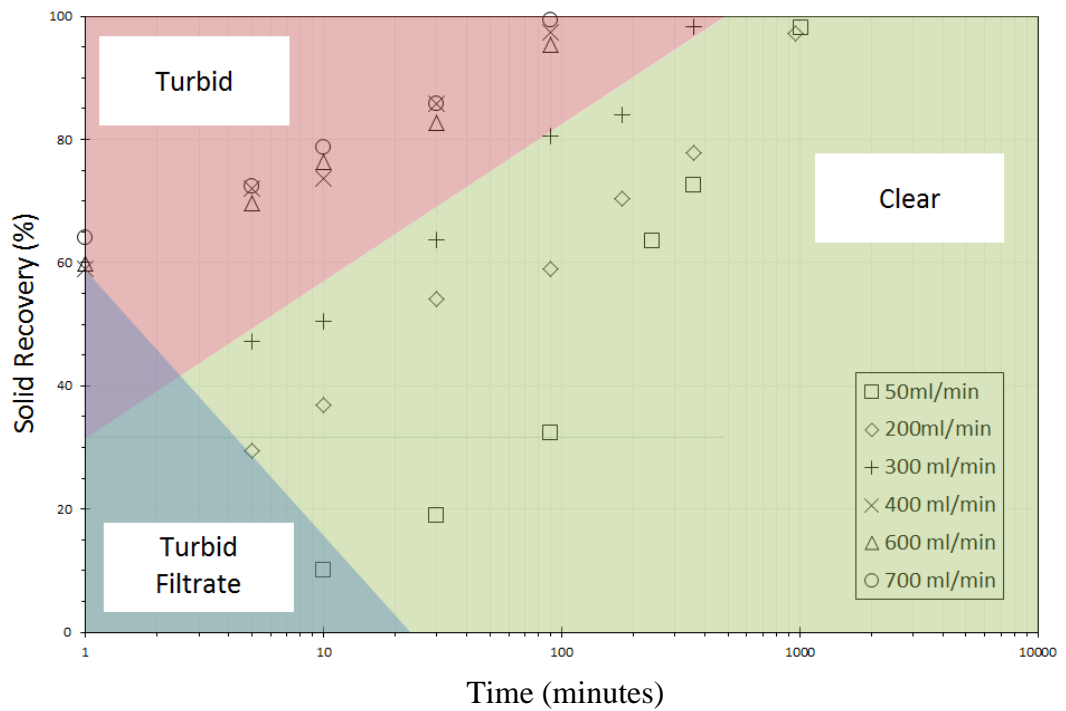


Figure 8.4. Time dependent solid recovery through 24mg/ml slice

Figure 8.4 shows the change in solid recovery with time at a 24 mg/ml slice through the contour plot of Figure 8.1. Interestingly, the solid recovery appears to be independent of flowrate at flowrates above 400ml/min. At inlet flowrates below this value, there was a reduction in solid recovery as a function of time. This reduction resulted in less turbidity and much larger particles. The change in turbidity from low to high is marked on Figure 8.4 as is the region where filtration induces crystallisation in the filtrate which retreats with increasing flowrate.

Figure 8.5 shows the surface weighted mean ($D_{3,2}$ - grey) and volume weighted mean ($D_{4,3}$ - black) as a function of inlet volumetric flowrate after 90 minutes (top , and at equilibrium (bottom). Better mixing results in a narrower particle size distribution than poorer mixing and also a reduction in particle size. After 200ml/min there is a rapid decrease in the final mean particle size which corresponds well to the transition region between the low and high flowrates.

At 90 minutes (Figure 8.5 – top) there is not a huge difference in particle size between the systems with the slow kinetics and the system with fast kinetics. The slow kinetic system (low flowrate) is approximately 25% to 50% larger in size than the fast kinetic system but considering the difference in solid recovery between the regimes, the fast system must have more particles. At low flowrate, these particles grow considerably over time whilst at high flowrate the solute is shared over more particles resulting in smaller sized particles with a narrower distribution.

Figure 8.6 shows the particle size distribution for different flowrates and times. The change in particle size distribution with time for 700ml/min (top left) clearly shows that the particles steadily get larger and the particle size distribution widens with time. Comparing the effect of mixing for the region of fast kinetics after 1 minute, this system shows the size decreasing and the distribution narrowing as mixing improves. All this is consistent with initial mixing controlling nucleation.

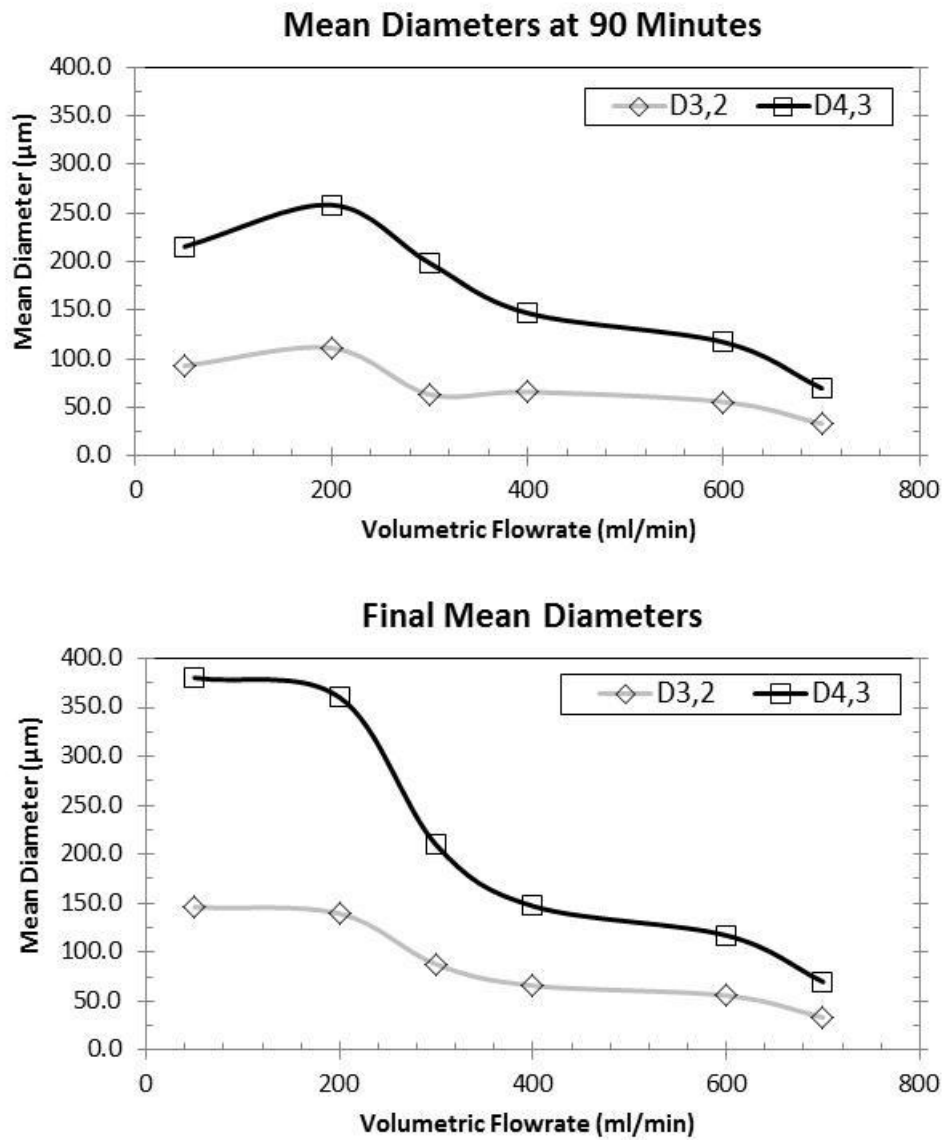


Figure 8.5. Influence of flowrate on mean particle size

After 90 minutes (top left) and at 100% Recovery (top right) and the change in size in the turbid region (bottom).

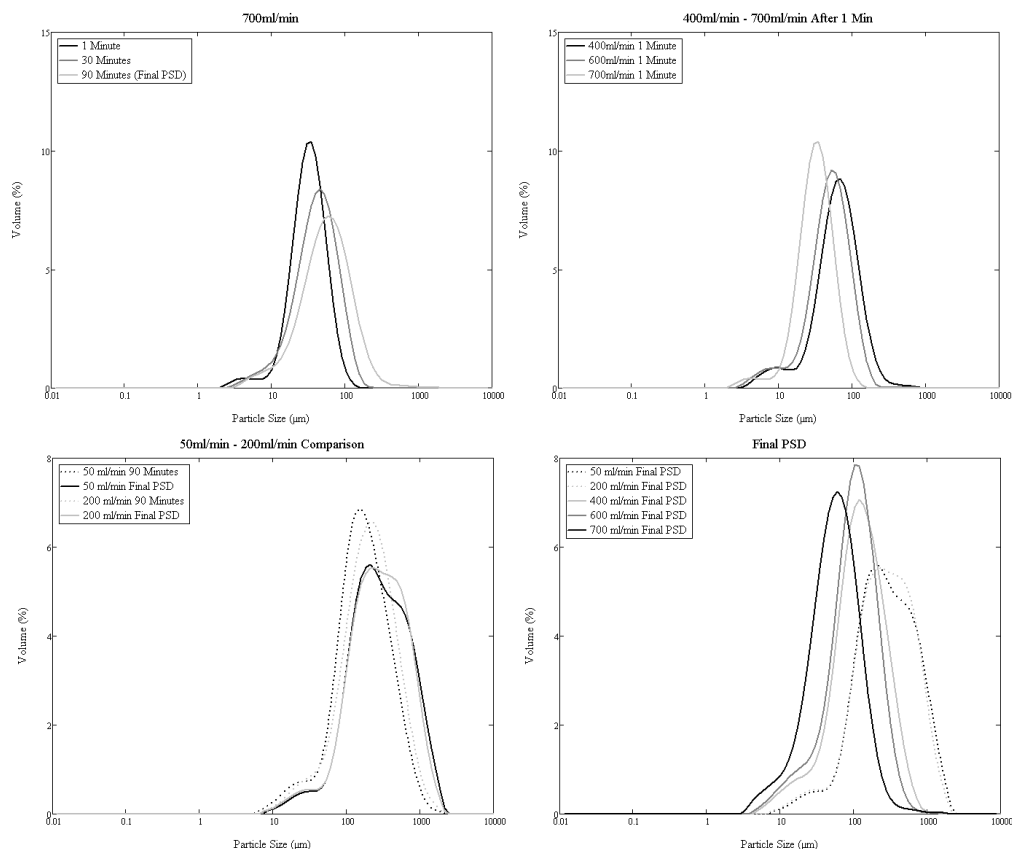


Figure 8.6. Particle Size Distributions at 24mg/ml

Sample particle size distributions showing growth after mixing with high flowrates (top left), the effect of flowrate on the PSD after 1 minute for high volumetric flowrates (top right), the PSD after 90 minutes and the final PSD for low flowrates (bottom left) and all the final PSDs (bottom right)

8.1.3 Closed loop crystallisation

These experiments were carried out in the scheme described in Figure 4.10. A solute concentration of 7mg/ml was chosen as when mixed with the antisolvent in the T-mixer the solution was undersaturated (Figure 4.13). This should prevent the possibility of precipitation in the T-mixer or capillary. The characterisation of the mixing performance of a T-mixer suggests that mixing in small T-mixer with a 10 cm capillary should be sufficient to complete mixing. Therefore it assumed that mixing occurs within the residence time and the solution which exits the capillary is molecularly mixed. The undersaturation prevents any crystallisation in the capillary. This means that the interaction between the jet from the capillary and the isopropanol in the vessel is what controls the mixing and subsequent nucleation process. This is therefore similar to a traditional semi batch crystallisation experiment.

Figure 8.7 and Figure 8.8 show that like in the previous experiments, two distinct behaviours occur. At high feed rates high turbidity and a large number of small particles were observed whilst at low feed rates lower turbidity and smaller number of larger particles were observed. Estimation of the radius of gyration is unreliable beyond 30% obscuration, so values were considered indicative rather than absolute beyond this value.

In the high feedrate experiments, crystallisation appeared to be finished after around 60-80 minutes on the basis of stable obscuration (Figure 8.7) and particle size (Figure 8.8). The first detectable particles appeared after about 15 minutes and were around 9 μm in size and grew to a final size around 20 μm although due to high obscuration this figure is unreliable.

For the low feedrates the first detectable particles appeared again after around 15 minutes but were around 20 μm in size. These grew steadily with time reaching around 30 μm after about 100 minutes. After this point the particle size and obscuration both continued to increase but there was more spread in the particle size data. This is likely due to a wider particle size distribution and the stochastic sampling of the analytical loop.

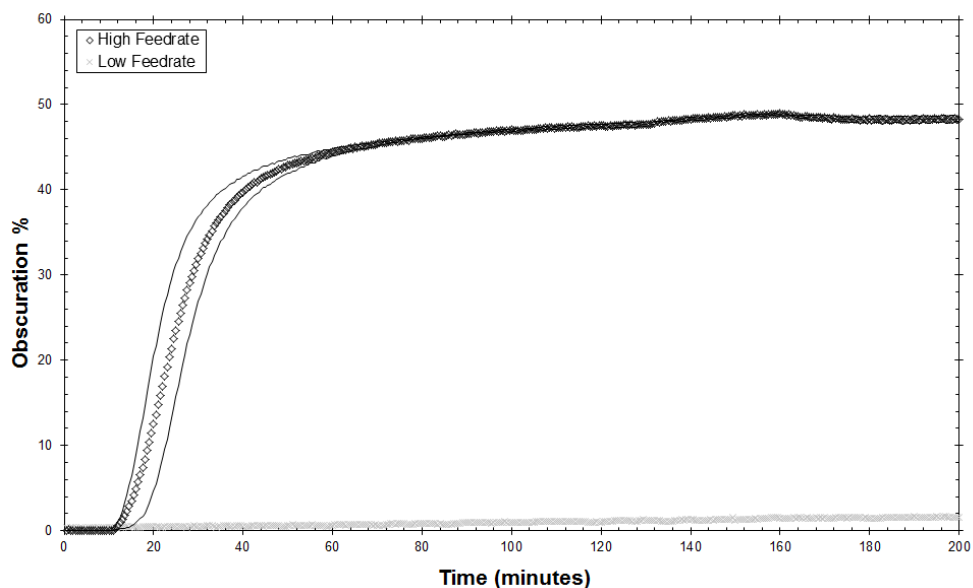


Figure 8.7. Obscuration vs. time

Obscuration as a function of time for a 1:1 flow ratio with a high feed rate (black diamonds) and low feedrate (grey crosses). As explained in chapter 4.2 it was not possible to achieve a flow ratio of 1:1 at a high feedrate, therefore two experiments were carried out one with 60:40 antisolvent flow ratio (upper black line) and one with 60:40 aqueous flow ratio (lower black). The high feedrate data points is a best estimate of a 1:1 flow ratio by taking an average of these two experiments.

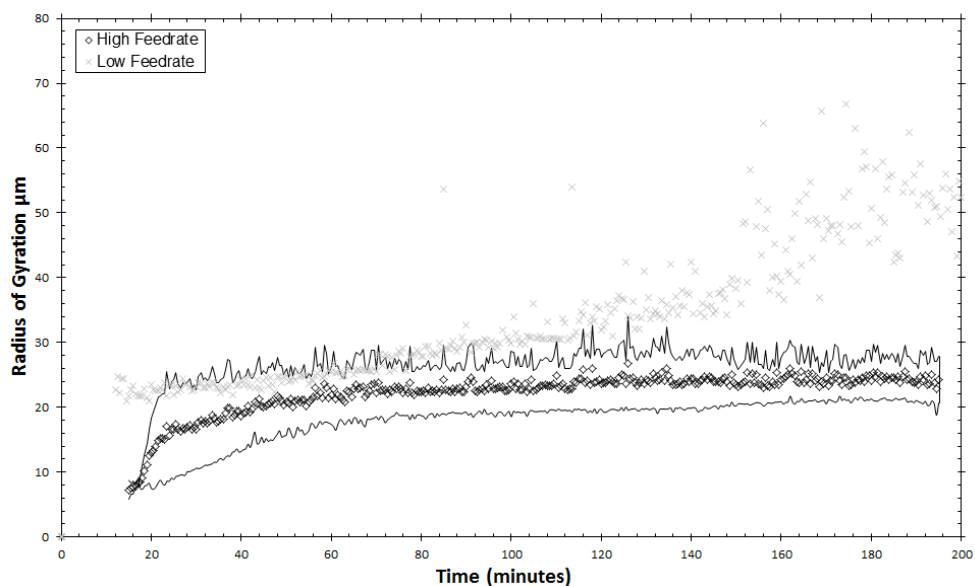


Figure 8.8. Radius of gyration vs. time

Radius of gyration as a function of time for a 1:1 flow ratio with a high feed rate (black diamonds) and low feedrate (grey crosses). As explained in chapter 4.2 it was not possible to achieve a flow ratio 1:1 at a high feedrate, therefore two experiments were carried out one with 60:40 antisolvent flow ratio (upper black line) and one with 60:40 aqueous flow ratio (lower black). The high feedrate data points is a best estimate of a 1:1 flow ratio by taking an average of these two experiments.

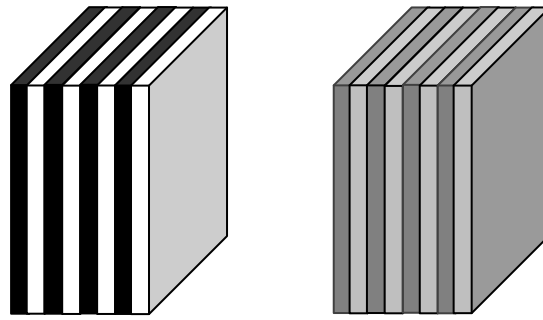
8.1.4 Discussion

A basic explanation of this behaviour relates to the interfacial area opened between the solvent and antisolvent. The greatest supersaturation occurs at the interface between the solvent and antisolvent. Therefore, a mixing process that maximises interfacial area should maximise local supersaturation and hence nucleation. Once mixed the supersaturation is below that required to overcome the energy barrier associated with establishing a new phase (nucleation) and therefore growth is the only mechanism after mixing by which supersaturation can be depleted towards equilibrium. Ignoring micromixing (Figure 8.9), if the energy dissipation rate is high (good mixing) then the Kolmogorov length scale is small which increases interfacial area and hence supersaturation and nucleation. Smaller energy dissipation rate on the other hand reduces the interfacial area and supersaturation which suppresses nucleation. In either case, micromixing eventually evens out the sub Kolmogorov concentration gradients but when bulk supersaturation is reached it is too low to induce nucleation leaving only growth. This results in fewer large particles for lower energy dissipation rates as fewer nuclei are created during initial mixing. Nucleation is controlled by the initial mixing.

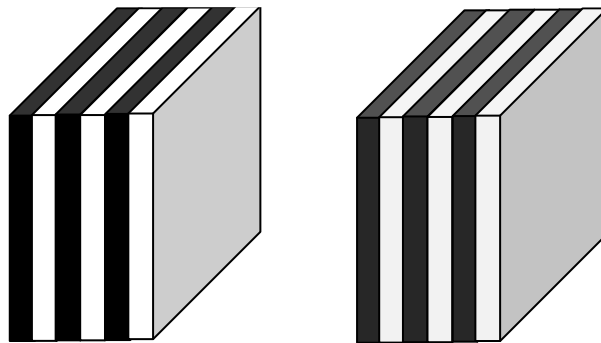
Such a mechanism would be dependent upon the characteristic timescale of nucleation being less than the characteristic timescale of mixing. In fact, regardless of the process which controls this behaviour, the characteristic timescale for the process has to be less than the characteristic timescale of the mixing process at 400ml/min. This is because 400ml/min is the first of the runs that exhibit fast kinetics and the last run that exhibits a degree of metastability which manifests in filtration induced crystallisation. Therefore, the timescale of the process governing this metastability (being nucleation or some other process) has a timescale similar to the mixing timescale of a CIJ at 400 ml/min.

The timescales of mixing in a CIJ mixer are shown in Figure 8.10 at a flow ratio of 1:1 for the modified system which has a viscosity difference approximately the same as isopropanol and water system. The mixing half-life, which is considered to be a characteristic timescale, is around 10ms and the 90% mixed time which is an estimate of mixing completion is around 20ms. Therefore, it is suggested that metastability is induced by a process that occurs in the first 10-20ms and if mixing is

not accomplished within this timescale it is too late and it goes down the metastable route. The first 10-20ms control which route is taken.



High energy dissipation rate



Low energy dissipation rate

Laminated substructure segregating the material down to the Kolmogorov length scale. Maximum local supersaturation at interface.

Figure 8.9. Laminated substructure caused by Kolmogorov scale segregation

Alternatively, stability could be induced by something like an interfacial tension that exists even between miscible liquids in the initial moments of mixing as discussed in section 7.5. This could then be further stabilised by solute which would precipitate at the interface in a process similar to that termed “quasi-emulsion precipitation” by Wang *et al.*[41], [42] This would possibly have a length scale rather than timescale controlling stability.

Taking the Kolmogorov length scale as representative of the mesoscale segregation achieved by turbulence, a length governing this stability can be estimated. The smaller the Kolmogorov scale, the quicker micromixing is to finish. Mesomixing controls mixing from the initial segregation down to the Kolmogorov length, so at this length scale there could be competition from micromixing (engulfment, deformation and molecular diffusion) which homogenises the system

and precipitation which could stabilise the segregation. Taking 400 ml/min as the point where the micromixing homogenises before the system can be stabilised allows an estimate of the Kolmogorov length scale that would control such behaviour. This is shown in Figure 8.11, with a value of around 10 μm at 100% of the total energy dissipation being utilised for mixing to 20 μm for 1%.

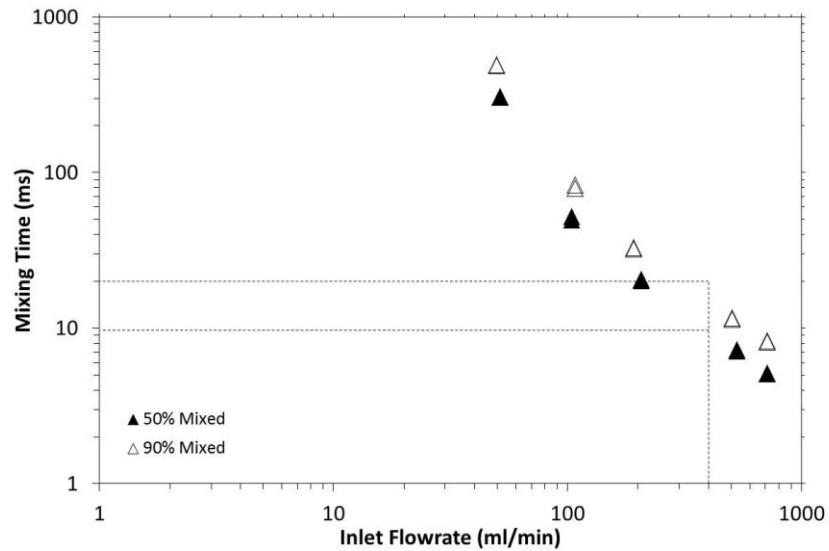


Figure 8.10. Mixing Characterisation of a CIJ Mixer

The mixing characterisation of a CIJ mixer as a function of inlet flowrate for the 1:1 MC system (viscosity difference) as outlined in the mixing characterisation section. The mixing half-life, which is being treated like a characteristic time is shown (left) as is the 90% mixed time (right).

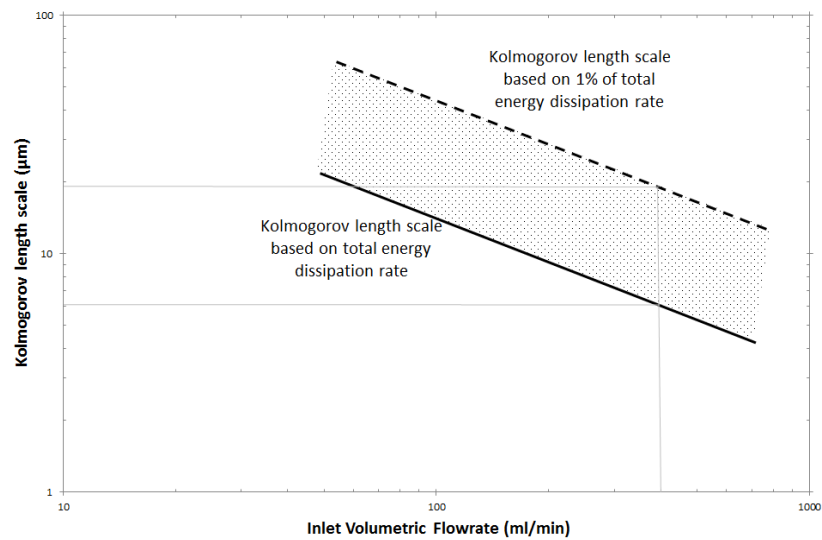


Figure 8.11. Kolmogorov length scale in a CIJ mixer

Kolmogorov length scale in a CIJ mixer based on 100% of the total energy dissipation rate (solid line) and 1% of the total energy dissipation rate (dashed line).

In the CIJ crystallisation experiments (Chapter 8.1.1 and 8.1.2) there remained the possibility that the low solid recovery was caused by the formation of a metastable phase that could be destabilised if exposed to agitation after the initial mixing rather than quiescent conditions, similar to that exhibited in the quasi-emulsion crystallisation mechanism.[41], [42] It appears from the closed loop crystallisation experiments in 8.1.3 (Figure 8.7 and Figure 8.8) that long term exposure to agitation does not destabilise the isopropanol/valine/water system and that everything is controlled by initial mixing.

It has been reported that for constant constant micromixing time the nucleation rate exhibits a maximum as a function of feedrate (mesomixing time).[87] At low feedrates the supersaturation is kept low by the small solute flowrate, this is analogous to adding reagents slowly in exothermic reactions to prevent runaway reactions. As the feedrate becomes larger the micromixing is eventually not sufficient to cope with the fresh feed addition which explains the maximum at constant micromixing time.

For the continuous CIJ experiments operating at a flow ratio of 1:1 the definitions of micromixing and mesomixing are less well defined. The streams are combined in their final mixed compositions and as the flowrate increases (increased energy dissipation) the solute is distributed over the whole volume and more interfacial area is opened between the solvent and antisolvent which increases the local supersaturation and therefore increases the nucleation rate.

8.2 Testing the vortex mixer in commercial applications

In the formation of protein coated microcrystals (see section 3.3) it would be sensible to assume that protein incorporation occurs on a timescale longer than crystallisation since the protein coats the outside of the crystals. The solid recovery is not strongly influenced by mixing, instead it seems to be largely fixed by the system. This is probably due to the rapid nature of the precipitation as the process is thought to be more of a spinodal decomposition due to the high supersaturation (high antisolvent content) than a classical nucleation and growth mechanism. However, the particle size is still sensitive to mixing and this is critical to control as this can determine suitability for certain applications e.g. pulmonary drug delivery requires a narrow distribution of small (less than 5 μm) particles.[88], [89]

The net protein recovery (NPR) is ultimately the critical parameter from a process economics view as this is the recovery of the expensive therapeutic molecule. Both the vortex mixer and X mixer produce an adequate NPR although the Kenics mixer resulted in higher NPR values.

8.2.1 F1 Formulation

In the F1 formulations there is no dependence of the solid recovery on mixer type and there is no improvement with the introduction of a Kenics style static mixer (Figure 8.12). In fact, the solid recovery in all instances is well over 90% and considering solid losses and other experimental error associated with gravimetric analysis plus the residual solubility in the mother liquor (solubility on mixing assumed 0 mg/ml due to high antisolvent content) it appears as though, from a solid recovery perspective, the precipitation is completely controlled by composition and is independent of mixing influences due to the high degree of thermodynamic instability caused by the high supersaturation.

The experimental error associated with the NPR experiments is estimated to be around 5%, therefore on two repetitions it is difficult to statistically determine if there is a benefit of the X mixer (poorer mixing) on protein recovery (Figure 8.13). The use of the Kenics (light grey) seems to increase the NPR for both the vortex and X mixers.

However, a comparison of the filter rates shows a clear difference between the vortex mixer and the X mixer (Figure 8.14). The vortex mixer takes considerably longer to filter in comparison to the X mixer.

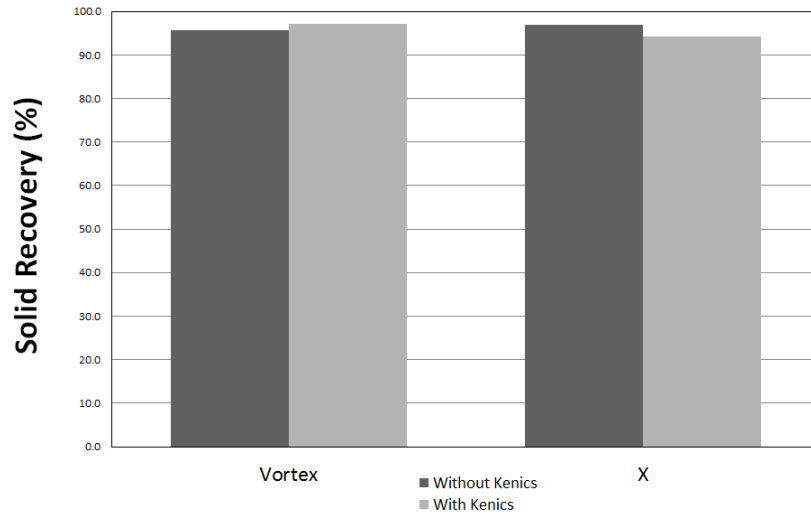


Figure 8.12. F1 solid recovery

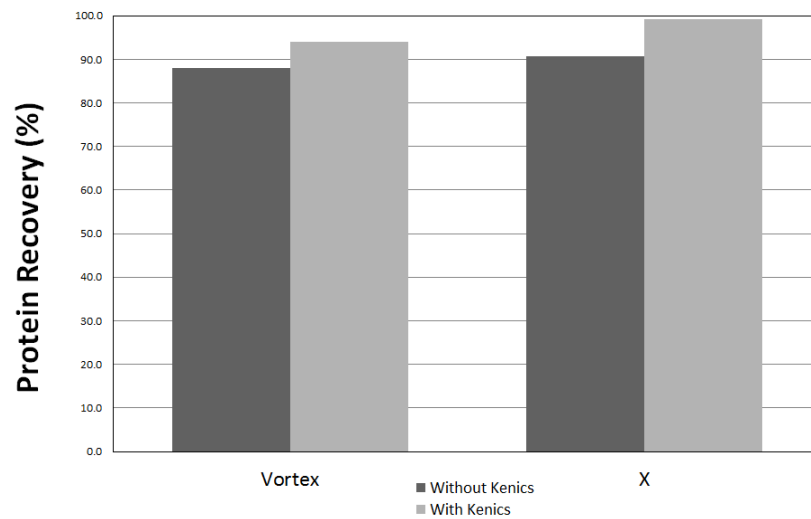


Figure 8.13. F1 net protein recovery

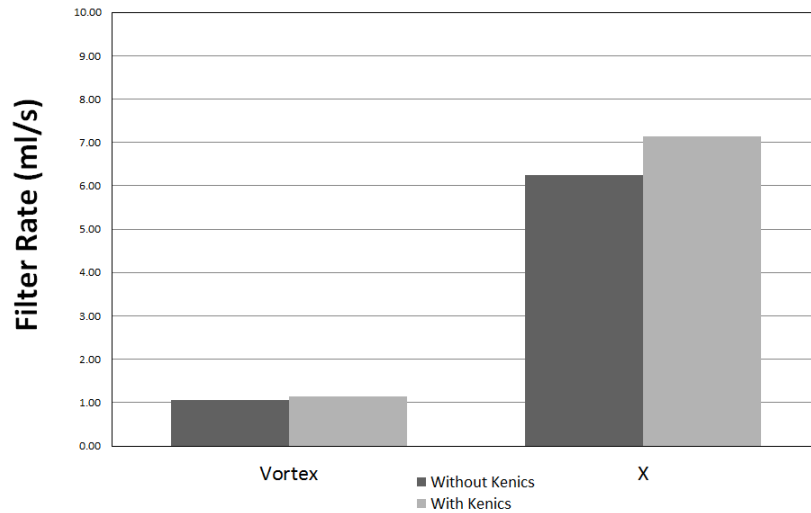


Figure 8.14. F1 filter rate

It is also obvious from the SEM images (Figure 8.15 and Figure 8.16) that there is a difference between the vortex mixer and the X mixer. The SEM image from the vortex reveals a lot of small material in the submicron range in addition to a few larger particles around 5 to 10 microns. The X mixer shows almost entirely the larger particles.

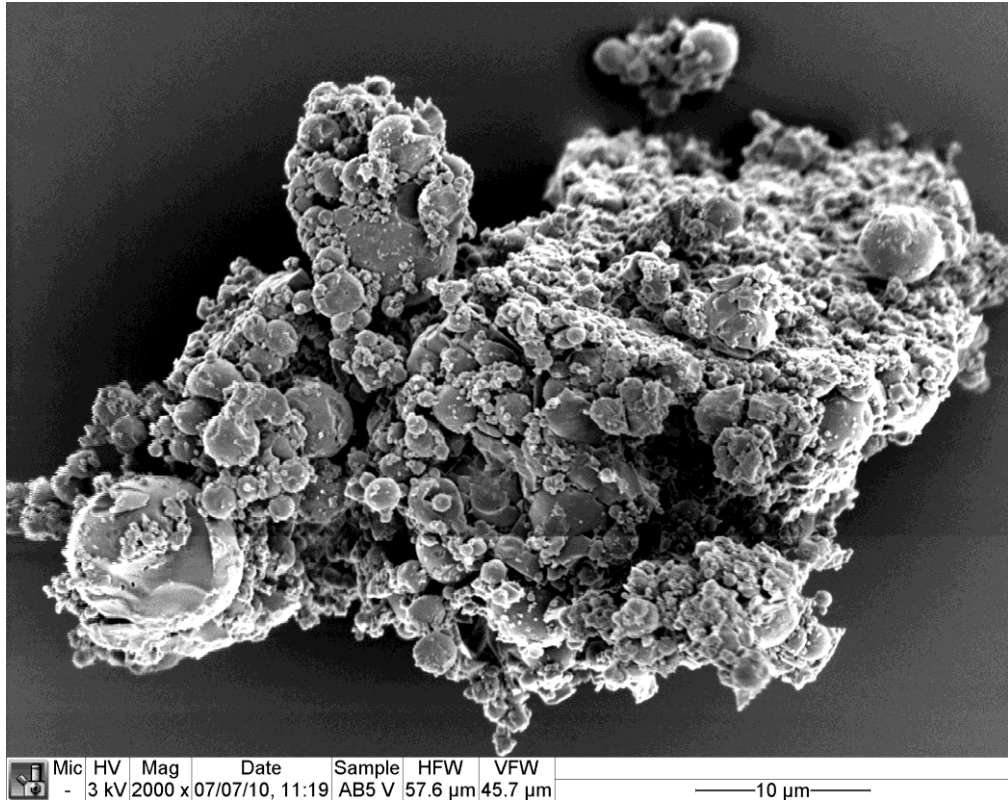


Figure 8.15. F1 in the vortex mixer (no Kenics) SEM 2000x magnification

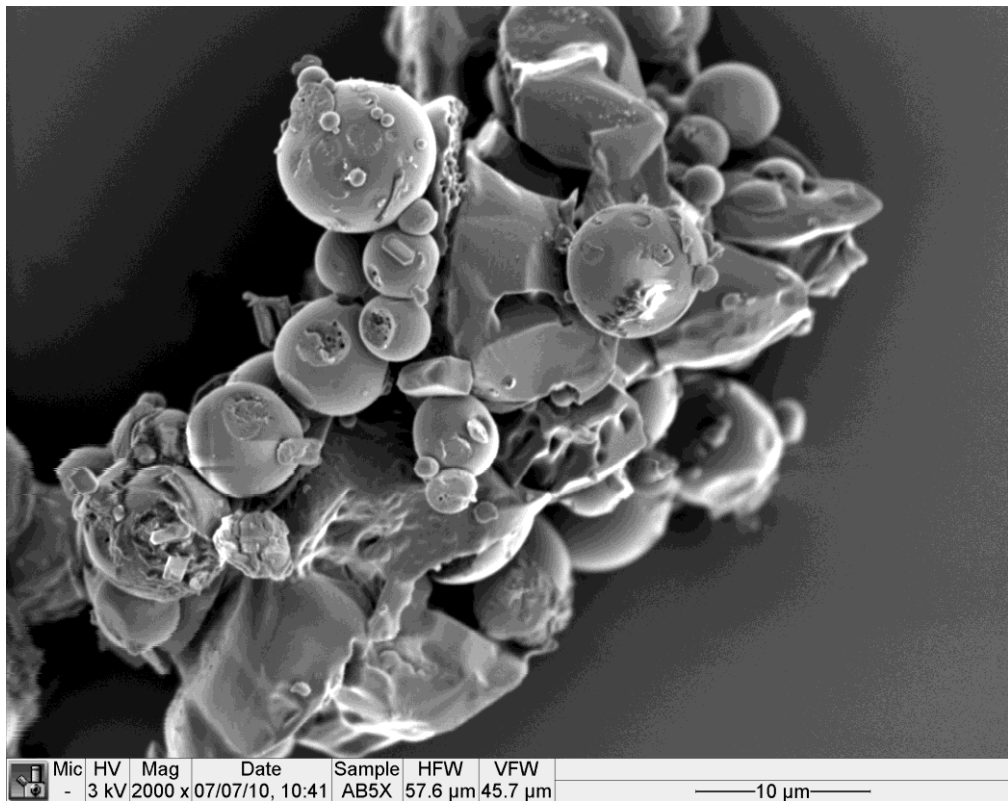


Figure 8.16. F1 in the X mixer (no Kenics) SEM 2000x magnification

8.2.2 F2 Formulation

For the F2 formulations, again there is little or no dependence of solid recovery (Figure 8.17) on mixer type. The solid recoveries are generally lower than the F1 formulations but again this is system influenced. The solid recovery is lower due to reduced supersaturation, which is caused by higher residual solubility as the excipient is known to be slow crystallising in comparison to the F1 formulations.

The use of the Kenics seems to again increase the NPR (Figure 8.18) for the vortex and X mixers and again the filter rate (Figure 8.19) is a lot slower when the vortex mixer is used than when the X mixer is used and the particle size of the material produced from the vortex mixer (Figure 8.20) is much smaller than that produced by the X mixer (Figure 8.21).

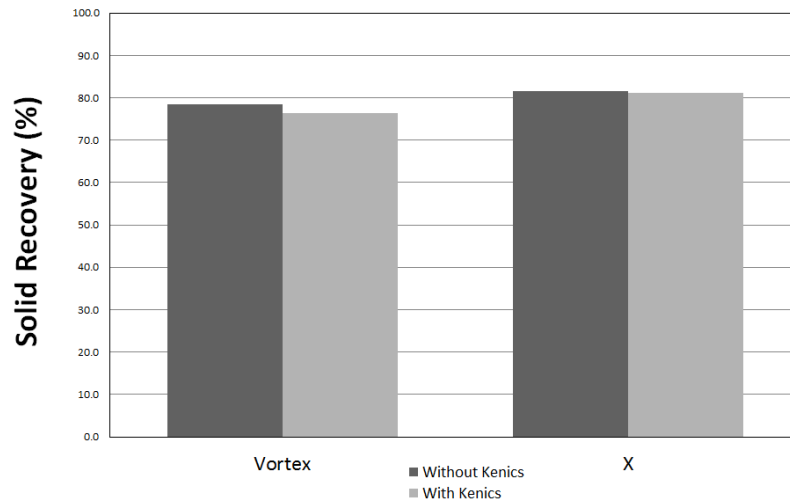


Figure 8.17. F2 solid recovery

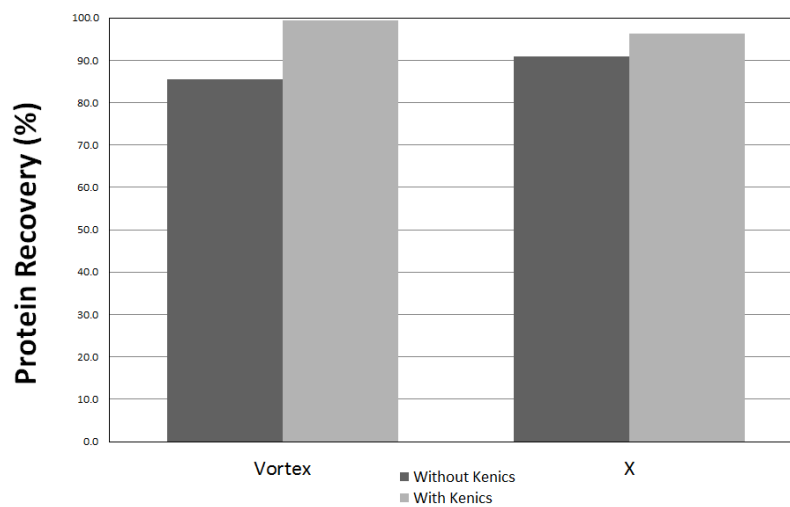


Figure 8.18. F2 net protein recovery

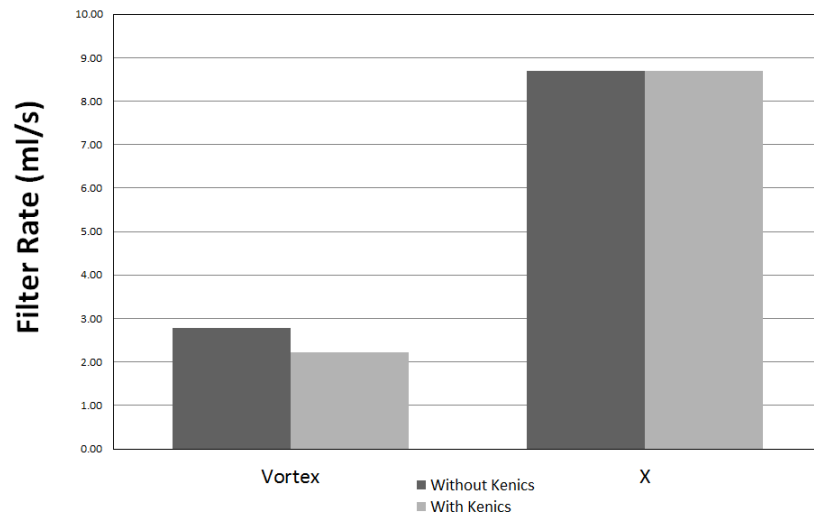


Figure 8.19. F2 filter rate

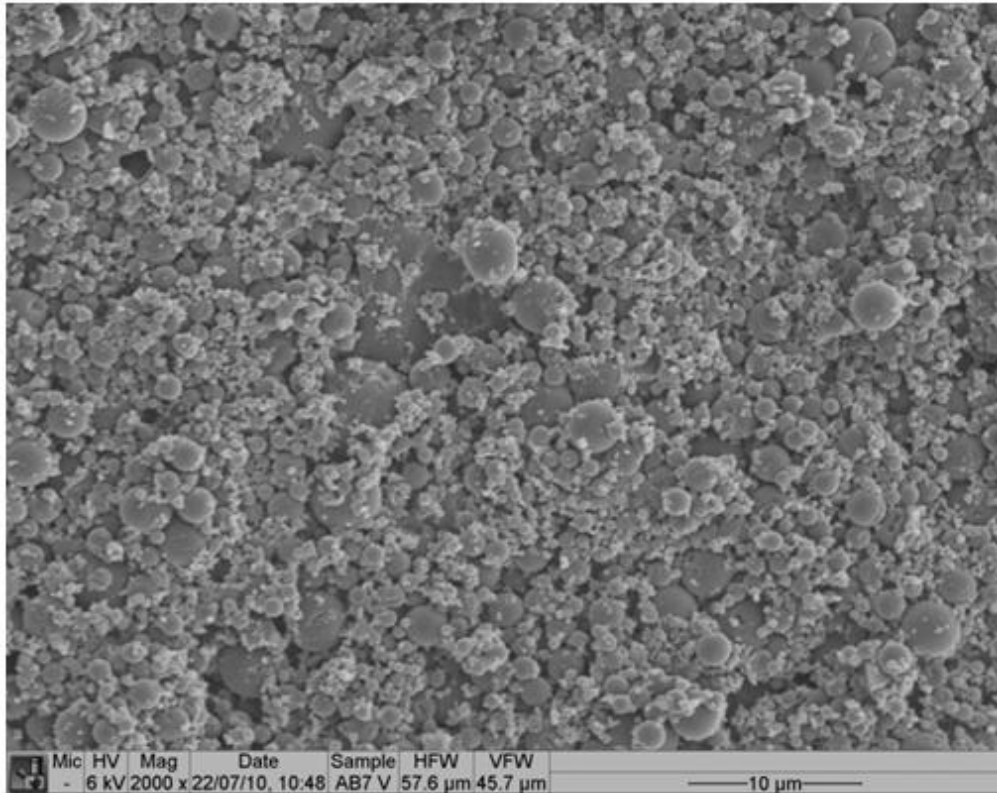


Figure 8.20. F2 vortex mixer (no Kenics) SEM 2000x magnification

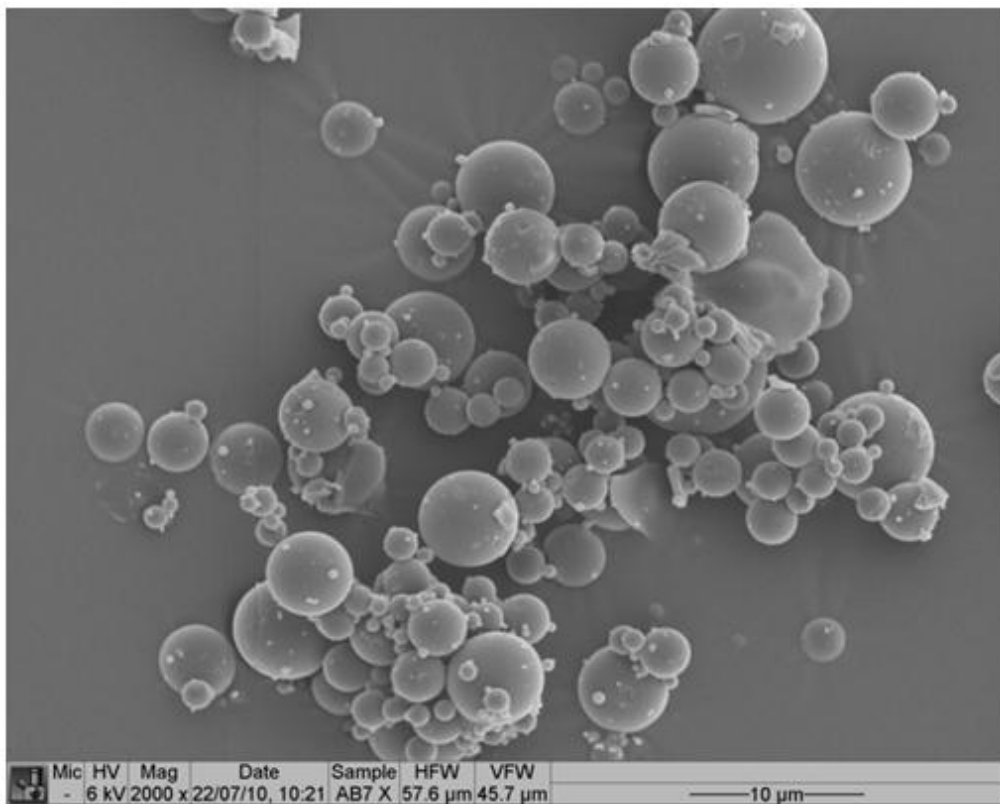


Figure 8.21. F2 X mixer (no Kenics) SEM 2000x magnification

8.2.3 Difference between mixers

The following general conclusions were made between how the different mixing conditions influence the various parameters of interest. The NPR in these experiments was affected only by secondary mixing (Kenics mixer), this could be because protein incorporation occurs over longer timescales (which is sensible due to the protein coating the excipient). The solid recovery is independent of both the primary and secondary mixing conditions – it was system dependent due to the high supersaturation. However, this does not mean the primary mixing is unimportant as indicated by the SEM images which showed that the vortex mixer produced much smaller particles than the X mixer and the filter profile which indicated that samples prepared using the vortex mixer required longer to filter than those prepared from the X mixer. Clearly the vortex mixer resulted in a different product to the X mixer.

There are two main parameters which control filtration behaviour – permeability and porosity.[90], [91] In filtration, finer particles are generally more difficult to separate than coarse ones. For example, doubling the particle size leads to a factor four reduction in cake resistance.[92] The small particles resist the flow, which gives rise to an enhanced pressure drop compared with unhindered flow.

The most important liquid property that influences filtration is the viscosity. Low viscosity fluids flow easier and hence have a lower pressure drop through the cake. In our case, the liquid physical properties are the same. Additionally, if we also assume the physical structure of the product varies only with formulation (i.e. varying the mixer type does not produce entirely different products, just the same product with different size distributions) then we can attribute differences in filterability to a different particle size distribution. Therefore it is concluded the longer filtration time exhibited by the vortex mixer was caused by a decrease in particle size.

As outlined in chapter 3 and confirmed in first part of this chapter (8.1) smaller particle size is characteristic of better mixing conditions. Therefore these results can be taken as verification of the experimental results outlined in chapter 7 which indicated that the vortex mixer was a substantially better mixer than the X mixer at volumetric flow ratios greater than 3:1.

Additionally, the formation of spherical particulate matter is not commonly observed in crystallisation. It would likely be driven by surface tension and therefore is perhaps indicative of a non-classical crystallisation route perhaps involving a liquid-liquid separation and then phase change and may perhaps be amorphous or nano/microcrystalline.

8.3 Conclusions - Mixing influenced precipitation

The precipitation of valine from an aqueous solution using isopropyl alcohol as an antisolvent is strongly influenced by the initial mixing conditions. Two distinct regions were observed, one that was turbid with fast kinetics and another that was clear with slow kinetics. This was observed in both a CIJ operating with a solvent to antisolvent ratio of 1:1 and in a semi-batch crystallisation with a ratio of 1:9.

The initial mixing determines the interfacial area between the solvent and antisolvent. At this interface lies the peaks in supersaturation and consequently the highest nucleation rates. Maximising this interfacial area requires energy in order to utilise the whole volume and to reduce the Kolmogorov length scale.

For the CIJ mixer operating at 1:1 there are two distinct zones with respect to the kinetics as characterised by the mass of crystal formation as a function of time. At low flowrates there is a steady increase in the rate of crystal formation with increasing flowrate until a breakpoint of 400ml/min when an improvement in mixing performance results in no improvement in kinetics. Taking this point as a Damköhler number of 1 results in an estimation of the timescale of nucleation, from the mixing characterisation work this corresponds to a time of around 10-20ms. After this breakpoint the reduction in particle size begins to slow down as the mixing improves.

In the early stages of crystallisation, for mixing before the breakpoint, crystallisation can be induced by filtration resulting in a turbid filtrate. The time window where this phenomenon can occur decreases as the flowrate increases.

The mixing characterisation experiments determined that at extreme flow ratios (much different to 1:1) the vortex mixer was a substantially better mixer than the other mixers. In order to test this performance of the vortex mixer in comparison to an X mixer was tested in pilot scale trials for the production of PCMCs. The crystalline material produced by the vortex mixer was substantially smaller than that produced by the X mixer as shown by SEM imaging and filter rates. This is a signature of improved initial mixing performance and corroborates the improved mixing performance as indicated by the mixing characterisation experiments.

9 Concluding Remarks

The Bourne IV competitive reaction scheme is a robust method for characterisation of mixer performance and can easily be extended to include volumetric flow ratios and the physical property differences that can be expected in common processing applications. It produces a characteristic quantity, the fractional conversion of the slow reaction, which is generally representative of the mixing conditions. This quantity can easily be converted to an estimate of a characteristic mixing time by implementing one of various mixing and reaction models.

The main limitation of such an approach is that it is limited to an average over the mixing volume. No information can be inferred about the spatial distribution of mixing efficiency. Mixers exhibit a spatial distribution of energy dissipation, a spatial distribution of mixing times and hence a distribution of residence and mixing times. Depth would be added to the analysis by implementing computational fluid dynamics, which would be capable of determining the spatial distribution of mixing performance. This would enable the ability to determine, for instance, the cause of the vortex mixer outperforming the others at a flow ratio of 10:1. Rather than simply saying that it translates a higher fraction of its energy and quantifying this, it could be explained how this happens. Is it due to the spatial distribution of energy dissipation rate or a narrower residence time distribution?

However, the main disadvantage of computational fluid dynamics is that it requires considerable skill and expertise to get results and considerable experience to determine the validity of these results. The method used in this thesis, on the other hand, only requires moderately difficult mathematics and despite the aforementioned limitations it still provides considerable insight.

The engulfment model was employed and has been experimentally verified to predict with reasonable accuracy the direction and magnitude of these concentration effects. It can also provide, with acceptable accuracy, a well-defined absolute mixing time. The IEM model was also utilised but it was found to deal poorly with the volumetric flow ratio changes. The IEM model was adequate at 1:1 flow ratio and consequently it is suggested that this may be a preferable formulation at this flow ratio due to its inherent simplicity. The fractional conversion of dimethoxypropane

has been found to have a linear relationship with mixing time until a fractional conversion of about 0.3. This is useful as it allows the interpretation of many mixing effects without the need to employ a time consuming model.

A stabilisation effect when the small stream is the more viscous stream has been noted. This is thought to be due to the difficulty of droplet breakup when a viscous stream is surrounded by a less viscous phase. No mixer was able to deal effectively with this. A practical example of such a system would be antisolvent precipitation of a solute from an organic solvent using an aqueous solution as the antisolvent.

One of the interesting and unanswered questions is how the difference in the way in which fluids are mixed rather than how quickly they are mixed influences mixing sensitive processes such as crystallisation. For instance, in comparing the particle size and morphology of the material produced by the vortex mixer with the X mixer it is unclear to what extent the reduction in particle size is as a result of faster mixing or some inherent geometrical advantage that perhaps results in smaller length scales of segregation.

The initial mixing determines the interfacial area between the solvent and antisolvent. At this interface lies the peaks in supersaturation and consequently the highest nucleation rates. Maximising this interfacial area requires energy in order to utilise the whole volume and to reduce the Kolmogorov length scale. The engulfment model currently utilised would be incapable of capturing such effects, the peaks in supersaturation would be the same only shifted in time. In order to capture such effects the model would have to be coupled with an inertial scale mixing model capable of capturing mixing from the integral scale down to the Kolmogorov scale. Therefore, the model becomes more complex and the benefit of a simplistic model over CFD becomes less clear.

In summary, the results in thesis were successful in characterising the mixing performance of a wide range mixers in a variety of mixing conditions in terms of average mixing performance. By implementing a micromixing model the fractional conversion was converted to a characteristic mixing time with a reasonable degree of accuracy. This approach has proven to be useful for the general comparison of mixing performance, the development of scaling methodologies or gaining insights

Concluding Remarks

into the behaviour of mixers. Unfortunately it does not divulge any information about the way in which fluids are mixed. This is sufficient for understanding how the kinetics of chemical reactions are influenced by mixing but for something more sensitive to molecular scale composition like nucleation in antisolvent crystallisation this approach only tells one part of story.

References

- [1] J. Baldyga, J. R. Bourne, and S. J. Hearn, 'Interaction between chemical reactions and mixing on various scales', *Chemical Engineering Science*, vol. 52, no. 4, pp. 457–466, 1997.
- [2] Edward L. Paul, Victor Atiemo-Obeng, and Suzanne M. Kresta, *Handbook of Industrial Mixing: Science and Practice*. Wiley.
- [3] J. R. Bourne, 'Mixing and the Selectivity of Chemical Reactions', *Organic Process Research & Development*, vol. 7, no. 4, pp. 471–508, Jul. 2003.
- [4] J. Baldyga and R. Pohorecki, 'Turbulent micromixing in chemical reactors - a review', *The Chemical Engineering Journal and the Biochemical Engineering Journal*, vol. 58, no. 2, pp. 183–195, Jul. 1995.
- [5] E. Paul and R. Treybal, 'Mixing and product distribution for a liquid-phase, second-order, competitive-consecutive reaction', *AIChE Journal*, vol. 17, no. 3, p. 6, 1971.
- [6] J. Baldyga, J. R. Bourne, and B. Walker, 'Non-isothermal micromixing in turbulent liquids: Theory and experiment', *The Canadian Journal of Chemical Engineering*, vol. 76, no. 3, pp. 641–649, 1998.
- [7] M.-C. Fournier, L. Falk, and J. Villermaux, 'A new parallel competing reaction system for assessing micromixing efficiency--Experimental approach', *Chemical Engineering Science*, vol. 51, no. 22, pp. 5053–5064, Nov. 1996.
- [8] A. G. Jones, *Crystallization Process Systems*. Butterworth-Heinemann, 2002.
- [9] J. W. Mullin, *Crystallization*, 4th Ed. Elsevier Butterworth-Heinemann, 2001.
- [10] A. S. Myerson, *Handbook of Industrial Crystallisation*, 2nd ed. Butterworth-Heinemann, 2002.
- [11] P. Danckwerts, 'The definition and measurement of some characteristics of mixtures', *Applied Scientific Research*, vol. 3, no. 4, pp. 279–296–296, Jul. 1952.
- [12] H. H. Shen, *Environmental fluid mechanics: theories and applications*. American Society of Civil Engineers, 2002.
- [13] J. R. Chasnov, 'The viscous-convective subrange in nonstationary turbulence', *Phys. Fluids*, vol. 10, no. 5, p. 1191, 1998.
- [14] A. N. Kolmogorov, 'Dissipation of energy in a locally isotropic turbulence.', *American Mathematical Society Translations*, vol. 8, p. 87, 1941.
- [15] B. K. Johnson and R. K. Prud'homme, 'Chemical processing and micromixing in confined impinging jets', *AIChE Journal*, vol. 49, no. 9, pp. 2264–2282, 2003.
- [16] S. Corrsin, 'The isotropic turbulent mixer: Part II. Arbitrary Schmidt number', *AIChE J.*, vol. 10, no. 6, pp. 870–877, 1964.
- [17] J. Baldyga and J. R. Bourne, 'Interactions between mixing on various scales in stirred tank reactors', *Chemical Engineering Science*, vol. 47, no. 8, pp. 1839–1848, Jun. 1992.
- [18] G. K. Batchelor, 'The Effect of Homogeneous Turbulence on Material Lines and Surfaces', *Proceedings of the Royal Society of London. Series A. Mathematical and Physical Sciences*, vol. 213, no. 1114, pp. 349–366, 1952.
- [19] J. Baldyga and J. R. Bourne, 'A Fluid Mechanical Approach to Turbulent Mixing and Chemical Reaction Part II Micromixing in the Light of Turbulence

-
- Theory', *Chemical Engineering Communications*, vol. 28, no. 4, pp. 243–258, 1984.
- [20] J. Baldyga and J. R. Bourne, *Turbulent Mixing and Chemical Reactions*. Wiley, 1999.
- [21] J. Baldyga and J. R. Bourne, 'Simplification of micromixing calculations. I. Derivation and application of new model', *The Chemical Engineering Journal*, vol. 42, no. 2, pp. 83–92, Nov. 1989.
- [22] G. K. Batchelor, 'Small-Scale Variation of Convected Quantities Like Temperature in Turbulent Fluid Part 1. General Discussion and the Case of Small Conductivity', *Journal of Fluid Mechanics*, vol. 5, no. 01, pp. 113–133, 1959.
- [23] B. K. Johnson, *PhD Thesis 'Flash NanoPrecipitation of Organic Actives via Confined Micromixing and Block Copolymer Stabilization'*. 2003.
- [24] J. Baldyga and J. R. Bourne, 'Simplification of micromixing calculations. II. New applications', *The Chemical Engineering Journal*, vol. 42, no. 2, pp. 93–101, Nov. 1989.
- [25] G. Patterson, 'Modeling and Scale-Up of Mixing- and Temperature-Sensitive Chemical Reactions', *Industrial & Engineering Chemistry Research*, vol. 44, no. 14, pp. 5325–5341, Jul. 2005.
- [26] J. R. Bourne, R. V. Gholap, and V. B. Rewatkar, 'The influence of viscosity on the product distribution of fast parallel reactions', *The Chemical Engineering Journal and the Biochemical Engineering Journal*, vol. 58, no. 1, pp. 15–20, Jun. 1995.
- [27] J. M. Ottino, 'Mixing and chemical reactions a tutorial', *Chemical Engineering Science*, vol. 49, no. 24, Part 1, pp. 4005–4027, 1994.
- [28] J. R. Bourne, F. Kozicki, and P. Rys, 'Mixing and fast chemical reaction 1 - Test Reactions to Determine Segregation.', *Chemical Engineering Science*, vol. 36, no. 10, pp. 1643–1648, 1981.
- [29] L. Falk and J.-M. Commenge, 'Performance comparison of micromixers', *Chemical Engineering Science*, vol. 65, no. 1, pp. 405–411, Jan. 2010.
- [30] J. R. Bourne, 'Comments on the iodide/iodate method for characterising micromixing', *Chemical Engineering Journal*, vol. 140, no. 1–3, p. 4, 2008.
- [31] J. Bourne and S. Yu, 'Investigation of Micromixing In Stirred-Tank Reactors Using Parallel Reactions', *Industrial & Engineering Chemistry Research*, vol. 33, no. 1, pp. 41–55, 1994.
- [32] J. R. Bourne, O. M. Kut, and J. Lenzner, 'An improved reaction system to investigate micromixing in high-intensity mixers', *Industrial & Engineering Chemistry Research*, vol. 31, no. 3, pp. 949–958, 1992.
- [33] Y. Liu and R. O. Fox, 'CFD predictions for chemical processing in a confined impinging-jets reactor', *AIChE J*, vol. 52, no. 2, p. 731, 2006.
- [34] E. Gavi, D. L. Marchisio, and A. A. Barresi, 'CFD modelling and scale-up of Confined Impinging Jet Reactors', *Chemical Engineering Science*, vol. 62, no. 8, pp. 2228–2241, 2007.
- [35] D. L. Marchisio, L. Rivautella, and A. A. Barresi, 'Design and scale-up of chemical reactors for nanoparticle precipitation', *AIChE J.*, vol. 52, no. 5, pp. 1877–1887, 2006.
- [36] S. W. Siddiqui, Y. Zhao, A. Kukukova, and S. M. Kresta, 'Characteristics of a Confined Impinging Jet Reactor: Energy Dissipation, Homogeneous and
-

-
- Heterogeneous Reaction Products, and Effect of Unequal Flow’, *Industrial & Engineering Chemistry Research*, vol. 48, no. 17, pp. 7945–7958, 2009.
- [37] Y. Liu, C. Y. Cheng, Y. Liu, R. K. Prud’homme, and R. O. Fox, ‘Mixing in a multi-inlet vortex mixer (MIVM) for flash nano-precipitation’, *Chemical Engineering Science*, vol. 63, no. 11, pp. 2829–2842, 2008.
- [38] C. Lindenberg, J. Scholl, L. Vicum, M. Mazzotti, and J. Brozio, ‘Experimental characterization and multi-scale modeling of mixing in static mixers’, *Chemical Engineering Science*, vol. 63, no. 16, pp. 4135–4149, Aug. 2008.
- [39] C. Lindenberg and M. Mazzotti, ‘Experimental characterization and multi-scale modeling of mixing in static mixers. Part 2. Effect of viscosity and scale-up’, *Chemical Engineering Science*, vol. 64, no. 20, pp. 4286–4294, Oct. 2009.
- [40] J. M. Gillian and D. J. Kirwan, ‘Identification and Correlation of Mixing Times in Opposed Jet Mixers’, *Chemical Engineering Communications*, vol. 195, no. 12, pp. 1552–1574, Dec. 2008.
- [41] X. Wang, J. M. Gillian, and D. J. Kirwan, ‘Quasi-emulsion precipitation of pharmaceuticals. 1. Conditions for formation and crystal nucleation and growth behavior’, *Crystal Growth and Design*, vol. 6, no. 10, pp. 2214–2227, 2006.
- [42] X. Wang and D. J. Kirwan, ‘Quasi-Emulsion Precipitation of Pharmaceuticals. 2. Application to Control of Polymorphism’, *Crystal Growth & Design*, vol. 6, no. 10, pp. 2228–2240, Oct. 2006.
- [43] R. J. Stokes and D. F. Evans, *Fundamentals of interfacial engineering*. Wiley-VCH, 1997.
- [44] D. D. Joseph, ‘Fluid dynamics of two miscible liquids with diffusion and gradient stresses.’, *Eur. J. Mech., B/Fluids*, vol. 9, no. 6, pp. 565–596, 1990.
- [45] S. E. May and J. V. Maher, ‘Capillary-wave relaxation for a meniscus between miscible liquids’, *Phys. Rev. Lett.*, vol. 67, no. 15, pp. 2013–2016, 1991.
- [46] W.-J. Ma, P. Koblinski, A. Maritan, J. Koplik, and J. R. Banavar, ‘Dynamical relaxation of the surface tension of miscible phase’, *Physical Review Letters*, vol. 71, no. 21, p. 3465, 1993.
- [47] B. Zoltowski, Y. Chekanov, J. Masere, J. A. Pojman, and V. Volpert, ‘Evidence for the Existence of an Effective Interfacial Tension between Miscible Fluids. 2. Dodecyl Acrylate–Poly(dodecyl acrylate) in a Spinning Drop Tensiometer’, *Langmuir*, vol. 23, no. 10, pp. 5522–5531, May 2007.
- [48] G. I. Taylor, ‘The Formation of Emulsions in Definable Fields of Flow’, *Proceedings of the Royal Society of London. Series A*, vol. 146, no. 858, pp. 501–523, 1934.
- [49] H. J. Karam and J. C. Bellinger, ‘Deformation and Breakup of Liquid Droplets in a Simple Shear Field’, *Industrial & Engineering Chemistry Fundamentals*, vol. 7, no. 4, pp. 576–581, 1968.
- [50] J. A. Lindley, ‘Mixing processes for agricultural and food materials: Part 2, highly viscous liquids and cohesive materials’, *Journal of Agricultural Engineering Research*, vol. 48, pp. 229–247, 1991.
- [51] M. Regner, K. Ostergren, and C. Tragardh, ‘Influence of Viscosity Ratio on the Mixing Process in a Static Mixer: Numerical Study’, *Industrial & Engineering Chemistry Research*, vol. 47, no. 9, pp. 3030–3036, May 2008.
- [52] W. D. Mohr, R. L. Saxton, and C. H. Jepson, ‘Mixing in Laminar-Flow Systems’, *Industrial & Engineering Chemistry*, vol. 49, no. 11, pp. 1855–1856, 1957.
-

References

-
- [53] P. . Smith, T. G. . van de Ven, and S. . Mason, 'The transient interfacial tension between two miscible fluids', *Journal of Colloid and Interface Science*, vol. 80, no. 1, pp. 302–303, Mar. 1981.
- [54] A. Mersmann, 'Crystallization and precipitation', *Chemical Engineering and Processing*, vol. 38, no. 4–6, pp. 345–353, Sep. 1999.
- [55] N. Doki, N. Kubota, M. Yokota, S. Kimura, and S. Sasaki, 'Production of Sodium Chloride Crystals of Uni-Modal Size Distribution by Batch Dilution Crystallization.', *J Chem Eng Jpn*, vol. 35, no. 11, pp. 1099–1104, 2002.
- [56] S. Mostafa Nowee, A. Abbas, and J. A. Romagnoli, 'Antisolvent crystallization: Model identification, experimental validation and dynamic simulation', *Chemical Engineering Science*, vol. 63, no. 22, pp. 5457–5467, Nov. 2008.
- [57] J. A. Dirksen and T. A. Ring, 'Fundamentals of crystallization: Kinetic effects on particle size distributions and morphology', *Chemical Engineering Science*, vol. 46, no. 10, pp. 2389–2427, 1991.
- [58] E. P. Favvas and A. C. Mitropoulos, 'What is spinodal decomposition?', *Journal of Engineering Science and Technology Review*, vol. 1, pp. 25–27, 2008.
- [59] H. Cölfen and S. Mann, 'Higher-Order Organization by Mesoscale Self-Assembly and Transformation of Hybrid Nanostructures', *Angew. Chem. Int. Ed.*, vol. 42, no. 21, pp. 2350–2365, May 2003.
- [60] A. W. Xu, Y. R. Ma, and H. Colfen, 'Biomimetic mineralization', *Journal of Materials Chemistry*, vol. 17, no. 5, pp. 415–449, 2007.
- [61] M. Volmer, *Kinetics of Phase Formation*. 1939.
- [62] R. Boistelle and J. P. Astier, 'Crystallization mechanisms in solution', *Journal of Crystal Growth*, vol. 90, no. 1–3, pp. 14–30, Jul. 1988.
- [63] F. Lince, D. L. Marchisio, and A. A. Barresi, 'Strategies to control the particle size distribution of poly- ϵ -caprolactone nanoparticles for pharmaceutical applications', 15-Jun-2008.
- [64] B. K. Johnson and R. K. Prud'homme, 'Mechanism for Rapid Self-Assembly of Block Copolymer Nanoparticles', *Phys. Rev. Lett.*, vol. 91, no. 11, p. 118302, 2003.
- [65] H.-C. Schwarzer and W. Peukert, 'Experimental Investigation into the Influence of Mixing on Nanoparticle Precipitation', *Chem. Eng. Technol.*, vol. 25, no. 6, pp. 657–661, 2002.
- [66] A. Nielsen, *Kinetics of precipitation*. Pergamon Press, 1964.
- [67] C. P. M. Roelands, J. J. Derksen, J. H. ter Horst, H. J. M. Kramer, and P. J. Jansens, 'An Analysis of Mixing in a Typical Experimental Set-up to Measure Nucleation Rates of Precipitation Processes', *Chemical Engineering & Technology*, vol. 26, no. 3, pp. 296–303, 2003.
- [68] M. Kreiner and M.-C. Parker, 'Protein-coated microcrystals for use in organic solvents: application to oxidoreductases', *Biotechnol. Lett*, vol. 27, no. 20, pp. 1571–1577, Oct. 2005.
- [69] J. Vos, 'Understanding the formation mechanism of protein coated microcrystals', PhD Thesis, University of Strathclyde, 2006.
- [70] M. Kreiner, J. F. Amorim Fernandes, N. O'Farrell, P. J. Halling, and M.-C. Parker, 'Stability of protein-coated microcrystals in organic solvents', *Journal of Molecular Catalysis B: Enzymatic*, vol. 33, no. 3–6, pp. 65–72, Jun. 2005.
-

-
- [71] J. Partridge and B. . Moore, 'Dry powder formulations of Protein-coated microcrystals prepared in the range of 30 % w/w- to 0.1 % w/w', 2007.
- [72] J. R. Bourne, J. Lenzner, and S. Petrozzi, 'Micromixing in static mixers: an experimental study', *Industrial & Engineering Chemistry Research*, vol. 31, no. 4, pp. 1216–1222, 1992.
- [73] E. F. Caldin and G. Long, 'Equilibrium between Ethoxide and Hydroxide Ions in Ethanol', *Nature*, vol. 172, no. 4378, pp. 583–584, print 1953.
- [74] K. Komers, J. Machek, and R. Stloukal, 'Biodiesel from rapeseed oil, methanol and KOH. 2. Composition of solution of KOH in methanol as reaction partner of oil', *Eur. J. Lipid Sci. Technol.*, vol. 103, no. 6, pp. 359–362, 2001.
- [75] J. F. Richardson and J. M. Coulson, *Chemical Engineering*, vol. 1. Butterworth-Heinemann, 1999.
- [76] C. F. Colebrook and C. M. White, 'Experiments with Fluid Friction in Roughened Pipes', *Proceedings of the Royal Society of London. Series A - Mathematical and Physical Sciences*, vol. 161, no. 906, pp. 367–381, 1937.
- [77] W. Jennings, E. Mittlefehldt, and P. Stremple, *Analytical Gas Chromatography*, 2nd ed. Elsevier, 1997.
- [78] G. Guiochon and C. L. Guillemin, 'Gas chromatography', *Rev. Sci. Instrum.*, vol. 61, no. 11, p. 3317, 1990.
- [79] R. Grob and E. Barry, *Modern Practice of Gas Chromatography*, 4th ed. Wiley, 2004.
- [80] O. D. Sparkman, Z. E. Penton, and F. G. Kitson, 'Gas Chromatography', in *Gas Chromatography and Mass Spectrometry: A Practical Guide (Second edition)*, Amsterdam: Academic Press, 2011, pp. 15–83.
- [81] 'Quantitative Analysis By Gas Chromatography Measurement of Peak Area and Derivation of Sample Composition', in *For Laboratory Analyses and On-Line Process Control*, vol. Volume 42, Elsevier, 1988, pp. 629–659.
- [82] A. Jawor-Baczynska, *PhD Thesis*. University of Strathclyde, 2010.
- [83] P. Costa and C. Trevisoi, 'Reactions with non-linear kinetics in partially segregated fluids', *Chemical Engineering Science*, vol. 27, no. 11, pp. 2041–2054, 1972.
- [84] J. Villermaux and L. Falk, 'A generalized mixing model for initial contacting of reactive fluids', *Chemical Engineering Science*, vol. 49, no. 24, Part 2, pp. 5127–5140, Dec. 1994.
- [85] J. Baldyga and J. R. Bourne, 'Comparison of the engulfment and the interaction-by-exchange-with-the-mean micromixing models', *The Chemical Engineering Journal*, vol. 45, no. 1, pp. 25–31, Nov. 1990.
- [86] J. M. Gillian, *Reactive precipitation of pharmaceuticals: Mixing, reaction and nucleation kinetics (PhD Thesis)*. University of Virginia, 2007.
- [87] R. Zauner and A. G. Jones, 'On the influence of mixing on crystal precipitation processes--application of the segregated feed model', *Chemical Engineering Science*, vol. 57, no. 5, pp. 821–831, Mar. 2002.
- [88] D. M. Ragab and S. Rohani, 'Particle Engineering Strategies via Crystallization for Pulmonary Drug Delivery', *Organic Process Research & Development*, vol. 13, no. 6, pp. 1215–1223, Nov. 2009.
- [89] N. R. Labiris and M. B. Dolovich, 'Pulmonary drug delivery. Part I: Physiological factors affecting therapeutic effectiveness of aerosolized medications', *Br J Clin Pharmacol*, vol. 56, no. 6, pp. 588–599, 2003.
-

References

- [90] J. M. Coulson, J. F. Richardson, J. H. Harker, and J. R. Backhurst, *Chemical engineering: Particle technology and separation processes*. Butterworth-Heinemann, 2002.
- [91] M. J. Matteson and C. Orr, *Filtration: principles and practices*. M. Dekker, 1987.
- [92] R. Wakeman, ‘The influence of particle properties on filtration’, *Separation and Purification Technology*, vol. 58, no. 2, pp. 234–241, Dec. 2007.

Appendix 1 - Physical Properties

All physical properties measured at 25°C and 1 atmosphere of pressure:

Bourne IV Scheme 1:1			
	ρ (kg.m ⁻³)	μ (mPa.S)	ν (m ² .s ⁻¹)
Acid	969.84	1.94	2.00E-06
Alkali	960.46	1.80	1.87E-06
Product	961.50	1.83	1.90E-06

Physical Properties 1:1 Same Solvent Composition

Bourne Scheme 3:1			
	ρ (kg.m ⁻³)	μ (mPa.S)	ν (m ² .s ⁻¹)
Acid	969.90	1.75	1.80E-06
Alkali	968.20	1.86	1.92E-06
Product	969.00	1.79	1.85E-06

Physical Properties 3:1 Same Solvent Composition

Reverse Bourne Scheme 1:3			
	ρ (kg.m ⁻³)	μ (mPa.S)	ν (m ² .s ⁻¹)
Acid	972.30	1.78	1.84E-06
Alkali	951.40	2.00	2.10E-06
Product	951.40	1.80	1.89E-06

Physical Properties 1:3 Same Solvent Composition

Bourne Scheme 10:1			
	ρ (kg.m ⁻³)	μ (mPa.S)	ν (m ² .s ⁻¹)
Acid	976.00	1.78	1.82E-06
Alkali	967.00	1.86	1.92E-06
Product	966.20	1.82	1.88E-06

Physical Properties 10:1 Same Solvent Composition

Composition Modified Bourne IV Scheme 1:1			
	ρ (kg.m ⁻³)	μ (mPa.S)	ν (m ² .s ⁻¹)
Acid	1003.20	0.91	9.09E-07
Alkali	920.30	2.32	2.52E-06
Product	969.50	1.87	1.93E-06

Physical Properties 1:1 Different Solvent Composition

Composition Modified Bourne Scheme 3:1			
	ρ (kg.m ⁻³)	μ (mPa.S)	ν (m ² .s ⁻¹)
Acid	1008.00	0.92	9.13E-07
Alkali	919.20	2.21	2.41E-06
Product	941.40	2.11	2.24E-06

Physical Properties 3:1 Different Solvent Composition

Composition Modified Reverse Bourne Scheme 1:3			
	ρ (kg.m ⁻³)	μ (mPa.S)	ν (m ² .s ⁻¹)
Acid	996.50	0.89	8.97E-07
Alkali	931.00	2.46	2.64E-06
Product	990.00	1.34	1.35E-06

Physical Properties 1:3 Different Solvent Composition

Composition Modified Bourne Scheme 10:1			
	ρ (kg.m ⁻³)	μ (mPa.S)	ν (m ² .s ⁻¹)
Acid	1011.60	0.96	9.49E-07
Alkali	915.30	2.22	2.43E-06
Product	930.00	2.17	2.33E-06

Physical Properties 10:1 Different Solvent Composition

Appendix 2 - Mixer Geometries

T-mixer

T-mixers were off the shelf Swagelok stainless steel union tees. Diameters are referenced to nominal external ID.



Swagelok 1/4" Union Tee – 1/4" external diameter

Swagelok 2/8" Union Tee – 1/8" external diameter

X-Mixer

X-mixers were off the shelf Swagelok stainless steel union crosses. Diameters are referenced to nominal external ID.

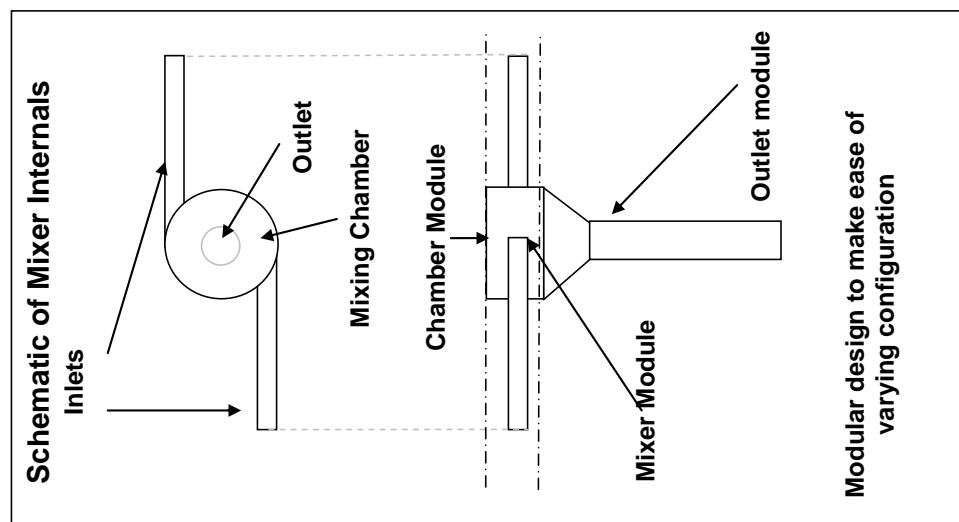
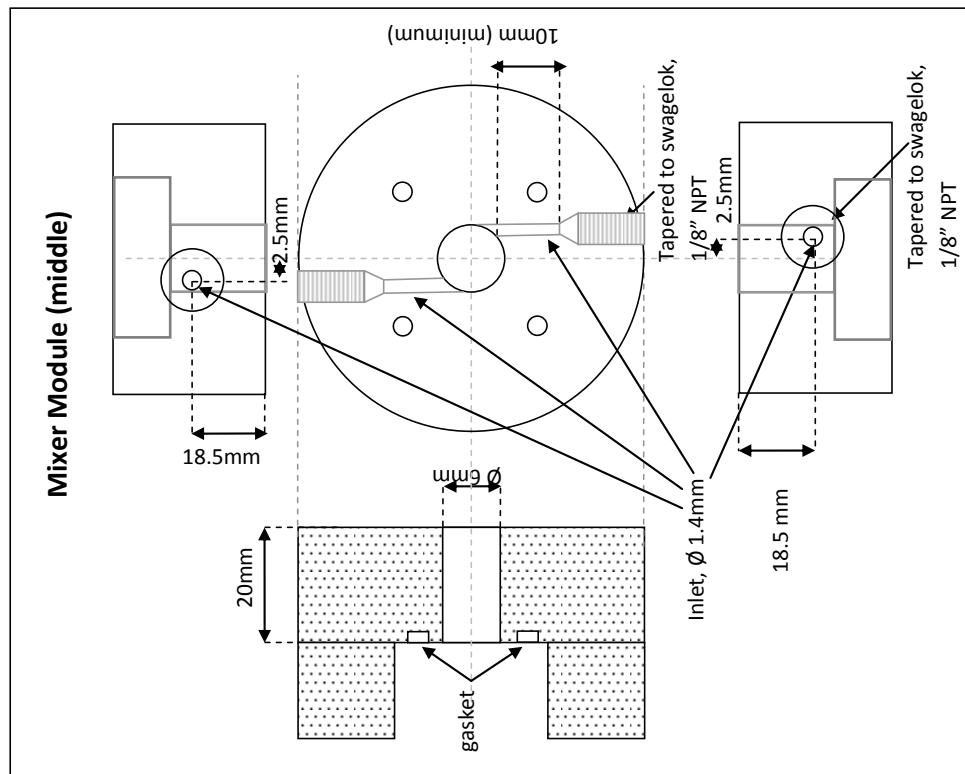


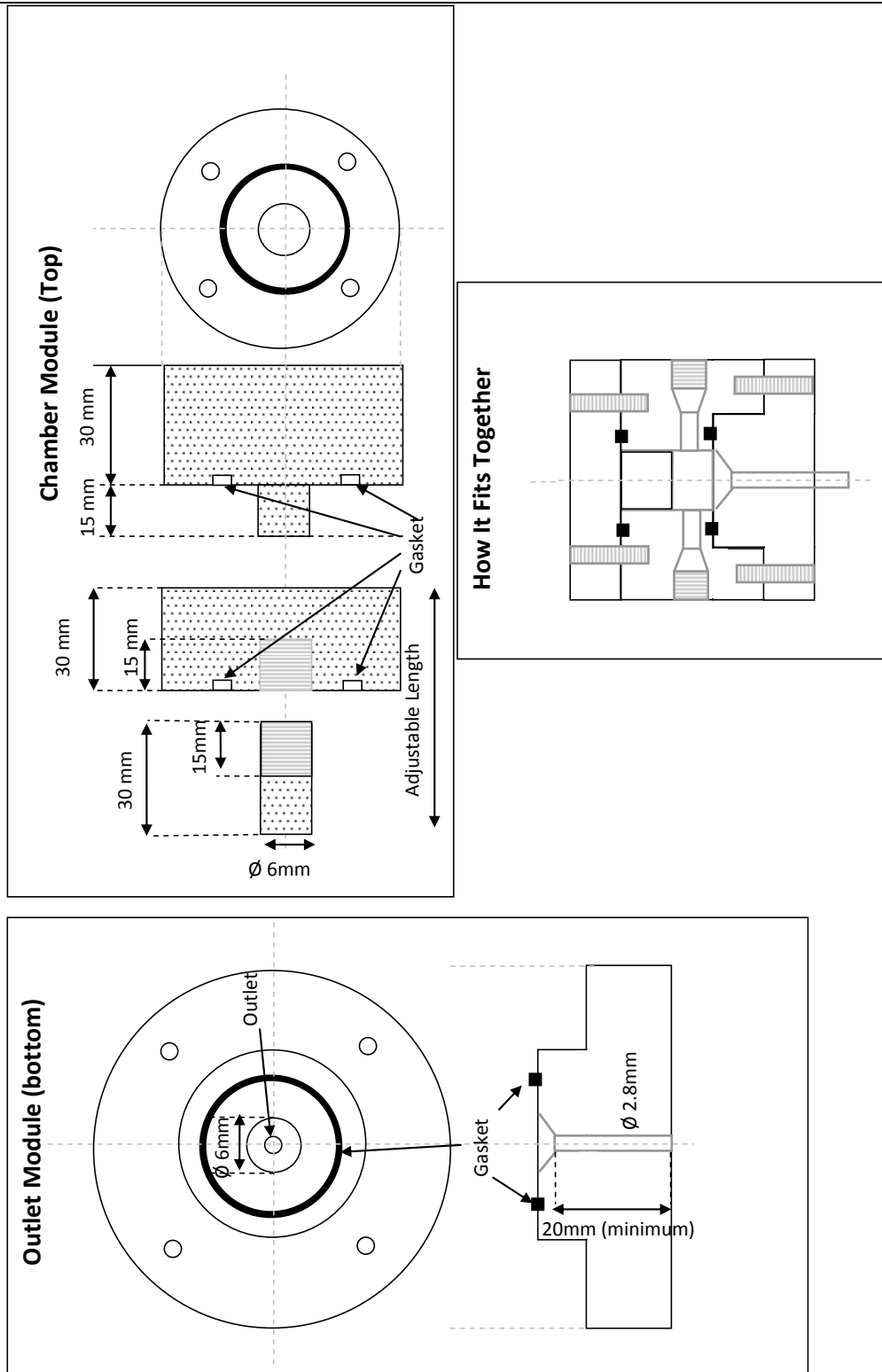
Swagelok 1/4" Union Cross – 1/4" external diameter

Swagelok 1/8" Union Cross – 1/8" external diameter

Vortex Mixer

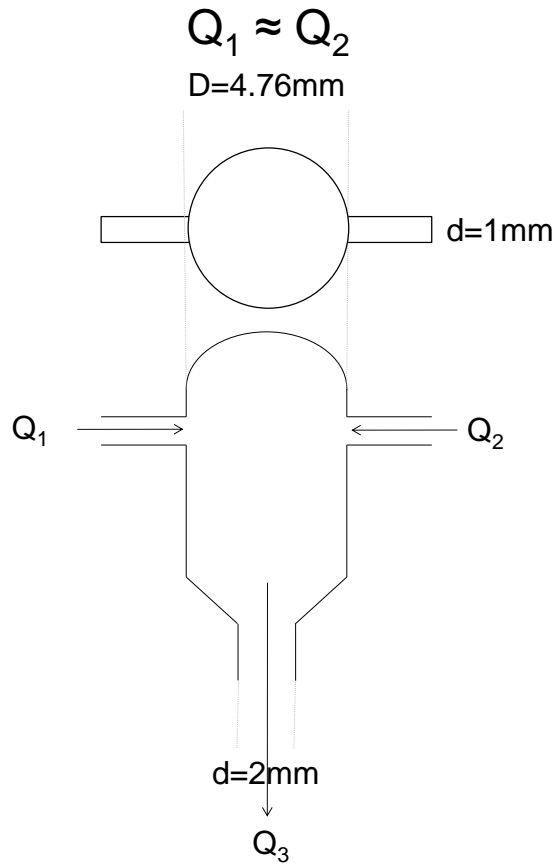
The vortex mixer was designed and fabricated in-house using the blueprint below. Some dimensions may vary slightly due to fabrication restrictions.





Confined Impinging Jet Mixer

The confined impinging jet mixer was fabricated externally to the following specifications:



Appendix 3 - Mixing Characterisation Data

1:1 no viscosity difference

1/4" X			1/4" T		
Q _{alkali} (ml/min)	ε _{total} (kj/kg)	X	Q _{alkali} (ml/min)	ε _{total} (kj/kg)	X
50.9	0.9	0.434	57.9	1.1	0.448
50.9	0.9	0.426	57.9	1.1	0.449
102.1	2.2	0.398	101.0	1.7	0.588
102.1	2.2	0.385	101.0	1.7	0.543
202.6	5.8	0.406	201.7	5.7	0.432
202.6	5.8	0.502	201.7	5.7	0.456
405.2	22.6	0.278	405.8	21.5	0.311
405.2	22.6	0.294	405.8	21.5	0.293
601.5	58.8	0.202	608.2	65.0	0.226
601.5	58.8	0.222	608.2	65.0	0.232
1/8" X			1/8" T		
Q _{alkali} (ml/min)	ε _{total} (kj/kg)	X	Q _{alkali} (ml/min)	ε _{total} (kj/kg)	X
50.3	17.6	0.283	50.4	15.6	0.466
50.3	20.3	0.283	50.3	17.9	0.433
101.8	105.6	0.139	101.7	81.9	0.187
100.7	104.7	0.131	102.0	86.3	0.195
204.4	654.0	0.078	203.9	544.6	0.084
202.8	708.4	0.087	203.4	592.9	0.101
419.7	5603.1	0.055	417.0	4370.2	0.045
421.4	5563.9	0.049	416.8	4492.7	0.044
611.2	14965.4	0.029	615.6	12751.8	0.031
607.1	15348.3	0.029	612.3	13840.9	0.032
Vortexer			CIJ		
Q _{alkali} (ml/min)	ε _{total} (kj/kg)	X	Q _{alkali} (ml/min)	ε _{total} (kj/kg)	X
49.5	22.5	0.231	51.4	21.7	0.274
49.3	21.3	0.252	51.4	21.7	0.277
99.6	140.9	0.113	104.1	120.5	0.150
99.4	141.3	0.119	104.1	120.5	0.155
200.7	1026.8	0.051	206.6	771.2	0.074
200.5	1039.8	0.056	206.6	771.2	0.073
406.5	8579.7	0.035	528.4	9999.8	0.044
409.9	9498.5	0.037	529.0	10176.7	0.038
608.1	25283.2	0.022	712.7	19915.4	0.032
614.0	25657.0	0.021	712.7	19915.4	0.038

1:1 no viscosity difference

1/4" X			1/4" T		
Q _{alkali} (ml/min)	ε _{total} (kj/kg)	X	Q _{alkali} (ml/min)	ε _{total} (kj/kg)	X
49.2	1.5	0.497	48.9	1.6	0.636
49.2	1.5	0.467	48.9	1.6	0.644
98.5	4.1	0.544	97.4	4.7	0.530
98.5	4.1	0.603	97.4	4.7	0.533
298.5	22.6	0.363	297.5	28.0	0.350
298.5	22.6	0.367	297.5	28.0	0.365
490.8	67.1	0.239	484.1	65.4	0.258
490.8	67.1	0.266	484.1	65.4	0.284
681.9	157.9	0.195	686.7	153.2	0.228
681.9	157.9	0.194	686.7	153.2	0.211
1/8" X			1/8" T		
Q _{alkali} (ml/min)	ε _{total} (kj/kg)	X	Q _{alkali} (ml/min)	ε _{total} (kj/kg)	X
49.0	31.5	0.451	50.7	23.5	0.389
49.2	31.5	0.468	50.7	23.5	0.402
97.8	177.3	0.258	99.9	127.3	0.264
98.4	175.3	0.293	99.9	127.3	0.268
194.8	855.2	0.150	195.4	747.2	0.160
194.4	1082.2	0.169	195.4	747.2	0.154
406.8	7751.6	0.087	407.7	5530.1	0.072
406.8	7751.6	0.077	407.7	5530.1	0.079
604.3	22178.0	0.057	604.7	16247.1	0.058
604.3	22178.0	0.048	604.7	16247.1	0.054
Vortexer			CIJ		
Q _{alkali} (ml/min)	ε _{total} (kj/kg)	X	Q _{alkali} (ml/min)	ε _{total} (kj/kg)	X
48.1	32.0	0.374	49.9	36.0	0.506
48.1	32.0	0.386	49.9	36.0	0.508
105.0	194.4	0.196	107.6	241.3	0.208
105.0	194.4	0.196	107.6	241.3	0.216
193.5	1113.8	0.115	191.4	1146.1	0.103
193.5	1113.8	0.128	191.4	1146.1	0.105
314.7	4183.2	0.074	503.4	10301.2	0.040
311.7	4131.4	0.085	503.4	10301.2	0.041
704.6	36116.4	0.053	711.0	23547.6	0.029
704.6	36116.4	0.042	711.0	23547.6	0.029

3:1 no viscosity difference

1/4" X			1/4" T		
Q _{alkali} (ml/min)	ε _{total} (kj/kg)	X	Q _{alkali} (ml/min)	ε _{total} (kj/kg)	X
52.6	0.2	0.408	52.6	0.6	0.503
52.6	0.9	0.415	52.5	0.6	0.536
106.0	1.9	0.494	105.8	1.0	0.597
105.9	1.8	0.554	105.9	1.0	0.585
209.3	4.3	0.434	210.5	3.1	0.496
208.7	4.2	0.455	209.8	2.9	0.476
409.5	14.4	0.377	407.9	11.6	0.360
407.8	14.6	0.397	407.3	11.6	0.417
613.5	37.0	0.235	609.8	33.9	0.294
617.0	34.9	0.268	610.0	34.0	0.302
1/8" X			1/8" T		
Q _{alkali} (ml/min)	ε _{total} (kj/kg)	X	Q _{alkali} (ml/min)	ε _{total} (kj/kg)	X
53.6	12.3	0.331	55.1	8.2	0.431
53.2	12.3	0.327	55.1	8.4	0.412
104.6	55.0	0.181	105.5	49.4	0.179
104.5	55.0	0.168	105.2	48.9	0.177
208.6	328.8	0.117	210.2	296.8	0.104
208.6	321.1	0.110	209.9	295.4	0.107
403.7	2062.6	0.067	407.5	1913.9	0.062
404.2	2066.7	0.068	407.5	1913.9	0.063
612.8	6338.9	0.042	616.2	6207.0	0.041
611.3	6304.4	0.044	616.2	6207.0	0.033
Vortexer					
Q _{alkali} (ml/min)	ε _{total} (kj/kg)	X			
54.4	9.6	0.368			
53.3	10.0	0.346			
104.2	54.3	0.187			
104.2	54.3	0.184			
209.0	406.7	0.097			
208.0	391.2	0.090			
405.4	3051.0	0.052			
405.2	3042.3	0.050			
616.2	9686.8	0.036			
615.8	9695.6	0.043			

3:1 with viscosity difference

1/4" X			1/4" T		
Q _{alkali} (ml/min)	ε _{total} (kj/kg)	X	Q _{alkali} (ml/min)	ε _{total} (kj/kg)	X
54.1	0.7	0.467	54.2	1.2	0.488
54.1	0.7	0.443	54.1	1.2	0.504
105.4	1.5	0.546	105.5	2.2	0.475
105.4	1.4	0.559	105.5	2.3	0.495
211.8	4.1	0.529	212.2	4.8	0.477
211.0	4.0	0.552	211.4	4.9	0.455
427.7	15.7	0.344	428.7	15.7	0.361
431.1	15.9	0.389	426.8	17.6	0.368
649.2	42.8	0.258	647.0	44.9	0.287
648.3	43.0	0.262	648.4	45.2	0.268
1/8" X			1/8" T		
Q _{alkali} (ml/min)	ε _{total} (kj/kg)	X	Q _{alkali} (ml/min)	ε _{total} (kj/kg)	X
54.1	13.0	0.293	54.2	11.5	0.320
54.1	13.1	0.315	54.1	11.1	0.314
105.4	59.7	0.194	105.5	45.2	0.197
105.4	57.9	0.180	105.5	44.9	0.190
211.8	340.8	0.114	212.2	282.3	0.105
211.0	336.3	0.116	211.4	276.1	0.108
427.7	2207.6	0.079	428.7	1758.1	0.066
431.1	2200.9	0.070	426.8	1783.9	0.069
649.2	7169.4	0.041	647.0	5896.4	0.046
648.3	7228.3	0.045	648.4	5935.1	0.048
Vortexer					
Q _{alkali} (ml/min)	ε _{total} (kj/kg)	X			
53.7	10.9	0.338			
53.8	11.2	0.324			
104.5	61.9	0.194			
104.6	62.0	0.202			
210.3	437.9	0.107			
209.4	428.9	0.107			
427.6	3322.1	0.064			
425.2	3279.4	0.064			
644.4	10969.2	0.049			
644.1	11331.2	0.046			

1:3 no viscosity difference

1/4" X			1/4" T		
Q _{alkali} (ml/min)	ε _{total} (kj/kg)	X	Q _{alkali} (ml/min)	ε _{total} (kj/kg)	X
34.2	1.1	0.641	35.0	0.9	0.510
34.2	1.1	0.660	35.0	0.8	0.479
68.7	2.6	0.401	68.0	2.6	0.389
68.7	2.3	0.389	68.0	2.5	0.342
135.4	11.1	0.375	135.9	11.5	0.252
135.4	11.3	0.414	135.9	11.5	0.269
205.5	33.8	0.302	203.3	33.6	0.225
205.5	31.0	0.312	203.3	33.3	0.229
1/8" X			1/8" T		
Q _{alkali} (ml/min)	ε _{total} (kj/kg)	X	Q _{alkali} (ml/min)	ε _{total} (kj/kg)	X
18.0	9.0	0.484	18.1	7.6	0.464
18.0	9.1	0.443	18.1	7.8	0.385
34.9	50.0	0.136	34.9	51.4	0.114
34.9	50.2	0.156	34.9	50.9	0.113
68.8	315.3	0.070	69.2	297.2	0.088
68.8	314.6	0.074	69.2	295.8	0.083
137.0	2118.8	0.041	137.6	2059.5	0.039
137.0	2147.2	0.043	137.6	2059.5	0.041
210.8	6778.6	0.018	210.3	6577.4	0.029
210.8	6789.0	0.021	210.3	6577.4	0.026
Vortexer					
Q _{alkali} (ml/min)	ε _{total} (kj/kg)	X			
18.2	8.5	0.256			
18.2	9.1	0.245			
35.6	53.0	0.133			
35.6	53.0	0.133			
69.5	397.5	0.066			
69.5	394.6	0.060			
140.4	3274.6	0.035			
140.4	3251.3	0.033			
218.8	10600.9	0.024			
218.8	10613.9	0.024			

1:3 with viscosity difference

1/4" X			1/4" T		
Q _{alkali} (ml/min)	ε _{total} (kj/kg)	X	Q _{alkali} (ml/min)	ε _{total} (kj/kg)	X
32.1	1.8	0.681	32.1	1.6	0.786
32.1	1.7	0.586	32.1	1.6	0.764
66.4	3.9	0.539	66.5	3.7	0.560
66.4	3.9	0.588	66.5	3.7	0.568
136.3	11.3	0.426	136.3	14.3	0.420
136.3	11.2	0.390	136.3	15.3	0.406
203.4	24.8	0.394	202.7	40.0	0.294
203.4	24.7	0.384	202.7	40.0	0.325
1/8" X			1/8" T		
Q _{alkali} (ml/min)	ε _{total} (kj/kg)	X	Q _{alkali} (ml/min)	ε _{total} (kj/kg)	X
16.9	14.0	0.641	16.8	12.2	0.485
16.9	14.0	0.611	16.8	12.2	0.523
30.6	44.8	0.500	31.3	37.3	0.458
30.6	44.6	0.471	31.3	37.1	0.381
61.9	217.5	0.208	61.5	201.5	0.301
61.9	217.3	0.201	61.5	200.2	0.307
133.9	1536.6	0.101	133.8	1456.2	0.123
133.9	1526.3	0.106	133.8	1461.9	0.105
187.7	4516.9	0.091	188.1	4473.4	0.115
187.7	4537.7	0.084	188.1	4458.6	0.110
Vortexer					
Q _{alkali} (ml/min)	ε _{total} (kj/kg)	X			
17.1	9.1	0.514			
17.1	9.0	0.538			
33.7	45.7	0.354			
33.7	45.7	0.339			
68.6	341.1	0.221			
68.6	340.2	0.194			
141.3	2942.0	0.135			
141.3	2944.6	0.147			
223.7	10782.0	0.103			
223.7	10860.0	0.098			

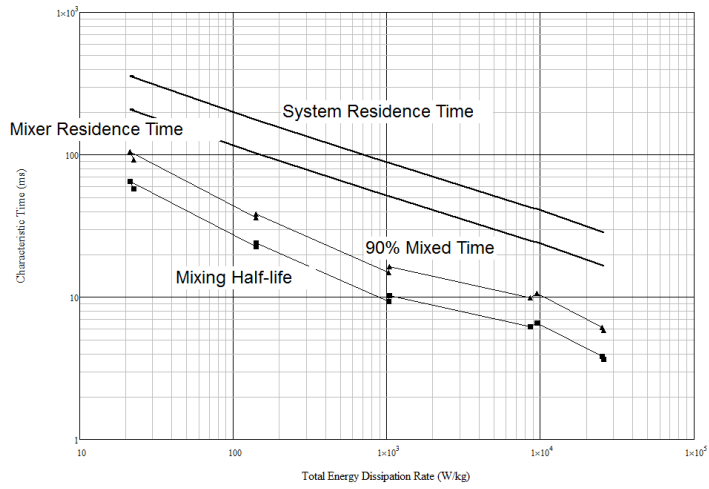
10:1 with no viscosity difference

1/4" X			1/4" T		
Q _{alkali} (ml/min)	ε _{total} (kj/kg)	X	Q _{alkali} (ml/min)	ε _{total} (kj/kg)	X
127.1	1.8	0.557	127.4	1.9	0.586
127.1	1.8	0.574	127.4	1.9	0.629
207.9	3.0	0.593	209.7	3.7	0.674
207.9	3.0	0.699	209.7	3.7	0.651
423.4	12.2	0.555	410.8	13.1	0.546
423.4	12.2	0.533	410.8	13.1	0.558
614.2	30.9	0.422	624.1	30.6	0.427
614.2	30.9	0.421	624.1	30.6	0.409
1/8" X			1/8" T		
Q _{alkali} (ml/min)	ε _{total} (kj/kg)	X	Q _{alkali} (ml/min)	ε _{total} (kj/kg)	X
127.1	68.9	0.319	127.4	48.1	0.274
127.1	68.9	0.350	127.4	48.1	0.296
216.7	300.5	0.237	209.7	204.0	0.230
216.7	300.5	0.245	209.7	204.0	0.238
416.1	2095.7	0.187	410.8	1478.7	0.181
416.1	2095.7	0.182	410.8	1478.7	0.178
613.2	7499.9	0.096	624.1	4052.9	0.152
613.2	7499.9	0.107	624.1	4052.9	0.135
Vortexer					
Q _{alkali} (ml/min)	ε _{total} (kj/kg)	X			
121.3	64.8	0.216			
121.3	64.8	0.208			
202.6	298.0	0.158			
202.6	298.0	0.139			
417.1	2620.6	0.072			
417.1	2620.6	0.060			
618.5	7141.9	0.047			
618.5	7141.9	0.051			

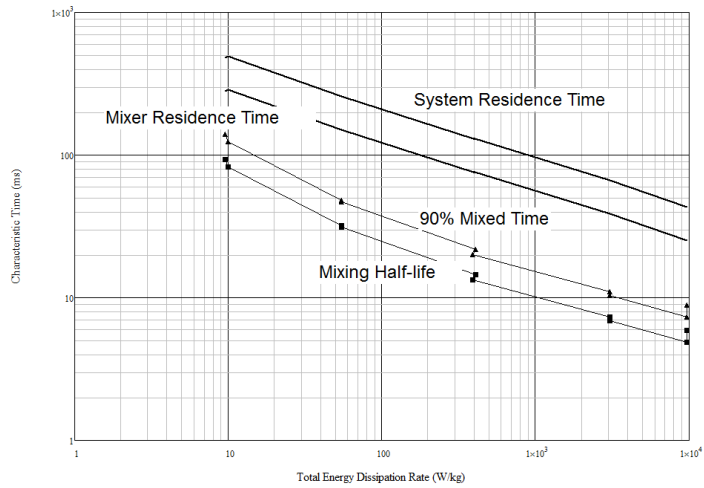
10:1 with viscosity difference

1/4" X			1/4" T		
Q _{alkali} (ml/min)	ε _{total} (kj/kg)	X	Q _{alkali} (ml/min)	ε _{total} (kj/kg)	X
126.0	2.2	0.631	126.1	2.2	0.608
126.0	2.2	0.558	126.1	2.2	0.632
209.0	4.8	0.682	209.1	2.4	0.609
209.0	4.8	0.726	209.1	2.4	0.557
418.4	16.1	0.495	418.9	13.5	0.504
418.4	16.1	0.468	418.9	13.5	0.406
615.0	39.1	0.294	619.0	34.4	0.366
615.0	39.1	0.300	619.0	34.4	0.335
1/8" X			1/8" T		
Q _{alkali} (ml/min)	ε _{total} (kj/kg)	X	Q _{alkali} (ml/min)	ε _{total} (kj/kg)	X
122.3	87.2	0.289	122.9	58.2	0.373
122.3	87.2	0.284	122.9	58.2	0.319
202.9	328.4	0.223	204.1	217.3	0.271
202.9	328.4	0.231	204.1	217.3	0.258
410.7	2129.2	0.166	408.5	1508.6	0.151
410.7	2129.2	0.154	408.5	1508.6	0.148
608.4	6469.0	0.066	609.5	4825.2	0.114
608.4	6469.0	0.072	609.5	4825.2	0.117
Vortexer					
Q _{alkali} (ml/min)	ε _{total} (kj/kg)	X			
122.0	81.1	0.182			
122.0	81.1	0.186			
202.0	322.7	0.125			
202.0	322.7	0.134			
408.9	2463.0	0.065			
408.9	2463.0	0.059			
604.2	7740.1	0.043			
604.2	7740.1	0.046			

Appendix 4 - Comparison of Timescales

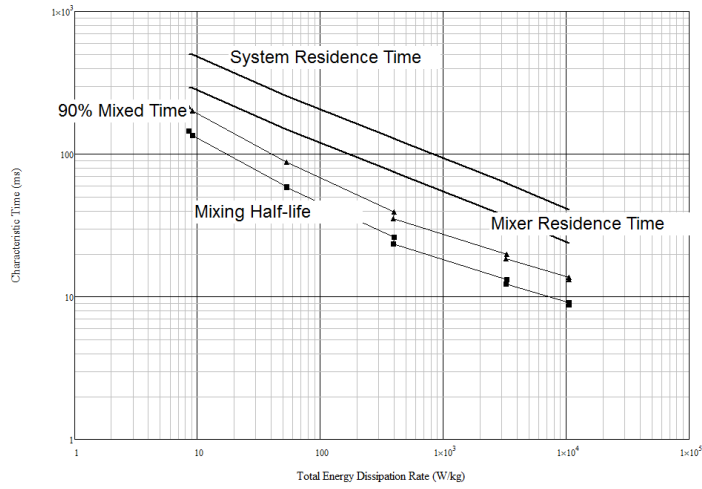


Vortex 1:1 Bourne Composition Timescale Comparison

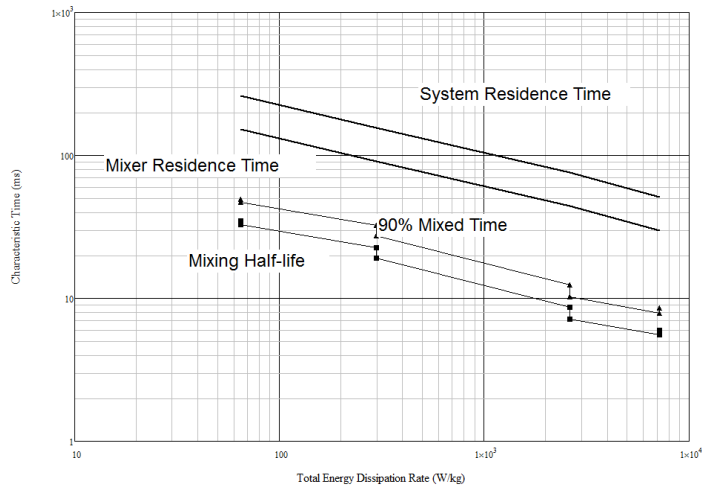


Vortex 3:1 Bourne Composition Timescale Comparison

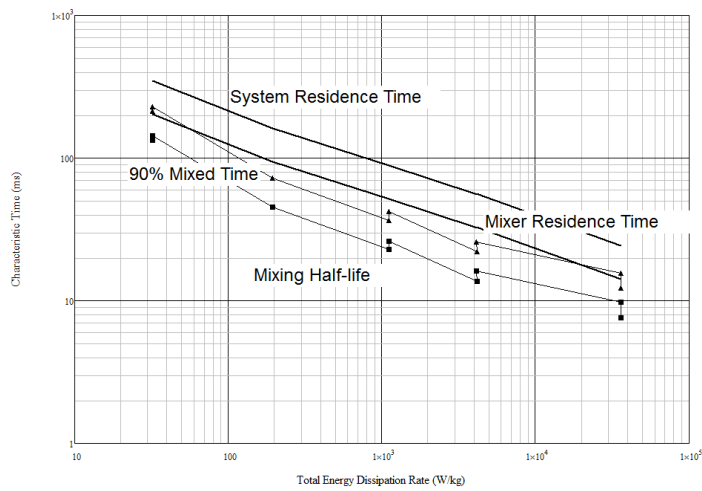
Appendix 4 – Comparison of Timescales



Vortex 1:3 Bourne Composition Timescale Comparison

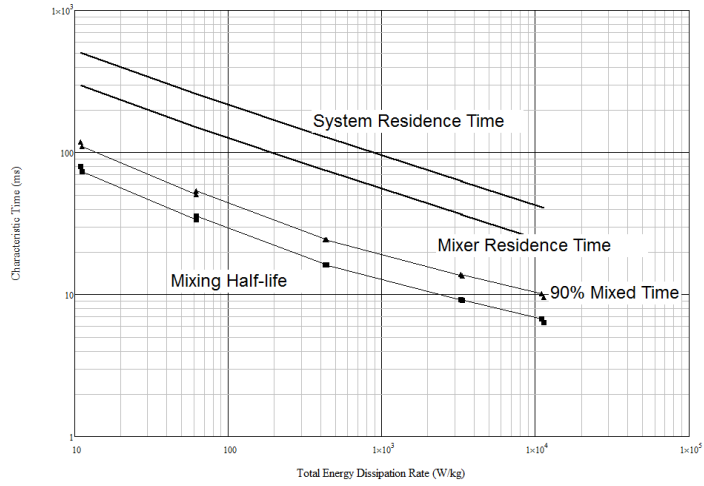


Vortex 10:1 Bourne Composition Timescale Comparison

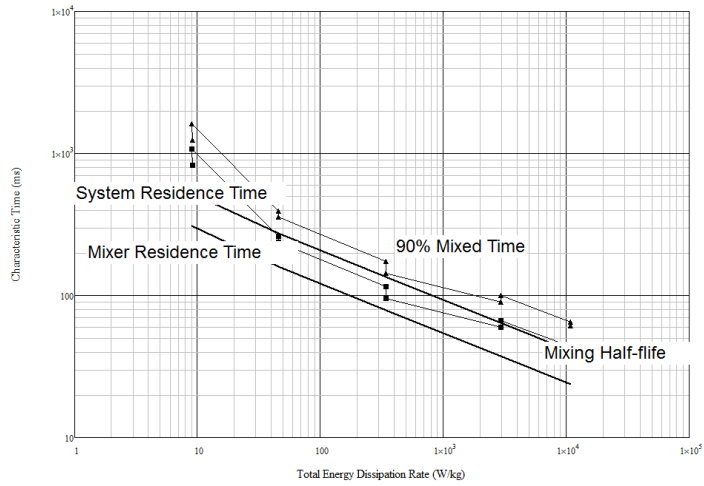


Vortex 1:1 Modified Bourne Composition Timescale Comparison

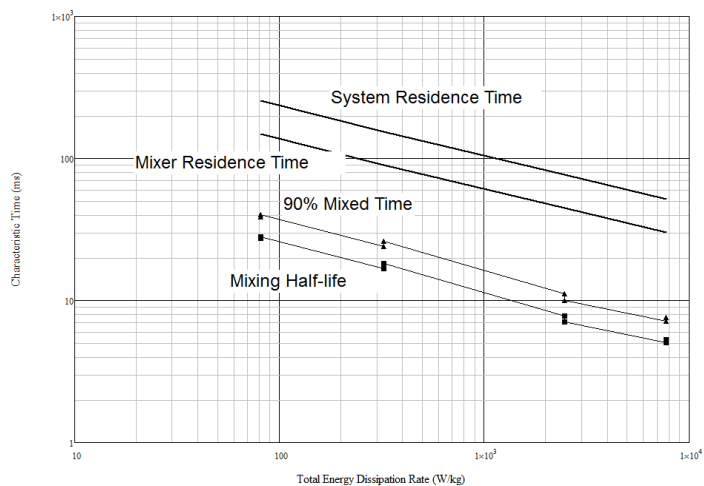
Appendix 4 – Comparison of Timescales



Vortex 3:1 Modified Bourne Composition Timescale Comparison

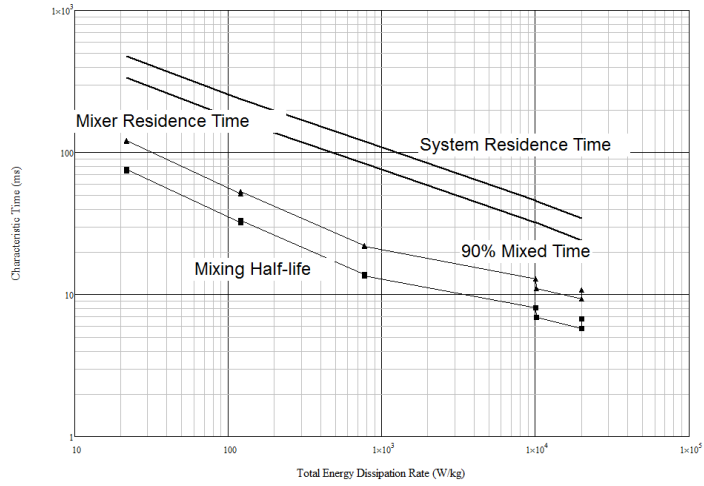


Vortex 1:3 Modified Bourne Composition Timescale Comparison

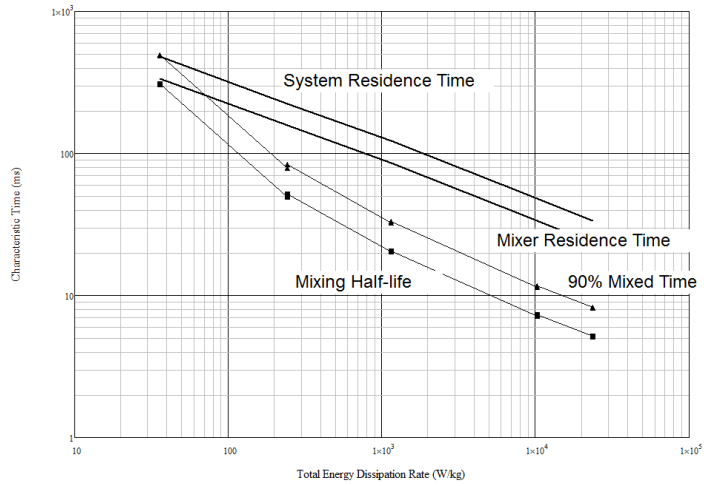


Vortex 10:1 Modified Bourne Composition Timescale Comparison

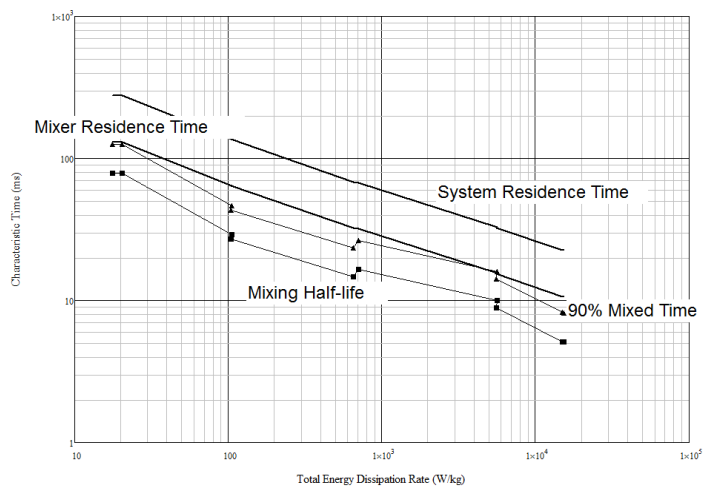
Appendix 4 – Comparison of Timescales



CIJ 1:1 Bourne Composition Timescale Comparison

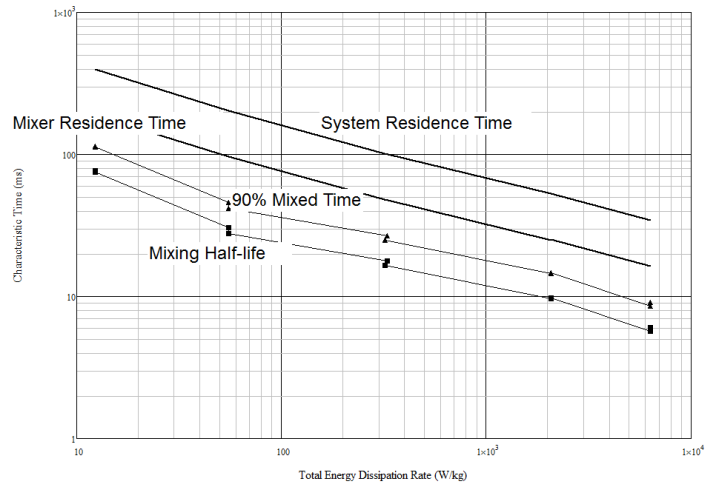


CIJ 1:1 Modified Bourne Composition Timescale Comparison

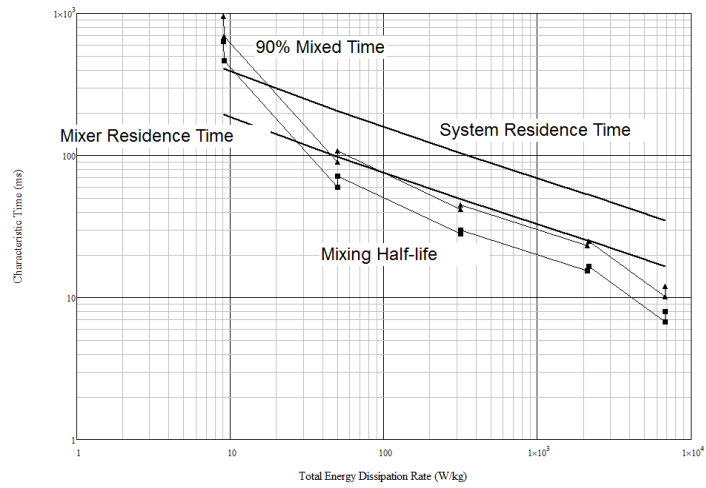


1/8" X Mixer 1:1 Bourne Composition Timescale Comparison

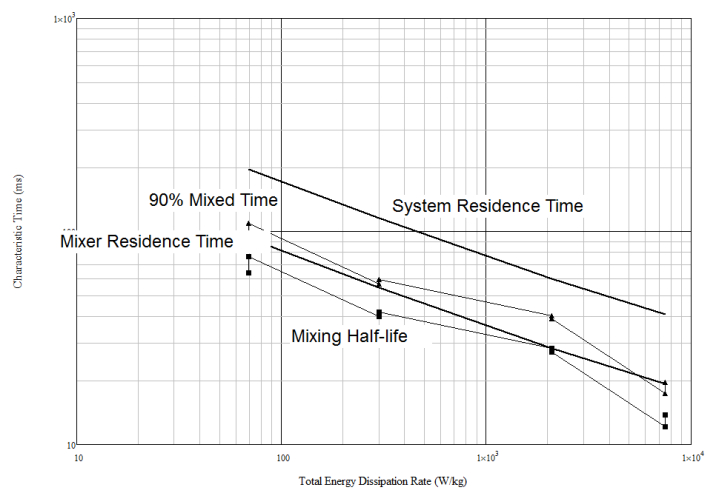
Appendix 4 – Comparison of Timescales



1/8" X Mixer 3:1 Bourne Composition Timescale Comparison

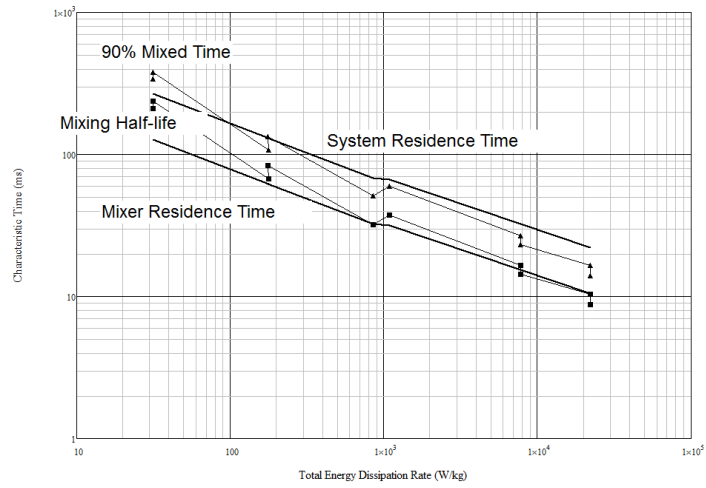


1/8" X Mixer 1:3 Bourne Composition Timescale Comparison

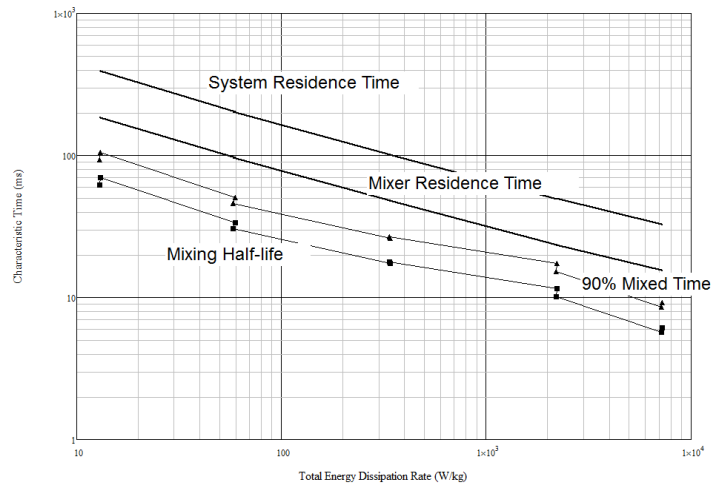


1/8" X Mixer 10:1 Bourne Composition Timescale Comparison

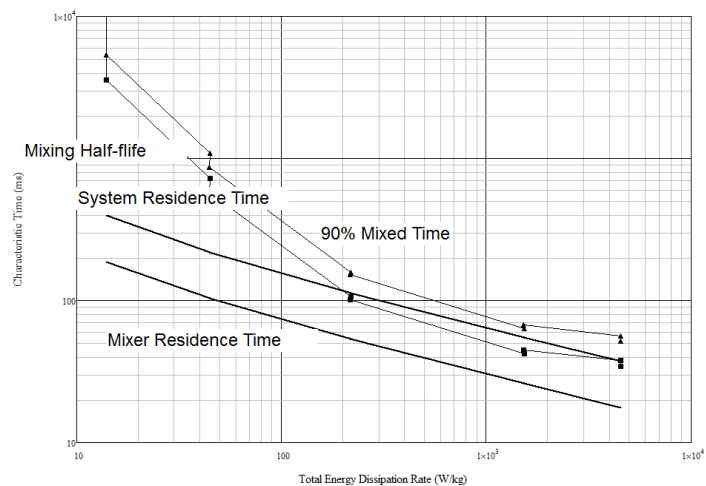
Appendix 4 – Comparison of Timescales



1/8" X Mixer 1:1 Modified Bourne Composition Timescale Comparison

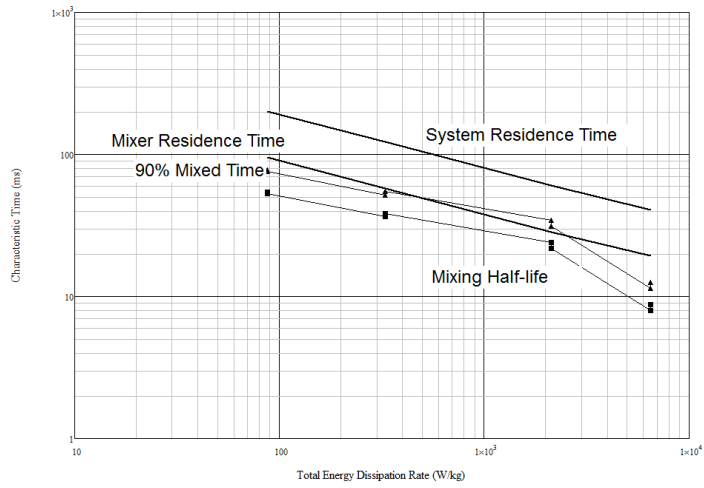


1/8" X Mixer 3:1 Modified Bourne Composition Timescale Comparison

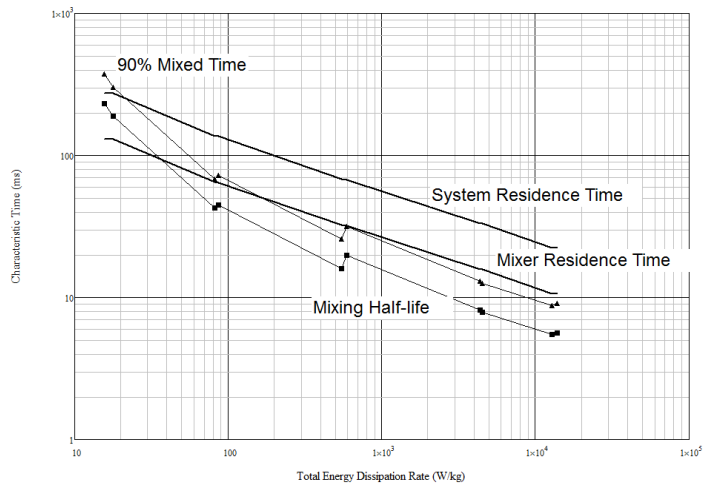


1/8" X Mixer 1:3 Modified Bourne Composition Timescale Comparison

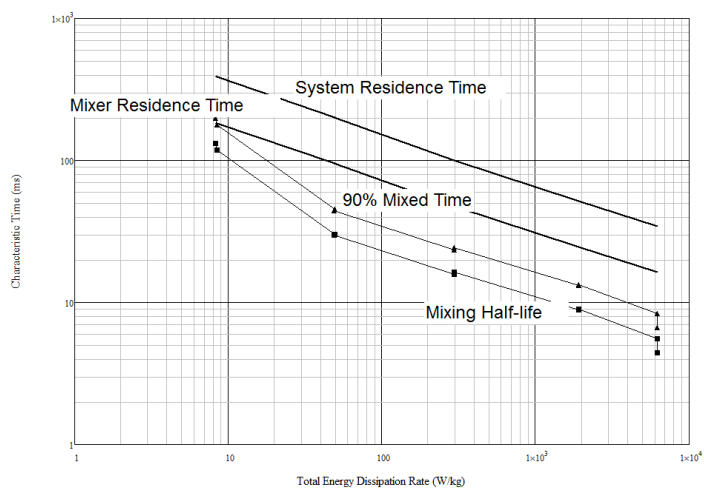
Appendix 4 – Comparison of Timescales



1/8" X Mixer 10:1 Modified Bourne Composition Timescale Comparison

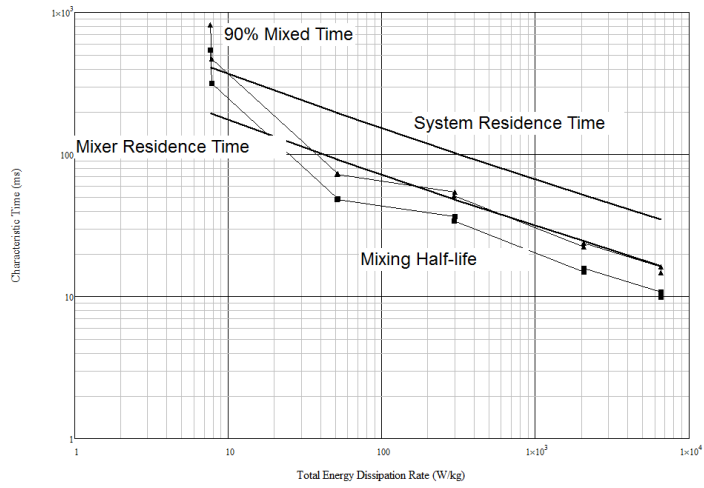


1/8" T Mixer 1:1 Bourne Composition Timescale Comparison

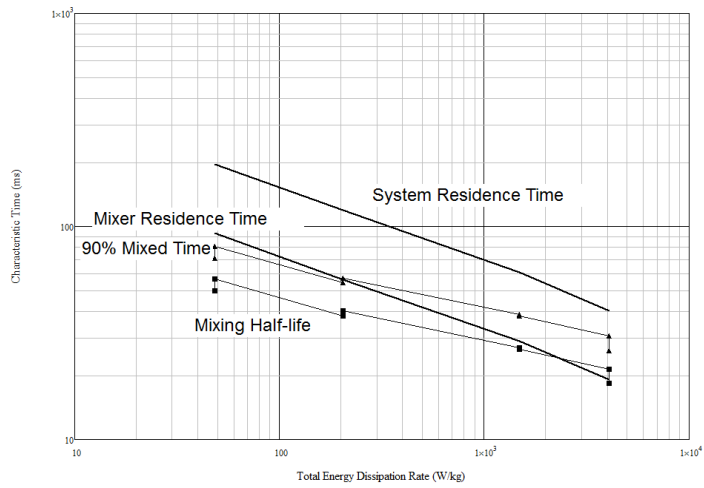


1/8" T Mixer 3:1 Bourne Composition Timescale Comparison

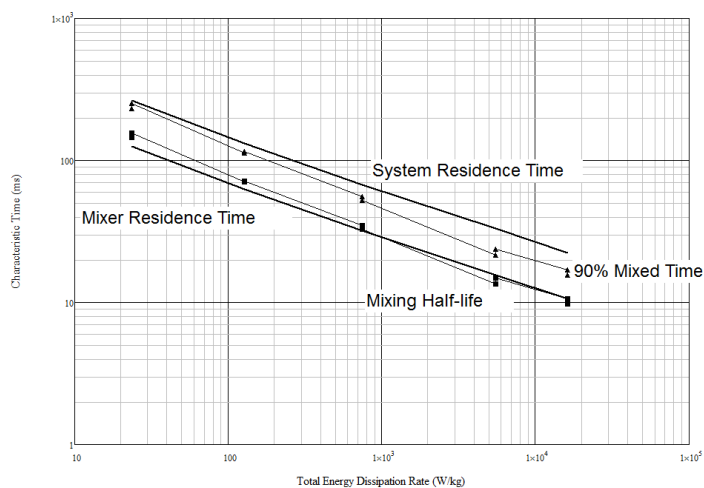
Appendix 4 – Comparison of Timescales



1/8" T Mixer 1:3 Bourne Composition Timescale Comparison

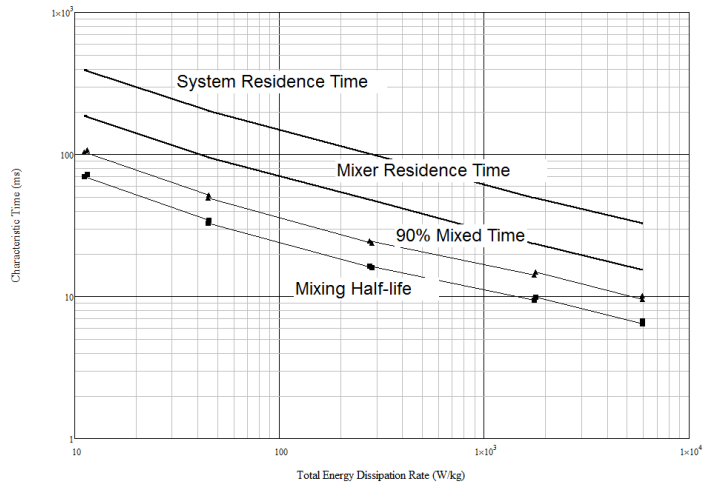


1/8" T Mixer 10:1 Bourne Composition Timescale Comparison

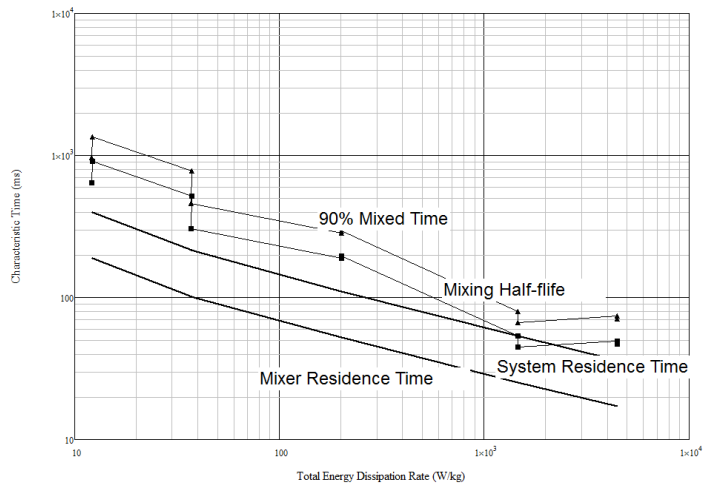


1/8" T Mixer 1:1 Modified Bourne Composition Timescale Comparison

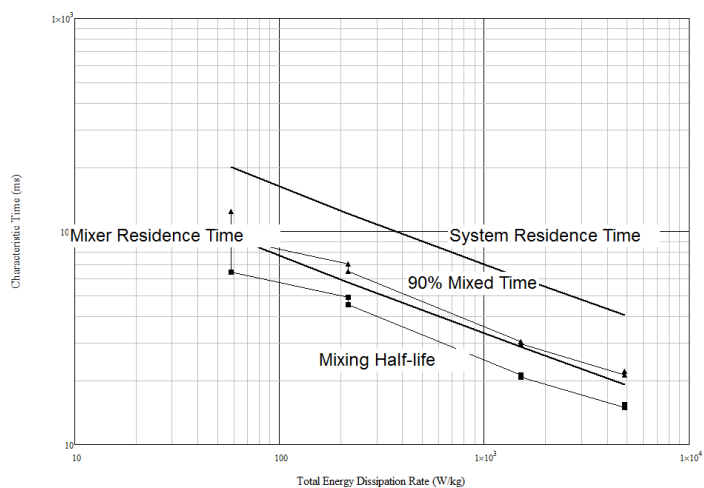
Appendix 4 – Comparison of Timescales



1/8 T Mixer 3:1 Modified Bourne Composition Timescale Comparison

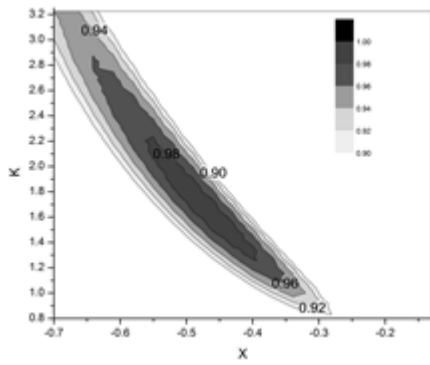


1/8 T Mixer 1:3 Modified Bourne Composition Timescale Comparison

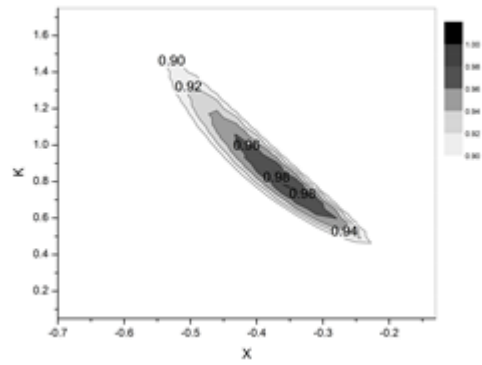


1/8 T Mixer 10:1 Modified Bourne Composition Timescale Comparison

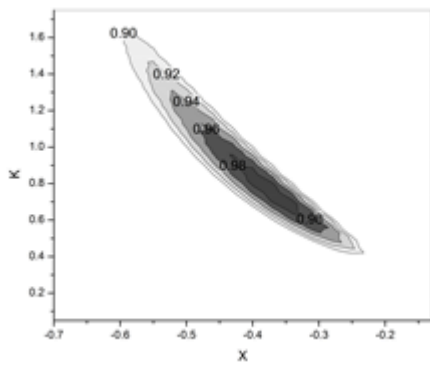
Appendix 5 - Fractional Conversion Regression Plots



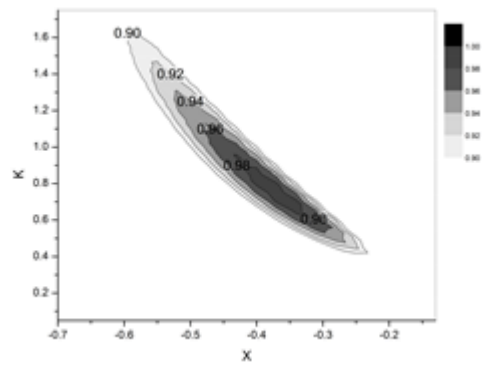
1/8" T 1:1 Bourne



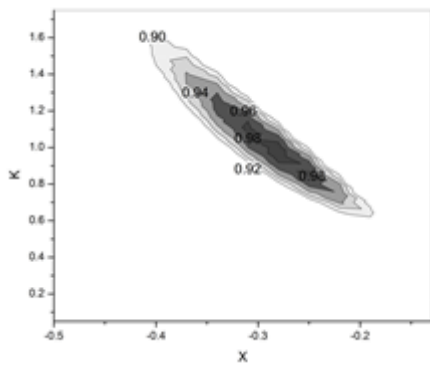
1/8" X 1:1 Bourne



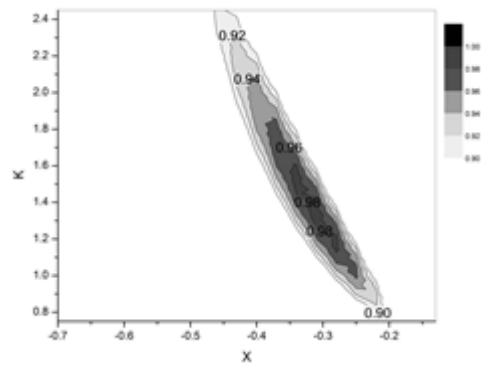
Vortex 1:1 Bourne



CIJ 1:1 Bourne

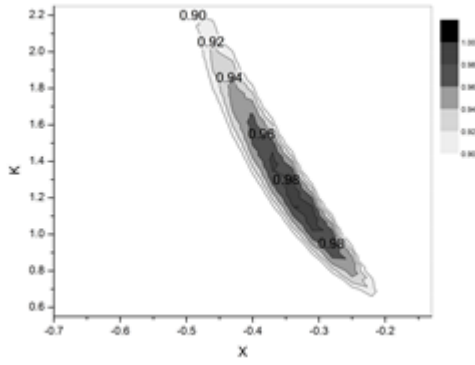


1/8" T 1:1 Modified Bourne

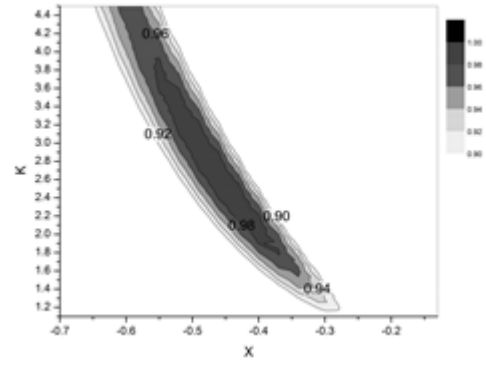


1/8" X 1:1 Modified Bourne

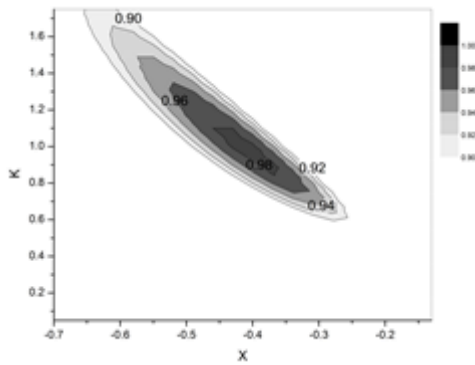
Appendix 5 – Solid Recovery Data



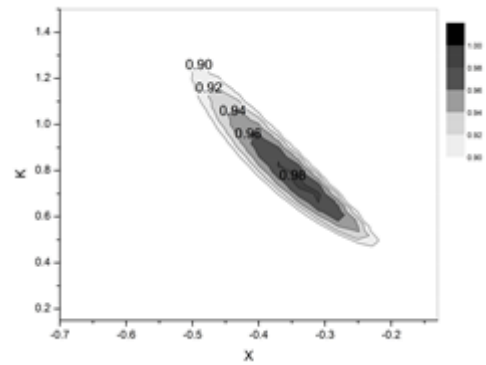
Vortex 1:1 Modified Bourne



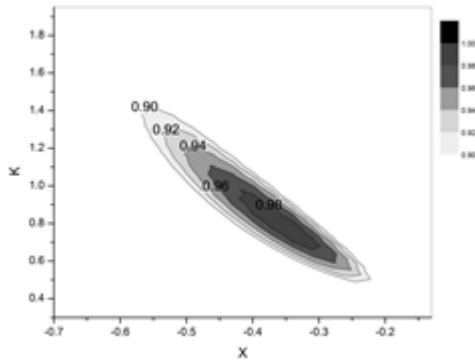
CIJ 1:1 Modified Bourne



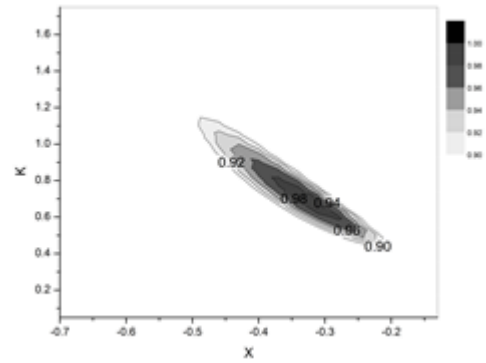
1/8" T3:1 Bourne



1/8" X 3:1 Bourne

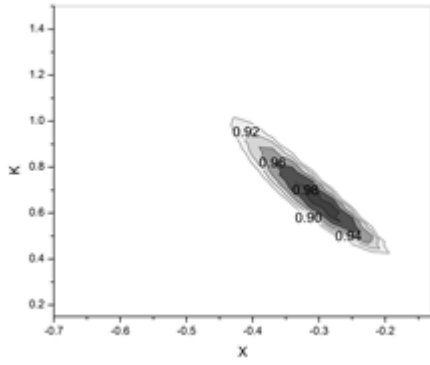


Vortex 3:1 Bourne

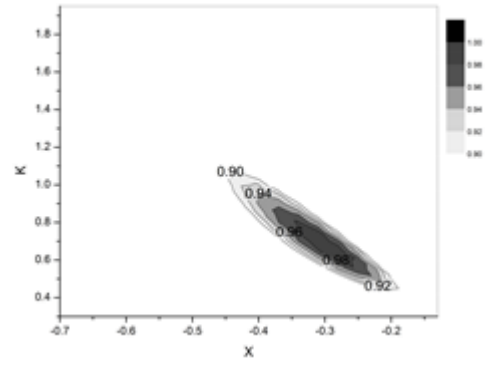


1/8" T 3:1 Modified Bourne

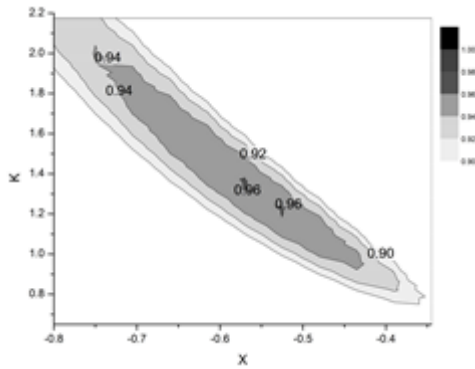
Appendix 5 – Solid Recovery Data



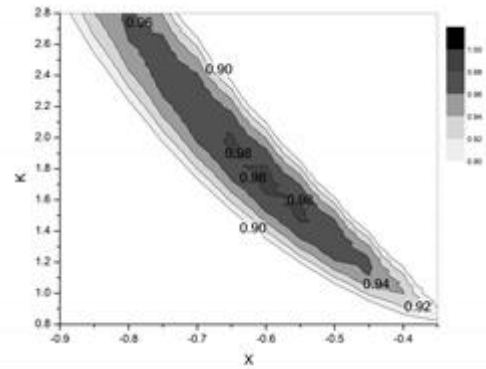
1/8" X 3:1 Modified Bourne



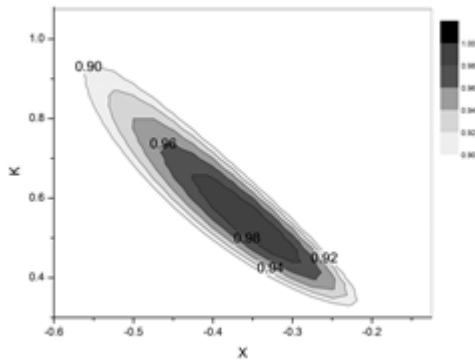
Vortex 3:1 Modified Bourne



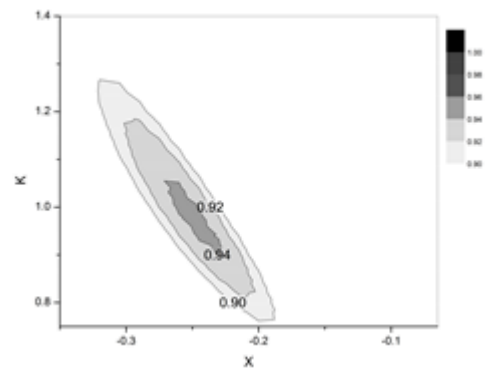
1/8" T 1:3 Bourne



1/8" X 1:3 Bourne

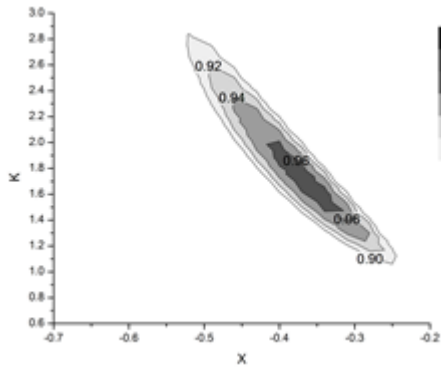


Vortex 1:3 Bourne

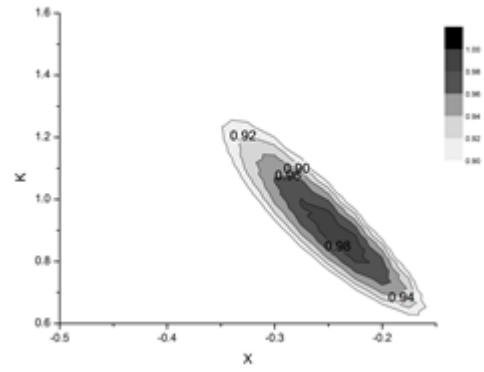


1/8" T 1:3 Modified Bourne

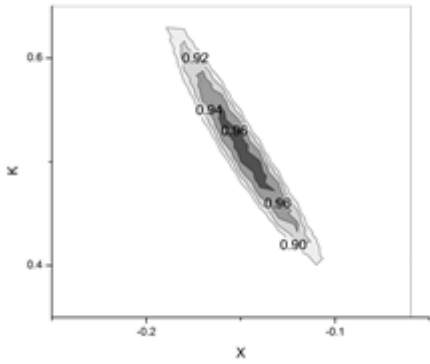
Appendix 5 – Solid Recovery Data



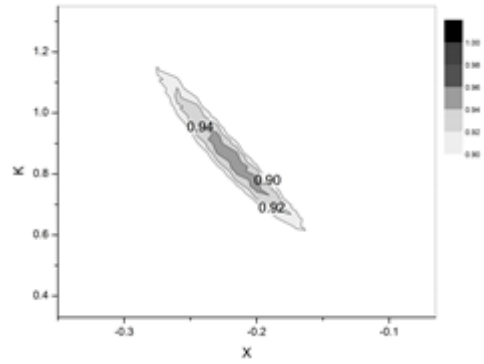
1/8" X 1:3 Modified Bourne



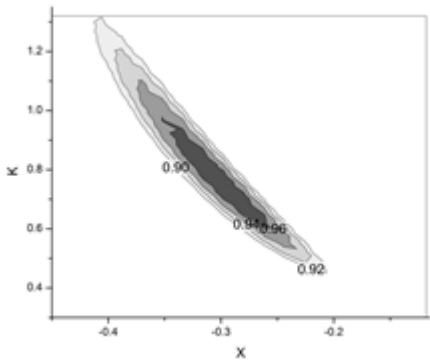
Vortex 1:3 Modified Bourne



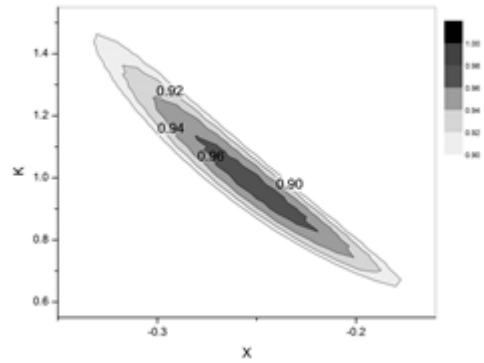
1/8" T 10:1 Bourne



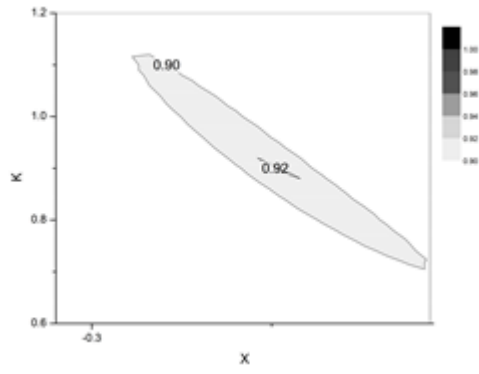
1/8" X 10:1 Bourne



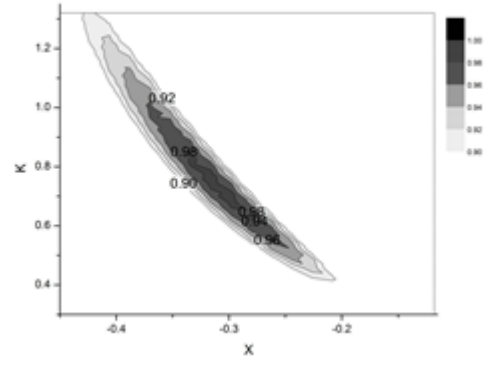
Vortex 10:1 Bourne



1/8" T 10:1 Modified Bourne



1/8" X 10:1 Modified Bourne



Vortex 10:1 Modified Bourne

Appendix 6 - Research Outcomes

- 2010 British Annual Crystal Growth (BACG) Poster presentation, Manchester
- “Influence of Rapid Initial Mixing on Particle Formation Kinetics”, 2011 International Symposium on Industrial Crystallization, Zurich
- Mixing Paper (Chapter 5,6 and 7) – Manuscript in progress
- Crystallisation Paper (Chapter 8) – Manuscript in progress